



ΕΘΝΙΚΟ ΜΕΤΣΟΒΙΟ ΠΟΛΥΤΕΧΝΕΙΟ

ΣΧΟΛΗ ΜΗΧΑΝΟΛΟΓΩΝ ΜΗΧΑΝΙΚΩΝ

**ΤΟΜΕΑΣ ΜΗΧΑΝΟΛΟΓΙΚΩΝ ΚΑΤΑΣΚΕΥΩΝ ΚΑΙ ΑΥΤΟΜΑΤΟΥ
ΕΛΕΓΧΟΥ**

**ΕΠΙ ΤΟΥ ΕΥΕΛΙΚΤΟΥ ΣΧΕΔΙΑΣΜΟΥ ΓΙΑ ΣΥΣΤΗΜΑΤΑ ΠΑΡΑΚΛΙΝΙΩΝ
ΑΝΟΣΟΛΟΓΙΚΩΝ ΔΟΚΙΜΩΝ**

ΔΙΔΑΚΤΟΡΙΚΗ ΔΙΑΤΡΙΒΗ

ΓΕΩΡΓΙΟΥ Π. ΚΑΝΑΚΑΡΗ

Διπλωματούχου Μηχανολόγου Μηχανικού Ε.Μ.Π.

ΕΠΙΒΛΕΠΩΝ

Λ. ΑΛΕΞΟΠΟΥΛΟΣ

Αναπληρωτής Καθηγητής Ε.Μ.Π.

ΑΘΗΝΑ, Νοέμβριος 2021



NATIONAL TECHNICAL UNIVERSITY OF ATHENS
SCHOOL OF MECHANICAL ENGINEERING
SECTION OF MECHANICAL DESIGN AND AUTOMATIC CONTROL

ON THE MODULAR DESIGN OF POINT-OF-CARE IMMUNOASSAYS

DOCTORAL DISSERTATION

GEORGIOS P. KANAKARIS
Mechanical Engineer, Dipl. NTUA

SUPERVISOR
L. ALEXOPOULOS
Associate Professor, NTUA

ATHENS, November 2021



ΕΘΝΙΚΟ ΜΕΤΣΟΒΙΟ ΠΟΛΥΤΕΧΝΕΙΟ

ΣΧΟΛΗ ΜΗΧΑΝΟΛΟΓΩΝ ΜΗΧΑΝΙΚΩΝ

**ΤΟΜΕΑΣ ΜΗΧΑΝΟΛΟΓΙΚΩΝ ΚΑΤΑΣΚΕΥΩΝ ΚΑΙ ΑΥΤΟΜΑΤΟΥ
ΕΛΕΓΧΟΥ**

**ΕΠΙ ΤΟΥ ΕΥΕΛΙΚΤΟΥ ΣΧΕΔΙΑΣΜΟΥ ΓΙΑ ΣΥΣΤΗΜΑΤΑ ΠΑΡΑΚΛΙΝΙΩΝ
ΑΝΟΣΟΛΟΓΙΚΩΝ ΔΟΚΙΜΩΝ**

ΔΙΔΑΚΤΟΡΙΚΗ ΔΙΑΤΡΙΒΗ

ΓΕΩΡΓΙΟΥ Π. ΚΑΝΑΚΑΡΗ

Διπλωματούχου Μηχανολόγου Μηχανικού Ε.Μ.Π.

ΤΡΙΜΕΛΗΣ ΣΥΜΒΟΥΛΕΥΤΙΚΗ ΕΠΙΤΡΟΠΗ

1. Λ. ΑΛΕΞΟΠΟΥΛΟΣ, Αν. Καθ. ΕΜΠ
2. Ε. ΠΑΠΑΔΟΠΟΥΛΟΣ, Καθ. ΕΜΠ
3. Ν. ΧΡΟΝΗΣ, Αν. Καθ. Παν. Κρήτης

ΕΠΤΑΜΕΛΗΣ ΕΞΕΤΑΣΤΙΚΗ ΕΠΙΤΡΟΠΗ

1. Λ. ΑΛΕΞΟΠΟΥΛΟΣ, Αν. Καθ. ΕΜΠ
2. Ε. ΠΑΠΑΔΟΠΟΥΛΟΣ, Καθ. ΕΜΠ
3. Ν. ΧΡΟΝΗΣ, Αν. Καθ. Παν. Κρήτης
4. Γ. ΒΟΣΝΙΑΚΟΣ, Καθ. ΕΜΠ
5. Β. ΣΠΙΤΑΣ, Αν. Καθ. ΕΜΠ
6. Π. ΜΠΕΝΑΡΔΟΣ, Επ. Καθ. ΕΜΠ
7. Χ. ΠΡΟΒΑΤΙΔΗΣ, Καθ. ΕΜΠ

ΑΘΗΝΑ, Νοέμβριος 2021



NATIONAL TECHNICAL UNIVERSITY OF ATHENS
SCHOOL OF MECHANICAL ENGINEERING
SECTION OF MECHANICAL DESIGN AND AUTOMATIC CONTROL

ON THE MODULAR DESIGN OF POINT-OF-CARE IMMUNOASSAYS

DOCTORAL DISSERTATION

GEORGIOS P. KANAKARIS
Mechanical Engineer, Dipl. NTUA

ADVISORY COMMITTEE

4. L. ALEXOPOULOS, Assoc. Prof. NTUA
5. E. PAPADOPOULOS, Prof. NTUA
6. N. CHRONIS, Assoc. Prof. UOC

EXAMINATION COMMITTEE

8. L. ALEXOPOULOS, Assoc. Prof. NTUA
9. E. PAPADOPOULOS, Prof. NTUA
10. N. CHRONIS, Assoc. Prof. UOC
11. G. VOSNIAKOS, Prof. NTUA
12. V. SPITAS, Assoc. Prof. NTUA
13. P. BENARDOS, Asst. Prof. NTUA
14. C. PROVATIDIS, Prof. NTUA

ATHENS, November 2021

ACKNOWLEDGMENTS

This work could not have been completed without the effort and patience of many people. First and foremost I would like to thank my supervisor, Dr. Leonidas Alexopoulos, Assoc. Prof. NTUA for his trust and guidance. I would also like to thank Dr. E. Papadopoulos, Prof. NTUA and Dr. N. Chronis, Assoc. Prof. UOC as well as their teams for the support in training, equipment and advice. Many thanks to Dr. M. Kandyla, Senior Researcher NHRF and Dr. E. Gogolides, research director NCSR Demokritos and their teams for their contributions.

I would also like to thank all those with whom we worked together over the years, Sofia Stamatatou for the unending support, Theodore Sakellaropoulos, Alexander Polesiuk, Yannis Melas, Yannis Pappas, the other Yannis Pappas, Chris Evangelakis, Dimitris Messinis, Nikos Kavalopoulos, Ilona Binenbaum, Chris Sotiropoulos and of course Dimitris Tzeranis for the support, advice and valuable help. I also deeply thank Aggeliki Minia, Stefania Tziola and Danai Zarifi for the time and effort they put into this work.

A big thank you to the friends who helped with all this, Christos A., Christos L., Natasa, Iasonas for being a role model, Alex, Vassilis for the heavy lifting, Makis and the team for pushing me as well as all the friends who put up with me throughout these years.

I will always be grateful for my parents, I know you would have liked to be here for this.

My biggest thank you belongs to Ifigeneia, for your never-ending love and support.

Blank Page

CONTENTS

Acknowledgments	5
Abstract	1
Figures and Tables	2
List of Figures	2
List of Tables	5
Abbreviations.....	6
Chapter 1: Introduction	7
1.1 Abstract	7
1.2 Motivation	7
1.3 Immunoassays for diagnostics and research.....	8
1.3.1 Microbeads for multiplexing and high-throughput	10
1.4 Point-of-Care Testing	14
1.4.1 Small Handheld devices	15
1.4.2 Small Benchtop Systems.....	16
1.4.3 Laboratory Systems	17
1.5 Point of Care technology	18
1.5.1 Immunoassay technology	18
1.5.2 Fluid handling in point of care systems	19
The realm of microfluidics	19
Main operating principles.....	20
Fluidic functions of a PoC system	22
1.5.3 Detection technology in point of care systems	25
1.6 Challenges of point of care systems	25
Affordability	25
Multiplexability.....	26
User friendly / Equipment free	26
Robustness / Rapidity	26
The immunoassay adaptation challenge	27
Open vs Closed technology.....	29
Rapid deployment	29
1.7 Towards modular Point-of-Care immunoassays.....	30
1.8 Thesis Structure	32

Chapter 2: Point of Care Systems Review	33
2.1 Abstract	33
2.2 Introduction.....	33
2.3 Commercialized Point of Care systems - Technology Categorization.....	34
2.3.1 Lateral Flow Assays.....	35
LFIA Principle of Operation.....	36
Design, Materials and Reagents in LFIA.....	36
Aspects of sensitivity and quantification in LFIAs.....	38
Multiplex analyses in LFIAs	40
2.3.2 Centrifugal Point of Care systems.....	41
LOAD Principle of Operation.....	42
Design, Materials and Reagents in LOAD	43
Aspects of Sensitivity and Precision in LOAD.....	44
Aspects of multiple measurements in LOAD	45
2.3.3 Electrochemical Sensing Systems	45
Electrochemical Sensing Systems principles of operation.....	46
Design, Materials and Reagents in Electrochemical Sensing Systems.....	46
Performance of Electrochemical PoC Systems	47
2.3.4 Nucleic acid testing systems	48
NAT principles of operation.....	48
NAT PoC systems performance	50
2.3.5 Blood Gas / Electrolyte benchtop systems	50
2.3.6 Other technologies	50
Physical determination of biomarkers (coagulation).....	50
Optical Detection Systems.....	51
2.4 Commercialized Point of Care systems - Biomarkers	52
2.5 Conclusions.....	67
Chapter 3: A Laboratory Device for Immunoassay protocols	68
3.1 Abstract	68
3.2 Introduction.....	68
3.2.1 Assay development for biomarker discovery	68
3.2.2 Laboratory automation for immunoassay protocols.....	68
Standard Instruments	68
Automated platforms	71

3.2.3 State of the art limitations.....	73
3.2.5 Objectives	74
3.3 Methods.....	75
3.3.1 Platform overview	75
Stacked plate architecture.....	76
3.3.2 Fluid handling system design.....	80
3.3.3 Magnetic separation system design	84
Magnetic separation system concept.....	85
Forces acting on a para/diamagnetic microbead	90
Definition of the problem	92
Finite element modelling Ring shaped magnet	94
Particle tracing Ring shaped magnet	101
Finite element modelling Quatrefoil magnet.....	114
Particle tracing Quatrefoil magnet	119
Magnetic separation system design Summary	127
3.3.4 Motion system.....	128
3.3.5 Electronics and system programming	131
3.3.6 Immunoassay process in SampleX.....	132
3.4 Results	134
3.4.1 Microbeads in pipette tips microscopy.....	134
3.4.2 Magnetic separation efficiency	140
3.4.3 SARS-CoV-2 ELISA protocol in SampleX	146
Assay principle	146
Assay Reagents and required equipment.....	147
Manual assay process	147
Process automation in SampleX	147
SARS-CoV-2 Results from SampleX.....	151
3.5 Conclusions and next steps.....	154
Chapter 4: Laser Activated Micropumps	155
4.1 Abstract	155
4.2 Introduction.....	155
4.2.1 Micropump technology	155
4.3 Materials and Methods	156
4.3.1 Expancel® expandable microspheres	156

4.3.2 Preparation of Laser Activated Expandable Mixtures	157
4.3.3 Chip design and fabrication	158
4.3.4 Experimental Setup	160
4.3.5 Video Analysis Tool	161
4.4 Results	162
4.4.1 Single Use Micropump Design	162
4.4.2 Volume displacement and flow rate experiments.....	164
4.4.3 Precise Volume Displacement	167
4.4.4 Pressure Testing.....	168
4.4.5 Dependency of expansion rate from laser power	169
4.4.6 Heat transfer Thermal imaging	170
4.4.7 Heat transfer The effect of chamber size	171
4.4.8 Heat transfer The effect of chip thickness	173
4.4.9 Heat transfer Using a Heatsink to reduce the size of heat affected zones	174
4.5 Conclusions and next steps.....	175
Chapter 5: Porous Hydrophobic Microvalves	177
5.1 Abstract	177
5.2 Introduction.....	177
5.2.1 Microvalve technology	177
5.2.2 Burst microvalves - Geometric approach	178
Hydrophobic valves	184
Assembled hydrophobic microvalves	186
5.6 Methods.....	186
5.6.1 Valving element fabrication.....	186
5.6.2 Chip design and fabrication	187
5.6.3 Experimental setup.....	190
Experimental process	191
5.7 Results	193
5.7.1 Standard chip design	193
5.7.2 Radial chip design	195
5.8 Discussion	196
Chapter 6: Point of Care concepts.....	198
6.1 Abstract	198
6.2 Introduction.....	198

6.3 Concept 1: Lab-on-a-Disk based on modular micropumps and microvalves.....	198
6.4 Concept 2: Lab-on-a-Disk based on self-contained reagent injectors.....	206
6.5 Conclusions and next steps.....	213
Chapter 7: Conclusions and Future work.....	214
7.1 Abstract	214
7.2 Summary.....	214
7.3 Conclusions.....	215
7.3.1 A Laboratory Device for Immunoassay protocols.....	215
7.3.2 Laser Activated Single-Use Micropumps	215
7.3.3 Porous microvalves.....	216
7.3.4 Modular PoC concepts.....	217
7.4 Future Work.....	218
7.4.1 Laboratory systems.....	218
7.4.2 On-chip fluid handling	218
Laser activated single-use micropumps.....	218
Porous microvalves.....	218
7.4.3 Modular PoC concepts.....	218
Supplementary Material	220
Chapter 4	220
A Discussion on the scalability of the proposed micropump design	220
Matlab video analysis tool for displacement results extraction.....	221
Chapter 7	227
Lab-on-a-Disk fluorescence detection system.....	227
Lab-on-a-Disk motion system	231
Περίληψη	234
Κεφάλαιο 1: Εισαγωγή	234
1.1 Κίνητρα ερευνητική εργασίας	234
1.2 Ανοσολογικές δοκιμές για διάγνωση και έρευνα	234
1.4 Έλεγχος στο σημείο φροντίδας.....	235
1.5 Ευέλικτος σχεδιασμός για συστήματα παρακλίνιων ανοσολογικών δοκιμών	235
Κεφάλαιο 2: Ανασκόπηση παρακλίνιων διαγνωστικών συστημάτων	235
2.1 Η τεχνολογία των παρακλίνιων διαγνωστικών συστημάτων.....	235
2.2 Τεστ lateral flow.....	236
2.3 Φυγοκεντρικά PoC συστήματα.....	236

2.4 Ηλεκτροχημικά PoC συστήματα	236
2.5 Συστήματα ανίχνευσης νουκλεϊκών οξέων	236
2.6 Συμπεράσματα	237
Κεφάλαιο 3: Ένα εργαστηριακό σύστημα για ανοσολογικά πρωτοκόλλα.....	237
3.1 Τεχνολογία ανοσολογικών δοκιμών με μικροσφαιρίδια	237
3.2 Μέθοδοι	237
3.3 Αποτελέσματα και Συμπεράσματα	238
Κεφάλαιο 4: Μικροαντλίες ενεργοποιούμενες με δέσμη laser.....	238
4.1 Τεχνολογία μικροαντλίων.....	239
4.2 Μέθοδοι	239
4.3 Αποτελέσματα και Συμπεράσματα	239
Κεφάλαιο 5: Πορώδεις υδρόφοβες μικροβαλβίδες	240
5.1 Τεχνολογία μικροβαλβίδων.....	240
5.2 Μέθοδοι	241
5.3 Αποτελέσματα και Συμπεράσματα	241
Κεφάλαιο 6: Εφαρμογές σε PoC συστήματα.....	242
6.1 Lab-on-a-Disk βασισμένο σε στοιχεία ευέλικτου σχεδιασμού.....	242
6.2 Lab-on-a-Disk βασισμένο σε αυτόνομους injectors	242
Κεφάλαιο 7: Συμπεράσματα και επόμενα βήματα.....	242
Δημοσιεύσεις.....	243
Bibliography	244

ABSTRACT

Medical testing at the Point of Care (PoC) is becoming essential for the timely diagnosis and monitoring of pathological conditions and infectious disease, for the proper treatment of the individual and for the protection of the community. The recent case of SARS-CoV-2 has outlined the need for decentralized immunoassay diagnostic technologies. The development of automated lab scale and benchtop point of care immunoassays is an actively pursued goal for both academia and industry. However, a gap between the rapid lateral flow test and the large, automated hospital analyzer still exists. Partly, this is because the miniaturization of laboratory immunoassay protocols remains elusive.

In this work, key concepts of immunoassays and point of care diagnostics are presented. The current state of the art is reviewed through literature and mostly through commercially available PoC systems. Their technology is discussed, and a list of their diagnostic targets is compiled.

Following this review, a point of care technology which can be shared across laboratory and benchtop systems is envisioned focusing on design modularity. A laboratory system for automated bead-based immunoassay preparation is developed, analyzed and its key components are presented. The system is then used to perform a full sandwich immunoassay for SARS-CoV-2 antibodies yielding promising results.

Following the development of the laboratory system, the building blocks for a benchtop point of care microfluidic disk that shares the same immunoassay technology are proposed. A new type of on-chip non-contact micropump that is activated using an IR laser beam is developed and tested. We report flow rates as high as 2 $\mu\text{l}/\text{sec}$ and total volumes over 160 μl with high displacement repeatability. The second development is a new type of burst microvalve that is based on hydrophobic porous glass microfiber filters. For this assembled part, we report burst pressures of 12.5 kPa which makes it suitable for use in centrifugal microfluidic systems. Both components follow the modularity concept pursued in this work. Using these two building blocks, some concept microfluidic disks for the performance of bead-based immunoassays are proposed and discussed. Initial prototyping work is presented along with motion system and detection concepts.

FIGURES AND TABLES

LIST OF FIGURES

- 1.1 The steps of a direct ELISA process
- 1.2 The steps of a sandwich ELISA process
- 1.3 Microarrays and superparamagnetic particles
- 1.4 The process of a bead-based immunoassay
- 1.5 A microbead detection system based on flow cytometry principles
- 1.6 Common examples of portable PoC systems: A glucose meter and a lateral flow test
- 1.7 Examples of Benchtop PoC systems: Piccolo Xpress and Siemens Stratus
- 1.8 Example of a high-throughput PoC system: Gyrolab
- 1.9 Key components of a sandwich immunoassay
- 1.10 A microfluidic chip example and laminar flows in microfluidic junction
- 1.11 Different fluid handling approaches in diagnostic PoC systems
- 1.12 Different functions of a PoC system for multistep protocols
- 1.13 Components for sample and reagent handling in PoC system
- 1.14 Immunoassay in the lab and PoC adaptations
- 1.15 Thesis breakdown structure
- 2.1 Inside a lateral flow test
- 2.2 Different lateral flow tests and reader system
- 2.3 Operation specific blocks found inside a lab on a disk disposable
- 2.4 Lab on a disk systems and consumables
- 2.5 A simplified design of an electrochemical sensing strip
- 2.6 4 electrochemical biosensing systems
- 3.1 Pipettes and microwell plates
- 3.2 A plate shaker and a plate washer
- 3.3 The main functions required for a bead-based immunoassay
- 3.4 An automated liquid handling system and assorted modules
- 3.5 Simplified configuration of a typical liquid handling platform
- 3.6 The proposed automated platform for bead-based immunoassays
- 3.7 Main components of the proposed platform
- 3.8 A simplified depiction of the SampleX platform logic
- 3.9 The process of capturing, moving and aligning a microtiter plate within the SampleX platform
- 3.10 Section view of the fluid handling head with washing-through capability
- 3.11 Section view of the fluid handling head without washing-through capability
- 3.12 The motion system for fluid handling operations in SampleX
- 3.13 A prototype of the fluid handling head used in SampleX
- 3.14 Microbead separation approach in SampleX
- 3.15 The magnetic separation system functionality in SampleX
- 3.16 A prototype of the magnetic separation system in SampleX
- 3.17 How magnetic separation is achieved inside pipette tips
- 3.18 Design constraints for a magnetic separation module 1
- 3.19 Design constraints for a magnetic separation module 2
- 3.20 Using a ring magnet for microbead separation
- 3.21 An axisymmetric model for magnetics and fluid flow analysis
- 3.22 Mesh size refinement for magnetics model

- 3.23 Magnetic forces on a superparamagnetic microbead from a ring magnet inside the pipette tip
- 3.24 Radial component of magnetic force from ring magnet on microbeads resting on the pipette wall
- 3.25 Radial component of magnetic force from ring magnet on microbeads floating in pipette cross section
- 3.26 Fluid flow and magnetics models for particle tracing in ring magnet arrangement
- 3.27 Time series of the motion of superparamagnetic microbeads inside a pipette tip under the influence of a ring magnet
- 3.28 Paths and end position of microbeads entering the pipette tip driven by a laminar flow under the influence of a magnetic field from ring magnets 1
- 3.29 Paths and end position of microbeads entering the pipette tip driven by a laminar flow under the influence of a magnetic field from ring magnets 2
- 3.30 Paths and end position of microbeads entering the pipette tip driven by a laminar flow under the influence of a magnetic field from ring magnets 3
- 3.31 Paths and end position of microbeads entering the pipette tip driven by a laminar flow under the influence of a magnetic field from ring magnets 4
- 3.32 Total magnetic attraction force on microbeads from promoted ring magnet designs at the pipette boundary
- 3.33 Time series of microbead travel paths from the lower part of the pipette tip
- 3.34 Total magnetic attraction force on microbeads from promoted ring magnet designs at the lower part of the pipette tip
- 3.35 A quatrefoil magnet arrangement for microbead separation
- 3.36 3D model for the quatrefoil magnet arrangement with quarter symmetry
- 3.37 Model mesh for quatrefoil magnet arrangement
- 3.38 Effect of magnet height and diameter in magnetic attraction force on pipette boundary for quatrefoil magnet arrangements
- 3.39 Fluid flow and magnetics models for particle tracing in quatrefoil magnet arrangement
- 3.40 Paths and end position of microbeads entering the pipette tip driven by a laminar flow under the influence of a magnetic field from a quatrefoil magnet arrangement 1
- 3.41 Paths and end position of microbeads entering the pipette tip driven by a laminar flow under the influence of a magnetic field from a quatrefoil magnet arrangement 2
- 3.42 Paths and end position of microbeads entering the pipette tip driven by a laminar flow under the influence of a magnetic field from a quatrefoil magnet arrangement 3
- 3.43 Total magnetic attraction force on microbeads from promoted quatrefoil magnet designs at the pipette boundary
- 3.44 Total magnetic attraction force on microbeads from promoted quatrefoil magnet designs at the lower part of the pipette tip
- 3.45 Motion system components of SampleX
- 3.46 SampleX Y-axis motion
- 3.47 Prototype for SampleX motion axes
- 3.48 Microwell plates and plate trays
- 3.49 Electronics and mainboard of SampleX
- 3.50 Standard mode and single plate mode of operation for SampleX
- 3.51 Optical microscopy setup to examine the behavior of superparamagnetic microbeads under the influence of the magnetic field of a ring magnet
- 3.52 Optical microscopy image of captured beads inside a pipette tip
- 3.53 Optical microscopy image of captured beads inside a pipette tip while the liquid solution is dispensed 1
- 3.54 Optical microscopy image of captured beads inside a pipette tip while the liquid solution is dispensed 2
- 3.55 Optical microscopy image of released beads inside a pipette tip while the liquid solution is dispensed

- 3.56 Plate layout for 3-step incubation test for bead capturing
- 3.57 Plate layout for a SARS-CoV-2 immunoassay in SampleX
- 3.58 A comparison of assay results for processes performed manually and using SampleX in bar graph visualization
- 4.1 Expansion in Expancel® microspheres
- 4.2 The expandable mixture used for this application
- 4.3 Experimental chip designs 1
- 4.4 Experimental chip designs 2
- 4.5 Experimental setup with laser activation of micropump and photopolymer solidification
- 4.6 Steps for data acquisition from recordings of micropump experiments
- 4.7 The micropump activation process
- 4.8 Results of micropump performance vs mixture composition experiments
- 4.9 Micropumping characteristics vs mixture composition
- 4.10 Experiments for controlled volume displacement
- 4.11 Evaluation of flow rate for increased circuit pressure
- 4.12 Evaluation of pressure capabilities of microfluidic pump
- 4.13 Dependency of flow rate from laser power
- 4.14 Thermal imaging of micropump during activation
- 4.15 FEA study of heat transfer during micropump activation 1
- 4.16 FEA study of heat transfer during micropump activation 2
- 4.17 FEA study of heat transfer during micropump activation 3
- 4.18 FEA study of heat transfer during micropump activation 4
- 5.1 Active and passive microvalves in literature
- 5.2 A basic design for a geometrical microfluidic valve 1
- 5.3 A basic design for a geometrical microfluidic valve 2
- 5.4 Geometrical burst valve inside a centrifugal microfluidic disc
- 5.5 Calculated burst pressure for varying channel widths and depths
- 5.6 Exerted pressure vs rotational frequency in a centrifugal microfluidic
- 5.7 Contact angle modification for burst microvalves
- 5.8 Burst pressure vs contact angle for burst microvalves
- 5.9 The concept of a modular hydrophobic microvalve
- 5.10 Contact angle measurement of processed filter
- 5.11 Test disk for hydrophobic porous valves
- 5.12 Test disk verification
- 5.13 Test disk preparation for experiments
- 5.14 A test disk for a radial valve positioning implementation
- 5.15 A prototype test disk with radial valve positioning implementation
- 5.16 Outline of experimental setup with strobe imaging and speed control
- 5.17 Implementation of the experimental setup with strobe imaging and speed control
- 5.18 Strobe images during microvalve testing
- 5.19 Burst frequencies of microvalves in standard chip design
- 5.20 Burst pressures of microvalves in standard chip design
- 5.21 Burst microvalve bypass by liquid reagent
- 5.22 Radial chip design burst frequency
- 5.23 Radial chip design burst pressure
- 6.1 Lab on a disk that makes use of laser activated micropumps and hydrophobic porous microvalves
- 6.2 A microfluidic disk for bead-based immunoassay protocols

- 6.3 An aliquoting operation implemented in the microfluidic disk
- 6.4 Laser activated micropumps in the microfluidic disk
- 6.5 Microbeads in the reaction channel of the microfluidic disk
- 6.6 An exploded view of the microfluidic disk and assorted device
- 6.7 Self-contained reagent injectors based on laser activated micropumps
- 6.8 A microfluidic disk based on self-contained injectors
- 6.9 An exploded view of the injector-based microfluidic disk and assorted device
- 6.10 A prototype of the injector microfluidic disk
- 6.11 A variation of the injector microfluidic disk utilizing an elastomer cartridge

LIST OF TABLES

- 1.1 The ASSURED criteria set by the World Health Organization
- 1.2 The different fluidic functions in a lab instrument and a PoC system
- 2.1 Main attributes of the different technological approaches for PoC systems
- 2.2 Extended list of conditions & biomarkers that are tested by PoC technologies (excluding SARS-CoV-2)
- 2.3 Different PoC tests related to SARS-CoV-2
- 2.4 A list of 125 PoC systems & companies reviewed in chapter 2
- 3.1 Standard vs SampleX bead-based immunoassay preparation process and required process stations.
- 3.2 Trapping efficiency for different ring magnet sizes
- 3.3 Promoted ring magnet designs for efficient bead trapping
- 3.4 Trapping efficiency of different magnet sizes for quatrefoil magnet arrangement
- 3.5 Promoted quatrefoil arrangement magnet designs for efficient bead trapping
- 3.6 Promoted solutions from ring magnet and quatrefoil arrangements
- 3.7 Separation efficiency results, experiment set 1
- 3.8 Separation efficiency results, experiment set 2
- 3.9 Separation efficiency results, experiment set 3
- 3.10 Separation efficiency results, experiment set 4
- 3.11 Separation efficiency results, experiment set 5
- 3.12 Reagents used for a SARS-CoV-2 antibody assay
- 3.13 Macros for incubation and washing in the SampleX platform
- 3.14 *A comparison of assay results for processes performed manually and using SampleX 1*
- 3.15 *A comparison of assay results for processes performed manually and using SampleX 2*
- 5.1 *Burst frequency and pressure for hydrophobic valves in standard chip design*
- 5.2 *Burst frequency and pressure for hydrophobic valves in radial chip design*

ABBREVIATIONS

Ab(s) : Antibody, Antibodies

Ag(s): Antigen, Antigens

ALP : Alkaline Phosphatase

CK-MB : Creatine kinase myocardial band

CMP : Comprehensive metabolic panel

COVID-19: Coronavirus disease 2019

DD : Doublet discriminator

ELISA : Enzyme linked immunosorbent assay

HRP : Horse Radish Peroxidase

LFIA : Lateral flow immunoassay

LOC : Lab on a Chip

LOAD: Lab on a Disk

PE : Phycoerythrin

POC : Point of Care

PT-INR : Prothrombin time, international normalized ratio

SARS-CoV-2: Severe acute respiratory syndrome Coronavirus 2

TBIL : Total bilirubin

CHAPTER 1: INTRODUCTION

1.1 ABSTRACT

In this introductory chapter, key concepts of immunoassays, microbeads and Point-of-Care (PoC) diagnostics are presented to set the groundwork on which this thesis is based. A categorization of PoC systems based on their setting and intended use is made and key aspects of their operating principles are discussed. Challenges of PoC systems as well as accepted guidelines for their development are presented. Based on the previous, it is argued that PoC diagnostic systems could benefit from technologies that would allow a modular approach towards their design. Key research directions towards the development of modular PoC systems are discussed and the structure of this work is outlined.

1.2 MOTIVATION

The need to diagnose, monitor or exclude a pathological condition when and where needed has always been a major healthcare challenge. The timely diagnosis of a disease will very often improve the outcome^{1,2} and the quality of life of the patient, while it is essential for the selection of appropriate treatment or the rejection of an ineffective one. For the case of gastric cancer, early diagnosis is associated with a 5-year survival rate over 90%, while this percentage drops significantly as the disease progresses³. In the case of HIV, early diagnosis is linked with improved health outcomes for the individual and public health benefits⁴, while in the case of malaria, the lack of early diagnosis is one of the main factors that have impeded the success of the global malaria program in reducing disease morbidity and mortality^{5,6} according to the World Health Organization. For the case of infectious diseases, early diagnosis is not only critical for the benefit of the individual patient but also to prevent population spreading⁷. The very recent case of the COVID-19 pandemic created a sudden and immense need for sensitive, remote diagnostics⁸ both to control the disease but also to relieve the strain from laboratory diagnostic settings and healthcare facilities. The outbreak of COVID-19 is a very prominent example for the need to have healthcare diagnostics as early as possible in the furthest locations.

For all but a few diagnostic targets, medical testing continues to be centralized, usually serviced by a clinical laboratory⁹. Such facilities are equipped with automated analyzers that can process multiple samples simultaneously for a wide range of analytes. The very existence of high-throughput, large footprint multi target analyzers is evidence of the centralized diagnostic model currently followed as the mainstream approach to medical testing. There are significant benefits from this approach, notably standardization and repeatability that stem from the automation of clinical diagnostics. However, a centralized testing model often results in long turnaround times from sample collection to actionable feedback¹⁰. Samples collected in decentralized locations, such as rural areas or even urban clinical laboratories that are serviced by larger clinical laboratories, need to be transported to the location of the analyzer, processed, batched, tested and then the results need to be communicated to the medical professional who will in turn inform the patient. This process can last several days, while often, a sample transportation service is not in place and the patient needs to travel to the centralized clinical setting in order to be tested. Even for the case of COVID-19 where rapid and accurate diagnosis is critical for decision making, it is observed that while commercial equipment exists for rapid molecular diagnostics¹¹⁻¹³ with protocol durations not exceeding 15 mins, the typical duration from sample to results in molecular testing may sometimes exceed 72 hours¹⁴. For patients with chronic conditions that need frequent testing or patients whose mobility is impaired by their condition, the centralized testing model can be especially challenging. For all of these reasons, the need for decentralized, rapid clinical diagnostics is being actively pursued both academically and commercially.

While there are numerous diagnostic fields for which the above apply, one of the major and most impactful is the field of immunoassays, which is the detection of antibodies/antigens in a sample. This work will focus on the analysis, challenges and proposed solutions for the development of decentralized immunoassays.

1.3 IMMUNOASSAYS FOR DIAGNOSTICS AND RESEARCH

Whenever the detection of a macromolecule such as a protein has diagnostic value, an immunoassay is typically used in order to verify and quantify the presence of the specific protein or a group of proteins in a sample. Immunoassays are biochemical detection techniques in which a detection reagent which can be an antibody or antigen is used to isolate or otherwise immobilize a target protein, often referred to as the “analyte”. The analyte binds to the detection molecules thanks to the ability of the later to recognize and attach themselves on specific macromolecule sites that are called epitopes. It is possible to use both antibodies or antigens as detection molecules to capture antigens and antibodies respectively. The captured protein is detected and quantified through the use of a label which can be based on color, fluorescence or other techniques such as radioactive isotopes or chemiluminescence. There are many variations of immunoassays, some of which will be presented in Ch.2 of this work (*see Lateral Flow Immunoassays or LFIA*).

One of the most researched and widely used immunoassays is the Enzyme Linked Immunosorbent Assay also known as ELISA. In ELISA, the captured proteins are detected by a reporter enzyme that is indirectly attached to the sample. The measured activity of this enzyme is usually related to color or fluorescence. There are several variations of ELISA. In the simplest case, the sample is immobilized on a substrate, and enzyme - linked antibodies are introduced to its environment. These antibodies, following an incubation period, will bind to their target antigens (*Fig. 1.1*). The remaining unbound antibodies will then be washed away. In a final step, a substrate that responds to the presence of the enzyme which is linked to the antibodies is added to the solution. The response, which is usually a color or translucency change, is measured using a spectrophotometer or an absorbance reader. An increased color change will indicate a high enzyme concentration which in turn indicates an initial high antigen concentration. This simple biochemical method is limited by its low specificity (because only one antibody is used) and by the fact that immobilizing the sample antigen in a non-specific way, will result in all proteins in the sample also adhering to the plate substrate. This makes the method unsuitable for low abundance targets where even a small concentration is of diagnostic value. To solve these problems, a more elaborate method called sandwich ELISA has been developed.

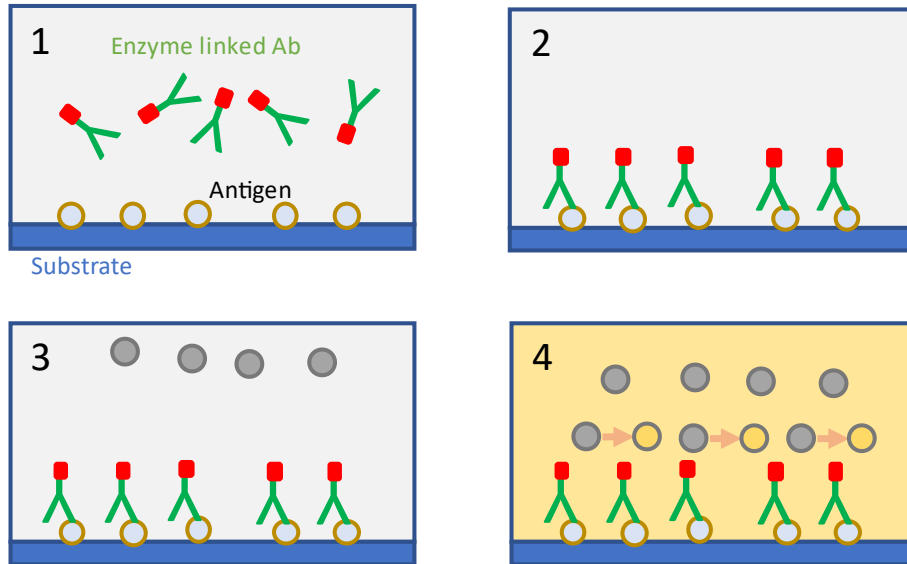


Fig 1.1 In direct ELISA, all proteins in the sample are immobilized and an enzyme-linked antibody specific to the target protein is added. If the protein is present in the sample, the antibody will bind to it. The unbound antibodies will be washed away. The detection happens by adding a substrate that responds to the presence of the enzyme (which is linked to the antibody) by changing its color or translucency)

In sandwich ELISA (Fig. 1.2), the target-specific antibody or primary antibody is immobilized on a surface, for example a well-plate bottom. The sample is introduced to the environment of the antibody but only the target protein can now bind to the surface through the primary antibody. The rest of the proteins are washed away. Following that, the secondary antibody is added to the solution. This secondary antibody is linked to an enzyme and it is also specific to the target protein. However, the primary and secondary antibody use different attachment sites on the antigen also known as epitopes so that they do not compete with each other. The secondary antibody will then bind to any target proteins that are already bound to the primary antibody. Unbound antibody is removed from the solution. As a final step, a labelling agent is added that responds or binds to the enzyme. In the simplest case, the enzyme is alkaline phosphatase (ALP) or horse radish peroxidase (HRP) and the label is P-Nitrophenyl-phosphate or hydrogen peroxide respectively. Both of these substrates change their color in the presence of the enzyme, and thus a colorimetric detection method is used to quantify the captured protein. However, another possibility is to use biotin-linked antibodies onto which a streptavidin-bound fluorophore such as phycoerythrin is attached in the labelling stage of the process. In this way, the quantification is done through measurement of fluorescence. The sandwich ELISA method is considered more sensitive than direct ELISA. There are some considerations since it is possible that the primary and secondary antibody will cross-react and yield falsely positive signals, however this method once optimized has great diagnostic value. Among other applications, it is used to detect different viruses and other pathogens through antibody response, toxins, cancer, and allergens. See Chapter 2 for a full list of conditions detected using immunoassays.

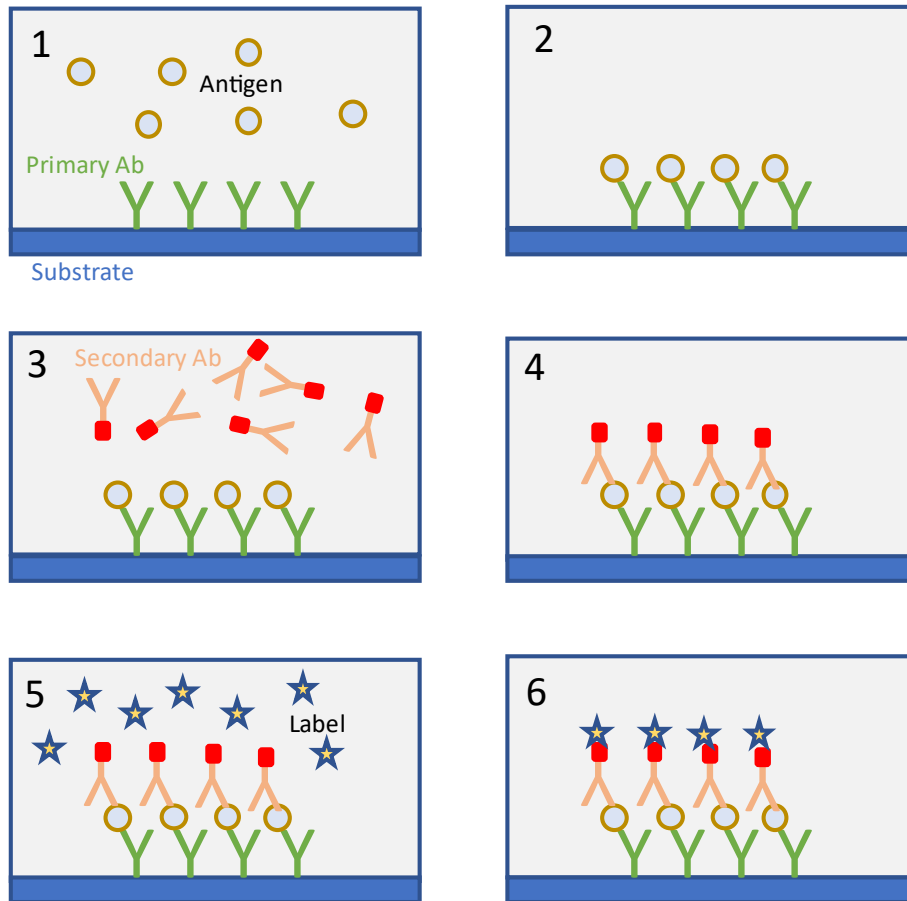


Fig 1.2 In sandwich ELISA, the target antigen is immobilized through the use of the primary antibody which is specific to the analyte. A secondary antibody which is enzyme-linked and is also specific to the analyte is used for the detection of the capture antigens. The use of two antibodies makes this method highly specific and sensitive.

1.3.1 MICROBEADS FOR MULTIPLEXING AND HIGH-THROUGHPUT

The sandwich ELISA method can be used to create immunoassays with high sensitivity and specificity. However, the mode of primary Ab immobilization requires the binding to a solid substrate, for example the bottom of a well plate. This is a time-consuming process and it requires large quantities of reagents and sample. More to that, if there is not one specific target analyte but several, or if the purpose of the immunoassay is to identify target analytes that can be used to develop diagnostic tests, an increased number of experiments may be required to acquire useful data. Assuming a case study in which 100 analytes are being examined as potential markers for a pathological condition in triplicates in 100 samples, this would require the preparation of 30k wells. But even for the purpose of diagnosis, an assay of 6 or more analytes is not uncommon. This requires the aliquoting of the sample in 6 different wells, which is typically performed by a liquid handling automation system in medical facilities or through the use of microfluidic aliquoting structures in PoC setups (see Chapter 2). Especially for the PoC setup, there are limited methods that can be employed to perform aliquoting and they tend to increase the chip footprint. There are two main approaches that tackle such challenges in immunoassays: Microarrays and Microbeads.

Microarrays are essentially the printing of antibodies/antigens/samples on a substrate in patterns. Using this method, discreet regions are created in which different reactions take place. For example, different primary antibody

spots can be printed on a glass slide in a grid and the entire slide could be processed with the same sample. Each spot would then behave as a separate well. If the labeling method is based on fluorescence and a fluorescent imaging system with the ability to scan different regions of the slide is available, then different analytes would be detected through a single experiment. This is referred to as multiplexing.

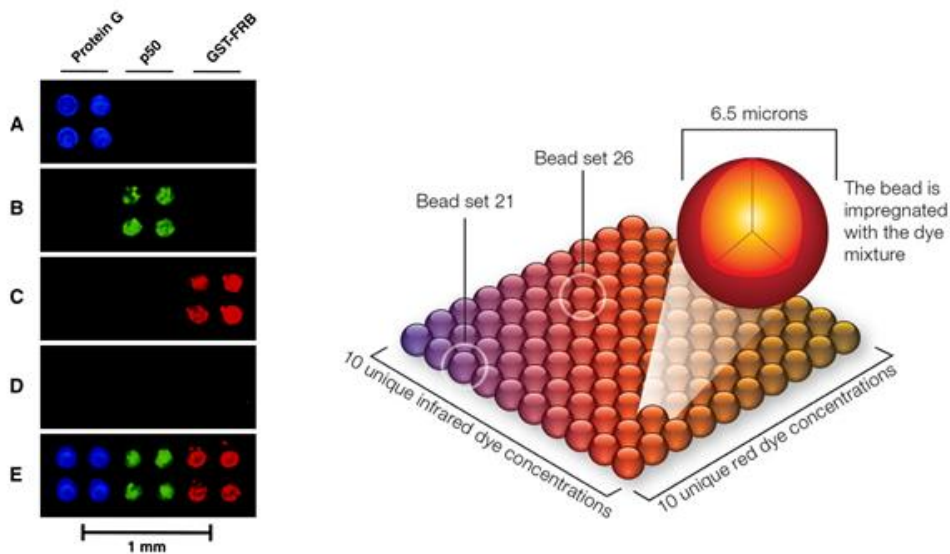


Fig 1.3 On the left¹⁵ A protein microarray of 150-200 μm diameter spots with a fluorescent label. On the right¹⁶, Luminex xMAP technology based on superparamagnetic color coded microbeads

There are different ways to prepare a microarray. Typically, either a jetting system or a contact deposition system are used. Spots can range from a few hundred microns down to submicron diameters (in this case termed nanoarrays). The process of creating a microarray requires specialized equipment, can be time consuming and increased volume of reagents and sample may be needed depending on the microarray surface that needs to be covered.

The second technology used to achieve multiplexing is based on microbeads. The idea had already been described in the 1960s¹⁷ but it was successfully commercialized for research and diagnostics by Luminex corporation¹⁸ in the late 1990s. In microbead technology, the substrate is replaced by polystyrene microspheres of 6.5 μm diameter (Fig. 1.3). The primary antibody is immobilized on the surface of these microspheres while the rest of the biochemical process remains unchanged. The microbeads have two additional properties from which the benefits of this process come from:

- Superparamagnetism¹⁹: The addition of metal oxide nanoparticles inside the polystyrene matrix of the microspheres makes them superparamagnetic. The nanoparticles are actually ferrimagnetic but because of their small size, they exhibit a random magnetization direction flip. This magnetization flip causes their average magnetization to be zero when not under the influence of an external magnetic field. However, in the presence of a magnetic field they display strong magnetic properties with high magnetic susceptibility. This provides the ability to manipulate the microbeads using magnetic fields.
- Color coding²⁰: Each microbead family has two or three different fluorescent dyes embedded in its matrix. The dye emissions under predefined excitation can be measured using flow cytometry-based methods. The ratio of each dye compared to the other one(s) is predefined per microbead family. This allows the use of multiple beads inside a single well in which each bead family targets a different analyte.

The process of a sandwich ELISA in a bead based -also known as suspension- assay is presented in *Fig 1.4*. In this case two beads are placed inside a saline solution. The beads represent two different bead families, 1&2 which carry different primary antibodies, also 1&2. In reality, 100s or 1000s of beads from each family are used for each assay. The different beads carry different ratios of fluorescent dyes and this is what makes it possible to differentiate between them. In step 2, the sample is introduced to the environment of the beads. The beads are suspended and this is also beneficial for the kinetics of the biochemical reaction. In step 3, some of the antigens for which Abs 1&2 are specific have been captured, while the rest of the sample proteins are still floating around.

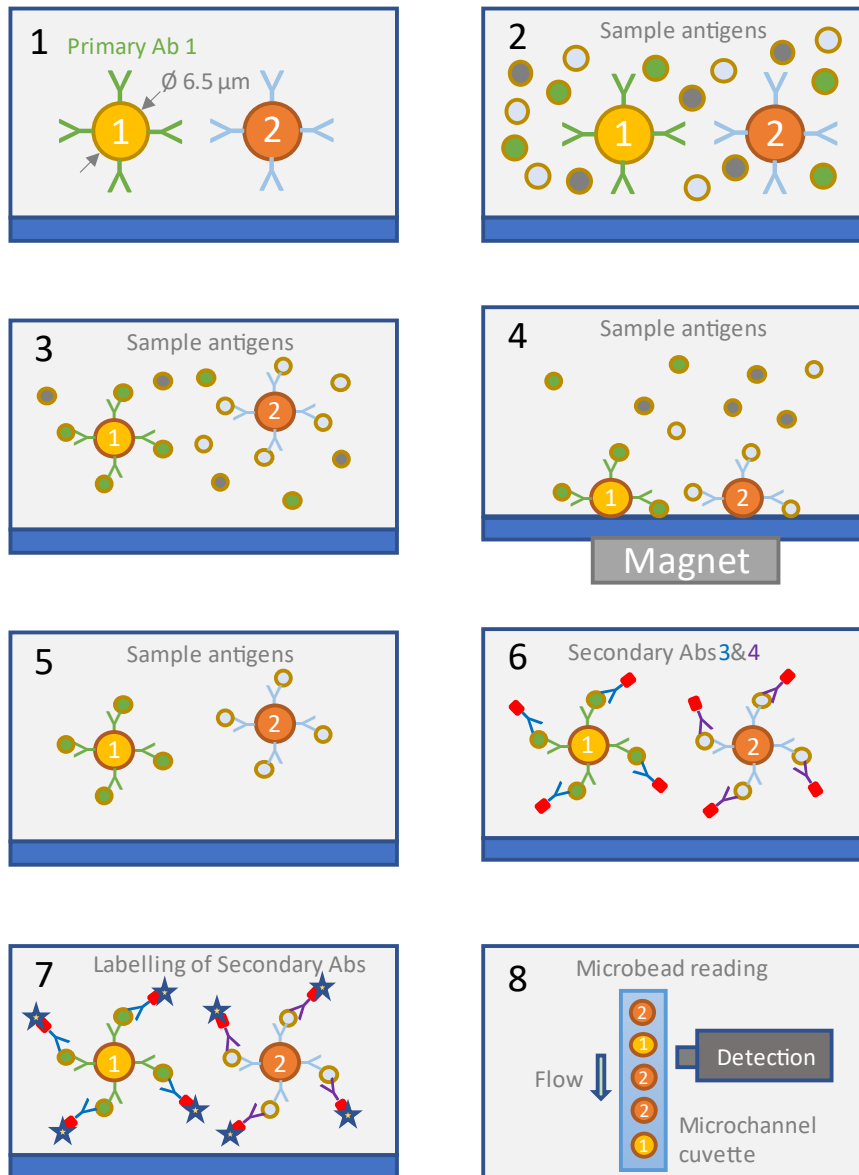


Fig 1.4 A microbead- based sandwich ELISA immunoassay. Additional steps are required such as washing is required to ensure that uncaptured molecules will not affect the biochemical process.

In step 4, a magnet is placed beneath the well and the superparamagnetic microbeads are attracted towards the bottom. Once the microbeads have been immobilized by the magnet, the solution can be disposed, aspirated or continuously diluted so that the uncaptured proteins are removed from the process and only the microbeads remain in the solution (5). Although not shown in the figure, this is repeated after each consecutive step. In (6), the secondary Abs are added. The secondary Abs are all biotinylated. Each of them has its own target analyte. In (7), the label is added. The label is typically a fluorescent agent -such as phycoerythrin- bound to streptavidin. The high affinity between the streptavidin and biotin results in the labelling of the beads that have captured their target analyte. The amount of captured analyte will result in a correlating fluorophore attachment/fluorescence emission. This is what makes the results quantitative. In (8), the beads will go through a flow cytometry-based system in which they are scanned and their identity (which family they belong to) as well as the amount of fluorophore (which is correlated to the captured analyte) are quantified. This system can be seen in *Fig 1.5*. The beads go through a cuvette microchannel which, just like in a flow cytometer, has a sheath flow aligning the beads in the microchannels center. Two laser sources, one at 532 nm (a suitable excitation wavelength for phycoerythrin) and one at 635 nm, aim towards the channel center. When a bead passes through this position, the dyes inside its polymer matrix and the fluorophore label are excited. The bead then emits radiation at 3 different wavelengths: The emission wavelength of the label fluorophore and the emissions of the classification dyes. Using suitable optics, the different wavelengths are filtered and measured using photodiodes (for the strong classification signals) and a photomultiplier (for the potentially weak label signal). A fourth sensor is measuring the scattered light from the excitation lasers to identify clusters of beads or debris that might be giving out false signals. The different signals can then be used to quantify the presence of different proteins inside the sample. Using this technology, up to 500 analytes can be tested in a single assay run. While multiple other issues such as cross reactivity between antibodies should be investigated for each multiplex assay, this method provides increased versatility and speed for life science and diagnostics.

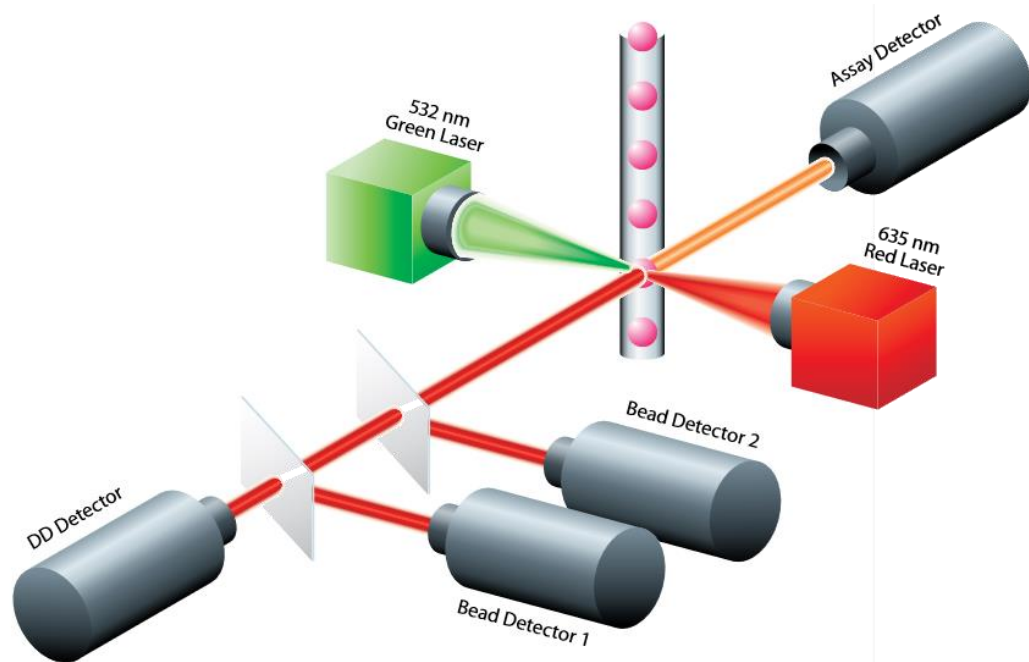


Fig 1.5²¹: The Luminex flow cytometry-based technology. Two excitation sources are used, one for the label and one for the microbead dyes. The emission signal is read by photodiodes for the dyes and a photomultiplier tube for the analyte signal, while a doublet discriminator is verifying that the beads are passing one by one and that there are no debris that could be affecting the measurement.

1.4 POINT-OF-CARE TESTING

Point-of-Care testing or PoC is the term that has been chosen to describe medical testing that is not strictly performed in a laboratory, instead it is done when and where it is required. This broad term encompasses multidisciplinary efforts for the development of technology that aspires to combine mobility and ease of use with the accuracy and sensitivity of laboratory equipment for the benefit of the patient. With multiple applications relevant to the decentralization of healthcare, PoC systems have been the focus of academic and industrial research with several new devices becoming available to the end user each year. One of the fields of PoC systems is infectious disease diagnosis in the developing world. In reference to the efforts for the development of such systems, the World Health Organization (WHO) created what has been known as the ASSURED²² criteria, which eventually came to apply to all PoC systems. ASSURED is an acronym that describes the ideal qualities of a Point-of-Care system. The exact criteria can be found in Table 1.1.

Affordable	Minimize cost
Sensitive	Minimize false positives
Specific	Minimize false negatives
User friendly	Minimize manual process steps
Robust & rapid	Ensure short time to result, minimize possibility or impact of error
Equipment free	Minimize auxiliary systems and tools
Delivered to those who need them	Make sure the logistics and infrastructure required for the test exist

Table 1.1: The ASSURED criteria set by WHO to describe the ideal qualities of a PoC system

The list created by WHO is an important set of guidelines to follow during the development of a PoC, but it is also helpful to understand the rules that formed existing Point-of-Care systems. A point of care diagnostic needs to be affordable to the ones who need it. It needs to be sensitive and specific so that false results are minimized. It must be user friendly to allow even untrained people to operate it. It may need to be rapid so that it can be easily integrated into everyday life. Its robustness ensures that it will deliver results with consistency. Auxiliary equipment must be kept to a minimum since it may not be available and finally, the test and its results must be able to be delivered to the end user. While not all of these criteria can be met for every PoC application, they serve as a set of general guidelines to be adapted to each specific scenario.

Two key variables that define the diagnostic scenario for PoC systems is the location and purpose of testing. Different settings include the patient's home, a primary care unit, an ambulance, a workplace, even a remote location with no access to healthcare. The purpose could be the confirmation or ruling-out of a specific condition, the general assessment of various biomarkers for the purpose of diagnosis or the monitoring of an already existing condition. This range of requirements leads to different specifications for the PoC depending on what need it aspires to cover. For the purpose of introducing point of care systems, three different device families are presented which answer to different needs: Small handheld devices, small footprint benchtop systems and laboratory systems.

1.4.1 SMALL HANDHELD DEVICES

The small, handheld device is the most well-known example of PoC systems. Devices in this category are designed to be completely portable, affordable and easy to use by the patients themselves. These requirements are translated into specifications: The systems need to be lightweight and have minimal size, autonomous in terms of energy - ideally not requiring a power source- and they should not require the use of peripheral equipment, for example pipettes, sample mixers etc. If some equipment is required, then it must be provided along with the test and follow the same rules as it. Additionally, a portable device made for the end user must be simple to operate and provide some sort of fail-safe features. Regarding the sample, such a device cannot require the use of special equipment or the skills of trained personnel to procure the test sample. As such, the sample is usually restricted to saliva, nasal swab, tears, urine or a single drop of blood obtained by the use of a fingerstick. A very common example from this category of POC tests is the glucose meter, a portable, low-cost device that allows people with diabetes to monitor and adjust their blood glucose levels (Fig 1.6 A). Another example is the SARS-CoV-2 rapid lateral flow test that quickly grew to become one of the key tools for the management of the COVID-19 pandemic (Fig 1.6 B). In both of these examples the tests are portable, lightweight and pocket-size. The glucose meter is powered using a battery, while the lateral flow test uses porous cellulose to pump sample and buffer liquids through the different assay steps. Both tests come with some auxiliary equipment: A fingerstick gun with disposable needles and disposable electrodes for the glucose meter. A swab and a buffer container for the lateral flow test. They are simple enough to be handled by the end-user and they provide fail-safe features: The glucose meter will alert the user if the sample is insufficient or if the electrode has been incorrectly inserted into the device. The lateral flow test includes a control line which indicates that the sample and key reagent have flown through the test. In summary, these tests are designed for portability and mass production. But there is a trade-off for this is, and it is usually sensitivity.



Figure 1.6: Common examples of portable point of care tests: (A)²³ a glucose meter measures blood glucose levels using a drop of blood. (B)²⁴ A lateral flow test for the detection of an antigen or antibody using immunochromatography, made widely known because of its usage for the detection of SARS-CoV-2 antigen.

In the example of rapid tests (also known as lateral immunoassays or LFIAs), while they do provide a fast and cost-effective way to evaluate the existence of a target molecule, they usually have no quantification features and their sensitivity is limited. In the recent case of SARS-CoV-2, rapid tests have been extensively used to rule-out infection, however the sensitivity of these tests is lower than what is obtained from standard laboratory immunoassays²⁵. In

practice, this means that a laboratory test is more likely to detect viral antigen than a rapid test, especially in the early days after symptom onset. In order to build POC tests that can approximate laboratory immunoassay results, it is necessary to include more complex functions, such as active fluid handling and optical detection methods. For example, the labelling method (the result readout) used in rapid tests is often based in colloidal gold. In this method, gold nanoparticle aggregates are used to produce a visible signal -most often a line- that indicates a captured molecule. In a laboratory test, a fluorescent molecule is often used for the same purpose, but in this case the signal is quantified using an appropriate sensor, for example a photodiode or a photomultiplier. This yields a much higher sensitivity, but it requires a higher level of complexity for the POC device. In another example, sample metering -a challenging task in rapid tests- is often approached by instructing the user to count sample droplets. In laboratory tests, sample metering and dilution is an essential step in quantitative assays which enables results consistency and biomarker monitoring over time. However, this requires metering equipment and mixing apparatus. Another key point for POC testing is that a single analyte is sometimes not enough to evaluate the patient's condition. For example, a physician will very often order a comprehensive metabolic panel (CMP) if they suspect a liver or kidney disease. The CMP is a test that measures 14 different substances whose levels and combinations of levels may indicate different pathology. The ability to test for multiple things at once is called multiplexing and it is a sought-after capability of POC systems²⁶ but with very limited applicability to handheld devices.

1.4.2 SMALL BENCHTOP SYSTEMS

In order to overcome the limitations of LFIA and other handheld devices, another category of POC systems has been the focus of research and development efforts. Small benchtop systems typically use different technology than portable POC tests and serve a different purpose. The aspiration for these devices is to combine the sensitivity of laboratory testing with the ease-of-use of a tabletop device by redesigning the components required to perform higher-level process steps. Creating devices that can run sensitive, multiplex, automated assays requires process miniaturization and automation capable to fit all the functions of a laboratory into a printer-sized device. Such functions may include sample and reagent metering, reconstitution, dilution, centrifugation, mixing, liquid dispensing and washing as well as various detection processes, either optical or electrochemical. Complexity, size and cost are the trade-off for the increased sensitivity and reliability in these systems.

Many different approaches exist for benchtop POC systems, some of which are analyzed in Chapter 2 of this work. This variety in technology and diagnostic targets is also reflected on the different diagnostic scenarios that are served by these systems. In Fig. 1.7, two benchtop POC systems are seen. On the left (A), a centrifugal system by Abaxis²⁷ uses disposable disks to perform a series of metabolic, electrolyte and general chemistry panels. Most of these panels have a CLIA waiver²⁸ by the US food and drug administration. This indicates that the level of automation of a test allows an untrained user to operate the device with minimal instructions. The purpose of this device is to provide accurate test results within ~15 mins in a primary care unit, in long term care facilities, in remote locations with no access to analytical laboratories and other similar settings where there is no access to testing facilities but there is a person with some medical training who can perform basic tasks, ex. draw blood and insert it into the test cartridge. On Fig. 1.7 B, the Stratus[®] system²⁹ by Siemens is a dedicated cardiac marker POC to help in the rapid diagnosis of myocardial infraction. The setting for this device is the acute care unit, for example the emergency room or even the hospital laboratory. The device is typically operated by a medical professional. Its purpose, unlike the Abaxis system, is not to provide test results in lack of lab facilities, but to bypass a time-consuming protocol in order to give stat results at the time of need.



Figure 1.7: Examples of benchtop point of care devices. (A)³⁰ Piccolo Xpress[®] by Abaxis, a blood chemistry analysis system. (B)³¹ Stratus[®] by Siemens, a cardiac panel POC for urgent care

Small benchtop systems manage to overcome the limitations of handheld, portable devices in sensitivity and multiplexing capabilities by introducing complex fluid handling and detection components. The size, cost and autonomy specifications that are imposed to make these systems ideal for the small clinic or the doctor's office make them a good choice for testing one patient at a time, but do not generally have the high-throughput capabilities required when multiple patients need to be tested simultaneously.

1.4.3 LABORATORY SYSTEMS

Arguably falling into the PoC definition, laboratory systems are automated, larger footprint and usually higher cost devices that provide high throughput and often increased versatility. Such systems are most often used when multiple samples need to be tested daily, for example in a hospital setting. However, the need to test multiple samples simultaneously is not restricted to hospitals. The COVID-19 outbreak has outlined the need for rapidly deployable immunoassays on a mass scale as a diagnostic but mostly as a screening measure. The same applies in a smaller scale for disease outbreaks in secluded or closed communities, refugee camps, prisons and military bases where timely diagnosis helps contain the contagion within the population. Interestingly, because these systems run in batch mode (multiple samples are loaded as a batch), the turnaround time is sometimes increased compared to small benchtop systems. This is also the case for large hospital analyzers where the requirement is not the timely diagnosis of a single sample but the high throughput testing of groups of people. Gyrolab[®] xP³² is a family of immunoassay systems by Gyros Protein Technologies based on the principles of centrifugal point of care systems (Fig. 1.8). The larger model can output up to 560 data points/hour. The platform is frequently mentioned in literature^{33–35} as a high throughput point of care system for in vitro diagnostics. However, its main application at the time of writing of this work is as a research tool for the optimization of immunoassays, for vaccine development as well as for cell and gene therapy. In conclusion, laboratory systems provide high throughput for multiple sample testing but are also very useful for the development of assays which can in turn be used in smaller point of care systems.



Figure 1.8: Gyrolab is a family of high-throughput centrifugal point of care immunoassay systems (A) ³⁶ The Gyrolab xPand system outputs up to 560 data point / hour (B)³⁷ The Gyrolab consumable disk

1.5 POINT OF CARE TECHNOLOGY

So far, different examples of POC system have been introduced with the key variable being their intended setting. It has been shown that the term point-of-care is in fact quite broad and can encompass different scenarios, ranging from the nasal swab rapid test to highly sophisticated benchtop analysis systems for decision making in the urgent care. The different settings call for different technology. Keeping the focus on point of care immunoassays, their technology can be divided in the following main areas:

- Immunoassay technology
- Fluid handling
- Detection technology

Immunoassay technology is the biochemical process used to separate and capture the target molecule. Fluid handling refers to the method by which reagents, buffers and samples are manipulated to perform this process. The detection method is the way by which the test result is detected or quantified. In the following paragraphs, a short introduction for each of these fields will be presented with more information being available in chapter 2 of this work.

1.5.1 IMMUNOASSAY TECHNOLOGY

The biochemical process is in the core of every PoC system and it drives the device specifications and requirements. The most common and versatile assay used in PoC systems but also in the lab is the sandwich ELISA³⁸ assay . In Fig. 1.9, the basic components of a sandwich ELISA can be seen. The target molecule is the antigen. It is contained in the sample and its presence is what needs to be quantified, verified or excluded. Two antibodies, the primary and secondary, are selected so that they are specific to this antigen. This means that each antigen and the antibody will form a bond if they are found close to each other and that other antigens will not as easily bind to these antibodies. The primary antibody will usually be bound to a substrate. The substrate can be a plastic surface in a chip or a magnetic microbead or even the interior of a microchannel. In most cases, the substrate is what is used to locate the conjugate of antigens or antibodies. The secondary antibody is usually the label antibody. It is bound to the label molecule. This can be a fluorescent molecule, a colored particle or even an enzyme that can catalyze a reaction. In short, the label is what translates information about the presence of the antigen into signal.

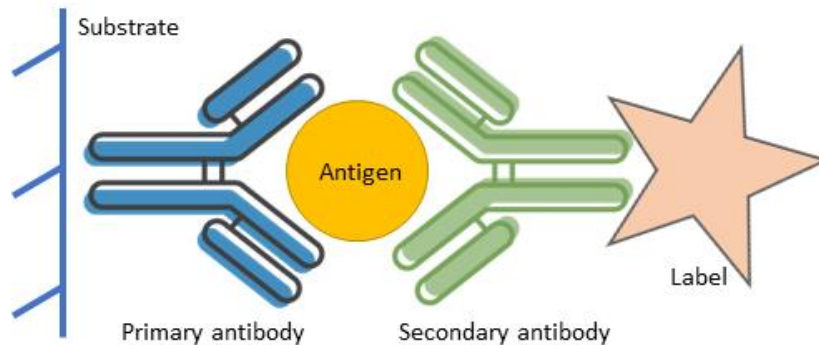


Figure 1.9: Key components of a sandwich immunoassay. In this scenario, the antigen is the target molecule. Many variants exist to allow adaptation immunoassays to PoC systems

Many different variants exist for sandwich immunoassays: The primary antibody can be bound to a part of the chip in which case this is also the reaction site of the chip. Alternatively, it can be bound to a paramagnetic microsphere which can be manipulated using magnetic fields. This is known as a suspension array. In the special case of AlphaLisa³⁹, the primary antibody is loose, but it is required to trigger the activation of the label in the secondary antibody. This way conjugates without a primary antibody do not emit a signal. Variants for the label include a fluorescent molecule that is excited using laser or led irradiation, colloidal gold or latex particles that have a distinct color when they accumulate, or an enzyme, which will catalyze a reaction in the surrounding medium causing a color change. One-site immunoassays, i.e. immunoassays with only one antibody, are also widely used and in fact are more common in some clinical analysis settings while several adaptations of immunoassays exist to make them compatible with PoC devices. Despite all these variants, the concept for these biochemical techniques is always the same: A protein is detected by attaching to it another protein which is somehow labelled.

1.5.2 FLUID HANDLING IN POINT OF CARE SYSTEMS

THE REALM OF MICROFLUIDICS

Every available point of care immunoassay method relies on the handling of fluids. In the examples that have already been presented in the previous section, different approaches for fluid handling are used depending on the application requirements. Rapid tests use wicking force to transport a fluid across different reagent zones. The fluid will carry with it the sample and conjugated reporter molecules such as colloidal gold particles. This is a cost effective and simple approach suitable for a disposable device. Abbott's i-stat is an electrochemistry based POC with disposable cartridges⁴⁰ where each cartridge includes all necessary buffers, reagents and sensors. The cartridge also includes a flexible portion over an "air bladder" which is actuated by the system to provide fluid handling. This is a mechanical approach that requires external actuators embedded in the POC device. The company Biosurfit, just like Abaxis, has launched a centrifugal point of care system called Spinit[®] for a variety of tests including the detection of covid-19 antibodies. Centrifugal point of care systems balance their fluid handling between the centrifugal forces acting on a fluid mass while the disk-cartridge is rotating and between the capillary forces which dominate when the disk is stationary. This allows the realization of multiple functions which will be presented in chapter 2 of this work.

The above examples represent just a few of the commercially applied technologies for fluid handling while several others are being researched. However, one thing that is common for almost all these technologies is that they are

designed to operate at the microscale. For this reason, they are called microfluidic technologies. Microfluidic technologies or microfluidics⁴¹ is the study of the behavior of fluids inside micron-sized channels and the exploitation of this behavior for various medical, research and other applications. The ability to reduce the size of the fluidics in a medical diagnostic system down to the microscale has several advantages:

- Complex, multistep processes can be miniaturized into small, portable devices
- Fluid flows are laminar due to the small channel size
- Reaction times are reduced
- Only a small quantity of sample and reagents is required
- Multiplex/ high throughput applications can be realized

To further elaborate on the above points, both diagnostic and bioresearch applications often require multistep, complex processes that include mixing, aliquoting, purging, priming and other fluid handling operations to be performed. Microfluidics provide the ability to perform all these processes in a single plastic device by miniaturizing them. The term given to such devices is “Lab on a Chip” to illustrate the potential of miniaturizing an entire lab into a small chip (Fig 1.10 A). Such chips are produced commercially using injection molding or embossing processes while soft lithography⁴² is a widely used technique for device prototyping in research. One of the unique characteristics of microfluidics is that in almost all cases fluid flows are laminar due to the very small size of the channels. This can be beneficial to applications which require a highly controllable liquid stream (ex. flow cytometry), but it can also be a challenge in other cases, especially when fluid mixing is required (Fig. 1.10 B). Yet, the controllability provided by laminar flows and the increased area-to-volume ratios in the chip can help to greatly reduce reaction times. Their small size also allows the use of small amounts of sample (one drop of blood, saliva, nasal swab) and reagents, which enables mobility and reduces costs. Both these attributes are important for point of care systems when examined through the ASSURED guidelines.

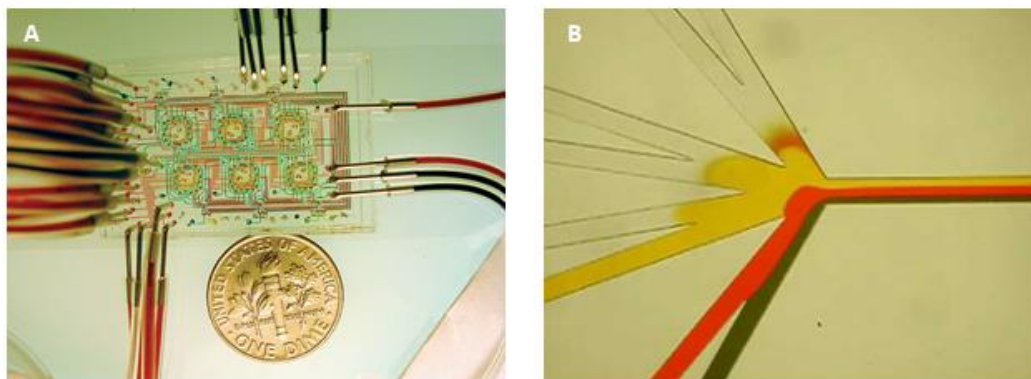


Figure 1.10: (A)⁴³ A microfluidic bioreactor for the study of bacteria (B)⁴⁴ Fluids remain immiscible in a junction because of flow laminarity

MAIN OPERATING PRINCIPLES

Within the context of microfluidics for point of care devices, there has been extensive research with many proposed technologies for fluid handling which have been thoroughly reviewed in the literature^{45,46}. These technologies include PDMS based active fluid handling⁴⁷, droplet based microfluidics⁴⁸, electrowetting fluid manipulation⁴⁹, acoustic methods⁴⁵ as well as other application specific methodologies. In the field of applied diagnostics, the fluid handling technologies that are employed are limited to the following:

- Passive fluid handling
- Centrifugal systems
- Mechanical interaction fluid handling

Passive fluid handling is the most commonly used approach because of its simplicity and low cost. This is the method used in rapid lateral flow tests and it is based on capillary action inside hydrophilic porous structures. In the simplest form, a nitrocellulose strip acts as a carrier for a fluid buffer and sample which are carried through a sequence of deposited, dried assay reagents. In more elaborate forms, the porous medium is processed by patterning⁵⁰ so that microchannels are formed. These systems are known as paper based microfluidics, and while they are not currently adopted commercially, they have significant potential to that end⁵¹. In Fig 1.11-A, the core of a rapid test is seen with different porous pads through which the sample and buffer solution travel during the test. Passive fluid handling is also achieved with hydrophilic microchannels in which the sample is inserted due to capillary forces. This is commonly used to absorb and meter blood samples for glucose measurement. In Fig. 1.11-B, the consumable chip of an electrochemical glucose point of care system uses microchannels formed between layers of plastic material to draw a nanoliter volume of blood through capillary action.

Centrifugal systems have already been mentioned in some of the previous examples. Also called lab on a disk or LOAD, centrifugal chips are disk-shaped microfluidics which are placed on a rotor of highly controlled angular velocity and acceleration. The chip itself contains chambers and structures connected with channels of controlled wettability and size. Hydrophilic channels will act as capillary pumps when the disk is not spinning, drawing the liquid until they are primed. When the disk does start to spin, centrifugal force overcomes capillary forces and a different flow sequence takes place. Numerous fluid handling functions have been realized commercially using centrifugal microfluidics, some of which are analyzed in chapter 2 of this work. In Fig. 1.11-C, the operating principle can be seen. A liquid volume moves outwards under the influence of the centrifugal force.

Other active fluid handling methods are employed through application specific solutions, usually involving a mechanical interaction. One example is the actuation upon an air bladder embedded in the chip that is connected pneumatically to a liquid reagent chamber. Another example is the interface of a microfluidic chip with an external positive displacement pump. In Fig. 1.11-D, an air bladder is above a reservoir of a liquid reagent. If the bladder is pushed using a mechanical interaction, the reagent will flow towards the other end of the circuit.

In summary, several approaches exist for fluid handling in point of care systems. Most of them operate in the realm of microfluidics because of their inherent benefits for medical diagnostics applications. Commercially, a narrower range of approaches exists which can be summarized in the following: Passive fluid handling using paper or capillary microchannels, centrifugal systems or application specific systems usually involving mechanical interaction.

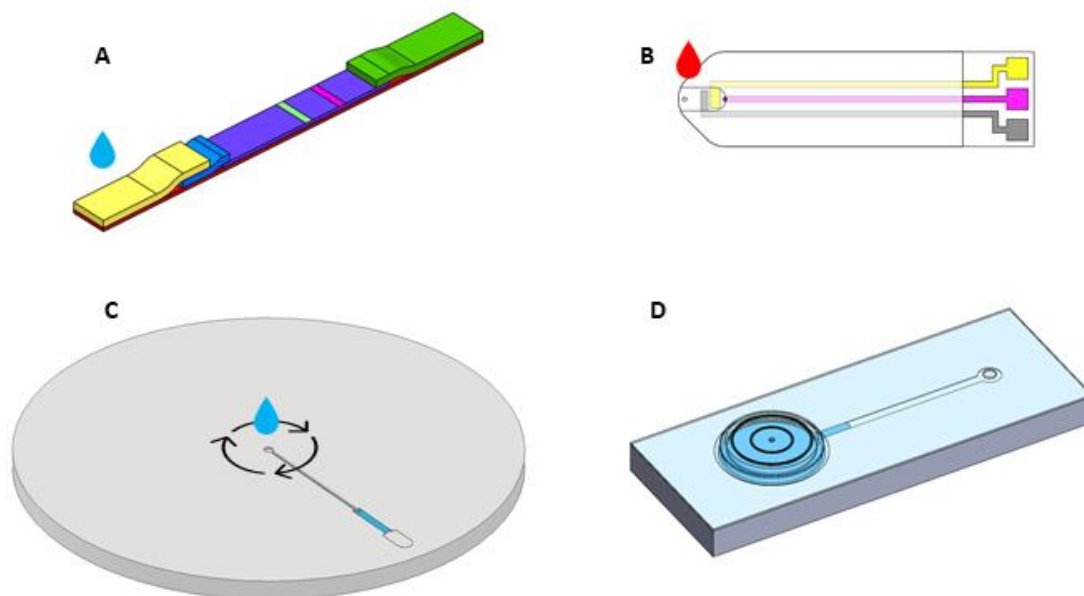


Figure 1.11: Different fluid handling approaches for point of care systems. (A) Rapid lateral flow tests use wicking action for the transport of sample and buffer across the reagent zones (B) In electrochemical glucose measurement tests, capillary action is used to draw and meter a nanoliter volume of blood (C) In centrifugal systems, a spinning disk is used for fluid handling (D) A mechanical interaction system with an air bladder connected to the microfluidic circuit.

FLUIDIC FUNCTIONS OF A POC SYSTEM

The ability to perform complex or multistep processes in a PoC, would require that common fluidic functions used in a laboratory assay can also be adapted to the PoC. In Table 1.2, common fluidic functions of PoC systems with active fluid handling are listed with their counterparts in laboratory practice and each function is analyzed below with examples from commercial PoC systems.

Function	Lab instrument	PoC system	Notes on PoC implementation
Pumping: Aspiration, metering, dispensing	Pipette	Capillary	Single use, passive component
		Centrifugal	Will work on demand but restricted by geometry
		External actuator	Requires auxiliary equipment and interface
Mixing	Plate shaker, vortex	Diffusion	Need to keep volumes low and contact area high
Aliquoting	Pipette, multipipette	Capillary	Single use, passive component
		Centrifugal	Strong point of centrifugal systems
Valving	-	Hydrophobic	Requires chip post processing, heavily dependent on geometry and surface roughness
		Sealed pouch	Single use, requires a bursting mechanism
Plasma extraction	Centrifuge	Centrifugal	Standard method, some challenges in PoC
		Filtration	Requires special membrane filter
		External	Limits PoC usability by non-trained users
Washing	Plate washer	Application specific solutions	By combining components seen above

Table 1.2: Different functions are implemented using different technology in the lab and in a PoC system

Pumping: The first function refers to all aspiration, dispensing and metering requirements for a laboratory multistep immunoassay. In a PoC application this would translate to moving a liquid volume from position A to position B within the circuit. Three ways are commonly used to achieve this: A capillary channel, centrifugal liquid handling and external pumps. Capillary channels are primed as soon as they come in contact with the liquid volume. In Fig. 1.12 A, the user dispenses a drop of blood in the sample port and the blood is automatically aspirated because of the capillary action of the microfluidic channel connected to the port. However, this is a constrained method. The user cannot delay the activation of this action. As such, microfluidics that rely solely on capillary fluid handling can only perform one-step assays. Centrifugal fluid handling relies on centrifugal force. In Fig. 1.12 B, a liquid volume starts from the position 1 and through centrifugal force moves to position 2. This is normally also constrained to one-step assays, however if position 2 is connected to the lower position 3 through a hydrophilic channel like the one seen in Fig. 1.12 B, it is possible to implement additional steps by stopping the disk until capillary action moves the fluid front below the level of 2 and then restarting the disk. This is called siphoning. However, this approach towards multistep protocols is constrained by the size of the disk and by the fact that spinning or stopping the disk will affect the entire circuit, not just the specific fluidic component.

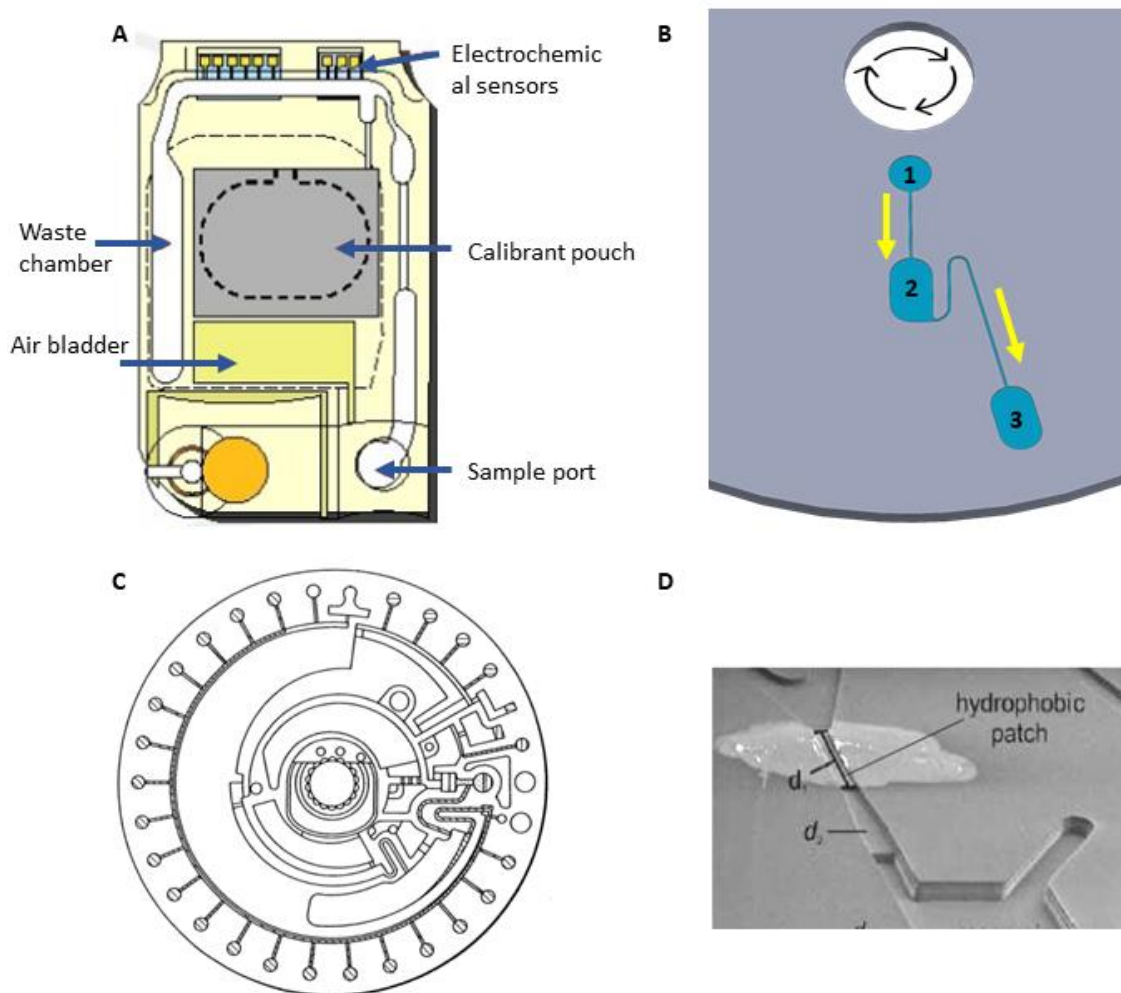


Figure 1.12: Different functions of a PoC system for multistep protocols. (A)⁵² Inside the fluidics of *I-stat*[®] by Abbott (B) Centrifugal fluid handling (C)⁵³ Aliquoting in an Abaxis disk, (D)⁵⁴ A hydrophobic patch created by deposition of a liquid patch

The last option seen in commercial PoC system is the use of an external pump or actuator. In Fig. 1.12-A, an external actuator will act upon the air bladder to do additional fluid handling. While external pumps and actuators are by default a modular option, they increase device complexity and costs for small benchtop and handheld systems, and they require interfacing with the microfluidic circuit which can be challenging plus it introduces failure modes into the system.

Mixing: Mixing in microfluidic systems is mostly achieved through diffusion since flows are almost always laminar, although there are several other methods that have been reviewed in literature⁵⁵. Mixing may require the use of special patterns on the microfluidic chip that enhance mixing, or the utilization of mixing aids, such as embedded spheres. The need to keep very small dimensions to reap the benefits of diffusion in microfluidics in combination with long mixing patterns can create clogging issues into the chip.

Aliquoting: Aliquoting is the distribution of a liquid volume into smaller, metered portions. This is useful for parallelization/assay multiplexing. In the lab, this is done using a pipette or multi-pipette. In PoC systems, this is either done using capillary channels or centrifugal action. For capillary systems, everything discussed in the pumping section also applies to aliquoting. Centrifugal systems have an inherent advantage for aliquoting since its implementation is somewhat straightforward. In Fig. 1.12 C, in an application by Abaxis⁵³, a liquid volume moves outward in a circular channels that is connected to multiple circular wells in the circumference of the chip. As each well is primed, the liquid moves to the next one until all of them are filled. The remaining volume usually ends up on a waste well at the end of the circular channel.

Valving: For PoC systems valving is used to allow, switch or prevent liquid flow on demand. A common way to achieve this, is by creating a hydrophobic barrier that prevents flow below a pressure threshold. This is in fact a relief valve and it is often used in commercial microfluidics. Some version of the relief valve is essential for most microfluidics, even the ones performing one-step protocols, because it is used at the venting positions of microchannels to prevent liquid from flowing out of the chip. The challenge with such valves is that they require post processing of the microfluidic chip, either by deposition of liquid or by plasma treatment. Additionally, they are heavily depended on geometry. In Fig. 1.12 D, a deposited hydrophobic patch can be seen.

Plasma extraction: Since many immunoassays require plasma or serum as sample, it is necessary to separate it from whole blood. Centrifugal systems achieve this through centrifugation. Other systems use plasma separation membranes to acquire the sample.

Washing: Washing is the removal of unbound assay reagents after each step of a multistep protocol to prevent them from causing unwanted interactions. It is a common step in immunoassays and often omitted in PoC systems, for example in rapid lateral flow assays.

1.5.3 DETECTION TECHNOLOGY IN POINT OF CARE SYSTEMS

So far, the methods employed to perform an assay in a point of care system have been described. The final step for the acquisition of the results is the detection of the target molecule. For immunoassays, this molecule is an antigen or antibody. Just like with fluid handling, there is a vast range of proposed solution for PoC sensing in literature which has been thoroughly reviewed⁵⁶⁻⁵⁸. The most widely used detection technologies in commercially available point of care systems are the following:

- Visual (rapid tests)
- Colorimetric
- Absorbance
- Fluorescence
- Electrochemical

Visual detection is the method employed in rapid lateral flow tests and is based on gold or latex particles that generate a visible band when they accumulate. For lateral flow assays, both colorimetry and fluorescence are used when the rapid test is combined with a reading system to increase its sensitivity and allow signal quantification. In this case a camera or photodiode is used to quantify the color intensity or the fluorescent signal of the test's detection line. However, colorimetry, fluorescence and absorbance are all classical detection techniques used in conventional assays that have been adapted to all types of point of care systems. Apart from lateral flow applications, they are widely used in microfluidic point of care systems to detect the signal emitted from a detection agent dispersed in a liquid volume or adhering to a chip's surface. The last category of detection methods is based on electrochemistry, which includes amperometry, potentiometry, conductimetry and impedance measurement techniques on electrodes. More information about sensors and their applications can be found on chapter 2 of this work.

1.6 CHALLENGES OF POINT OF CARE SYSTEMS

Analytical diagnostics for the point-of-care is a field that is continuously increasing in attention both academically and commercially. Its integration into healthcare practice can be quantified by the increasing market size of PoC systems which is expected to exceed \$28B BY 2026⁵⁹. More to that, their usage during the Covid-19 pandemic as a screening or diagnostic tool is proof of their potential. Yet, commercial applications of PoC immunoassays remain limited to a small number of technological approaches which is in contrast to the research conducted in this field as represented in literature⁶⁰. Part of the reason is that there are still unmet challenges for PoC systems. The challenges can be in part be traced back to the ASSURED criteria while at the same time there are additional technological and performance challenges that create a gap between research and application in the field of PoC systems:

AFFORDABILITY

The cost of a system is dependent on many factors which may include R&D costs, intellectual property, marketing and approval costs. However, a more tangible factor is the complexity of the PoC system. Highly precise positive displacement pumps (Fig 1.13 A), valves, automation and mechanical actuators (Fig 1.13 C), all increase the device's complexity and cost. Rapid tests, the most successful example of immunoassay PoC system to date, partly owes its popularity to its simplicity, low cost and availability. More elaborate and much more sensitive/ precise systems

exist^{61,62}, which are not as frequently used partly because of their increased acquisition and consumables cost. This is not to say that such systems will not become more widely available with the increasing demand for PoC testing, however the takeaway lesson from rapid tests adoption is that simplicity is an important factor. Another challenge stemming from the affordability guideline is the need to keep consumable manufacturability within industry standards. While lithography and PDMS techniques have been widely adopted in the research lab, the ability to produce chips using injection molding or embossing is important for their commercial applicability. The same applies for further localized processing such as the deposition of surface energy modifiers and wetting agents to produce fluidic control elements (Fig 1.13 B).

MULTIPLEXABILITY

Multiplexability is the ability of a PoC system to conduct multiple tests simultaneously. Multiplexing emerges as an increasing requirement for the complete evaluation of a pathological condition. For example, multiplexing could give the ability to discriminate between different subtypes of a pathogen. Furthermore, it is often necessary to monitor multiple biomarkers in order to evaluate just one condition, ex. cardiac markers, while in some diagnostic scenarios, multiple conditions exist that could explain the patient's symptoms, all of which need to be tested for. Multiplexing also allows to enhance the detection of even a single biomarker either by adding positive and negative controls into the assay or by detecting the same biomarker with different sensitivity levels, which eventually increases the dynamic range of the test. Multiplexing becomes a significant challenge for PoC systems when complex fluidics are required to perform the diagnostic protocol.

USER FRIENDLY / EQUIPMENT FREE

Keeping a PoC system user friendly can be about the interface or the user input or the interpretation of the results, which are real challenges and are optimized by the test manufacturers. A major challenge that is also related to the "Equipment free" guideline, is the sample and reagent preparation. Especially when the sample is blood, it is often required to remove red and white blood cells to get plasma. This may require the use of micropipettes and centrifugation equipment which severely restricts the accessibility of the test to most people. The same applies to reagents when there is the need to reconstitute dried or lyophilized components and place them into the PoC system. The challenge stemming from these guidelines is how to completely integrate sample preparation and reagent fluidics into the PoC system (Fig 1.13 D).

ROBUSTNESS / RAPIDITY

A robust system needs to minimize errors and be able to detect them if they happen and perform accordingly. And if most of the previous guidelines were pushing towards microfluidic PoC systems with the power of a lab analyzer, robustness is one of the weak spots of microfluidic systems. Clogging, air bubbles, insufficient mixing, connectivity issues with peripheral pumps and valves, volume displacement control, reagent damage due to poor storage, leaks and wetting irregularities are common challenges into developing a PoC system. Rapid response is usually dependent on surface-area-to-volume ratio for which microfluidic systems have an inherent advantage, although reducing the test volumes increases the severity of the aforementioned challenges. Most commercial PoC systems in the United States of America aim to acquire a CLIA waiver from the US Food & Drug Administration. This is achieved by introducing failsafe measures into the PoC system so that even if an error occurs, the system is able to detect it and not output a result that could be wrong or even harmful.

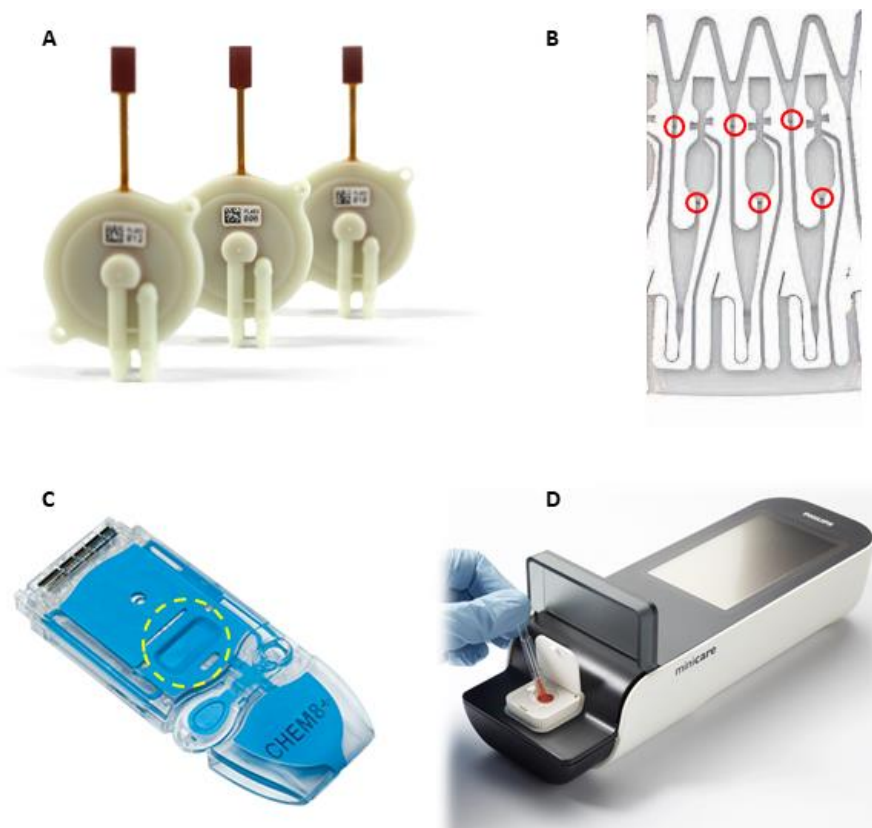
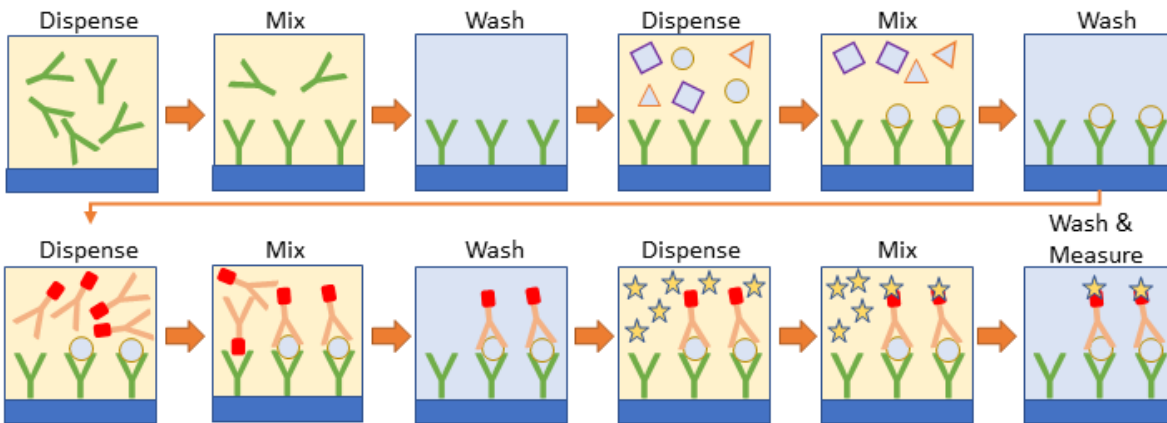


Figure 1.13: Components for sample and reagent handling in PoC systems. (A)⁶³ a diaphragm precision pump by TTP Ventusfor microfluidic applications. (B)⁶⁴ Hydrophobic patch valving in Gyrolab discs requires localized treatment for surface modification (C)⁶⁵ I-stat[®] by Abbott uses cartridges with an elastic bladder (encircled in yellow). A mechanical actuator pushes or releases the bladder to move the liquid forward or to make it reciprocate in order to perform a mixing step. (D)⁶⁶ Siemens minicare[®] includes an embedded filter on each disposable disk that separates blood cells from the plasma before the sample enters the microfluidic circuit

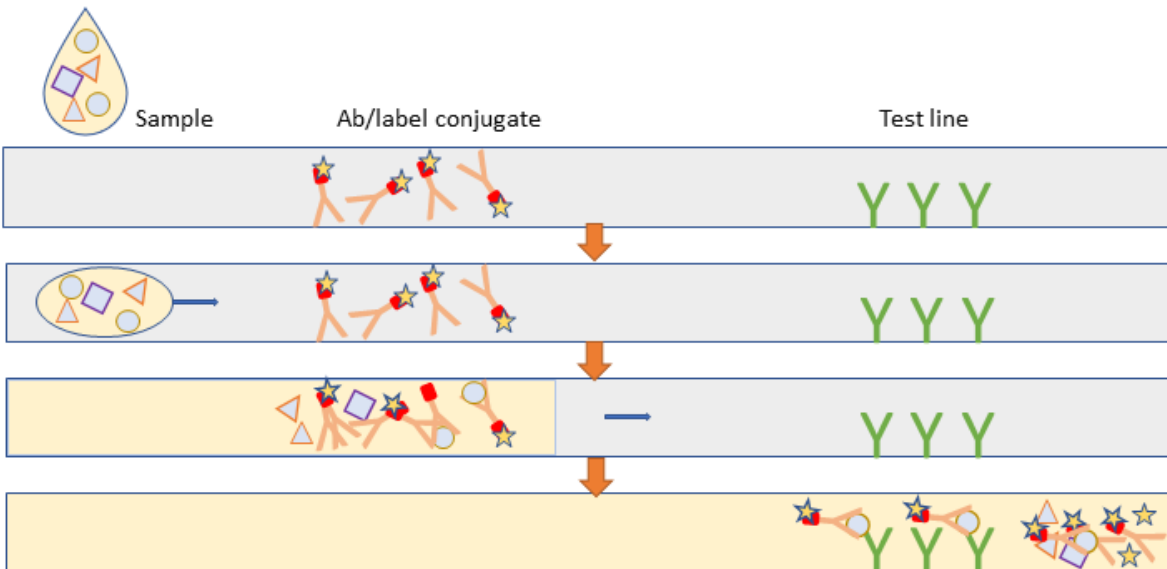
THE IMMUNOASSAY ADAPTATION CHALLENGE

In the beginning of this chapter, the basic steps for a sandwich immunoassay have been described. This standard practice that is used in the laboratory and requires a multistep protocol, is not employed in PoC systems. The reason is the complexity of implementing multistep protocols in miniature, autonomous devices. Instead, adaptations of immunoassays are used. In Fig. 1.14, different protocols for immunoassays are presented. On the top (A), the standard process for a laboratory sandwich immunoassay is presented. It is a 12-step process including timed mixing, washing and precision metering/dispensing steps. This step sequence has been established to ensure that non-specific binding is minimized and that captured reagents do not need to compete with uncaptured species for reaction sites. The sandwich format increases specificity further by using two sites on the antigen, one for each antibody. The final result is measured in a device that typically includes a photosensitive diode, ccd camera or photomultiplier. This process requires a level of automation which is not available in PoC devices. For this reason, different versions that simplify the immunoassay process are typically used. In Fig. 1.14B, the lateral flow immunoassay process is shown. The diluted sample is transferred through wicking force on the Ab/label conjugate site where the two mix. The bound as well as the unbound proteins move together to the test line where the primary antibody captures the antigen which should now be conjugated to the secondary antibody and the label. The result is observed rather than measured.

A: Sandwich ELISA



B: Lateral flow immunoassay



C: Turbidimetric immunoassay

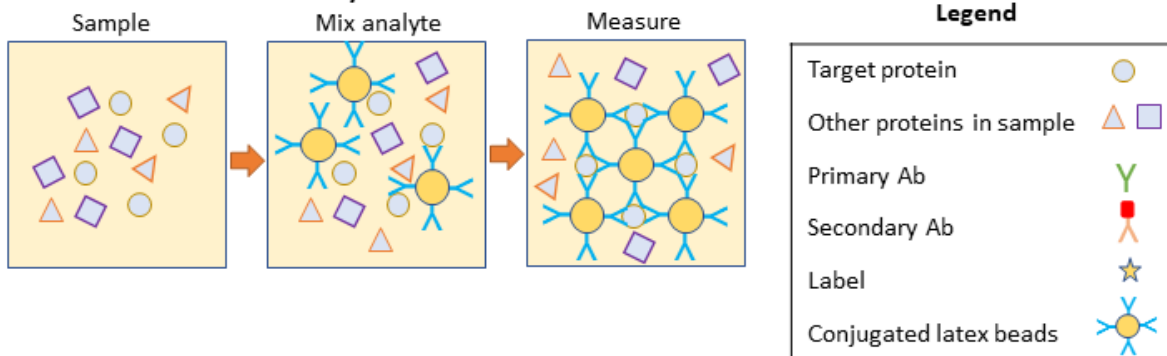


Figure 1.14: A laboratory immunoassay (A) and two adaptations: (B) an immunoassay for lateral flow rapid tests and (C) A turbidimetric immunoassay for centrifugal PoC systems

The lateral flow immunoassay adaptation is a simple, one-step process which omits all washing steps and has limited capabilities when it comes to mixing and controlling incubation times. This simplification is necessary in order to perform a complex immunoassay in a completely passive device. However, it results in decreased sensitivity compared to full immunoassay protocols⁶⁷. In Fig. 1.14 C, a latex turbidimetric immunoassay process is shown. In this assay, the target molecules bind to conjugated latex microspheres. The antigen-antibody-microbead complexes have the ability to scatter incident light. By placing a light source and a detector across the measured solution, the transmitted light can be measured, which in turn is correlated to the amount of antigen in the solution. This process only requires mixing the sample with the assay reagents. Abaxis Piccolo Xpress CRP measurement⁶⁸ is based on this technique. While these simplified assays may be optimized individually to yield acceptable clinical results, they need to be treated per case and cannot be compared to gold standard processes such as sandwich ELISA when it comes to sensitivity. The immunoassay challenge is therefore the requirement to adapt the assay to what the fluidic technology permits because the implementation of a full immunoassay is considered not feasible.

OPEN VS CLOSED TECHNOLOGY

The ability to create a technology that is open and can be used by others to develop their own tests, is an unmet challenge for PoC systems. With the exception of rapid lateral flow tests, all other devices are made to operate with a limited range of assays which is developed by the device manufacturer. This results in most of these devices having a limited range of available tests.

RAPID DEPLOYMENT

This challenge became more obvious during the Covid-19 pandemic: In the case of novel infectious disease, a PoC system should be able to be readily adapted and deployed in order to be usable in an emergency situation. Rapid lateral flow systems are produced by depositing and then drying reagent lines on a sheet of porous material which is then sliced into the strips that are inserted into the plastic test cassette. By changing the deposited antibody solutions, the test is adapted to a new target molecule. But first, any new assay would need to be developed in the laboratory, tested for affinity, specificity, cross reactivity, stability and more. The transferability of a test from the laboratory protocol to a PoC system is also a challenge. For optimal integration, the PoC and the laboratory test should be using the same technology.

In summary, several challenges remain unmet for PoC systems. The ASSURED criteria can partly be used as a starting point to delve into why some technologies are commercialized and some are not, or why from already commercialized technologies, some are widespread, and some are not. The example of the rapid lateral flow test in the case of Covid-19 shows that there is a need to meet challenges of cost, simplicity, reliability and accessibility to be able to provide usable solutions to the community that can be rapidly deployed.

1.7 TOWARDS MODULAR POINT-OF-CARE IMMUNOASSAYS

This work aims to propose technologies that help meet the challenges mentioned in the previous paragraph. The aspiration behind the different research objectives is the ability to create modular point of care immunoassays. A modular system implies that it can be pieced together by individual modules that exist as standalone components^{69,70}. Preferably, these components are produced elsewhere and are assembled in, inserted to or used by the immunoassay system. In the context of immunoassay PoC systems, modularity could apply to the following:

- *Immunoassay substrate*: The immunoassay substrate is the location of the primary antibody. If the antibody needs to be covalently bonded to a microfluidic chip surface this creates the necessity for individual chip treatment. However, if the substrate is produced externally, it becomes a modular component that can be inserted to the chip on demand
- *Development platform*: Disconnecting the substrate from the PoC system would allow the assay development to be done externally and only replicate the developed process in the PoC system
- *Fluid handling method*: Regarding the fluid handling method, the creation of modular fluidic components such as micropumps and microvalves, can enable the replication of full sandwich immunoassay protocols on chip
- *Reagents and their storage*: Reagent storage and reconstitution is an important challenge for the creation of functional diagnostic devices as it often requires on-chip lyophilization of reagents.

In the beginning of this chapter, superparamagnetic bead-based technology was presented for immunoassays. Bead-based technology is a modular immunoassay substrate since the primary antibodies are coupled on the surface of suspended microbeads. Luminex[®] beads allow multiplexing for up to 500 targets in a single sample volume. While other technologies exist⁷¹, which use graphical barcodes and lithography-based particles for increased multiplexability, color coded microbeads is a mature technology with multiplexing limits that already exceed the limit imposed by antibody cross reactivity. Additionally, they are an open technology as the manufacturer provides them with surface carboxyl groups so that the user can couple them with the antibodies required for their application. Microbead technology also covers the rapid deployment challenge described in the previous chapter, since once the assay has been developed, microbeads can be produced and distributed for use in any instrument that is compatible with bead-based assays. Lastly, since the beads are superparamagnetic, they can be manipulated using magnetic fields which is a big benefit for washing and mixing applications in the point of care. Due to these merits, superparamagnetic microbeads are adopted in this work as the key immunoassay technology.

With bead-based technology in the center of research efforts, the vision of this work is that it is possible to create a fully modular technology for PoC systems, which includes both laboratory and small benchtop devices that use the same immunoassay methods. Laboratory systems can be used for assay development or for centralized testing. Small benchtop devices can be used for decentralized testing and rapid diagnostics deployment. Several unmet challenges need to be addressed in order to move closer to this vision. In Fig. 1.15, core technologies that could support this vision are shown. In this work, three out of these topics will be addressed: Laboratory immunoassay automation for assay development and diagnostics, on-chip micropumps and on-chip microvalves. Using these technologies, concept microfluidic designs will be described as examples of the applicability of the developed components.

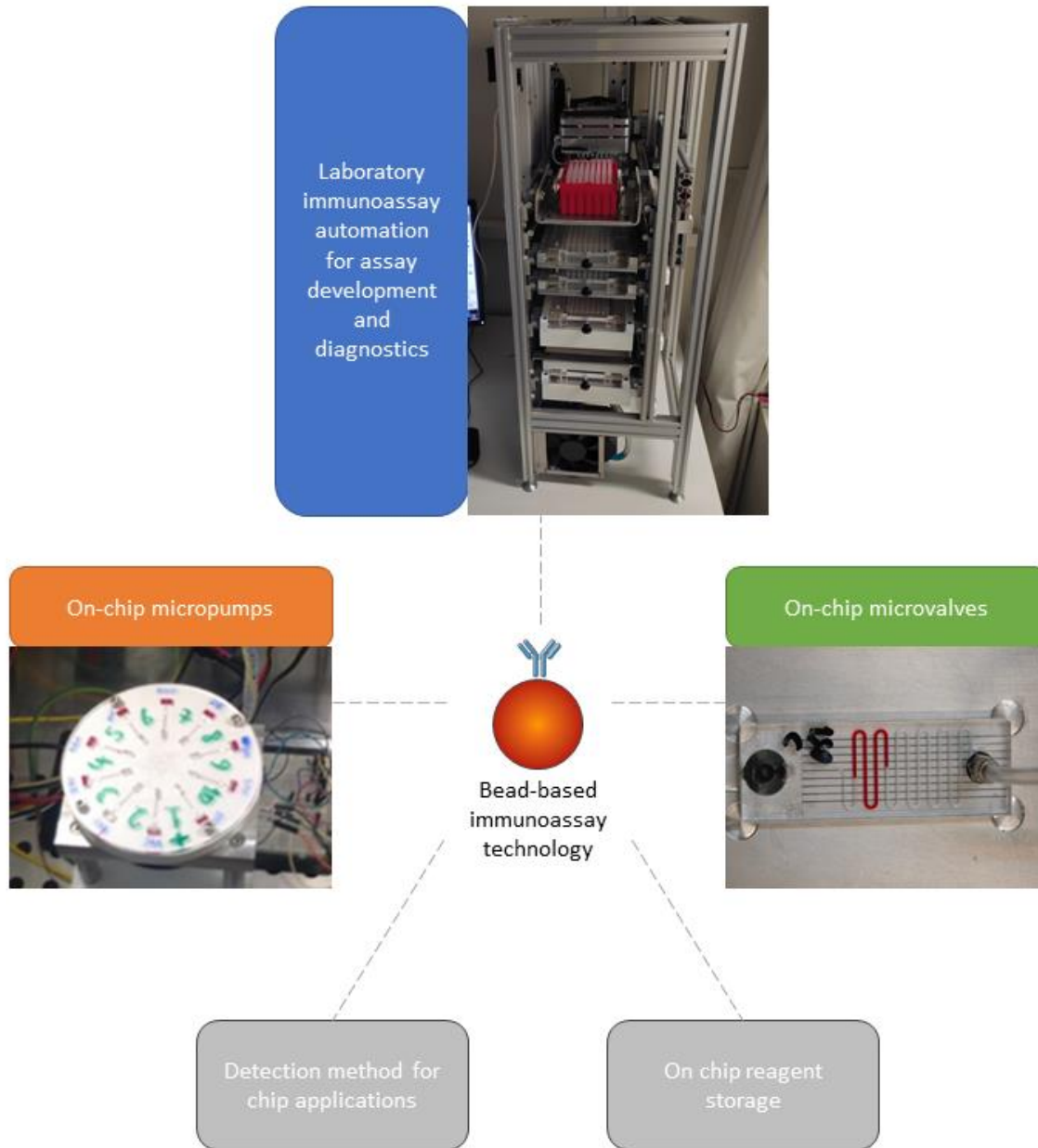


Figure 1.15: A breakdown structure of the technologies needed to enable the vision of this work for modular PoC systems. In the scope of this thesis, three out of these topics will be addressed: Laboratory immunoassay automation for assay development and diagnostics, on-chip micropumps and on-chip microvalves

1.8 THESIS STRUCTURE

In the introduction of this work, Point-of-Care systems have been presented. Their merits and challenges have been briefly discussed along with a short introduction into PoC technology that is currently used in clinical practice.

- In chapter 1, introduction, key concepts and thesis objectives have been discussed
- In chapter 2, an analysis of commercialized PoC system, their technology and diagnostic targets is presented
- In chapter 3, a benchtop ELISA system is presented for the development and performance of immunoassays
- In chapter 4, a modular micropumping method for microfluidic devices is presented
- In chapter 5, a modular microvalving method for microfluidic devices is presented
- In chapter 6, microfluidic immunoassay concepts based on the developed methods are discussed
- In chapter 7, conclusions and future work is discussed

CHAPTER 2: POINT OF CARE SYSTEMS REVIEW

2.1 ABSTRACT

This chapter⁷² examines current trends in PoC technology for diagnostics. Using 105 PoC manufacturers as a starting point, the most represented technologies are reviewed as per their fluid manipulation, signal detection, footprint, main applications, multiplexing and diagnostic targets. Principles of operation for each of the main categories are described based on literature and patents. Common design principles, materials and reagents as well as aspects of sensitivity and quantification are described. A comprehensive list of the diagnostic targets used in commercial PoC systems is compiled. Finally, the traits of applied PoC systems are discussed as a reference frame for developmental efforts in the field.

2.2 INTRODUCTION

Point of Care (PoC) diagnostics have grown to become both academically and commercially a very challenging but also rewarding field of research, development, innovation and commercialization. PoC systems can be found in the ambulance, the hospital, the clinic, a doctor's office, a pharmacy, a patient's home or the bedside. For all of these settings, there is a growing need for easier, less costly and more reliable diagnostic solutions for a wide range of diagnostic, prognostic and predictive targets. The recent SARS-CoV-2 pandemic outbreak underlined the already existing need for decentralized diagnostic. PoC systems aspire to cover that need. The systems and technologies envisioned by researchers as future PoC in-vitro-diagnostic (IVD) candidate solutions are numerous, often very exciting as to their potential impact on clinical care and have been thoroughly reviewed in literature⁷³⁻⁷⁷. However, it is true that the staggering number of proposed technologies for PoC seen in literature is disproportionate to the ones that are eventually adapted in commercial systems. This disconnect has been attributed to the fact that academia has for long been focused at methods that are not easily transferable to industry⁷⁸, while it is often the case that a scientific achievement of the field might not present with a clinical impact that justifies the effort or cost of the implementation. In recent years a number of excellent review articles have been published⁷⁹⁻⁸¹ regarding Point of Care systems commercialization. There are different viewpoints that can be used to describe this subject, notably market size, state of the art technological applications or promising research findings with potential impact on commercial IVD systems. In this work, we shall attempt to review the status of Point of Care IVD as can be seen through commercialized applications alone, with a focus on handheld and small benchtop systems. The specific viewpoint is based on the technological and diagnostic target decisions of 105 PoC manufacturers that were selected based on site visits on international trade fairs⁸², PoC conferences and market reports⁸³ for the PoC industry. The selection process for trade fair participation was the inclusion of any company offering a PoC solution on settings ranging from clinic to what is referred to as extreme point of care⁸⁴. The scope of the selection is to get a comprehensive image of the commercialized PoC landscape while minimizing bias in the inclusion process. Subsequently, we proceed to categorize the technologies used by each of these companies. We identify 5 major groups: 1) Lateral flow assays, 2) centrifugal microfluidics systems, 3) electrochemical systems 4) nucleic acid testing systems 5) Blood gas analyzers. Those 5 technological categories encompass 98 out of 105 companies whereas 14 systems cannot be grouped into these categories. The technological groups are not strictly related to the sensing approach or the fluidic manipulation approach, rather in key design similarities. However, PoC systems are at the epicenter of a very active research field with new principles being applied constantly that may very well render this categorization obsolete in the near future. In this sense, this article can be viewed as a snapshot of the commercial PoC landscape at the time of writing that is sure to evolve in coming years. Using as a starting point the previously mentioned 105 PoC firms, this review outlines the most prevalent technologies in the field and provides some insight

on their functions, attributes and limitations. Furthermore, using the same starting point, we present a thorough list of biomarkers that are currently the diagnostic objective of systems reviewed in this work. PoC systems for the detection of SARS-CoV-2 antigens, antibodies or molecular targets are discussed in a separate paragraph at the end of this chapter because of the staggering number of tests that have been issued with an emergency use license (152 in EU at the time of writing of this report)⁸⁵

2.3 COMMERCIALIZED POINT OF CARE SYSTEMS - TECHNOLOGY CATEGORIZATION

A categorization of the commercially available PoC systems based on their technology is presented on the following table with basic information on applications, attributes and adaption.

	Lateral flow tests and systems	Lab on a Disk	Electrochemical sensing systems	Nucleic acid detection	Blood Gas and electrolyte systems	Other
Number of companies	81	4	10	6	4	15
Number of biomarkers	143	36	30	12	13	59
Signal detection	Visual, colorimetric, absorbance, fluorescence	absorbance, fluorescence	Amperometry, potentiometry, conductimetry, impedance	Fluorescence, impedance	Amperometry, potentiometry, fluorescence	Physical, optical
Fluid manipulation	Capillary	Centrifugal / capillary	Capillary / active	Capillary / active	Active	Various
Device Size	No device, Pocket size, benchtop small	Benchtop, small	Pocket size, benchtop small	Pocket size, Benchtop small and large	Benchtop large	Various
Main applications	Infectious disease, cardiac stat testing, Pregnancy	Clinical Biochemistry, Hematology	Glucose, Coagulation, Hematocrit, Blood gas, electrolytes, cardiac stat testing	Infectious disease, mutation	Blood gas, electrolytes, metabolites	Clinical Biochemistry, Hematology, coagulation
Quantitative	Usually no, semiquantitative, quantitative when coupled with detection device	Yes	Yes	Yes	Yes	Yes
Multiplexing	Multiple test lines (limited), Multiple strips	Multiple test chambers	Multiple electrodes	Multiple fluorescent probes, multiple electrodes	Multiple electrodes	Yes

Table 2.1: Main attributes of the different technological approaches for PoC systems.

2.3.1 LATERAL FLOW ASSAYS

Lateral Flow Immunoassays or LFIA for short, constitute by far the most represented technology in terms of number of companies as well as diversity of analytes commercially available for PoC settings. It is indicative that 81 out of the 105 companies reviewed in this work deal partially or exclusively with LFIA and LFIA readers. Furthermore, 143 out of 173 biomarkers reported here are being detected also or exclusively using LFIA technology alone, or coupled with a detection system at various levels of sensitivity, resolution and multiplexibility. The apparent domination of these capillary-driven disposable tests be can traced into their inherent merits^{78,86}, which are compactness, simplicity in both manufacturing and operation, compatibility with small sample volumes and affordability. Closely modeled to ELISA, this technology is not only rapidly growing on its current capabilities^{75,87}, but is also emerging as a potential alternative in the league of quantitative biomarker detection⁸⁸. Still, the innate simplicity of traditional LFIA comes with the cost of incompatibility with automated multistep protocols, detection limits that are often incompatible with low abundance targets and the need to translate ELISA assays into their one-step counterpart for each individual test, which can pose severe challenges both in porous media design and in reagent selection.

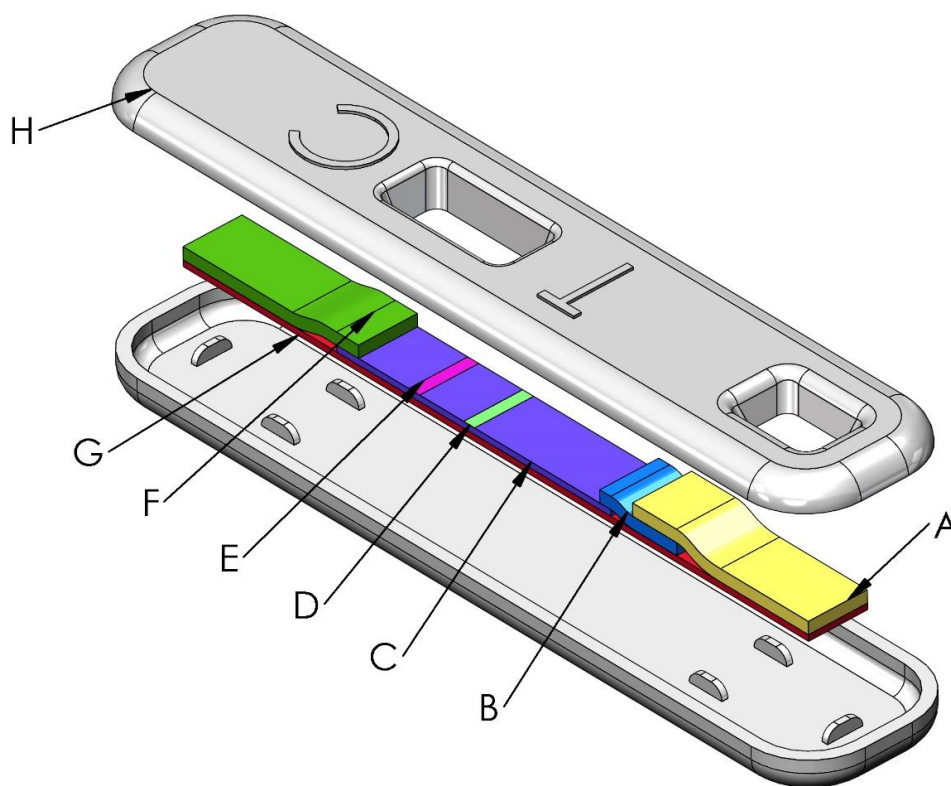


Figure 2.1. Inside a typical lateral flow test. (A) Sample pad, (B) Conjugate pad, (C) Reaction membrane, (D) Test line, (E) Control line, (F) Wick pad, (G) Backing strip, (H) Cassette

LFIA PRINCIPLE OF OPERATION

The driving force of lateral flow immunoassays is capillary flow in porous pads. Fig. 2.1 shows the main components of a typical lateral flow test format. The strip assembly comprises 4 consecutive absorbing pads into which the sample will flow in-line. There are 2 main architectures commonly used, the sandwich format and the competitive inhibition format⁸⁹.

The sandwich format is primarily used when the target analyte is a large compound with multiple antigenic sites. In this case, the conjugate pad (Fig. 2.1-B) embeds an air dried or lyophilized solution of a label (typically latex or gold nanoparticles)⁹⁰ conjugated with a recognition antibody or antigen specific to the target biomarker. The Reaction membrane (Fig. 2.1-C) carries the test and the control line (Fig. 2.1-D&E), which are bound to its matrix. The test line is a capture antibody or antigen specific to a targeted biomarker epitope. The control line is usually a species-specific anti-immunoglobulin⁹¹ that will bind the initial recognition conjugate stored in the conjugate pad. The assay process starts with the introduction of the sample and often an added buffer solution on the sample pad (Fig. 2.1-A). Capillary forces drive the sample inside the pad in which a pretreatment may take place for pH adjustment, retention of interfering components or removal of particulates and cells. Consequently, the assay-ready sample moves on to the conjugate pad where the analyte, if present, will bind to the label conjugate and move on to the reaction membrane. Once the sample reaches the test line, the analyte/label conjugates complex will bind to the immobilized capture molecules and accrue thus forming a visible band. As the sample solution continues to flow on, excess or unbound conjugates reach the control line and form a second visible band, that is, an accumulation of immobilized label conjugates to confirm successful assay completion. The last pad (Fig. 2.1-F) will gather excess solution and labels thus clearing the view from unbound label conjugates to the reaction matrix. Typical tests that utilize the sandwich approach are the SARS-CoV-2 antigen test, HIV, hCG, Dengue IgG/IgM and Ag NS1, Troponin I and many others.

The competitive inhibition format is less common and is primarily used when the target analyte is a small molecule with a single available antigenic site. In this case, the test line is drawn with an immobilized antigen which competes for the same antibody epitope of the label conjugate as the analyte itself. This way, once the sample reaches the conjugate pad, any present analyte will bind the label conjugate to epitope depletion thus preventing the downstream binding that would occur on the test line. As such, in competitive assays the formation of a test line is negatively correlated to the presence of the biomarker. The control line does not compete for the same binding site, so it forms upon successful completion of the assay. In some cases the analyte may be incubated with the label conjugate externally prior to strip usage⁹². A typical test that utilizes competitive inhibition is the detection of microalbumin in human urine specimens for the diagnosis of renal dysfunction⁹³.

DESIGN, MATERIALS AND REAGENTS IN LFIA

Lateral flow immunoassays are mostly found in the encased format (Fig. 2.1) or the dipstick format, a usually exposed strip assembly which is dipped inside a sample container. Dipstick formats are more often used when there is a need for larger sample quantities or a pretreated sample and may not include all of the pads seen in the previous paragraph. Encased formats include the serial arrangement of pads which starts with the sample pad. The sample pad is typically fabricated from cotton linter, glass fiber or cellulose⁸⁹ strips or sheets and serves the purpose of pretreatment and smooth and homogeneous transportation of the sample to the conjugate pad. Filtration of particulates, pH adjustment and leakage prevention are key design parameters. The conjugate pad contains the recognition molecule bound on a label. Conjugate pads are commonly made from glass fibers, polyester or rayon⁷⁸ and are impregnated or sprayed with the label conjugate solution and eventually dried or lyophilized to store the reagent. Design parameters here include the reproducible volumetric priming of the membrane with the reagent

and consistent release of conjugates during use. Attached to the conjugate pad lies the reaction matrix, a long strip of porous membrane typically made from nitrocellulose onto which the capture and control molecules are immobilized in discrete lines. This hydrophobic component by nature, needs to be treated with surfactants but at the same time retain the ability to electrostatically adsorb antibodies⁹⁴. But the most important design parameter of the reaction matrix is the capillary flow time – the time it takes for a sample to travel through the membrane laterally, as it directly affects the time available for antibody-antigen interaction both for capture and recognition molecules. Faster membranes make for faster tests but put stress both on quantity and association rate in the reagent selection. Slower membranes allow for slow association rates and less reagents but increase the waiting time of the user. Connected to the reaction matrix is the wick, the end station of the sample. The wick is typically made from cotton linter or high density cellulose and is used to collect the sample after it goes over the control line and keep the flow running. All the porous components are joined together and supported with a plastic backing strip whose purpose is to keep everything together for easy manufacturing and assembly (Fig. 2.1- G). This final, processed and supported strip is placed within a plastic cassette (Fig. 2.1-H) that exposes only the inlet and the test lines to the user and protects the components from damage.

Labels are key components in the LFIA industry. While a variety of different components is proposed in the literature^{89,95}, the ones applied commercially are colloidal gold nanoparticles, monodisperse latex colored particles and fluorescent particles. Gold nanoparticles are low cost, available in a variety of sizes and present high sensitivity compared to latex. However, the quantification of a colloidal gold assay is limited, it is a sensitive label to pH and salts, may not be suitable for multiplex systems and does not offer control over the orientation of the bound antibody/antigen or covalent conjugation, rather passive adsorption^{87,92}. Latex on the other hand is also cost effective, comes at a variety of colors, is amenable to a variety of surface chemistries and covalent conjugation of recognition molecules, but it requires the use of surfactants as it is hydrophobic in its untreated form and it generates a weaker signal thus it is not as sensitive. Fluorescent labels are used in device-based LFIA to further increase sensitivity or when the goal is quantification and can be organic or quantum dots.

While all of the above are essential components of an LFIA, antibodies are in the core of immunoassay technologies⁸⁷. Aside from specificity and affinity, parameters such as the association rate constant and long term storage become critical. Absent a sample incubation step, the performance of recognition element binding for an antibody with a given association rate constant is directly linked to the capillary flow time of the porous components. The same applies for the test line, where incubation is not an option at all. Slow kinetics will result in unbound but also bound labels bypassing the test line for this reason. The available binding time is specified in literature⁹⁶ as 1-6 s for the test line and 10-20 s for the conjugation pad. Both monoclonal and polyclonal antibodies are used in commercial LFIA, often in combination. Monoclonal Abs ensure consistency among product batches, are specific and can achieve higher immobilization surface densities, however they are expensive to develop and produce and may not achieve high affinities. Polyclonal Abs are inexpensive in comparison and can achieve high affinities but are less specific and present variability between batches. A third option that is currently available from reagent vendors are aptamers, single strands of DNA or RNA that can bind to target molecules, such as proteins and peptides. Aptamers present great advantages over antibodies⁹⁷: They have increased stability and tolerance to temperature and pH, they are produced using chemical or enzymatic synthesis and as such are highly reproducible, they can be more economical and they can achieve high specificity and affinity. To the authors' knowledge, at the time of writing, aptamer technology has not been applied commercially in LFIA. However it is the epicenter of a lot of discussion and research⁹⁸ and it is considered a good candidate for LFIA applications^{97,99}. The use of aptamers for SARS-CoV-2 antigen detection is investigated for applied diagnostic applications¹⁰⁰.

ASPECTS OF SENSITIVITY AND QUANTIFICATION IN LFIAs

Lateral flow immunoassays can be described as a smart way to greatly simplify an ELISA assay into a low cost, one step, rapid test. There is however a tradeoff to all this inherent simplicity and it lies in test sensitivity, quantification of the results and the dynamic range of the test. Unlike its multistep counterpart, commercial LFIA technology is mostly qualitative, giving a yes/no answer to a threshold related question. Part of this problem is implicit to the LFIA architecture and part of it is user related. LFIA is typically a one-step assay that relies on a homogeneous distribution and flow of reagents at all phases including reconstitution, mixing and binding to the capture molecules. Additionally, many parameters such as membrane speed, capture Abs, label conjugate reagents and sample quantity are subject to error due to manufacturing and fabrication tolerances of components and equipment, storage or environmental conditions during use. The test line itself is typically visible to $\sim 10 \mu\text{m}$ depth¹⁰¹ exposing less than 1/10th of the bound label conjugates to the user thus making the test susceptible to errors arising from wetting irregularities and batch to batch variations⁹⁴. The user related limitation arises from the fact that even a perfectly correlated signal with an assorted color chart is susceptible to subjective interpretation, perception of color, visual impairment and psychological factors. More so, while adding an additional step to the rapid assay may improve the sensitivity of the test, for example a sample pretreatment in a competitive assay or an enzymatic enhancement of the signal generation, it also makes the test result susceptible to human error and deviations from the assay protocol. As such, LFIAs have been mostly designated for cases in which a binary answer will suffice, such as infectious and venereal disease diagnosis. Independent studies have been conducted to evaluate the performance of LFIAs in such diagnostic scenarios. In the case of SARS-CoV-2, rapid tests were one of the first tools that were used for population screening and for decentralized diagnostics. However, in a meta-analysis of 17171 cases, the sensitivity of these tests has been reported to be less than 69% for suspected patients most of whom were symptomatic or confirmed positive at the time of testing¹⁰² compared to 92% for RT-PCR testing¹⁰³ and over 80% for laboratory serological tests¹⁰⁴. HIV rapid testing is considered to be one of the most successful implementations of lateral flow technology in terms of sensitivity, with performance reaching that of laboratory testing. For HIV Antibody testing, high sensitivity values are being reported¹⁰⁵⁻¹⁰⁷ ranging from $\sim 97.5\%$ to 100% for more than 10 LFIA brands with the lower values being reported for patients taking antiretroviral medication. Specificity values (percentage of true negatives) are being reported to be over 99% in 2 of the studies and 86% to 100% in the third with an outlier at 75%. In a different application¹⁰⁸, 4 LFIA tests for the detection of norovirus in fecal samples were evaluated for 3 virus genogroups. The results show specificity equal to 100% for all manufacturers, but the sensitivity ranges from 17% to 52% for the genogroup I, 39% to 64% for genogroup II and 59% to 78% for genogroup GII.4 with the latter being the most common. As such, it was concluded that LFIA alone is not an acceptable solution if the goal is to rule out this condition. Another diagnostic target for which LFIAs have been developed is visceral leishmaniasis. A global comparative evaluation¹⁰⁸ of 5 different brands showed sensitivity of 92.8%-100% and specificity of 96% to 100% for panels performed using archived samples from the Indian subcontinent. However these values were significantly lower for samples from Brazil and East Africa (sensitivity 61.5%-91%, specificity 36.8% - 87.2%). For non-infectious disease applications, a common LFIA product marketed by manufacturers is a rapid troponin I test. One study¹⁰⁹ examines 4 different LFIA tests for cardiac troponin I and reports Positive Predictive Values (PPV) reaching 100% for 3 of the tests with Negative Predictive Values (NPV) ranging from 57.6% to 91.6% for the same tests. One test performed differently with NPV over 99% and PPV less than 60%. Regarding sensitivity, out of the 4 tests only one gave a positive result for Tp-I less than 0.5 ng/ml while the rest gave negative results for Tp-I less than 1.6 ng/ml. Many other studies exist, both independent and ones conducted by manufacturers, that demonstrate performance ranging from poor to as good as lab testing, depending on the diagnostic target, the manufacturer and the setting. However, yes/no results cannot fully describe every clinical condition. For example, quantifying the b-hCG value can assist in ruling out ectopic pregnancy, while quantification of CRP can assist in the differential diagnosis between a viral or microbial infection. For this reason, quantitative LFIA technologies have been developed.

There are both instrumented and stand-alone methods to render LFIAs quantitative or semi-quantitative. The ones that are frequently seen in commercial applications are color comparison charts, ladder bar assays, colorimetric strip readers and fluorescent systems. Color comparison charts are found in the packages of urinalysis strips, drug, adulteration and alcohol test dipsticks, which do not share the definition of lateral flow tests. Less commonly this method can be found in lateral flow tests for cholesterol (Prima[®] hometest)¹¹⁰. This method is most susceptible to human error and thus not very frequently used. As such, for biomarkers such as C-Reactive protein and fecal calprotectin where screening and rapid testing is desirable, but clinical intervention may vary depending on the concentration range, a ladder bar¹¹¹ is introduced. This method is based on the careful deposition of specific concentration and volume of capture Ab on two or more subsequent test lines. This way, in lower concentrations of the analyte, the bound conjugate will be depleted before the final test line, so if the test includes two test lines, only one will become visible. In larger concentrations the conjugate will be enough to bind both test lines and both lines will appear. Since lateral flow tests lack the flexibility of analytical devices in detector adjustments, the dynamic range of the measurement is often quite limited. As such, ladder assays exist for various ranges. For example the diagnostics company Preventis[®] offers 2 different versions of a calprotectin rapid test, with cutoffs at 60 and 200 µg/g of fecal sample respectively. Another method with multiple bars is the deposition of reference lines along with the test line (ABON[™] CRP). This way, the intensity of the test line is compared to the intensity of two reference lines (high and low) in order to evaluate whether the sample concentration is above, below, or between the two reference concentrations. Many tests based on variations of this principle are marketed as semi-quantitative tests with one (PreventID[®] CRP 1/3) or two reference lines in sandwich or competitive (Cortez Diagnostics inc. CRP) formats. However, these non-instrumental approaches could not cover the market demands for more sensitive, user-independent quantitative tests. For this reason, device-based and device-compatible LFIAs as well as LFIA-compatible devices have been introduced to the market by a number of manufacturers, usually at a low cost. Among the 81 LFIA rapid test companies examined in this study, 17 produce some sort of chromatographic imaging device and 9 offer a urinalysis strip reader, while companies such as Skannex, Qiagen, Bioscitech, Cellmic and Axxin deal exclusively with imaging technologies for LFIAs. The typical strip reader¹¹²⁻¹¹⁴ includes a controlled illumination source (LED/Laser diode), a detector which can be a CCD, CMOS or photodiode and suitable optics for colorimetric, fluorescent (Trinity Biotech - Meritas[®], Micropoint ezLabs[®]) or refractometric (ReaScan[®]) analysis. The advantages of using such a system are numerous: subjective interpretation of the results is replaced with a machine interpretation of the test line, either numeric or in the yes/no format that leaves no room for ambiguity. As such, the user sourced errors are ruled out and it becomes possible to acquire quantitative results based on the test line coloration/intensity. Also, in multi-pixel or scanning schemes, averaging over a non-uniform test line and white balance/background removal assist in more robust quantifications/interpretations of the results. Typical detection ranges for colorimetric systems are 0.5-50 and 0.2-20 ng/ml for Troponin I (Concile[®] Ω100, Humasis HUB-QUANpro) and typical ranges for fluorescent systems are 50-10000 ng/ml for D-Dimer (Micropoint mLabs[®]) and 0.012-30 ng/ml¹¹⁵ for Troponin I (Trinity Biotech - Meritas[®], Fig. 2.2-D). Considering that the sensitivity of the plain immunochromatographic lateral flow test for Tn-I is usually 1 ng/ml (Teco Diagnostics TnI, PreventID TnI and many others) and that the diagnostic limit is set at 0.04 ng/ml¹¹⁶, one can see the value of using colorimetric and fluorescent systems coupled with LFIAs. The downside in using such systems is losing the inherent simplicity of these stand-alone disposable tests. Analytical devices even at this level require calibration, standards and even maintenance, although much less than the typical clinical analytical instrument. An interesting line of products for the digitization of an LFIA result are smartphone based systems, either devices that actually embed a smartphone (Skannex Skansmart) or adapters that allow the user's own smartphone to be used as an imaging and image processing device for lateral flow tests (CellMic – HRDR 200). Since most modern smartphones include quality CMOS sensors and illumination LEDs, they make a good fit for colorimetric applications at low cost. Cellmic has even introduced a smartphone-compatible multi-wavelength fluorescence reader (CellMic HRDR-300). These solutions remove the need for an elaborate optical system putting the pressure on the analysis software and making the

technology ideal for e-health applications. However, they do suffer from platform obsolescence⁸⁷ due to the constant evolution of smartphone hardware and software.



Figure 2.2: Lateral flow rapid tests and system: (A) an HIV rapid test (B) a multiplex rapid test for Troponin I, Myoglobin and Creatine Kinase-MB (C) a semi quantitative rapid test for CRP based on reference lines (D) Meritas by Trinity Biotech: a device-based LFIA with fluorescence detection for quantitative testing of Troponin I and Brain Natriuretic Peptide.

MULTIPLEX ANALYSES IN LFIAS

The need for multiple measurements in a single disposable strip/cartridge is a constant challenge in PoC systems design. A typical example is the cardiac triple test (Troponin I, Myoglobin, CK-MB), where different combinations of even qualitative (threshold) results indicate different stages of myocardial infarction and cell necrosis. Other examples include the differentiation between influenza types A or B, malaria types Pf or Pv and HIV types 1 or 2. In all those cases, detection of multiple analytes can assist in the identification of the subtype of the disease, the selection of a suitable treatment and/or the prognosis of the disease outcome. In lateral flow tests there are two main strategies to detect multiple analytes: The first method is simply the attachment side by side of two or more strips in a common cassette. This technique is common in ToRCH rapid combo tests where newborns and pregnant women are screened for Toxoplasmosis, Rubella, Cytomegalovirus and Herpes simplex virus antibodies. This method does not share the classical definition of multiplex since a number of different samples is introduced to the same number of different strips resulting in more steps needed by the user and more sample requested from the patient. However it does have the advantage of being as robust and reliable as the individual tests. The second method – that is common in cardiac triple, HIV and influenza multiplex tests- involves the deposition of multiple test lines and the corresponding detection Abs in a single strip. The advantage in this “true multiplex” method is that a single drop of sample can be used for two or more tests, which is compatible with finger-prick sampling, involves only one step and does not suffer from sample aliquot variations. The disadvantage is that just like in multiplex ELISA, non-specific binding and cross-reactivity raise the bar for the selection of good quality antibodies¹¹⁷, while all assays must be compatible with a single selection of membrane, sample pretreatment and incubation times that are dependent on the positioning of the test lines. A third strategy, not frequently seen in commercial products, is the implementation of a single sample pad that feeds multiple strips. While such a technique introduces parallelization into the assay, it may not be compatible with conventional LFIA production equipment.

2.3.2 CENTRIFUGAL POINT OF CARE SYSTEMS

Centrifugal PoCs, also known as Lab on a Disk or LOAD, are a group of analytical microfluidic systems that share common fluid manipulation techniques based on the centrifugation of a disk-like consumable microfluidic chip. In these systems, samples and reagents are transferred and mixed in a network or microfluidic channels and chambers within a rotating disk to perform diagnostic assays. This technology is only employed by 4 out of 105 companies examined here, however it is unique in many ways and also quite new in the field of commercial PoC systems with increasing interest from diagnostics companies¹¹⁸. The main benefit of centrifugal microfluidics is that traditionally troublesome aspects of Lab on a Chip such as pumping, aliquoting, bubble formation, plasma/serum extraction and peripheral equipment necessities suddenly become a lot easier to tackle with simple exploits of geometry, spin and wetting properties of the substrate. More so, LOAD can be designed in a way that fluid motion is discrete, from one position to another with no stable intermediate states, which makes it conceptually and operationally preferable to systems where everything is continuous and thus in need of carefully designed closed loop control. Having strong affiliations with the optical disc industry, this technology has been commercially applied so far in quantitative PoC devices for blood chemistry, hematology and limited immunoassay tests, however it possesses inherent universality and parallelization capabilities that suggest there is more to come. That being said, these systems are by default hard to miniaturize to a handheld level and they are more costly than LFIAs for low throughput settings.

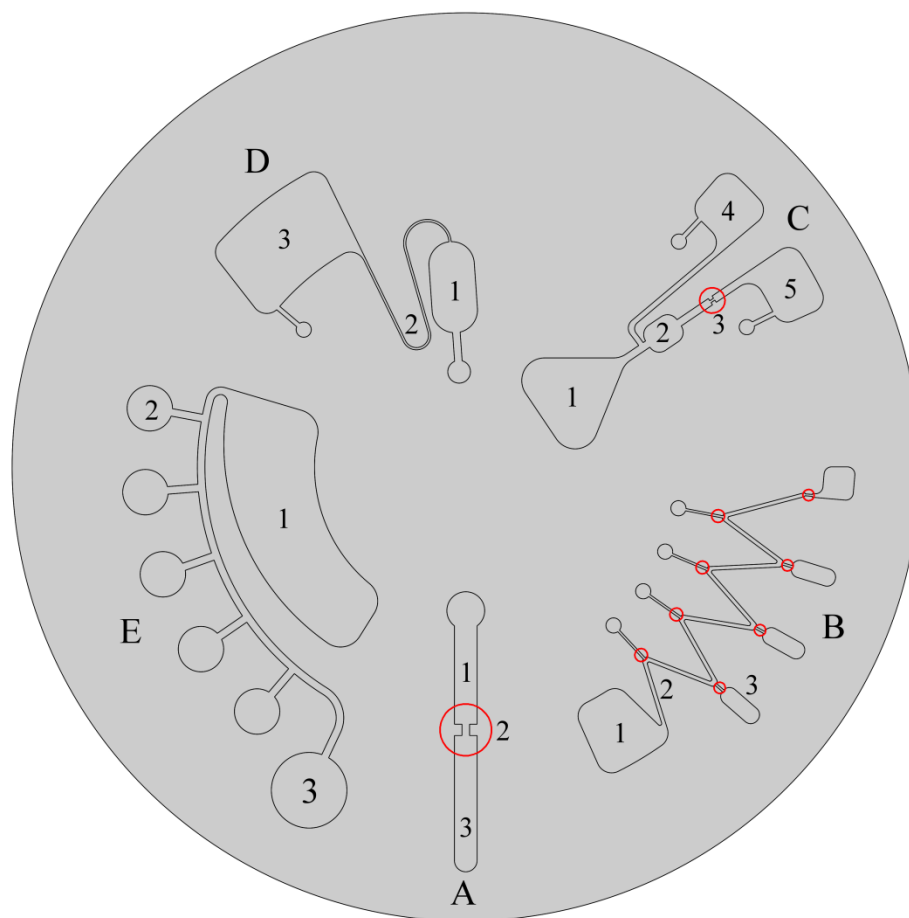


Figure 2.3: Operation specific blocks that are found inside a LOAD disposable. (A) Hydrophobic valving block (B) Aliquoting block with vents (C) Metering block (D) Siphon structure (E) Overflow aliquoting block

LOAD PRINCIPLE OF OPERATION

Lab on a Disk operations rely on 4 different forces: Centrifugal, Capillary, Euler and Coriolis¹¹⁹. Centrifugal force is used to pump fluid outwards. Capillary force is used for the initial sample priming and to move fluid in sufficiently small channels where capillary effects are prevalent. Euler force is used to mix components when inertial forces are large enough. Coriolis force is mostly used experimentally in flow direction switching schemes¹²⁰. Aside from these 4 (pseudo)forces, the enabling technology for LOAD systems is the local hydrophobic patching of flow channels which allows on/off valving dependent on rotational speed of the disc. However, unlike LFIA, LOAD does not have a single operating sequence adopted in all systems, rather consists of design blocks that perform a specific task and whose interconnection results in a protocol-specific chip. Fig. 2.3 shows the typical blocks found in a LOAD consumable. (A) is a simplified example of hydrophobic valving¹²¹, where hydrophilic channels A1 and A3 are connected through a smaller and hydrophobically treated section (A2, enclosed in a red circle). Liquid that is initially present in A1 will not be able to move to A3 when the disc is motionless because of the contact angle difference at the intersection with the hydrophobic patch. If the disc starts spinning, the liquid volume will experience a centrifugal force pushing it against the hydrophobic barrier. Should this centrifugal force become large enough, the exerted pressure on the fluid front will counter the superficial force at the air/fluid interface and the hydrophobic valve will open, i.e. it will be wetted allowing the liquid to flow to A3. The structures are often vented so that air pressure buildup will not interfere with pumping. (B) is a method of aliquoting of sample and reagents patented by Gyros¹²², a company that pioneered the field of commercial centrifugal microfluidics. In (B), a sample originally stored at B1 flows inside the meander (B2) by capillary force alone while the disk is stationary. Hydrophobic patches (encircled sections) allow venting of the channel but are not wetted by the inflowing liquid. Once the meander has been primed, the disc spins, outer hydrophobic patches burst and the liquid gets distributed at the respective chambers (B3). (C) shows a metering chamber. At low rotational speed, sample stored in chamber C1 flows outwards, filling chamber C2 but stopping at C3 due to the hydrophobic patch. Once C2 is full, all excess liquid will flow towards C4. Once C1 is empty, the disc is accelerated up to a point when C3 bursts and the metered liquid flows in chamber C5. In (D), a siphoning block is depicted. In this arrangement, while the disc is spinning, fluid within D1 will flow due to capillary and centrifugal force in channel D2 until the radial level in D1 matches the radial level in the first turn of D2. If the disc stops, then the flow will continue up to the entrance of D3 where it will stop absent capillary force. However, since the entrance of D3 is outwards in comparison to the exit of D1, upon spinning the disc again, D1 will empty. (E) is again an aliquoting arrangement used by most commercial LOAD systems. In this block, when the disc is spinning, liquid stored in E1 flows outwards priming each chamber consequently starting with E2. The last chamber (E3) is used to gather excess liquid. Sufficiently large channels or vents are used to allow air to escape. Mixing can be achieved in chambers of suitable size and shape by abruptly slowing down or stopping and then reaccelerating the disk. Most systems are designed using variations and combinations of these blocks along with mixing chambers, sample and reagent ports or liquid containing pouches embedded in the disk. Centrifugation adds the great benefit of plasma/serum separation within the chip so typically these systems provide sample to result functionality without the need for external separation steps. The result of the test is acquired using photometric or fluorescence sensing in detection chambers¹²³.

DESIGN, MATERIALS AND REAGENTS IN LOAD

Centrifugal microfluidic design, while mostly based on the same operating principles, are quite diverse. Interestingly, each LOAD system researched in this article employs its own unique and innovative techniques of liquid handling and detection. LOAD solutions dealing with blood chemistry (Abaxis - Piccolo Xpress¹²⁴⁻¹²⁹, Cobas® b 101¹³⁰⁻¹³³) typically use a spectrophotometric method of analyte detection, much like in a standard laboratory clinical analyzer. In this type of measurement, the sample is diluted within the chip and then mixed with a detection reagent for analyte quantification. The final fluid absorbs light at specific wavelengths in correlation to the concentration of the sample/reagent reaction product. In order to produce measurable absorbance, the fluid needs to be accumulated in a cuvette-like chamber measuring a few millimeters in layer thickness, much like in clinical analyzers. For this reason, these disks are a lot thicker than typical microfluidic structures, embedding chambers and channels that are well within the mesoscale. Since in centrifugal systems the fluid handling force acts on the entire mass of the liquid, larger structures along with microchannels do not pose a problem. Cobas b 101 (Fig 2.4-D) takes advantage of this thick design by incorporating a lateral sampling port protected by a hinged lid. Upon closing this lid, buffer/reagent solution is released in the chip and thus the problem of reagent storage/reconstitution is solved. Similarly, Abaxis (Fig 2.4-B) stores the buffer solution in a separate container at the center of the disk which opens by mechanical interaction when the consumable is inserted in the machine. Biosurfit, (Fig 2.4-C) with their system Spinit¹³⁴⁻¹⁴⁰, use a different approach that allows for a thinner design. The incident light is forced to undergo multiple internal reflections within the detection chamber using a diffractive reflective layer at the bottom of the chamber. This gold layer traps specific biomarkers using surface immobilized antibodies. The refractive index of the biomarker layer is measured as light reflects out of the disk and is used to quantify the bound analyte¹⁴¹. A different issue that LOAD designers need to address is that when the disk keeps spinning, the radial “gravitational” field keeps fluids secure against a wall. However, if the disk stops, then capillary forces once again become predominant and in a half full mixing/detection chamber this can be a problem. For this reason, it is often a requirement to do detection while the disk is spinning. This can only be done stroboscopically. Abaxis uses a Xenon arc lamp to counter this problem. The source is only open for 5 microseconds with a 50 kW radiant power output. The light travels through the sample and apertures and ends up in a series of dichroic mirrors and interference filters where it is broken down into wavelengths and measured by individual light detectors. This arrangement allows multiple measurements at 1200 rpm to acquire an average absorption per cuvette in the desired wavelengths. Biosurfit has patented plain LED source illumination with CCD/CMOS detection for a 200 μm sample layer. This 2D approach, in conjunction with the internal reflection format and carefully designed apertures, allows simultaneous measurements that correspond to different optical path lengths within the sample. A special case in the family of commercial LOAD is that of Samsung-Nexus and their systems LABGEO¹⁴²⁻¹⁴⁴ IB10 (Fig 2.4-A) and PA20. In this format, the disk is a carrier for up to 3 LFIA strips, performing fully automated quantitative immunoassays for cardiac markers from whole blood. It is mentioned in literature¹⁴⁵ that this system, at least initially, used fluorescence with lanthanides to provide high sensitivity with inexpensive optics. The typical materials used for centrifugal disk microfluidics are Polycarbonate (PC) and Polymethyl Methacrylate (PMMA) because of their good optical characteristics, low cost and compatibility with mass production methods such as injection molding. The hydrophobic treatment¹⁴⁶⁻¹⁵⁰ can be done using silane derivatives or PTFE in spray or plasma deposition while superhydrophobic treatment is also possible by using surface micropatterning¹⁵¹ prior to treatment. Apart from the fluidic aspects of LOAD, a key consideration is the storage of the reagents within the chip. All 4 companies investigated here use dry reagents which are reconstituted during usage of the disks. The drying can be conventional (ex. atmospheric or hot air) or by lyophilization when the required stability cannot be achieved using other methods or when a porous structure of the pellet or spot is necessary for rapid reconstitution and mixing. Taking into consideration all of the above, one can observe that centrifugal microfluidics constitute a good canvas for a variety of design approaches and seem to be able to perform in different types of tests such as immunoassays and clinical chemistry.

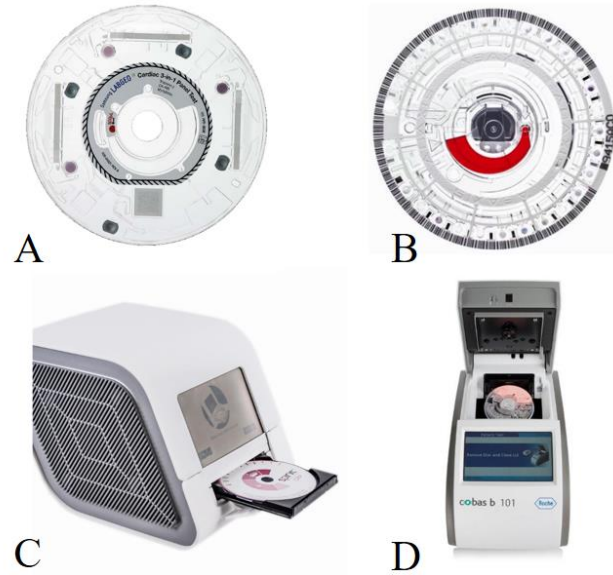


Figure 2.4: Lab on a Disk systems and consumables: (A) The disk used in Samsung LabGeo IB10 (B) The Disk used in Abaxis' Piccolo Xpress (C) The system Spinit from Biosurfit (D) The system b 101 from Cobas.

ASPECTS OF SENSITIVITY AND PRECISION IN LOAD

Commercialized centrifugal microfluidics, as it has been described in the previous paragraph, utilize standard and non-standard optical arrangements to acquire measurements indicative of the quantity or absence of an analyte. A big benefit of this technology is the inclusion of control spots into the disposables to calibrate the device and assess the state of the reagents^{124,126,127}. These sophisticated systems clearly do not aim for the rough estimation in an extreme point of care setting⁸⁴, rather aspire to become mobile or benchtop, low cost alternatives to clinical analyzers. Abaxis offers 26 different clinical chemistry tests in 17 individual disks/panels. Independent studies¹⁵²⁻¹⁵⁵ produced generally favorable results with most measurements conforming with laboratory standards. For example, liver function panel intra-assay precision, linearity and accuracy have been found to be acceptable for clinical usage^{152,154} with the exception of TBIL. Also, lipid panel results have been found to be within the limits set by the National Cholesterol Education Program with HDL falling out of the limit in one study¹⁵⁶. Abaxis reports¹⁵⁷ linear ranges for its assays with a wide dynamic range but less sensitivity than a clinical analyzer¹⁵⁸, especially for electrolyte panels¹⁵⁹, although within the limits of diagnostic significance. Cobas offers a lipid panel and glycated hemoglobin measurement, with independent studies¹⁶⁰⁻¹⁶³ for the latter reporting CVs ranging from less than 3% to more than 7%. Biosurfit offers complete blood count and a CRP immunoassay as well as SARS-CoV-2 serological antibody testing. For the CBC, the company reports¹⁶⁴ CVs ranging from 4.8% for Hematocrit to 13.5% for Monocyte differentiation in WBC. For CRP, the analytical range of the measurement is reported¹⁶⁵ to be 4-180 mg/L with a CV of 6.6% against a standard. Samsung offers immunoassays for cardiac and cardiac STAT testing, thyroid function, pregnancy and procalcitonin measurement. For cardiac triple measurements, Samsung's LabGeo is reported¹⁶⁶ to have high sensitivity (0.05-30 ng/mL Tpl, 2-60 ng/mL CK-MB, 30-500 ng/mL Myoglobin) with a total CV in the range of 11%. It can be deduced from all of the above that these devices present high sensitivity in most cases, but sometimes lack in repeatability when compared to standard clinical analyzers. However, their compactness, cost

and ease of use might outweigh these drawbacks when there is no alternative for an in-situ measurement, such as a doctor's office, an ambulance or any other emergency or decentralized setting.

ASPECTS OF MULTIPLE MEASUREMENTS IN LOAD

Centrifugal microfluidics are inherently a multiple measurement technology, since parallelization and aliquoting are easily accomplished using standard techniques. These multiple measurements can be used for multiplexing, for real time optics calibration, for disk and reagent stability assessment and for control measurements. The disks manufactured by Abaxis and Biosurfit are prime examples of multiple measurements using a single disk. Panels like CBC, cardiac triple and clinical chemistry analytes have already been implemented in centrifugal technology systems. However, a multistep protocol, such as ELISA has yet to be realized in commercial PoC LOAD systems, and is perhaps a natural next step for this technology that would also presumably have a positive effect on the coefficients of variation of the devices.

2.3.3 ELECTROCHEMICAL SENSING SYSTEMS

Along with LFIAs, electrochemical sensing systems constitute the most established and applied technologies for PoC settings. 10 out of 105 companies examined here deal with purely electrochemical or hybrid technology that may also include optical detection. In these systems, the presence of an analyte is correlated to an electrical signal at the electrodes of a disposable strip. With blood glucose portable meters being the most prominent of applications, electrochemical sensors have been embedded into a wide range of commercial PoC systems covering blood gases, electrolytes, metabolites and other analytes. Typically, in less the size of a smartphone, these systems are solid state, low cost, highly sensitive and robust. These merits, along with the fact that they cover analytical targets incompatible with LFIAs, have established them in a number of settings, such as home monitoring and emergency testing for specific biomarkers. However, there are drawbacks to consider, including limited specificity from the electrochemical activity of species other than the analyte, limited shelf life, and non-specific binding^{167,168}. Nonetheless, electrochemical sensing systems' impact can be appreciated when considering that millions of people rely on them every day to regulate medication intake of insulin and oral anticoagulants.

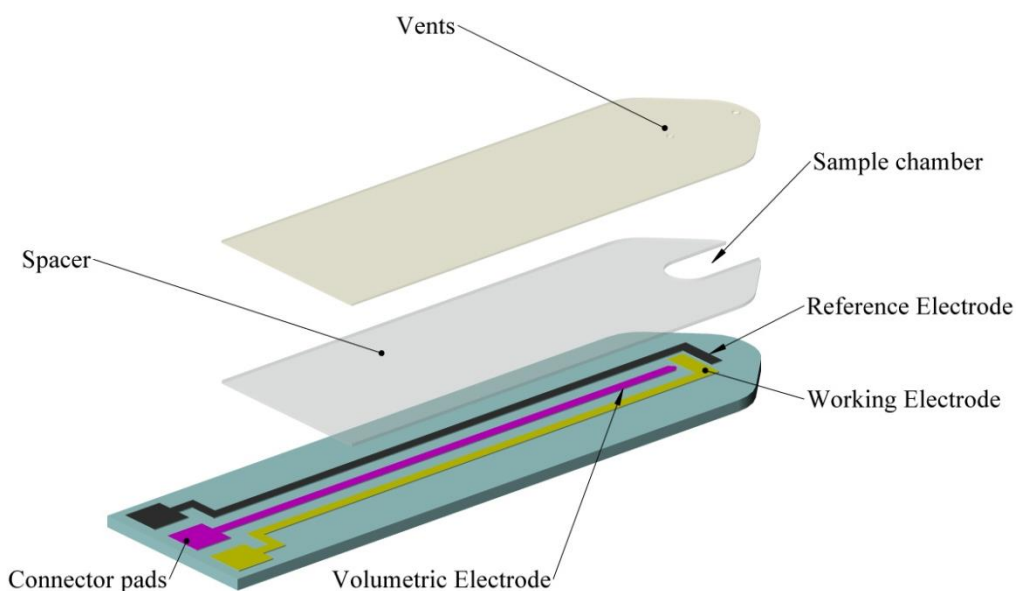


Figure 2.5: A simplified design of an electrochemical sensing disposable strip

ELECTROCHEMICAL SENSING SYSTEMS PRINCIPLES OF OPERATION

Commercial PoC systems with an embedded electrochemical sensor are quite diverse in terms of operation and analytical targets. Fig. 2.5 shows a simplified disposable electrode strip similar to the ones used for glucose monitoring. In this embodiment, the sample, which can be a drop of blood from finger-prick, is metered in a vented sample chamber. A volumetric electrode verifies that the chamber is full while a working and a reference electrode are used to acquire the measurement. Electrochemical sensing PoC applications can be subdivided into different categories as per their recognition element and the method of measurement. In regards to the recognition element, the two main categories are Biocatalytic and Affinity biosensors¹⁶⁷. In Biocatalytic sensors, the recognition element is an enzyme that catalyzes the formation of an electroactive product when the sample is introduced to the cell. In Affinity biosensors, the recognition molecule is most commonly an antibody that captures the antigen biomarker while a secondary antibody, labeled with an enzyme, will complete the sandwich format. This enzyme label is responsible for the formation of the electroactive product in affinity biosensors. As per the method of measurement, the four main approaches are amperometry, potentiometry, conductometry and impedance spectroscopy. In Amperometry^{167,168} the analyte and the sensor reagents are involved in reduction-oxidation reactions at inert metal electrodes. During this process, the electrode gains electrons from the analyte. This results in a measurable current that is linearly proportional to the concentration of the analyte. This technique is used for the quantification of metabolites, such as glucose, cholesterol and lactate. In potentiometry, a potential difference described by the Nernst equation is measured between two electrodes with minimal current drawn. The measurement has a logarithmic dependence to the analyte concentration. Potentiometry is commonly used with ion selective electrodes for electrolyte (K^+ , Na^+ , Cl^-) quantification. Conductometry is the measurement of the sample's conductivity that is in turn related to the concentration of electrolytes. Since red blood cells have insulating properties due to their lipid bilayer membrane, this method is used for hematocrit measurements. Impedance spectroscopy is primarily used in affinity biosensors, in which a sinusoidal excitation signal with varying frequency is used to acquire the impedance spectrum of the test zone. The measurement is proportional to the real time binding activity on the test zone¹⁶⁹.

DESIGN, MATERIALS AND REAGENTS IN ELECTROCHEMICAL SENSING SYSTEMS

Point of Care devices that embed an electrochemical sensor come in a wide range of footprints and designs, the most common one being pocket size instruments for blood glucose monitoring. All of these systems share in common the use of disposable strip in which the electrodes and reagents are packed and a device that connects electrically to this strip. The disposable is in most cases a single use strip into which the sample, most commonly whole blood, is inserted directly into a metering/testing chamber much like Fig. 2.5. However, more elaborate approaches have been successfully commercialized. Abbot's i-STAT^{170,171} (Fig 2.6-B) combines active and passive microfluidic components with electrochemical sensing within a disposable plastic cartridge to perform a wide range of tests including cardiac triple, blood gas, coagulation and electrolytes. Different cartridges utilize potentiometry, amperometry and affinity methods depending on the analyte, however all are compatible with a single handheld device containing pumps, actuators, heater and all necessary electronics to perform measurements in situ. In a similar approach, Alere's Epc¹⁷² (Fig 2.6-D) can perform 11 tests including blood gas, electrolytes and metabolites in a single disposable cartridge utilizing microfluidics and different sensor technologies. The technological advantage of such systems is the ability to perform multiplex assays with sample pretreatment and on-chip calibration. Another notable approach is that of mobile phone integration. Just like in LFIA readers, the smartphone race to provide high quality consumer goods has provided the technological basis that is compatible with some PoC specifications^{173,174}. For example Dario¹⁷⁵(Fig 2.6-C) offers glucose meters that utilize the audio jack of smartphones, an I/O port able to both record and generate signals that can be used for electrochemical sensing. Regarding the electrode design in electrochemical sensor systems, configurations include the use of at least two electrodes: a reference electrode and a working electrode, while commonly an auxiliary electrode is included to function as a source or sink of electrons. Additional probes can be used for volumetric verification or to compensate for working electrode fouling or non-

specific binding. Electrodes are fabricated using either screen printing or laser ablation patterning on thin layers of metal made with vapor deposition¹⁷⁶. Materials include carbon, platinum, gold, silver and palladium. In biocatalytic sensors¹⁶⁷, the functionalization of the electrode is achieved by making sure that the targeted enzyme and the electrode surface are in contact and that the enzyme remains functional. Methods to achieve this include entrapment of the enzyme between membranes on the electrode surface, covalent bonding, encapsulation, inclusion in a gel or paste, adsorption, and biotinylation of the enzyme to form a biotin-avidin complex with the electrode. The enzymes used depend on the application. Glucose meters use glucose oxidase along with a redox mediator often in the form of immobilized enzyme in a redox polymer^{177, 178}. For Cholesterol, cholesterol esterase and cholesterol oxidase are used often in combination, while for electrolytes ion selective electrodes¹⁷⁹ are integrated in the strips. Miniaturized Severinghaus and Clark electrodes are used for CO₂ and O₂ measurements respectively. For prothrombin time (PT/INR) measurements, human recombinant thromboplastin is commonly used along with buffer solution and human plasma-extracted coagulation factors for control purposes.



Figure 2.6: Electrochemical biosensing systems: (A) Typical glucose meter (B) i-STAT handheld blood analyzer, Abbott Point of Care inc. (C) Dario's smartphone compatible glucose meter (D) Epoc PoC system by Alere

PERFORMANCE OF ELECTROCHEMICAL PO C SYSTEMS

Electrochemical methods are broadly applied in clinic analysis among other reasons because of their increased sensitivity and selectivity. Their implementation in point of care systems has resulted in a wide range of devices that provided access to measurements typically done in the lab, for example glucose or lipid panels, or replaced testing principles with solid state technology, for example PT/INR measurements. Portable glucose meters have been stringently evaluated as per their performance. Independent studies^{180,181} have reported the accuracy of 43 and 27 commercial self monitoring blood glucose (SMBG) systems respectively according to ISO 15197:2003¹⁸². This standard stipulates that 95% of measurements below 75 mg/dL must fall between a ± 15 mg/dL zone from laboratory results while measurements over 75 mg/dL must fall between $\pm 20\%$ from laboratory results to acquire a CE mark. In these studies approximately 21% and 41% of the product did not perform according to these standards. It is worth mentioning that the 2013 revision of ISO 15197 sets tighter standards for the regulation of SMBG systems, notably by requiring that 99% of measurements should fall within the error margin. Interfering factors in SMBG have been

widely investigated^{183,184}. Temperature, altitude, certain drugs, such as acetaminophen and substances such as maltose can significantly affect the reliability of the measurement. In PT/INR monitoring, where once again frequent testing is used for the regulation of drug dosage, electrochemical systems have partly replaced classical methods based on magnetic/mechanical principles to detect clotting. With companies generally abiding by an allowable ± 0.3 INR (International Normalized Ratio for prothrombin time) bias in comparison to a reference system, we examine the coefficients of variation published by manufacturers for their systems. Alere's INRatio¹⁸⁵ is reported by the manufacturer to have an 8% CV for normal and 7.7% CV for therapeutic samples in a wide range of 0.7-7.5 INR values. Siemens, with Xprecia Stride¹⁸⁶, in a similar range of 0.8-7 INR reports CVs of 5.9% for INR<2, 4.1-4.2% for INR ranging from 2 to 4.5, and 3.6% for INR>4.6 up to 8. Cobas with CoaguChek¹⁸⁷ reports a CV of 2.6% for venous blood and 3.5% for capillary blood for samples with INR<4.5. Abbott, with i-STAT¹⁸⁸, reports a CV of 4.7% for venous blood with mean INR=2.4 and CV of 4.6% with mean INR=2.5. The ISO standard 17593:2007 defines that for samples with INR<2 in a reference system, 90% of the allowable differences between the PoC and the reference system must be ± 0.5 INR. For samples with INR from 2-4.5, this becomes $\pm 30\%$ with an allowable bias of ± 0.3 INR. For values larger than those, no performance criteria are set¹⁸⁹.

2.3.4 NUCLEIC ACID TESTING SYSTEMS

Nucleic acid testing (NAT), as a diagnostic tool at the Point of Care, is a rapidly evolving field with potentially great impact. Out of 105 companies reviewed in this work, 5 offer diagnostic tools based on NAT with company provided assays, whereas 2 offer general use amplification/detection systems that are claimed to be directed for PoC applications. In NAT PoC systems, the diagnostic targets are most commonly (1) DNA/RNA segments of bacteria/viruses or (2) human genetic material. In the first case, human body fluids such as plasma, sputum, or nasal swab are tested in an attempt to diagnose an infectious disease and differentiate between possible subtypes that would alter the therapeutic intervention. In the second case, the clinical significance lies in the detection of mutations or oncogenes, with the most widespread application being cancer treatment or prevention. One key advantage of molecular diagnostic systems lies in their ability to amplify their target sequence, a trait that is unique in comparison to other diagnostic approaches. This allows for extremely high sensitivity and specificity even at early disease stages where immunological PoC methods fail to report a positive result due to lack of sufficient analyte. As per the target analytes, nucleic acid methods ultimately look for the most primary pieces of information that describe pathogenesis, and in this sense they can deliver high quality information to the Point of Care. These can be in regard to, for example, the specific subtype of an influenza infection, or a mutation in a tumor suppressor gene. On the downside, nucleic acid detection systems can only confirm the presence of a target sequence within the sample, without providing any information on whether, for example, a microorganism is alive or dead, or whether there is colonization without disease¹⁹⁰. Additionally, polymerase chain reaction (PCR), the most widely adopted method employed in NAT, is a slow process that is hard to implement in PoC and has led to the introduction of alternative amplification strategies¹⁹¹. Finally, the nucleic acid testing industry faces tremendous financial pressure from the technological strides of the whole-genome sequencing technology and is thus limited to scenarios where a centralized health structure is not present.

NAT PRINCIPLES OF OPERATION

Nucleic acid detection presents significant diversity as to the methods applied to make it compatible with diagnostics¹⁹¹⁻¹⁹⁴. This is true for both amplification and detection of the amplicons. The first step in all of these techniques is releasing the DNA/RNA into a buffer in order to perform amplification. This is most commonly achieved

using chemical or enzymatic agents, however other methods, such as sonication and mechanical lysis have been employed¹⁹³. This step is commonly followed by purification and removal of particulates. At this point, the analyte, if present, can be at very low numbers, so it is necessary to amplify, i.e. multiply the segments of interest. If the target is a DNA segment, PCR is the most widely adopted approach. In PCR, the double DNA helix is denatured at high temperatures (~98°C) to allow separation of the two strands. Once this step is complete, the temperature is lowered to allow chemically synthesized oligonucleotides called primers to pair with the separated strands on the location of interest. After this, the enzyme polymerase is used to extend the primer with complementarity to the preexisting strand in a way that it forms a copy of the previously separated strand, at least for the length of the sequence of interest. The process is usually repeated for up to 30-35 times to acquire exponentially increasing number of copies. If the target is RNA, a variation of this technique is used in which another enzyme, reverse transcriptase, is first used to create complementary DNA to the RNA of interest. Biocartis with their system Idylla (Fig. 2.7-A), Quantum DX (Fig. 2.7-C) with Q-POC, and NanoBiosys all use PCR as their amplification strategy. Another approach to amplification is loop mediated isothermal amplification, or LAMP¹⁹⁵. In this method, the temperature is constant at ~65°C and amplification takes place using 4 to 6 primers. An enzyme initiates synthesis by strand displacement and 2 of the primers form loop structures to facilitate subsequent rounds of amplification¹⁹⁶. This technique is used by HiberGene in their systems HG Swift and by Optigene in Genie (Fig 2.7-B). A third approach which is utilized by Alere in their system Alere-i (Fig 2.7-D), is called Nicking Enzyme Amplification Reaction. NEAR employs a nicking enzyme along with polymerase to exponentially amplify DNA at constant temperature. Both NEAR and LAMP are faster than PCR and easier to integrate in PoC systems since no thermocycling is required. Regarding detection, 5 out of 6 companies reviewed here use fluorescence in 2 or more channels, out of which 4 use a real time method, meaning that the amplification and the detection of amplicons are done simultaneously. Quantum DX uses nanowires with DNA probes whose impedance changes as DNA sequences hybridize onto their surface. Cepheid¹⁹⁷, a US based molecular diagnostics company, is considered to pioneer the field of molecular PoC systems. The company has developed GeneXpert, a range of PoC benchtop devices that use a disposable cartridge to perform 6-plex real time PCR for infectious and venereal disease, oncology and nosocomial infections.



Figure 2.7: Nucleic acid testing PoC systems: (A) Idylla system from Biocartis (B) Genie III system from Optigene (C) Q-poc system from Quantum DX (D) Alere-i system from Alere.

NAT POC SYSTEMS PERFORMANCE

Nucleid acid testing systems, have the inherent advantage of amplification, which allows for very high sensitivity. This feature has made them especially useful for SARS-CoV-2 screening and diagnostics in remote locations, although performance has been found to vary among manufacturers. Alere's ID-now has a reported average sensitivity of 73% and a specificity of 99.7%, while Cepheid's Xpert Xpress model is reported to have a 100% sensitivity and a 97.2% specificity¹⁹⁸. Alere-ID NOW is also being used to test nasal swab samples for the diagnosis of influenza A and B. Alere reports¹⁹⁹ sensitivity of 97.9% with specificity of 89.2% for influenza A against viral culture in a clinical study of 571 patients, while the same values are calculated for influenza B at 92.5% and 96.5% respectively. Results regarding the limit of detection for this assay are also presented, with values ranging from 1.88×10^5 TCID₅₀/mL for subtype A/H1N1 to 5.55×10^2 TCID₅₀/mL for subtype B/Yamamata lineage for direct swab testing. The same device is used for the detection of *Streptococcus pyogenes* in throat swab. Alere reports²⁰⁰ 95.9% sensitivity and 94.6% from a clinical study of 481 patients against bacterial culture. The system HG-Swift by HiberGene is used for the detection of *Meningococcus* in a variety of samples. The company reports²⁰¹ sensitivity and specificity equal to 100%, however using as a reference a laboratory PCR assay for a total of 137 samples. Additionally, the limit of detection of the assay is claimed to be 1.4 copies/ μ L for whole blood and 1.9 copies/ μ L for respiratory swab. Idylla by Biocartis is used for oncology assays but also for a respiratory panel to identify influenza virus subtypes and RSV. The company claims to be able to provide high sensitivity however the clinical trials are ongoing at the time of writing of this paper²⁰².

2.3.5 BLOOD GAS / ELECTROLYTE BENCHTOP SYSTEMS

Blood gas and electrolyte testing is a requirement in critical care and emergency room testing to diagnose acute conditions relating among others to respiratory problems, lung disease, kidney disease, dehydration or heart condition. In this sense, centralized testing often needs to be circumvented in order to get stat measurements at the point of care²⁰³. Various companies have developed benchtop systems with larger footprint compared to the devices that have been presented so far to cover the needs of such settings. The specifications of these systems usually include compatibility with capillary blood which is extremely useful in neonatal care, cartridge based reagents and controls, reliability, operating simplicity and the ability to integrate into a broad data management system. These devices are usually based on electrochemical sensing, however fluorescent based systems have been developed²⁰⁴. In this review 4 out of 105 companies have developed one or more blood gas/electrolyte PoC analyzers. Gem 4000²⁰⁵ from Instrumentation Laboratory, Rapid Point 500²⁰⁶ from Siemens, Cobas b 123²⁰⁷ as well as Cobas b 221²⁰⁸ from Roche and OPTI CCA-TS2²⁰⁴ from OPTIMedical perform blood gas and electrolyte testing, while some also include a metabolic module, a co-oximetry module and hemoglobin measurement. Blood gas and electrolyte analyzers are in general highly automated sophisticated devices that have become pretty much standard equipment in modern clinical facilities.

2.3.6 OTHER TECHNOLOGIES

PHYSICAL DETERMINATION OF BIOMARKERS (COAGULATION)

Apart from electrochemical approaches, coagulation disorders can be diagnosed and monitored using physical determination relating to the change of viscosity in a blood sample in the presence of clotting reagents. Accriva diagnostics have developed a whole blood microcoagulation system called Hemochron Signature Elite²⁰⁹. In this system the blood is introduced in a disposable cartridge which in turn is inserted in a pocket-size point of care device. Using a pumping system embedded in the device, the sample is mixed with coagulation reagents and forced into a reciprocating motion within the cartridge. This motion is directly affected by the formation of clots and is monitored

optically within the device²¹⁰. The cessation of movement marks a clinically important clotting time and is used to provide a series of measurements, such as PT/INR, activated partial thromboplastin time (APTT), citrated APTT and activated clotting time. Similarly, Coagusense has developed a PT/INR monitoring system called Coag-Sense²¹¹. In this system, a rotating spoke wheel is operating inside a mix of sample and recombinant rabbit thromboplastin. When the sample clots, the clot is caught up in the spokes and interrupts a beam/sensor couple. Physical methods are promoted by their manufacturers on the basis that alternative systems, such as electrochemical sensors, are affected by the concentration of red blood cells or other substances in the sample.

OPTICAL DETECTION SYSTEMS

Optical detection in clinical testing is probably the most applied technology of all for the detection of biomarkers²¹². Optical techniques such as fluorescence, turbidimetry, nephelometry, spectrophotometry, chemiluminescence and others are routinely used in clinical settings. In fact, apart from electrochemical systems, most other automated PoC systems mentioned in this article fall into this sensing category. However, the viewpoint of this article is the categorization of devices based on discreet set of design choices that go beyond the sensing or the fluidic manipulation method alone. In this sense, the single unifying principle of devices presented in this paragraph is an optical detection method around which the system is built.

Immunofluorimetric²¹³ methods have been employed widely in clinical testing. Siemens has developed the Stratus CS200²¹⁴ which utilizes immunofluorimetry to perform STAT cardiac tests, notably CK-MB, Tp-I, Myoglobin and D-Dimer. This device accepts whole blood in a test tube with anticoagulant. Test reagents are inserted in individual single use cartridges. Up to 4 different cartridges can be used each time to create the emergency panel that is deemed most useful at the time of measurement. The device contains a centrifuge and fluidic samplers and components to perform the automated assay. This system has a comparably large footprint and a level of automation complexity that exceeds what is commonly seen in point of care systems as they have been described so far. However, it represents a different category of PoC systems, the ones that are placed inside a clinic or emergency room to provide fast and reliable information outside the normal pipeline of biochemical testing. In this sense, such devices are autonomous and easy to use, provide lab-quality results and have low sample to result times. As such their intended use justifies a higher design sophistication and cost.

Siemens has also developed the DCA Vantage analyzer, that uses a colorimetric method along with a multi point absorbance measurement from a competitive latex agglutination assay²¹⁵. The device is used to monitor glycemic control and detect early kidney disease by measuring glycosylated hemoglobin ratio and urine albumin and creatinine in self-contained immunoassay cartridges. In a similar approach by Alere with the system Affinion²¹⁶, glycosylated hemoglobin is measured using a boronate affinity assay. A spectral reflectance method is used to measure different colors that correlate to the glycosylated and total hemoglobin in the sample, and whose ratio is proportional to the required measurement. The same device with a different cartridge can be used to quantify albumin and creatinine in human urine. These devices are simple to use, table top systems that are compatible with finger-prick sample acquisition and are directed towards decentralized diabetes/hypertension management.

In a different application, Diagon with Coag S^{217,218} use optical turbidimetry to quantify cloudiness generated by a reaction between the sample and recombinant thromboplastin. A disposable cuvette which includes lyophilized reagents and a steel ball is introduced with the sample (whole blood) after being placed in the PoC device in a controlled temperature position. The sphere is moved using a rotating magnetic field and clotting is monitored using turbidimetry.

A common application of optical detection is the quantitative determination of hemoglobin using a disposable chip and a table top small footprint device. Alere's Hemopoint^{219,220} is an example of such systems. In this device a disposable microcuvette is primed with finger prick blood and placed in the system. Reagents stored in the microcuvette hemolyze the sample. A modified azide methemoglobin method is utilized, and the colored product which is proportional to the Hgb concentration is quantified using an absorption method at 570 nm with an additional wavelength at 880 nm for turbidity compensation. Alere has also developed a lipid panel PoC system called Cholestech²²¹⁻²²⁴. This device is used to measure total cholesterol, high density lipoprotein cholesterol, triglycerides and glucose in a single disposable cartridge from finger prick blood collected with a heparin coated capillary tube. The device uses reflectance photometry to quantify quinoneimine dye produced by a series of reactions²²⁵ for each individual analyte.

Of special interest to critical care testing is the measurement of ammonia in blood in order to assist in the diagnosis of liver disease, kidney failure or a urea cycle disorder. Menarini diagnostics²²⁶ is one of the companies from this list that produces a portable ammonia meter. These devices typically utilize a strip into which ammonium ions are separated from whole blood vertically to react with a reagent producing a color change. This change is detected using reflectance measurements at an appropriate wavelength typically provided using LED technology.

Finally, in a different application, DIESSE has developed Chorus^{227,228}, a cartridge based ELISA benchtop device for a wide range of immunoassay tests ranging from infectious disease to autoimmunity markers. This system uses self contained reagent cartridges and performs full ELISA protocols with washing steps to acquire results photometrically. A carousel-type design allows for up to 30 different cartridges to be analyzed in one run with integrated fluidic components handling all protocol steps.

2.4 COMMERCIALIZED POINT OF CARE SYSTEMS - BIOMARKERS

Selection of biomarkers/conditions has a great impact on the commercialization success of a PoC system. On the first part of this work different technological approaches applied in commercial PoC systems have been described. This second part will address the targeted biomarkers of these systems. While review articles referenced throughout this work present notable applications of their reviewed technology, to the best knowledge of the authors, an extended list of the conditions/biomarkers currently being tested using PoC technology has not been published. The purpose of the second part of this work is to present a thorough list of biomarkers that are currently the diagnostic, prognostic or predictive objective of the systems that have been investigated in this work. While it would fall outside of the scope of this review to investigate each biomarker separately, it is the hope of the authors that this tabulated form of analytes with their respective technologies could assist researches into identifying technological and diagnostic gaps in PoC applications.

Table 2 includes 173 targets categorized based on their type and the sample that is used to perform the PoC test. For each target all relevant tests/devices from companies investigated in this work are cited and categorized based on their technology. Companies that deal exclusively with glucose monitoring and pregnancy testing and applications dealing with allergen identification and veterinary testing have not been included in this table. Hematology panels are grouped into one entry due to the low number of PoC systems currently performing them. SARS-CoV-2 is listed separately on Table 3. The devices have been categorized based on the first section of this article. Table 4 includes the references to the system presented in Tables 2 & 3.

Table 2: An extended list of conditions/biomarkers excluding SARS-CoV-2 that are tested by PoC technologies and the companies investigated here that have developed relevant systems listed by technology: Lateral flow immunoassays (LFIA), Lab on a Disk (LOAD), Electrochemical systems (EC), Blood gas and electrolyte PoC systems (BG) and Other systems.

Test Category	Sample type	Diagnostic target	LFIA	LOAD	EC	NAT	BG	Other
Clinical Biochemistry								
Lipid panel	S/P/WB	CHOL Cholesterol	94,119	121,122	27,32, 33			7,10,20
Lipid panel	S/P/WB	HDL (Direct)	119	121,122	32			7,10,20
Lipid panel	S/P/WB	LDL		122				
Lipid panel	S/P/WB	TRIG Triglyceride	94,119	121,122	27,32, 33			7,10,20
Lipid panel	WB	Lipid Panel (Cholesterol, LDL,HDL,Triglyce rides)		122	27			
Atherosclerosis Marker	WB	sPLA2-IIA (Atherosclerosis)	57					
Cardiac panel	S/P/WB	BNP (Brain Natriuretic peptide)	41,57,72,111	124,125				10,19
Cardiac panel	S/P/WB	CK-MB	40,41,44,47,49,5 4,64,67,69,72,75 ,76,88,93,96,107 ,111,114	124,125	29			10,19
Cardiac panel	S/P/WB	CK Creatine Kinase	119	121				20
Cardiac panel	S/P/WB	h-FABP	57,67,72,76,96					
Cardiac panel	S/P/WB	Myoglobin	40,41,44,47,49,5 4,64,67,69,72,75 ,76,77,88,93,96, 107,111,114	124,125	29			10,19
Cardiac panel	S/P/WB	Troponin I	40,41,44,47,49,5 2,53,54,57,64,67 ,69,70,72,74,75, 76,77,82,83,88,9 3,96,99,107,108, 111,114	124,125	29			10,19
Liver panel	S/P/WB	ALT Alanine Aminotransferas e	119	121				7,20
Liver panel	S/P/WB	AST Aspartate Aminotransferas e	119	121				7,20
Liver panel	S/P/WB	Gamma GT						7,20
Liver panel	S/P/WB	ALP Alkaline Phosphatase	119	121				7,20

Test Category	Sample type	Diagnostic target	LFIA	LOAD	EC	NAT	BG	Other
Liver panel/Anemia Marker/Body Fluid analysis	S/P/WB	LDH Lactate dehydrogenase		121				20
Liver panel/Anemia marker	S/P/WB	TBIL Total Bilirubin	119	121			3,4,5	7,20
Liver panel/Hemolytic Anemia Marker	S/P/WB	DBIL Direct Bilirubin		121				7
Liver panel/Renal panel/Nutritional status	S/P/WB	ALB Albumin	42,64	121				7,20
Liver panel/Nutritional Status Marker	S/P/WB	TP Total Protein		121				7,20
Liver disease/ Kindey failure/ Reye syndrome	WB	Ammonia						20
Renal panel	S/P/WB	BUN Blood Urea Nitrogen	119	121	29		1,3	7,20
Renal panel	S/P/WB	CREA Creatinine	119	121	29,35,36			7,13,20
Renal panel	S/P/WB	Cystatine C	72					
Gout/Kidney disease/Monitoring cancers treatment Marker	S/P/WB	UA Uric Acid	119		38			7,20
Electrolytes/Renal panel/Acid-base balance Marker	S/P/WB	K+ Potassium	119	121	29,35		1,2,3,4,5,6	7
Electrolytes/Renal panel/Acid-base balance Marker	S/P/WB	NA+ Sodium		121	29,35		1,2,3,4,5,6	7
Electrolytes/Acid-base balance Marker	S/P/WB	Cl- Chloride		121	29,35		1,2,3,4,5,6	7
Electrolytes/Renal panel/Parathyroid Function Marker	S/P/WB	Ca Calcium		121	35		1,2,3,4,5,6	7,20
Electrolytes/Renal panel	S/P/WB	iCa ionized Calcium			29			
Electrolytes/Renal panel/Parathyroid Function Marker	S/P/WB	PHOS Phosphorus, inorganic		121				20
Electrolytes/Renal disorders	S/P/WB	Magnesium		121				20
Pancreatic Function Marker	S/P/WB	AMY Amylase	119	121				20
Pancreatic Function Marker	Stool	Pancreas Elastase 1	60					

Test Category	Sample type	Diagnostic target	LFIA	LOAD	EC	NAT	BG	Other
Diabetes disease/Pancreatic Function Marker	S/P/WB	Insulin	72					
Diabetes disease Marker	S/P/WB	Fructosamine						20
Diabetes disease Marker	WB	Glycated Hemoglobin		122	27,32,37			7,11,13
Diabetes disease Marker	Urine	Ketoacidosis (β-hydroxybutyrate)	114		36,37			
Diabetes disease Marker	Urine	Microalbumin	44,54,69,70,71,72,114		39			
Diabetes Disease Marker	S/P/WB	GLU Glucose	94,119	121	27,29,32,33,35,36,37		1,3,4,5,6	7,10,20
Acid-base balance Marker	S/P/WB	LAC Lactate		121	29,33,35,36,37		1,3,4,5,6	
Blood Gases/Acid-base balance Marker	S/P/WB	pO2			29,35		1,2,3,4,5,6	
Blood Gases/Acid-base balance Marker	S/P/WB	pCO2			29,35		1,2,3,4,5,6	
Blood Gases	S/P/WB	sO2			29		1,2	
Blood Gases/Acid-base balance Marker	S/P/WB	tCO2 Total Carbon Dioxide		121				7
Thyroid Function Marker	S/P	TSH	40,57,64,70,72,75,77,94					
Thyroid Function Marker	S/P	Thyroxine free	57					
Sex Hormone (Female)	Urine	Luteinizing Hormone (Ovulation)	40,44,45,47,49,54,57,64,67,70,72,73,74,76,77,80,82,83,84,85,88,93,94,97,99,107,114					
Sex Hormone (Female)	Urine	FSH- Follicle Stimulating Hormone	44,47,54,57,64,67,70,72,73,80,84,93,94,99,107					

Test Category	Sample type	Diagnostic target	LFIA	LOAD	EC	NAT	BG	Other
Sex Hormone/Pregnancy Marker	Urine	b-hcG	40,44,45,47,48,49,50,53,54,57,64,67,69,70,71,72,73,74,76,77,80,82,83,84,85,88,92,93,94,96,97,99,102,104,107,112,114		29			19
Sex Hormone	S/P	Testosterone	40,57					
Tumor Markers	S/P	AFP	40,47,49,54,57,64,67,72,73,74,75,76,77,85,93,99,114					
Tumor Markers	S/P	CA-125	57,72					
Tumor Markers	S/P	CA-15-3	57					
Tumor Markers	S/P	CA-19-9	57					
Tumor Markers	S/P	CEA	40,47,49,54,57,64,67,72,73,74,75,76,77,85,93,114					
Tumor Markers	Stool	M2-PK	60					
Tumor Markers	S/P/WB	PSA	40,54,64,67,72,74,75,76,77,85,94,96,99					
Tumor Markers	S/P	PSA	47,49,52,54,72,73,93,96,114					
Tumor Markers	Urine	PSA	83					
Tumor Markers	Urine	Urinary Bladder Cancer Ag	44,57,70,75,104					
Metastatic cancer Marker	P	ctBRAF mutation				25		
Urinalysis	Urine	Urinalysis Strip Test	44,46,53,54,69,71,72,73,74,75,77,82,85,93,94,99,107,114,115		38			
Other	Urine/WB	Drugs/Alcohol/A adulterants	44,47,49,54,61,64,65,71,72,73,74,75,77,83,85,88,91,93,94,98,100,107,116					10
Hematology								
Complete Blood Count/Anemia Marker	WB	Hgb Blood Hemoglobin	72,107,119		27,37,39		1,2,5	12

Test Category	Sample type	Diagnostic target	LFIA	LOAD	EC	NAT	BG	Other
Complete Blood Count/Anemia Marker	WB	Hct Haematocrit		123	29,35,37,38		2,3,4,5	
Complete Blood Count/Inflammation Marker	WB	WBC White Blood Cell count		123	39			
Complete Blood Count	WB	Haematology Panels*		123,124				8,9
Anemia Marker	WB	Ferritin	64,72,94					
Hemolytic Anemia Marker	WB	G6PD deficiency	63					
Other	WB	Blood type classification	55					
Coagulation								
Haemostasis status/Coagulation disorders	P/WB	INR PT			28,29,30,34			17,18
Coagulation Disorders Marker	P/WB	D DIMER	41,42,44,57,64,70,72,75,76,106,111	124				10,19
Inflammation								
Inflammatory Marker	S/P/WB	CRP - C Reactive Protein	42,44,51,54,57,64,70,72,75,97,104	121,123				19
Inflammatory Marker	S/P	Neopterin	57					
Inflammatory Marker	S/P/WB	Procalcitonin	47,72					
Inflammatory Marker	Tear	MMP-9 (Dry eye disease)	51					
Inflammatory Bowel Disease (IBD) Marker	Stool	Calprotectin	57,58,68,70,78,86					14
Inflammatory Bowel Disease (IBD) Marker	Stool	Lactoferrin	47,68,86,112					
Oxidative stress Marker	Urine	Malondialdehyde (ROS indicator)	114					
Rheumatoid Arthritis Marker	S/P/WB	Anti-CCP	59					14
Rheumatoid Arthritis Marker	S/P/WB	Anti-MCV	62,70					
Rheumatoid Arthritis/Autoimmune Diseases Marker	S	Rheumatoid Factor	75,97					14

Test Category	Sample type	Diagnostic target	LFIA	LOAD	EC	NAT	BG	Other
Infections Differential Diagnosis tests								
Bacterial serology tests	S/P/WB	<i>Borrelia burgdorferi</i> IgG Ab	72					14
Bacterial serology tests	S/P/WB	<i>Borrelia burgdorferi</i> IgM Ab	72,75					14
Bacterial serology tests	S/P	<i>Brucella spp.</i> Abs	73					
Bacterial Antigen Detection tests	Stool	<i>Campylobacter spp.</i> Ag	56,68,86					
Bacterial Antigen Detection tests	Stool	<i>Vibrio cholerae spp.</i> (serotypes O1 & O139) Ag	75,93,96					
Bacterial Antigen Detection tests	Stool	<i>Clostridium Difficile</i> Ag	56,66,68,72,86,108,112					
Bacterial Antigen Detection tests	Stool	<i>Clostridium Difficile</i> Toxin A/B	50,56,68,72,75,86,108,112					
Bacterial Antigen Detection tests	Stool	<i>Clostridium perfringens</i> Ag	68					
Bacterial Antigen Detection tests	Stool	<i>E.coli</i> (serotype O157) Ag	47,56,68,75,86,112					
Bacterial serology tests	S/P/WB	<i>Helicobacter pylori</i> IgG Ab	40,44,45,47,49,52,53,54,61,64,67,69,70,71,72,73,74,75,76,88,92,93,94,99,102,107,112,114					14
Bacterial Antigen Detection tests	Stool	<i>Helicobacter pylori</i> Ag	40,44,47,50,54,56,57,58,61,66,68,69,70,71,72,73,74,75,78,85,86,88,93,96,104,108					
Bacterial Infection Marker	Biopsy sample	<i>Helicobacter pylori</i> (Liquid Urease Test)	109					
Bacterial Antigen Detection tests	Urine	<i>Legionella pneumophila</i> Ag	49,54,56,57,72,73,75,80,86,93,104,108,112					14

Test Category	Sample type	Diagnostic target	LFIA	LOAD	EC	NAT	BG	Other
Parasite Antigen Detection tests	S/P	<i>Leishmania spp.</i> (Kala-Azar) Ag	47,54,66,73,75,96,101					
Bacterial serology tests	S/P/WB	<i>Leptospira spp.</i> IgG/IgM Abs	47,48,52,64,75,79,96					
Bacterial Antigen Detection tests	Stool	<i>Listeria monocytogenes</i> Ag	68,86					
Bacterial Antigen Detection tests	WB, CSF, Nasophagal swab	<i>Neisseria meningitidis</i> (serogroups A, B, C, 29E, W135, X, Y, Z) Ag				21		
Bacterial serology tests	WB	<i>Orientia tsutsugamushi</i> IgM Ab	63					
Bacterial Antigen Detection tests	(Stool)/S/P	<i>S. typhi</i> / <i>S.paratyphi</i> Ag	47,49,52,53,64,68,74					
Bacterial Antigen Detection tests	Stool/S/P	<i>S. typhi</i> Ag	44,47,49,54,56,64,68,73,74,86					
Bacterial serology tests	S/P/WB	<i>S.typhi</i> IgG/IgM Abs	44,47,49,53,73,74,79,93,96					
Bacterial serology tests	S/P/WB	<i>Rickettsia rickettsii</i> IgG/IgM Abs	44,49					
Bacterial Antigen Detection tests	Stool	<i>Shigella spp.</i> Ag	56,68,86					
Bacterial Antigen Detection tests	Throat Swab	<i>Streptococcus group A (S.pyogenes)</i> Ag	44,45,47,49,50,54,57,64,68,69,70,71,72,73,74,75,80,86,88,92,93,96,102,103,104,107,112			26		14
Bacterial Antigen Detection tests	Throat Swab	<i>Streptococcus group B (S.agalactiae)</i> Ag	47,50,64,69,70,71					
Bacterial Antigen Detection tests	Urine	<i>Streptococcus group B (S.agalactiae)</i> Ag	44					
Bacterial Antigen Detection tests	Nasal & Rectal swab	<i>Streptococcus group B (S.agalactiae)</i> Ag	72			21		
Bacterial Antigen Detection tests	Urine	<i>Streptococcus pneumoniae</i> Ag	57,72,75,86,108,112					
Bacterial Antigen Detection tests	WB	<i>Mycobacterium tuberculosis</i> IgG Ab	44,49,70,72					

Test Category	Sample type	Diagnostic target	LFIA	LOAD	EC	NAT	BG	Other
Bacterial Antigen Detection tests	WB	<i>Mycobacterium tuberculosis</i> IgM/IgG Abs	44,75,85,93,96					
Bacterial serology tests	S/P/WB	<i>Mycobacterium tuberculosis</i> Abs	40,52,64,73,83,88			23		
Bacterial Antigen Detection tests	Stool	<i>Yersinia enterocolitica</i> (serotypes O:3) Ag	68					
Bacterial Antigen Detection tests	Vaginal swab	<i>Chlamydia spp.</i> Ag	50,54,64,67,69,71,72,74,77,88,92,93,96			23		14
Parasite Antigen Detection & serology tests	WB	<i>Plasmodium spp.</i> (malaria Pan) Ag & Abs	40,44,47,48,49,54,64,66,67,72,73,74,75,79,82,88,93,96,101,104,112			23		
Parasite Antigen Detection & serology tests	WB	<i>Plasmodium falciparum</i> (malaria Pf) Ag & Abs	40,44,47,48,49,52,53,54,63,64,67,72,73,74,75,76,79,82,83,88,93,96,104,105,112,114			23		
Parasite Antigen Detection & serology tests	WB	<i>Plasmodium vivax</i> (malaria Pv) Ag & Abs	40,44,47,49,52,53,54,63,64,67,73,74,75,76,79,82,83,93,96,105,114			23		
Parasite serology tests	S/P	<i>Trypanosoma cruzi</i> Ab	54,64,72,73,75,96					
Parasite Antigen Detection tests	Stool	<i>Entamoeba spp.</i> Ag	68,75					
Parasite serology tests	S/P/WB	<i>Wuchereria bancrofti</i> , <i>Brugia malayi</i> or <i>B. timori</i> IgG/IgM (Filariasis)	47,75					
Parasite Antigen Detection tests	Stool	<i>Giardia lamblia</i> Ag	47,50,58,61,68,71,72,75,86,108,112					
Parasite Antigen Detection tests	Urine	<i>Schistosoma spp</i> (<i>mansoni</i> , <i>japonicum</i>) Ag	73,75,95					

Test Category	Sample type	Diagnostic target	LFIA	LOAD	EC	NAT	BG	Other
Parasite Antigen Detection tests	Stool	<i>Cryptosporidium parvum</i> Ag	50,58,68,75,86,108,112					
Parasite serology tests/ToRCH	S/P/WB	<i>Toxoplasma gondii</i> IgG/IgM Abs	47,53,73,93,96					14
ToRCH Panel	S/P/WB	ToRCH Panel (TOX, CMV, RUB, HSV-1,HSV-2) Abs	47,53,64,73,74,93					
Sexual Transmitted Diseases (STDs) panel	Vaginal/Throat swab	<i>Neisseria gonorrhoeae</i> Ag	47,54,64,73,77,88,93,96			23		
Sexual Transmitted Diseases (STDs) panel	S/P/WB	<i>Treponema pallidum</i> IgG/IgM/IgA Abs	40,44,47,48,49,52,54,61,67,72,73,74,76,82,83,85,88,90,93,96,108,114					14
Sexual Transmitted Diseases (STDs) panel	Vaginal Swab	<i>Trichomonas vaginalis</i> Ag	45					
Virus Antigen Detection tests	Tear	Adenovirus Ag	51					
Virus Antigen Detection tests	Stool	Adenovirus Ag	40,47,49,50,54,57,58,61,64,66,68,72,74,75,78,80,86,87,88,93,97,104					
Virus Antigen Detection tests	Nasal/Throat swab	Adenovirus Ag	45,68,86					
Virus serology tests	Stool	Astrovirus Ag	44,68,75,86					
Virus serology tests	S/P/WB	Chikungunya virus IgG/IgM Abs	47,49,64,75,79,82					
Virus serology tests/ToRCH	S/P/WB	Cytomegalovirus (CMV) IgG/IgM Abs	47,53,73,93,96					14
Virus serology tests	S	Dobrava-Hantaan virus IgM Ab	110					
Virus serology tests	S/P/WB	Dengue virus IgG/IgM Abs	40,44,47,48,49,52,54,63,64,74,75,79,82,88,93,96,101,114					

Test Category	Sample type	Diagnostic target	LFIA	LOAD	EC	NAT	BG	Other
Virus Antigen Detection tests	S/P/WB	Dengue virus Ag (NS1)	40,54,63,75,79,82,93,101					
Virus serology tests	S/P/WB	Ebola virus IgG/IgM Abs	47,91					
Virus Antigen Detection tests	Stool	Enterovirus Ag (VP1 Peptide)	68,86					
Virus serology tests	S/P	Epstein Barr virus VCA-IgG/IgM Abs	45,54,64,69,71,72,74,75,88,92,101,102,107,112					14
Virus serology tests	WB	Hantavirus IgG/IgM Abs	49,64					
Virus serology tests/Viral liver disease	S/P	Hepatitis A virus IgM Ab	53,64,73,93,96					
Virus serology tests/Viral liver disease	S/P/WB	Hepatitis C virus Ab (anti-HCV)	40,44,47,52,53,54,64,67,69,71,72,73,75,76,79,82,83,88,91,93,114					
Virus Antigen Detection tests/Viral liver disease	S/P	Hepatitis B virus HBsAg	40,44,47,48,50,52,53,54,64,67,69,71,72,73,74,75,76,82,85,88,93,96,114					
Virus serology tests/Viral liver disease	S/P/WB	Hepatitis B virus Panel (HBsAg, HBsAb, HBeAg, HBeAb, HBcAb)	42,47,64,72,73,75,79,83,104					
Virus serology tests/ToRCH/Sexual Transmitted Diseases(STDs)	S/P/WB	HSV 1 IgG/IgM Abs	40,47,73,80,93					14
Virus Antigen Detection tests	Nasal Swab	Influenza A+B (differentiates) Ag	40,44,45,47,49,54,67,68,70,72,74,75,76,77,78,80,86,88,91,92,96,97,103,104,112,114			25,26		14

Test Category	Sample type	Diagnostic target	LFIA	LOAD	EC	NAT	BG	Other
Viral Infection Marker	S/P/WB	Myxovirus resistance A protein	51					
Virus Antigen Detection tests	Stool	Norovirus Ag	40,47,68,75,86,87					
Virus serology tests	S/P/WB	PUUMALA virus IgM Ab	110					
Virus Antigen Detection tests	Stool	Rotavirus Ag	40,44,47,50,54,57,58,61,64,66,68,72,74,75,78,80,86,87,88,93,97,104					
Virus Antigen Detection tests	Nasal Swab	RSV virus Ag	45,47,50,57,61,67,68,72,75,80,86,92,103,112			25		14
Virus serology tests/ToRCH	S/P/WB	Rubella virus IgG/IgM Abs	47,73,93					14
Virus serology tests	S	Tickborne encephalitis virus IgM Ab	110					
Virus serology tests	S/P/WB	Zika Virus IgG/IgM Abs	49					
Virus serology tests/ToRCH/Sexual Transmitted Diseases (STDs) panel	S/P/WB	HSV 2 virus IgG/IgM Abs	47,73					14
HIV treatment Marker	WB	HIV (CD4 Cell Count for treatment determination)	48					
Sexual Transmitted Diseases(STDs)/HIV marker	S/P/WB	HIV 1/2 Abs	40,44,47,48,49,50,54,64,67,69,71,72,73,74,75,76,77,79,82,83,85,88,90,91,93,96,101,104,105,108,114					
Sexual Transmitted Diseases(STDs)/HIV marker	S/P/WB	HIV 1/2 Tri-Line Abs	40,47,53,64,73,74,75,79,82,88,93,96,101					

Test Category	Sample type	Diagnostic target	LFIA	LOAD	EC	NAT	BG	Other
Sexual Transmitted Diseases(STDs)/HIV marker	S/P/WB	HIV 4th generation tests (Ag & Abs)	47,75,79,96,112					
Fungus Antigen Detection tests	Vaginal Swab	<i>Candida spp.</i> Ag	50					
Other	WB	<i>Clostridium tetani</i> anti-toxoid Ab (Immunization status)	72,75,94					14
Other	Vaginal Swab	Sialidase Activity (Bacterial Vaginosis)	45					
Miscellaneous								
Gastrointestinal bleeding Marker	Stool	Transferrin	47,68,93					
Gastrointestinal bleeding Marker	Stool	occult blood (Hb)	40,45,47,54,57,58,60,64,67,68,69,70,71,72,73,74,75,76,77,84,85,92,93,94,96,99,102,104,107,114					16
Gastrointestinal bleeding Marker	Stool	occult blood (Hb/Hp)	44,61,66,70,75,86					
Other	Breast milk	Creamatocrit (optical)			37			

Table 3. Different PoC tests related to SARS-CoV-2 and their manufacturers

Test Category	Sample type	Diagnostic target	LFIA	LOAD	NAT	Other
SARS-CoV-2	Nasal swab, sputum	Ag	20,40,41,48,49,50,51,57,61,63,65,66,67,68,69,72,73,74,78,81,82,83,85,86,91,92,94,96,101,103,105,106,107,109,111,112			14,20
SARS-CoV-2	S/P/WB	IgA, IgG, IgM, total Abs	20,40,47,48,50,52,57,60,61,63,66,67,69,72,73,74,78,82,83,85,86,88,94,96,98,105,106,107,109,113,117	123		14,20
SARS-CoV-2	S/P/WB	Anti-S1/RBD	40,72,73,85,86,94			14
SARS-CoV-2	Nasal swab, sputum	RNA			20,21,22,23,24,25,26,126	
SARS-CoV-2 & Flu A&B	Nasal swab, sputum	Ag	40,67,68,73,103		45	14

Table 4. The list of 125 systems/companies investigated in this work. The reference number corresponds to the biomarker list in table 2.

Reference Number	Company/Product Name	Category	Reference Number	Company/Product Name	Category
1	Optimedical	Blood Gas / Electrolyte analyzer	64	Amgenix	LFIA
2	Cobas-Roche b 121	Blood Gas / Electrolyte analyzer	65	BioGMS	LFIA
3	Cobas-Roche b 221	Blood Gas / Electrolyte analyzer	66	Apacor	LFIA
4	Cobas-Roche b 123	Blood Gas / Electrolyte analyzer	67	Humasis	LFIA
5	Instrumentation Lab	Blood Gas / Electrolyte analyzer	68	Certest Biotech	LFIA
6	Siemens RAPIDPoint 500	Blood Gas / Electrolyte analyzer	69	Futura System	LFIA
7	Nexus - Samsung LABGEO PT10	Other - Clinical chemistry	70	Preventis	LFIA
8	Nexus - Samsung LABGEO HC10	Other - Hematology	71	Sanymed Diagnostics	LFIA
9	Norma Diagnostica	Other - Hematology	72	VedaLab	LFIA
10	Alere Cholestech	Other	73	Atlas Link	LFIA
11	Alere Afinion	Other - Diabetes	74	Dialab	LFIA
12	Alere Hemopoint	Other Hemoglobin	75	Nal von minden	LFIA
13	Siemens DCA Vantage	Other - Diabetes	76	HBI 21	LFIA
14	DIESSE	Other - Immunoassays	77	MH Medical	LFIA
15	OJ Bio	Other	78	Generic Assays	LFIA
16	Accumetrics	Other - Coagulation	79	Jmitra. Co	LFIA
17	Coagusense	Other - Coagulation	80	SAS Scientific	LFIA
18	Diagon	Other - Coagulation	81	Rapigen	LFIA
19	Siemens Stratus CS 200	Other	82	BHAT biotech	LFIA
20	Menarini Diagnostics	Other	83	Intecasi	LFIA
21	Hibergene	Nucleic Acid Testing	84	Lobeck	LFIA
22	NanoBioSys/ Mico Bio	Nucleic Acid Testing	85	Victorch	LFIA
23	QuantumDX	Nucleic Acid Testing	86	Vidia	LFIA
24	Optigene	Nucleic Acid Testing	87	Rimco	LFIA
25	BioCartis	Nucleic Acid Testing	88	Prometheus Bio	LFIA
26	Alere - Alere i	Nucleic Acid Testing	89	Hemaprompt	LFIA
27	BioSys	Electrochemical	90	Biolytical	LFIA
28	Alere INRatio	Electrochemical	91	Orasure	LFIA
29	Abbott i-stat	Electrochemical	92	Quidel	LFIA
30	Siemens Xprecia Stride	Electrochemical	93	Aluxbio	LFIA
31	MagellanDX	Electrochemical	94	Primahometest	LFIA
32	PTSdiagnostics	Electrochemical	95	Rapid Medical	LFIA
33	Cobas-Roche Accutrend	Electrochemical	96	Audit Diagnostics	LFIA

34	Cobas-Roche Coagucheck	Electrochemical	97	EVL	LFIA
35	Alere epoc	Electrochemical	98	Drugcheck	LFIA
36	NovaBiomedical	Electrochemical	99	Teco diagnostics	LFIA
37	EKF Diagnostics	Electrochemical	100	DST Diagnostics	LFIA
38	Urit	Electrochemical	101	BioRad	LFIA
39	Hemocue	Electrochemical	102	Beckman Coulter	LFIA
40	Nanoentek	LFIA	103	Becton dickinson	LFIA
41	Alere / Triage (Abbott)	LFIA	104	Biomerieux	LFIA
42	Technoclone	LFIA	105	Atomo Diagnostics	LFIA
43	Siemens Urinalysis	LFIA	106	Micropointbio	LFIA
44	Dutch Diagnostics	LFIA	107	Clarity Diagnostics	LFIA
45	Sekisui Diagnostics	LFIA	108	IMMCO	LFIA
46	YD Diagnostics	LFIA	109	AB Analytica	LFIA
47	Biocan Diagnostics	LFIA	110	Reagen	LFIA
48	Omega Diagnostics	LFIA	111	Cobas-Roche	LFIA
49	Lumiquick Diagnostics	LFIA	112	Alere Rapid (Abbott)	LFIA
50	Sanyon Diagnostics	LFIA	113	Sugentech	LFIA
51	RPS Diag. / Lumos	LFIA	114	DFI Care	LFIA
52	LabCare Diagnostics	LFIA	115	77 Elektronika	LFIA
53	Spectrum Diagnostics	LFIA	116	Cellmic	LFIA - Devices
54	Cortez Diagnostics	LFIA	117	Abingdon Health	LFIA - Devices
55	MTC InVitro	LFIA	118	Skannex	LFIA - Devices
56	Pro-Lab Diagnostics	LFIA	119	Cobas-Roche Reflotron	LFIA
57	Concile	LFIA	120	Bioscitech	LFIA - Devices
58	Epitope Diagnostics	LFIA	121	ABAXIS - Piccolo Xpress	Lab on a Disk
59	Eurodiagnostica	LFIA	122	Cobas-Roche b101	Lab on a Disk
60	Schebo Biotech	LFIA	123	Biosurfit Spinit	Lab on a Disk
61	Biomaxima	LFIA	124	Nexus - Samsung LabGeo IB10	Lab on a Disk
62	Orgentech	LFIA	125	Nexus - Samsung LabGeo PA20	Lab on a Disk
63	Accessbio	LFIA	126	Cepheid Xpress	NAT

2.5 CONCLUSIONS

In this review, a total of 105 PoC companies have been reviewed as per their technology, design, and target analytes/applications. We identified 5 distinct technological approaches relating to the PoC design configurations and sensing decisions. These are: 1) Lateral flow tests with or without a reader system, 2) Centrifugal systems (Lab on a Disk) with optical sensing, 3) Handheld or small benchtop electrochemical systems 4) Handheld or small benchtop nucleic acid testing systems 5) Benchtop blood gas and electrolyte analysis systems. One thing that immediately becomes evident is that simpler approaches such as standalone LFIA tests or direct electrochemical strip-based systems greatly outnumber more sophisticated systems such as lab on a disk or cartridge based microfluidic devices, presumably because it is a well-established, accessible technology with off the shelf production equipment available for most applications. The rapid development of LFIA diagnostics for SARS-CoV-2 is indicative of the accessibility of this technology. This also becomes evident from the variety of analytes detected by such systems. However clinical biochemistry and hematology measurements, but also all measurements for which the objective is high quality quantitative testing in panels, are mostly designated to more complex systems. It is also evident that from a large pool of fluidic and sensing methodologies reviewed in literature, only a few seem to make their way into commercial applications. Centrifugal microfluidics, capillary microfluidics and active pump-based systems seem to have become the gold standards when it comes to reagent and sample handling. Electrochemical sensing is the prominent detection method for blood gases, electrolytes and metabolites. Immunochromatography, absorbance, reflectance and fluorescence are mostly applied for immunoassays, however there are targets for which both methods are used. In addition, the implementation of user-friendly embellishments (device integrated lancets, modified protocols to allow sample pretreatment in the device) defines a focus point of commercial systems that is seldom seen in research efforts: usability might outweigh technology refinement or even new, groundbreaking principles of operation. Moreover, it is clear that no single approach is better than all others for all settings and all applications. Quantitation, detection limits, and repeatability are important specifications, although it is often the case that an extremely sensitive system with unprecedented resolution might not justify its development costs when examined against its impact in clinical practice. In the specific field of immunoassays, we identify two trends, the lateral flow technology and the automated assay in a device approach. In LFIA it is pretty much established that the vision is a one-step assay for all applications. As such, efforts are being directed into improving the antibody performance, the labels and the instrumented quantification methods. In automated device-based immunoassay PoC systems, the efforts are also directed into assimilating multistep and multiplex lab protocols, with a successful example being the Lab on a Disk. Nucleic acid testing PoC systems are emerging as a highly sensitive and specific method for infectious disease differential diagnosis with the focus being on reagents, the amplification and the detection methodology. The targeted biomarkers of PoC systems are numerous and each has its own impact in a wide range of diagnostic settings: SARS-CoV-2 Ag, antibodies including anti-spike Ab and viral RNA, β -hCG, Tp-I / CK-MB / Myoglobin, fecal occult blood, Helicobacter Pylori, influenza A/B, HIV 1/2, Malaria species and glucose are the most prominent diagnostic targets of PoC. As a concluding remark, it is the authors' viewpoint that innovative and applicable ideas in the field of PoC systems engineering have yet a lot to offer to this field as long as their implementation is realistic and their merits outweigh the effort and cost of their development and production.

CHAPTER 3: A LABORATORY DEVICE FOR IMMUNOASSAY PROTOCOLS

3.1 ABSTRACT

In this chapter, the development of an automated system for bead-based immunoassays is presented. Standard laboratory practices and equipment for bead-based assays are outlined and their challenges and limitations are discussed. The specifications for an automated system for life science and clinical applications are set. System architecture, basic modules and operations are presented and analyzed. A platform is developed combining fluid handling, magnetic manipulation and motion system for microwell plate handling. The platform is presented and basic tests to evaluate its functionality are conducted. Having established basic system functionality, the platform is used for a diagnostic application where SARS-CoV-2 antibodies are quantified in a multiplex assay.

3.2 INTRODUCTION

3.2.1 ASSAY DEVELOPMENT FOR BIOMARKER DISCOVERY

The discovery of biomarkers for existing as well as for novel diseases is of high clinical importance for the early diagnosis, prognosis and monitoring of a pathological condition, as well as for predicting and monitoring therapeutic response. In the second chapter of this work, diagnostic solutions for the point-of-care have been reviewed along with their respective biomarkers or biomarker combinations. However, apart from the adaptation of a diagnostic test for the remote setting, the identification of the biomarker is often the bigger challenge. The multiple steps of the biomarker discovery process have been discussed in literature²²⁹. The unbiased discovery process deals with a large pool of potential targets. Starting from 1000s of analytes with only 10s of samples and gradually moving to 1000s of samples with less than 10 analytes, the process requires different combinations of multiplexing and high-throughput. In the early phases, liquid chromatography with tandem mass spectrometry^{230,229,231} is a tool with the ability to detect multiple different candidate biomarkers in a small number of samples. As the list of candidate biomarkers becomes more narrow and the process more targeted, the need for multiplexing capacity is replaced by the requirement for multiple sample processing. At the final stages of biomarker discovery, an immunoassay, possibly relying on bead-based fluorescent technology, is employed due to the high sensitivity and specificity of the method. In this chapter, an automated device that can perform immunoassays for life science or diagnostics is presented, analyzed and tested in a diagnostic scenario.

3.2.2 LABORATORY AUTOMATION FOR IMMUNOASSAY PROTOCOLS

STANDARD INSTRUMENTS

Laboratory clinical testing as well as life science research practice are based in accurate and repeatable liquid handling at the micro- or nanoliter level. Immunoassay protocols but also other genomics and proteomics assays are based in aliquoting, mixing, diluting, aspirating and dispensing liquid samples and reagents. In laboratory practice, such process steps are performed using manual pipettors, either single or multi-channel (Fig. 3.1). These are piston-based liquid handlers in which the piston travel is adjustable and calibrated. This way, the user can define the aspiration/dispense volume in ranges around 0.1 μ l to several ml, depending on the instrument size. Since it is most often desirable to perform more than one reaction, either because the requirement is high-throughput or several

simultaneous immunoassays or several repetitions of the same assay, the protocols are performed in multiple position components that are called microtiter plates (Fig. 3.1). These are inert, plastic multi-well parts, usually in a 96, 384 and even 1536 position format in a standard size of 127.8 x 85.6 mm. With the 96/384 formats mostly used for immunoassay protocols, the need for high throughput in life science research and diagnostics becomes apparent.



Figure 3.1: On the left are single channel and an 8-channel pipette by Eppendorf. On the right, a standard 96-well plate by NEST.

With the pipettor and the microwell plate being the core components for most assays, additional instruments are typically required, such as shakers and washers (Fig. 3.2). Shakers are used to accelerate diffusion of different species into the microwells or mixing between different reagents, samples and diluents. This is typically achieved mechanically, by placing the microwell plate on an orbital or oscillatory motion system that is moving with a frequency ranging from a few hundred RPM to 10s of thousands RPM. The use of shakers is widespread for volumes over 10-20 μ l, however mixing becomes especially challenging as volumes become smaller. This is because inertial forces at the microscale become less important, while surface tension forces become dominant. Plate washers are used to rinse microwells during process steps. The operating principle of washers relies on two needles that are immersed in each well of the plate. The first needle rinses the well with diluent, while the second needle aspirates the excess volume so that the well does not overflow.



Figure 3.2: On the left is an orbital mixer by SciLogex. On the right is a plate washer by DAS.

Focusing on bead-based immunoassays, the function of mixers and washers can be better understood through Fig. 3.3. Beads are mixed, captured and washed using specially designed equipment in order to perform the necessary steps of an immunoassay.

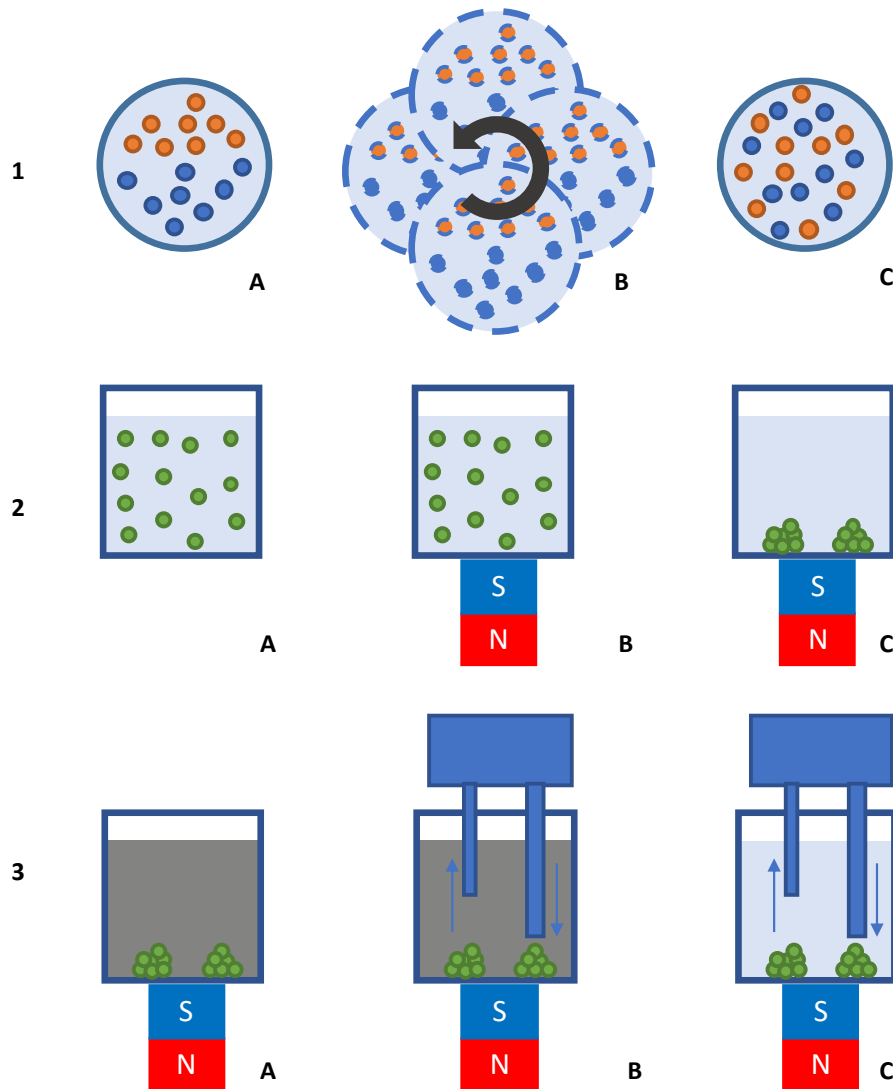


Figure 3.3: The main functions required to perform a bead-based immunoassay protocol are shown graphically. (1) is a mixing step in a microtiter well shown from a top view. The well contains reagents and microbeads that are mixed using orbital shaking (1B). In bead-based immunoassays, the separation of the magnetic particles from the solution is required. In (2) a microtiter well shown from a front view has several microbeads dispersed within its volume. Placing a permanent magnet on the bottom of the well will cause the microbeads to temporarily adhere to the bottom. This way, a microplate washer can be used (3). The microplate washer includes an inlet and an outlet for buffer solution which work in parallel until the original solution has been diluted to the point that it is considered completely replaced by buffer solution. The magnetic microbeads remain trapped from the magnet and thus avoid being aspirated from the inlet channel.

AUTOMATED PLATFORMS

In diagnostic or life science scenarios it is often required to test 100s or 1000s of samples for a single or multiple analytes. In this case immunoassay protocols cannot be performed manually. In life science research, drug discovery and diagnostics, automatic liquid handling is an essential tool²³². While not often reviewed in literature, laboratory automation is an enabling technology which has allowed the scaling up of research and diagnostics to tens of thousands datapoints per assay or more. The requirements for high precision and accuracy, high throughput and low sample/reagent volumes have led to the development of automated liquid handling platforms by several manufacturers.

A typical liquid handling platform such as the one seen in Fig. 3.4 consists of a cartesian 3-axis motion system and a pipetting module which performs the liquid handling (also called a pipette head). The pipetting module usually includes one or more automated syringe pumps which may be moving on motion axes, or they can be stationary but hydraulically connected to pipette tip adapters on the travelling effector. In Fig. 3.4-C, a standalone syringe pump module by Tecan can be seen. These modules are mounted on a fixed position inside the platform and a liquid-filled tube connects them with the pipette tip adapters. The pipette head can move over the platform work area where microtiter plates, reagent and sample tubes as well as waste and cleaning positions can be found. In the most common case, the pipette head consists of 8 or 12 liquid handling channels. For a 96-well format, the pipette head will need to continuously load and unload pipettes so that there is no cross-contamination between the wells. For this reason, 96 channel pipette heads also exist that allow simultaneous processing of the entire plate. Using the pipette head and the motion system, aspiration and dispensing of ml / μ l volumes can be moved from plate to plate or aliquoted from larger containers to microwell plates. However, just like for the manual liquid handling, additional modules are often required to complete diagnostic/life science assays. For example, washing modules and shakers can be embedded inside the work area. For the special case of magnetic microbead assays (Refer to Ch. 1), a magnetic trapping module (Fig. 3.4-B) is required to work together with the blade washer.

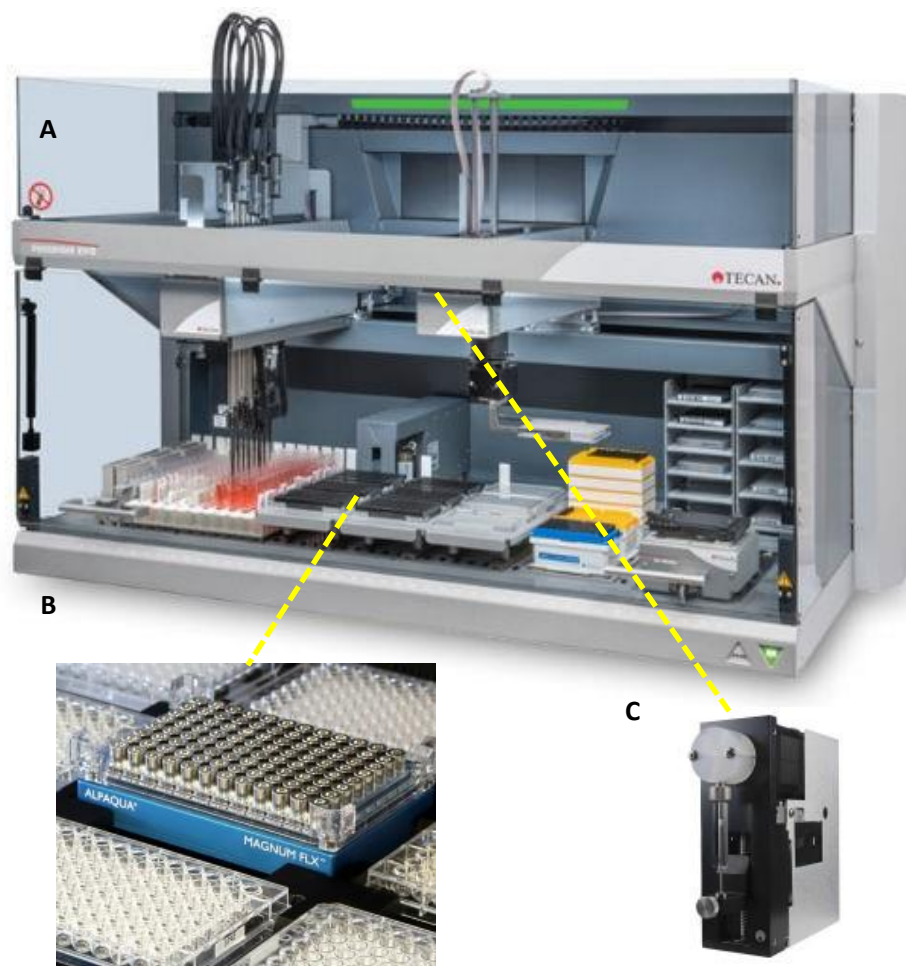


Figure 3.4: (A)²³³Freedom Evo by Tecan is a liquid handling automation system with different configurations that are intended for diagnostic and life science applications. Syringe pumps (C)²³⁴ are stationary but hydraulically connected to the travelling pipette tips. (B)²³⁵ Different modules can be used for different applications, for example a magnetic plate by Alpaqua is used for magnetic bead-based assays.

To better understand the modules of a typical liquid handling platform, a simplified configuration has been prepared in Fig 3.5. A pipetting head (A) is seen mounted on a 3-axis motion system. In this configuration, the pipetting head consists of a single syringe pump on which the pipette tip is attached directly, i.e., the syringe pump is moving on the motion axes. On other configurations, more syringe pumps might be used either moving or stationary, operated by a single actuator or independent from one another. The pipetting head needs to load pipetting tips which can be found in position (B) in a typical 96-format pipette tip box. Since only one syringe pump is available, the pipette head will need to unload the old tip and load a new one when moving from well to well. In some configurations the tips may be washed between steps using an ultrasonic bath. In (C), tubes containing reagents, samples or buffers are located. From there, the pipette head will aspirate the required quantity and distribute it to the reaction wells of the microtiter plate (D) which in turn may already contain different samples or assay reagents. The reaction will commonly take place using some mixing strategy, either with the aid of a plate shaker or by consecutive aspiration and dispensing steps from the pipette head. Finally, a plate washer such as the one seen in (E) may be required in between steps to facilitate assay protocols. If the assay is based on magnetic beads, then the washer will also need to have an embedded magnetic separator or a filter plate for a washing through strategy (see Fig 3.3-2&3). In most

platforms, waste stations such as the one seen here in (F) are included. In these stations, waste products from the assays as well as pipette tips can be disposed from the pipette head

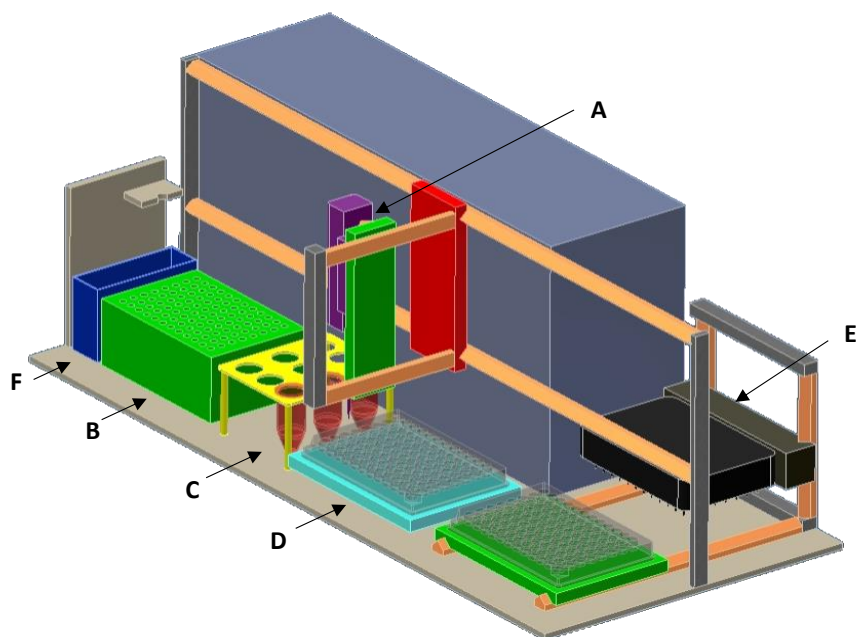


Figure 3.5: A simplified configuration of a typical liquid handling platform. (A) Pipetting head, (B) Pipette tip loading station, (C) Reagent station, (D) Microwell plate, (E) Microwell plate in washing station, (F) Waste station.

3.2.3 STATE OF THE ART LIMITATIONS

The current state of the art in laboratory automation extends from robust robotic platforms for clinical settings to highly versatile systems for life science research where manufacturers such as Agilent²³⁶, Tecan²³⁷ and Hamilton²³⁸ are offering configurable systems for applications such as cell culture, Immunoassays, protein purification, PCR and several others. The field is very wide with many available solutions and technical approaches often tailored for individual applications. In this work, the method of focus is magnetic bead-based ELISA for life science applications or diagnostics. As such, any attempt to identify technology limitations or challenges only aims at configurations relevant to this method. On this basis, there are 3 main dimensions that are critical for bead-based ELISA protocols and create room for improvement:

1. Efficient handling of beads
2. Process stability when reagent/sample volumes decrease
3. Automation simplicity and device footprint

Efficient handling of beads refers to the ability of the platform to magnetically manipulate the microbeads during and between process steps. Bead-based sandwich ELISA, when compared to traditional sandwich ELISA where the reaction takes place on immobilized antibodies on the well bottom, has the added requirement of bead immobilization or release into the solution. However, this also requires the use of permanent magnets below the microwell bottom or the inclusion of a full plate washer with a magnetic module inside the platform. Integrating the trapping system into the platform is not trivial since an additional mechanical motion is usually required that will

either move the magnets away from the plate or the plate away from the magnets. This may require custom solutions for each platform further complicating the assay automation process.

Process stability with decreasing immunoassay volumes is an important dimension in assay development and automation. Often, the minimum volume of reagents or samples that can be used in an immunoassay is driven by the liquid handling capabilities. Lowering the assay volume is almost always desirable because of the several benefits that come with it: decreased assay cost, faster reaction times and the ability to use larger plate formats (ex. 384 well plates). However, as volumes move more into the microfluidic realm, mixing through orbital shakers becomes increasingly more difficult and surface tension forces can create significant challenges. Pipetting also becomes more challenging and the possibility of bubbles due to aspiration of air increases.

Automation simplicity is a requirement for immunoassay applications. In the case of bead based immunoassays, the automation options mostly come from highly versatile fluid handling platforms such as the freedom EVO²³⁷ which can be adapted to embed several additional modules, for example plate washers, magnetic modules and even plate readers. However, this may require increased customization and development of modules adapted to fit a commercial fluid handler. The need to fit additional modules into an already existing platform results in high footprint systems with increased complexity in their programming and functionality.

The present work deals with the development of a system that is optimized for bead-based immunoassays and can provide novel, technical solutions to the aforementioned limitations.

3.2.5 OBJECTIVES

As seen on the previous analysis, a system that could function as an assay development tool or diagnostic tool and that could bridge the laboratory assay process and the Point of Care process could contribute to the faster development of diagnostic assays, assist the biomarker discovery process and be used as a large scale PoC tool for diagnostic. The main functions that are required to perform a bead-based immunoassay have been analyzed and the standard laboratory automation to perform these tasks has been presented. For the case of bead-based immunoassays, specific dimensions that have significance for the performance and scalability of the assay have been discussed. Based on these dimensions, the development objectives of a novel bead-based immunoassay liquid handling platform could be defined:

1. Compatibility with bead-based immunoassay technology
2. Small footprint
3. Ability to employ magnetic trapping methods for superparamagnetic microbeads
4. Ability to perform aspiration, dispensing and mixing operations for microliter volumes
5. Ability to perform washing operations
6. Compatibility with laboratory practices and formats, for example the use of 96-well plates and standard pipette tips
7. Fully automated system with no need for user intervention for the completion of the assay
8. Fully programmable in a conceptually uncomplicated way

3.3 METHODS

3.3.1 PLATFORM OVERVIEW

Based on the previous analysis, several objectives have been set in the form of functions and compatibilities that an automated system should have in order to be able to be used as an assay development tool and as a diagnostic system. The main reasoning and concepts behind such a platform have been analyzed in the diploma thesis of the author²³⁹. In that work, concept architectures were proposed and discussed. In this work, the completed system (Fig 3.6) will be presented and discussed. The platform has been named SampleX combining the word “Sample” and the letter “X” from the Xmap technology which is the most prominent bead-based immunoassay tech during the platform’s development.

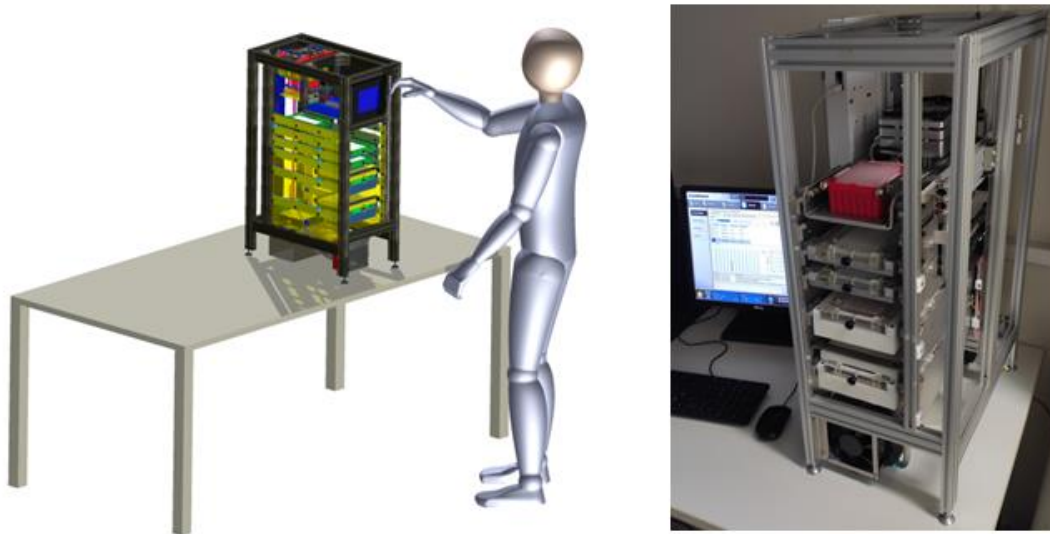


Figure 3.6: The automated platform which was named SampleX was designed to perform fluid handling operations and magnetic trapping of microbeads for ELISA protocols. On the left is a 3d model of the system, on the right a photo of the actual system

The system consists of three main parts (Fig. 3.7):

1. The fluid/microbead handling head
2. The motion system
3. The sample/reagent plate carriers

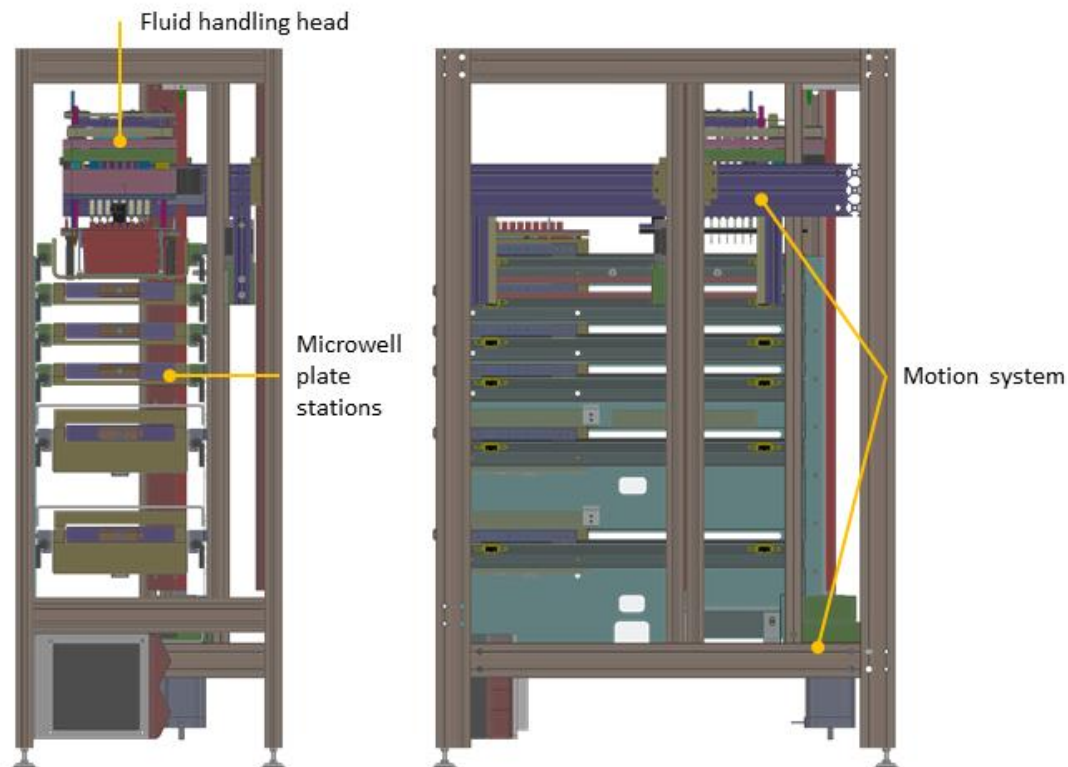


Figure 3.7: The main components of the platform are the head, the motion system and the microplate carriers

In part, the platform concept is similar to commercial fluid handling robots. The fluid handling head is positioned over the sample plates using a motion system. The sample/reagents are metered, aspirated and released by the fluid handling head in order to perform the experimental protocol. However, additional ideas are employed to tailor the platform's functionality to bead-based immunoassay protocols. The different ideas employed to match the required objectives are listed and analyzed below:

1. Stacked plate architecture
2. A fluid handling head with a 96-tip design for high-throughput
3. Magnetic trapping within the pipette tip
4. Washing through the pipette tip

STACKED PLATE ARCHITECTURE

The standard architecture for a fluid handling robot like Tecan Freedom Evo includes a worktable space with an overhanging XYZ motion system onto which the fluid handler is mounted. The reagent and sample plates are placed on the worktable and the robot is programmed to perform the experimental protocol. The fluid handler is typically an 8-channel or 96-channel pipette head which is positioned over the microtiter plates and can aspirate or release reagents and samples in microliter quantities. This format is highly flexible and allows for many different configurations. Different modules such as plate shakers and magnetic bead separators can be embedded in the platform which makes it suitable for multiple applications. The drawback from this design is that the work envelope can result in a large system footprint. Also, the need of accurate alignment of the fluid handler with the plates necessitates a closed loop motion system.

The proposed architecture relies on a stacked plate format where plates are placed one on top of another (Fig 3.8). Each plate lies on its own slide and can be moved in (towards the fluid handling head) or out (towards the user). The motion system has 2 axes, a Z motion for the head to move to the position of each microtiter plate and a Y motion which pulls the plate in towards the fluid handling position. This allows for a much smaller footprint than commercial fluid handling robots and at the same time simplifies the operation of the system since only two positions exist for any plate: the “user” position when the plate is on the outer side of the platform and thus accessible by the user and the “head” position when the plate is below the fluid handling head and can be processed. A typical sequence can be seen in the Fig 3.8: In frame A the fluid handling head (purple) is on the top position and all the plates (blue) are on the user side. In B, the head is moving downwards to the position of the first plate. The Y end effector (green) grabs the first plate handle and in frame C the plate is pulled below the head. In D, the head moves downwards for the pipette tips to reach within the microtiter plate wells. In this position the liquid handling steps and magnetic manipulation of microbeads take place. When this is complete, the head and Y end effector move to the previous position (D) to grab the plate and in (E) it is returned to its original position. The above process can be repeated for each of the 6 plate positions in order to complete an immunoassay protocol.

The benefits of this format over the standard XYZ architecture is a reduced platform footprint since the work envelope is much smaller. The first version that has been developed has a footprint of 300 x 500 x 800 mm (XYZ) whereas a standard small format automated fluid handler is close to 4 times that in X and 2 times in Y. An additional benefit of this format is that the user and head positions for each plate are terminal positions and no intermediate positions exist that need to be attained as part of the system’s normal functionality. This, in combination with contact switches both for the plate positions and the contact of the head with each plate, allows the use of stepper motors with open loop controls for all motion axes and a simplified automation strategy that does not rely in precision positioning. The Y axis effector moves the plate from the user to the head position. There, the fluid handling head is aligned with the plate and can perform the various processes. This can be viewed in more detail in Fig 3.9, where essentially the same steps described in Fig 3.8 can be seen performed by the platforms head (Z) and plate (Y) motion subassembly mechanism. In 3.9 D the Y effector has captured a plate and brought it in to the head position. Locating pins are used for final plate alignment which can be seen in a magnified view. In 3.9 C, the Y effector has moved below the gripping point of the plate and the plate is now aligned using the locating pins.

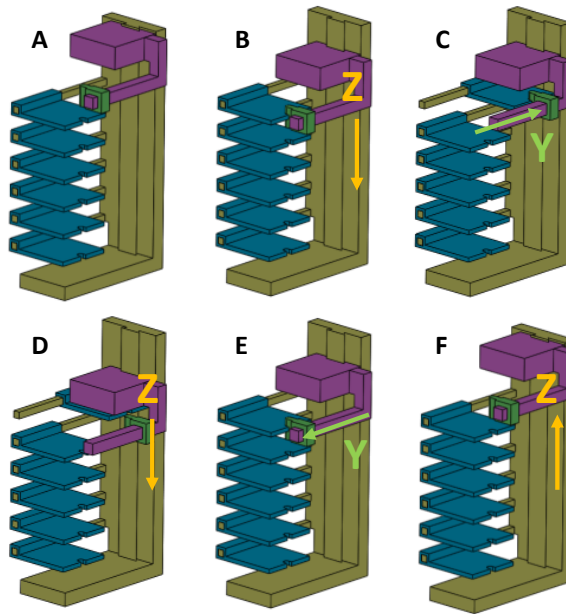
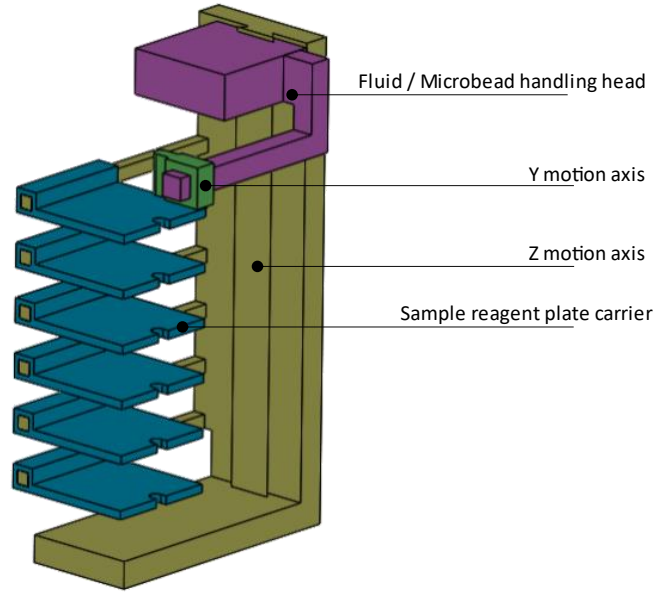


Figure 3.8: A simplified depiction of the SampleX platform logic. Plates (blue) are pulled inwards by a Y effector (green) towards the liquid & microbead handling head (purple). The platform is based on a 2 axis motion system where plates are either at an outward (user) position or inward (process) position.

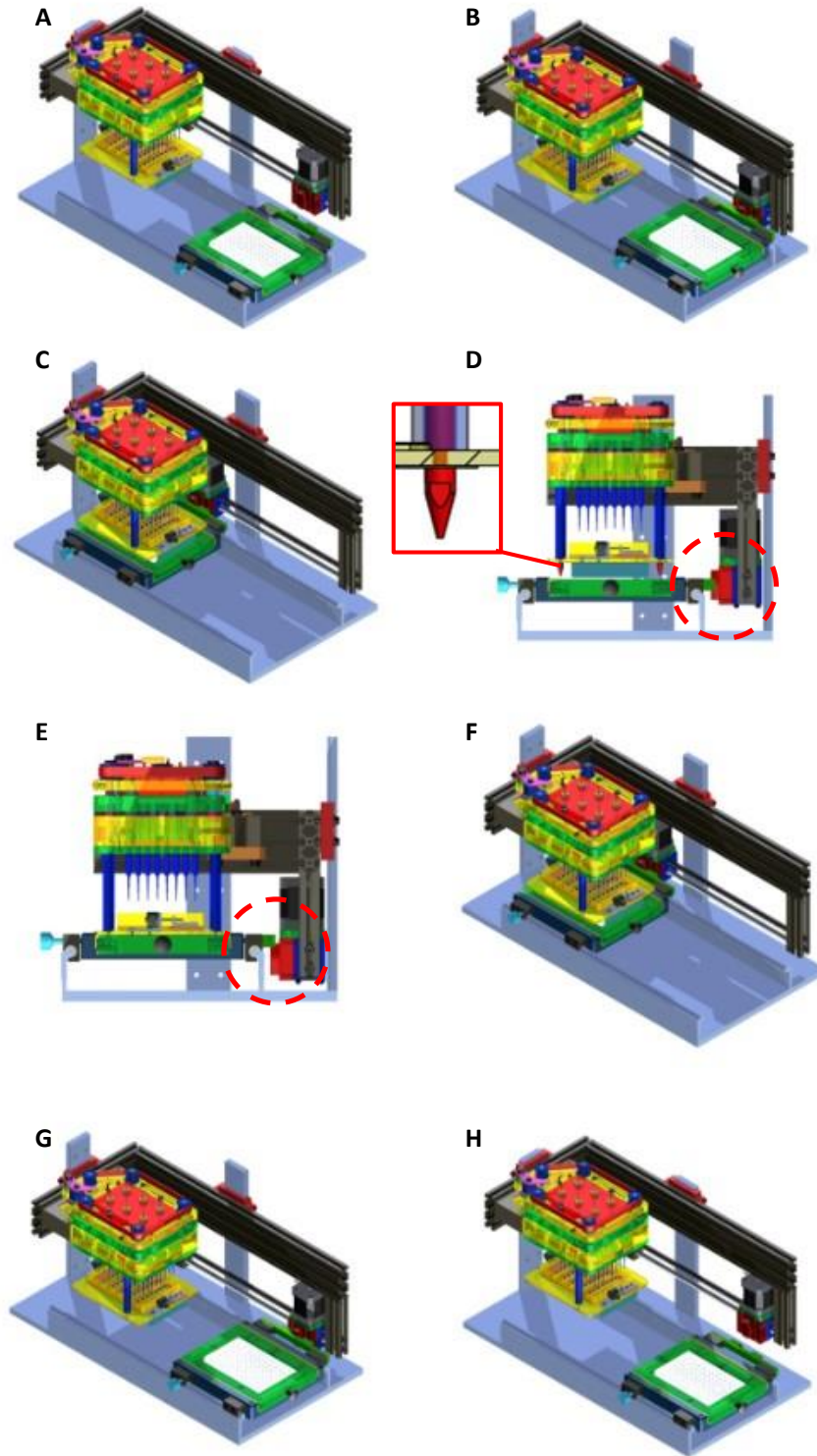


Figure 3.9: The process of capturing, moving and aligning a microtiter plate within the SampleX platform. The steps are the same as in the previous figure and the role of the alignment pins can be seen in positions D&E.

3.3.2 FLUID HANDLING SYSTEM DESIGN

Fluid handling in life science automation typically requires precision metering of low viscosity liquids for transfer between microtiter plates, tubes and other liquid containers. The standard functions for fluid handling system are aspiration and dispensing. Depending on the application the volumes that need to be transferred range from 1-2 ml down to nl. For laboratory suspension immunoassay applications, a typical range is 1-100 μ l. The fluid handling system of the platform was designed for that range in a 96-well format.

The standard operating principle for precision aspiration and dispensing are plunger-based pumps like the Cavro syringe by Tecan which is seen in Fig. 3.4. These pumps operate just like a plain syringe. The plunger is moved using a linear actuation system such as a leadscrew or a ballscrew. The plunger tip is typically manufactured from a low friction plastic, for example PTFE, while the syringe sleeve is usually made from borosilicate glass. A three-way valve is sometimes used to allow the pump to handle larger volumes by resetting the plunger position while the flow channel is isolated.

The liquid handling system of SampleX follows the same operating principle with multiple plungers being actuated together. In Fig. 3.10, a section of the liquid handling head is shown. The plungers are sliding in the pump sleeves to aspirate or dispense liquid volumes in and out of the pipette tips. The sealing between the plungers and the sleeves is achieved using two EPDM o-rings. In order to maintain a low friction between moving parts, PTFE tubing with a \varnothing 3.5 mm ID was used for the sleeves. The plungers are mounted to a main actuated plate which moves upwards for aspiration and downwards for dispensing. The fluid handling heads includes a plate with adapters sized for disposable 20 μ l pipette tips. For each pipetting position, a washing channel is included. The outlets for washing buffer that can be seen in Fig. 3.10 are 26S needles (\varnothing 130 μ m ID) connecting each channel with a main washing buffer container. The washing container needs to be primed with buffer before any pipetting operation takes place. Due to the small gauge and the length of the needles, there is significant pressure drop across their length. This allows aspiration and dispensing to happen without drawing buffer from within the washing circuit. In order to perform washing, assay buffer is pumped to the container using an external peristaltic pump. The washing buffer is pumped from the needle into the pipette tip and then towards a waste container on the lower part of the platform. Once the washing process is completed, a quantity of washing buffer remains in the pipette tip and needs to be emptied using the plunger. In summary the fluid handling system has been designed in order to perform the following functions:

- Fluid aspiration by moving the actuated plate upwards
- Fluid dispensing by moving the actuated plate downwards
- Flow-through washing by pumping washing buffer through the pipette tips
- Fluid mixing by oscillating the actuated plate upwards and downwards continuously

Going back to Fig. 3.2, the fluid handling system in this case also performs the function of a microplate mixer and the function of a plate washer.

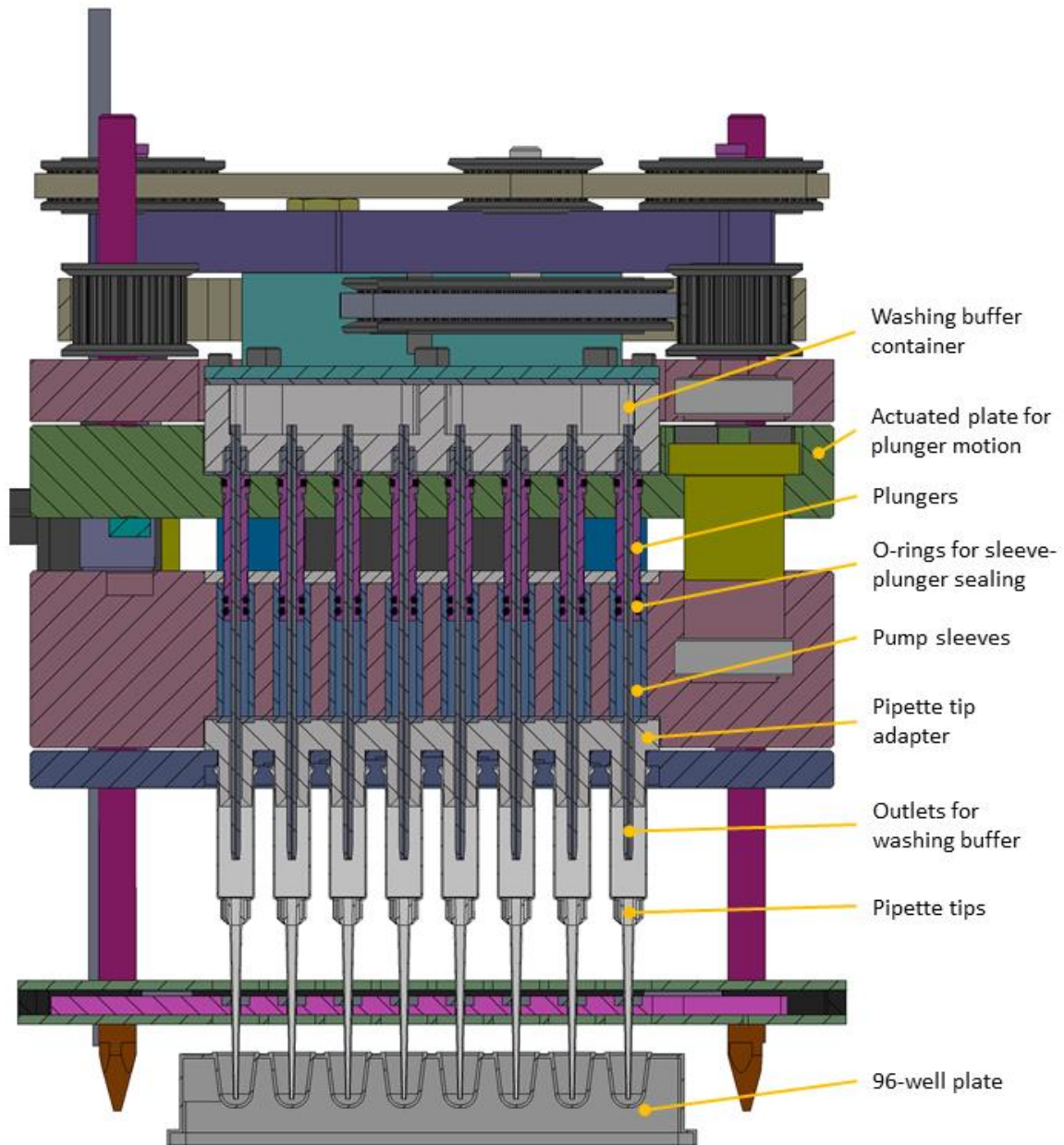


Figure 3.10: A section view of the fluid handling head. The components participating in the fluid handling operations are noted.

The arrangement with the flow through washing system, while very similar to commercial washing systems for bead-based applications, can become a source of error when combined with a pipetting system, for example if a pipette tip becomes blocked during an aspiration step or if the washing buffer flow through one of the needles is obstructed. For this reason, a second arrangement for the fluid handling system exists (Fig. 3.11) in which the washing through capability is not used and the washing buffer container is replaced with a sealing plate that isolates each channel from the rest. In this arrangement the washing buffer outlets are not used and washing steps are done using buffer-containing microtiter plates. This arrangement will be used throughout for the experimental section of this work.

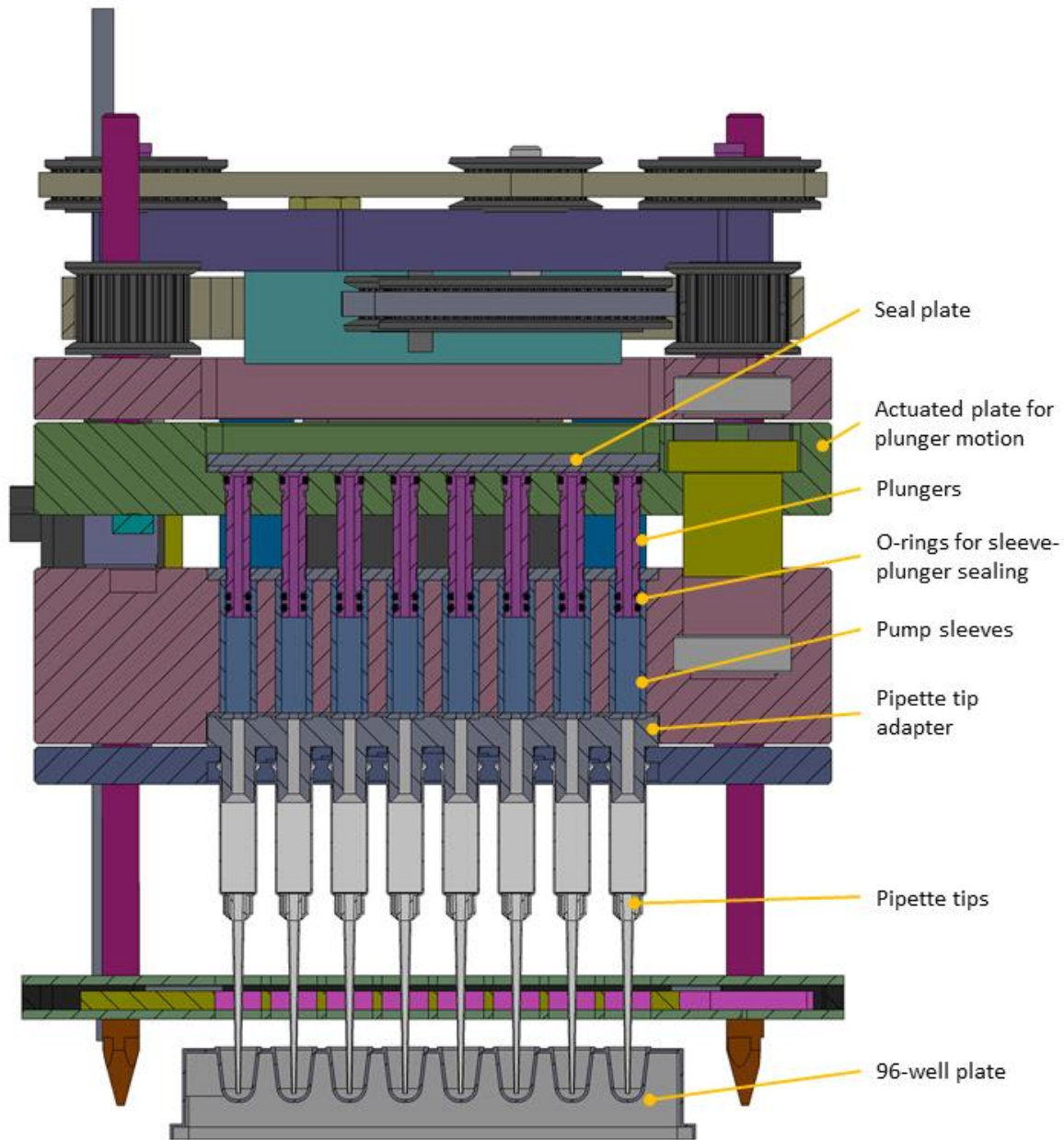


Figure 3.11: A section view of the fluid handling head showing an arrangement without washing-through capabilities.

The motion system of the fluid handling module is presented in Fig. 3.12. The main plunger plate is moved upwards and downwards using two leadscrews which are located diagonally on two out of its four edges. The leadscrews are rotated using a timing belt which is driven by a stepper motor mounted on the head's top plate. In total, there are five timing pulleys participating in the motion system: One driving pulley, two pulleys which are mounted on the leadscrews and two idler pulleys. The shafts on which the idler pulleys are located are also used for the mounting of linear ball bearings on which the actuated plunger plate is sliding during its vertical motion. For an S3M driving pulley with a 1:1 transmission ratio and a leadscrew with 2 mm pitch, the calculated resolution of the vertical motion axis

is 10 μm for a full step of the motor (standard 200 steps/rev). This, combined with the sleeve's internal diameter, yields a volumetric resolution of 0.1 μl for the motor's full step.

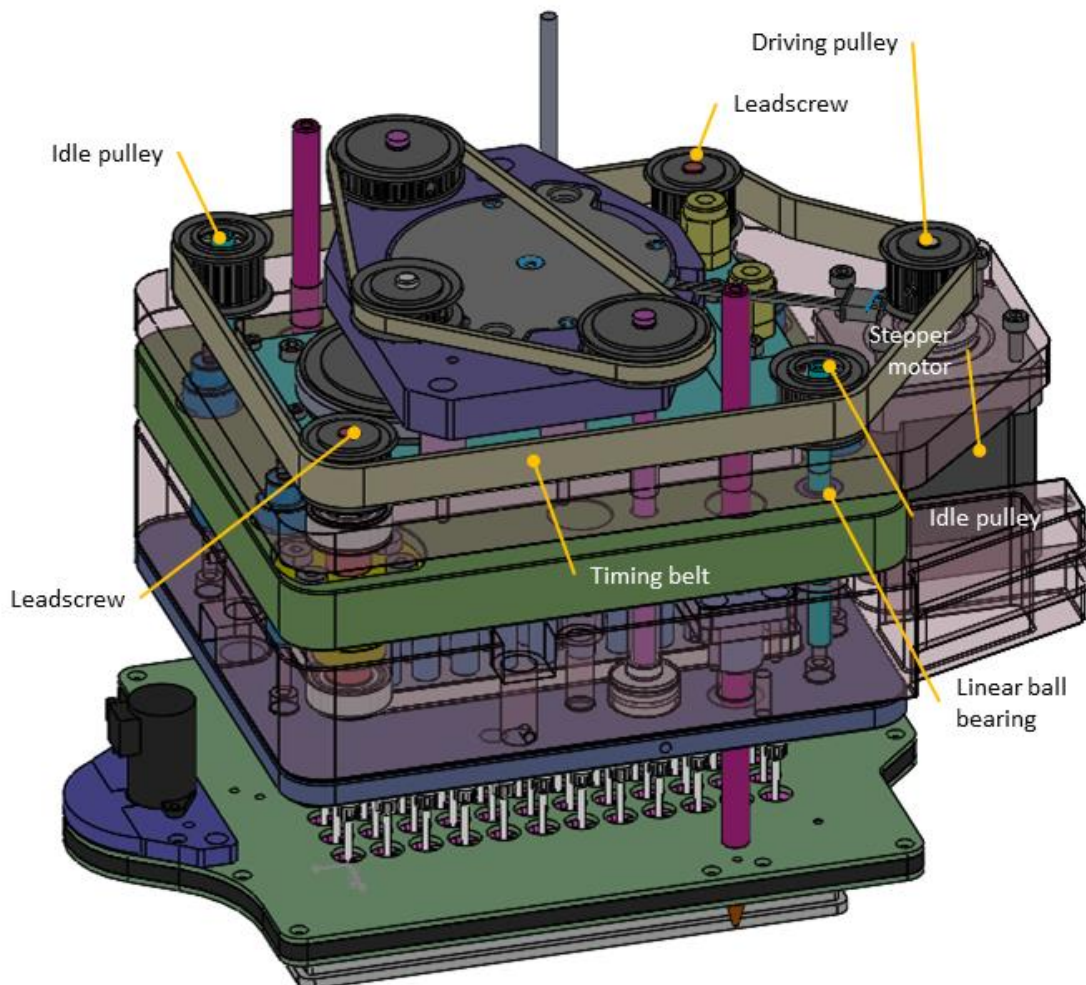


Figure 3.12: The motion system for the fluid handling operations. A driving pulley rotates two leadscrews which move the main plunger plate in the vertical direction.

In summary, the fluid handling system of the SampleX platform includes 96 plunger-based pipettes which operate in parallel with a resolution of 0.1 μl . The key functions of this module are aspiration and dispensing, mixing and washing. Two different arrangements exist, one with a washing through module in which washing buffer is directly run into the pipette tips and a simpler one in which the washing is not performed automatically but needs to be done using a washing buffer containing a microtiter plate. A prototype fluid handling head can be seen in Fig 3.13.

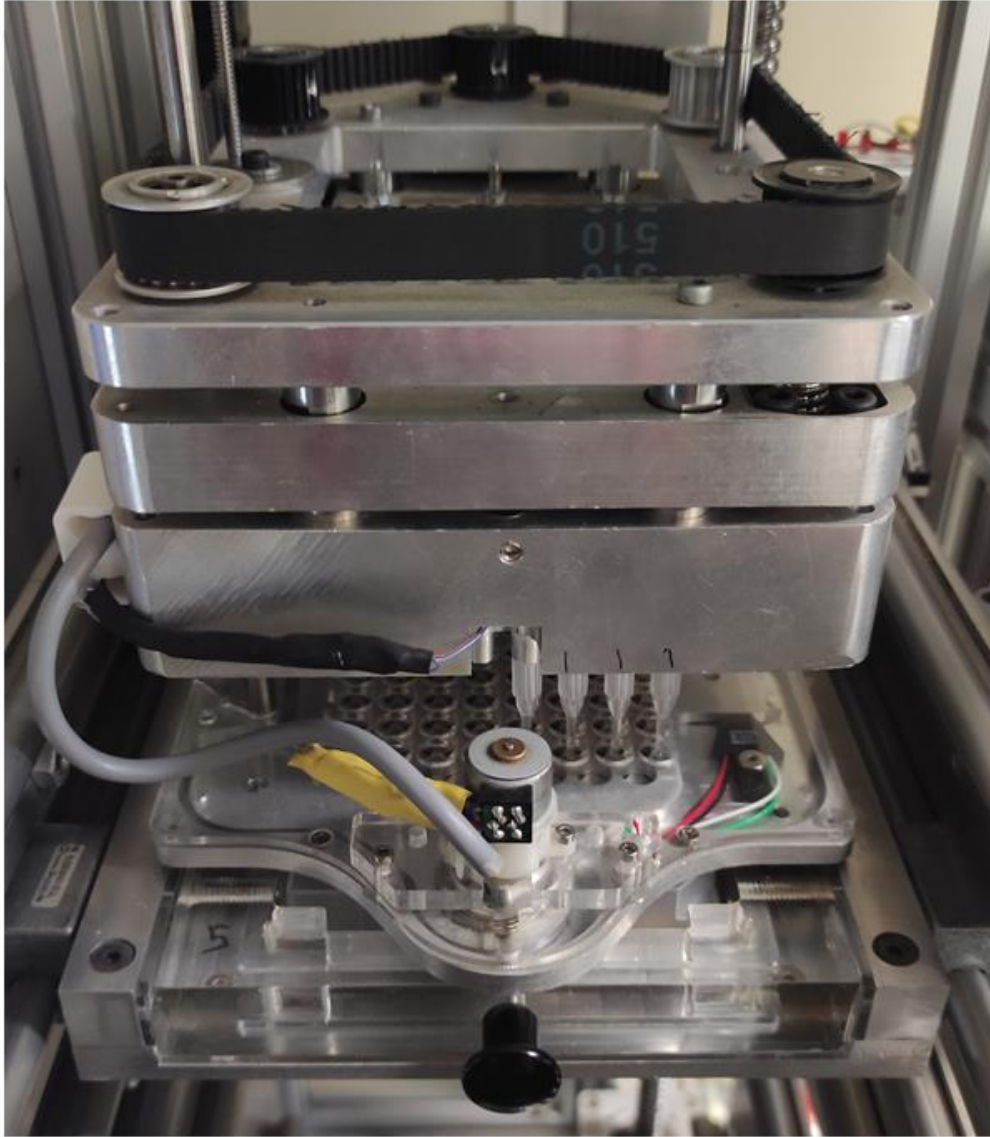


Figure 3.13: A prototype of the fluid handling head used in the SampleX platform during an assay

3.3.3 MAGNETIC SEPARATION SYSTEM DESIGN

Magnetic separation of superparamagnetic microbead for immunoassays is typically achieved using strong permanent magnets to attract the microspheres towards a physical barrier. The objective is to exert a magnetic attraction force that is stronger than the fluid flow or other forces that will be applied during assay steps such as washing or aspiration. While stationary magnetic separation modules usually rely on large block magnets, this is not possible for the configuration that is attempted in this work. For this reason, alternative designs have been explored, modeled and tested.

MAGNETIC SEPARATION SYSTEM CONCEPT

The magnetic separation procedure in an automated system requires that a permanent magnet is manipulated so that microbeads can be trapped or released depending on the requirement of the process step. In bead-based assays, this is typically achieved using a magnet plate such as the one seen in Fig. 3.4B. The solution containing the microbeads which need to be separated, is dispensed in a standard microtiter plate. The microtiter plate is then placed on a magnetic separation plate. When the microbeads settle on the bottom of the plate drawn by the attractive magnetic force, the liquid solution is removed using aspiration or simply by emptying the entire plate by turning it over. The plate is then refilled with a different reagent or a washing buffer. This process requires the use of a separate magnetic plate as well as fluid handling steps to move the beads from plate to plate whenever a separation step is required. An alternative method is proposed here, in which the beads are trapped within pipette tips. Using this approach, the process can potentially be simplified by turning the pipette tip into a reaction site. By doing so, the need to transfer reagents and buffers between plates is removed. This greatly simplifies the protocol required to perform an immunoassay in an automated environment. The concept can be seen in Fig 3.14, where initially a bead-containing solution is aspirated using a pipette tip. A permanent ring magnet is then placed around the pipette tip, which results in the microbeads being drawn towards the magnet and eventually trapped on the inner pipette tip walls. Once the beads have been immobilized, the solution can be dispensed leaving only the microbeads in the tip. If necessary, a washing step can take place using an additional buffer-containing plate or the fluid handling head's washing system (see previous section). Following that, the protocol can continue by aspirating the sample, the secondary Ab and finally the label substance while the beads remain in the pipette tip. The comparison of the proposed process against a conventional protocol for bead-based assays can be seen in Table 3.1 with plates A to E corresponding to the reagents used for a bead-based sandwich ELISA immunoassay. Compared to the current state of the art, the proposed method requires less actions for each assay step while the different stations-equipment required, have been replaced by the fluid handling head.

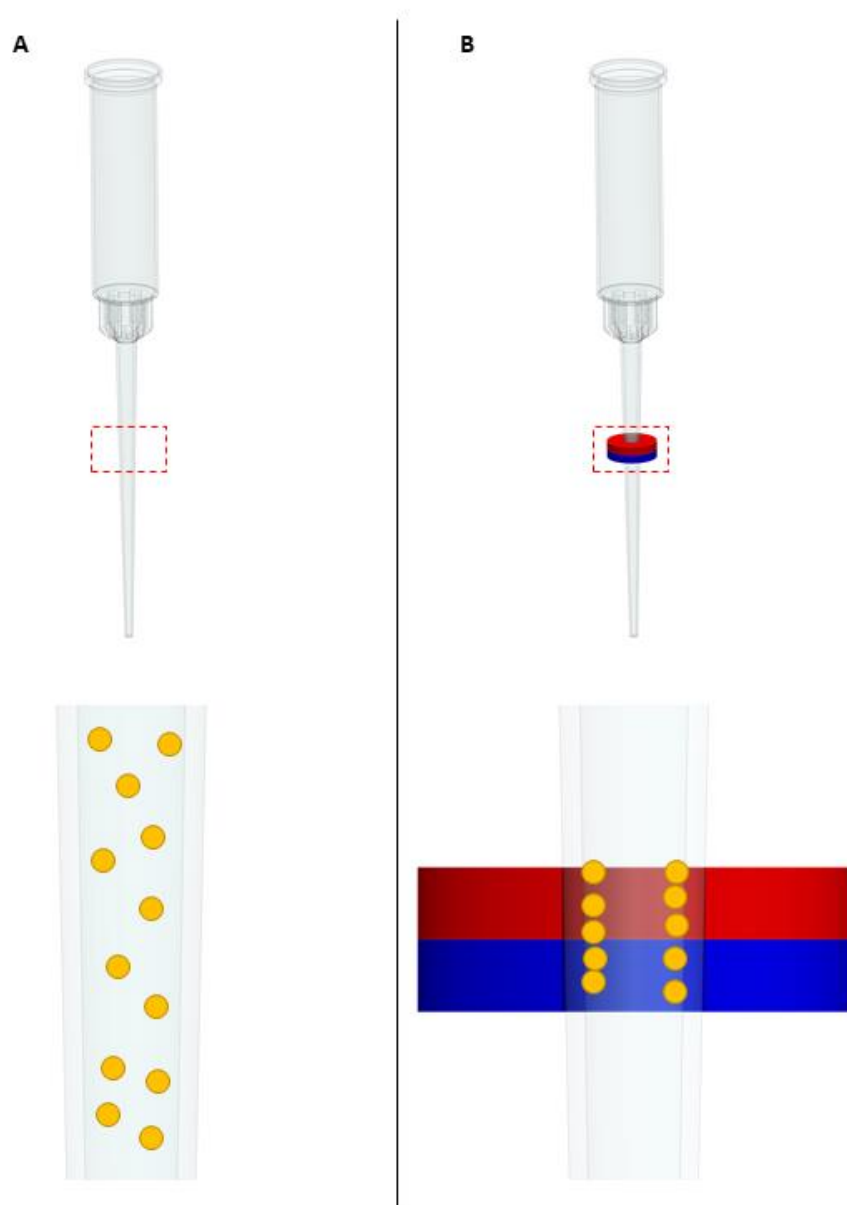


Figure 3.14: A microbead separation approach is proposed in which the bead trapping happens within the tip. In (A) a bead-containing solution is aspirated and the beads are suspended in the pipette tip. In (B), a permanent magnet is placed around the tip which attracts and eventually traps the microbeads. Once the microbeads are immobilized, the rest of the solution can be disposed of in its original plate

Assay step	Standard process - Action	Standard process- Station	SampleX process - Action	SampleX process- Station
Introduce Sample	1. Separate beads	Magnet plate	1. Dispense solution – retain beads	Fluid handling head
	2. Aspirate solution	Fluid handler & magnet plate	2. Aspirate sample	Fluid handling head
	3. Wash	Washing system with magnet plate	3. Pipette up & down for incubation	Fluid handling head
	4. Move sample from plate B to plate A	Fluid handler		
	5. Incubate	Mixer		
Introduce secondary Ab	1. Separate beads	Magnet plate	1. Dispense solution – retain beads	Fluid handling head
	2. Aspirate solution	Fluid handler & magnet plate	2. Aspirate contents of plate C	Fluid handling head
	3. Wash	Washing system with magnet plate	3. Pipette up & down for incubation	Fluid handling head
	4. Move Ab from plate C to plate A	Fluid handler		
	5. Incubate	Mixer		
Introduce label	1. Separate beads	Magnet plate	1. Dispense solution – retain beads	Fluid handling head
	2. Aspirate solution	Fluid handler & magnet plate	2. Aspirate contents of plate D	Fluid handling head
	3. Wash	Washing system with magnet plate	3. Pipette up & down for incubation	Fluid handling head
	4. Move label from plate D to plate A	Fluid handler		
	5. Incubate	Mixer		
Prepare for reader	1. Separate beads	Magnet plate	1. Dispense solution – retain beads	Fluid handling head
	2. Aspirate solution	Fluid handler & magnet plate	2. Dispense beads on plate E	Fluid handling head
	3. Wash	Washing system with magnet plate		
	4. Move buffer from plate E to plate A	Fluid handler		

Table 3.1: Standard vs SampleX bead-based immunoassay preparation process and required process stations. Plates used for this example: A: Microbeads with primary Ab, B: Sample & standards, C: Secondary Ab, D: Label (Streptavidin-PE), E: Buffer solution

The development of a system that allows the introduction and removal of permanent magnets on 96 positions simultaneously requires the design of a magnet plate with an arrangement of magnets. In order to be able to switch in and out of the separation mode, the magnet plate, driven by a stepper motor, aligns with the pipette tips in two distinct positions: A position where 96 magnets are aligned with the tips and a position where through holes are aligned with the tips. The functionality of this submodule can be seen in Fig 3.15. The magnet plate can move upwards and downwards so that the magnets can be placed around the pipette tips. Moving at the upper position (A) the magnet plate is brought at the pipette tip level, while moving at the lower position (B) the magnet plate is no longer interfering with the pipette tips. At the same time, the entire magnet plate can perform a translation on a cyclic path which switches between the magnets on (C) and the magnets off (D) positions. The magnets-off position is an array of 96 holes on the magnet plate which are offset at 180° from the magnet positions on the cyclic translation path of the plate. These holes are larger than the largest diameter on the pipette tip, so when the magnet plate is moved at the uppermost position, pipette tips can be loaded and unloaded through the plate.

In summary, the magnetic separation system of the fluid handling unit includes a magnetic plate which can move upwards or downwards and switch between a magnets-on and a magnets-off position. The purpose of these motions is to use permanent magnets to separate microbeads from their carrier solution and subsequently release them into other positions according to the immunoassay protocol. The purpose of this 2-axis design is to be able to perform bead separation in a fully automated platform without the need for auxiliary equipment and multistep processes such as the ones typically used in conventional bead-based immunoassays. A prototype of the magnetic separation system can be seen in Fig. 3.16.

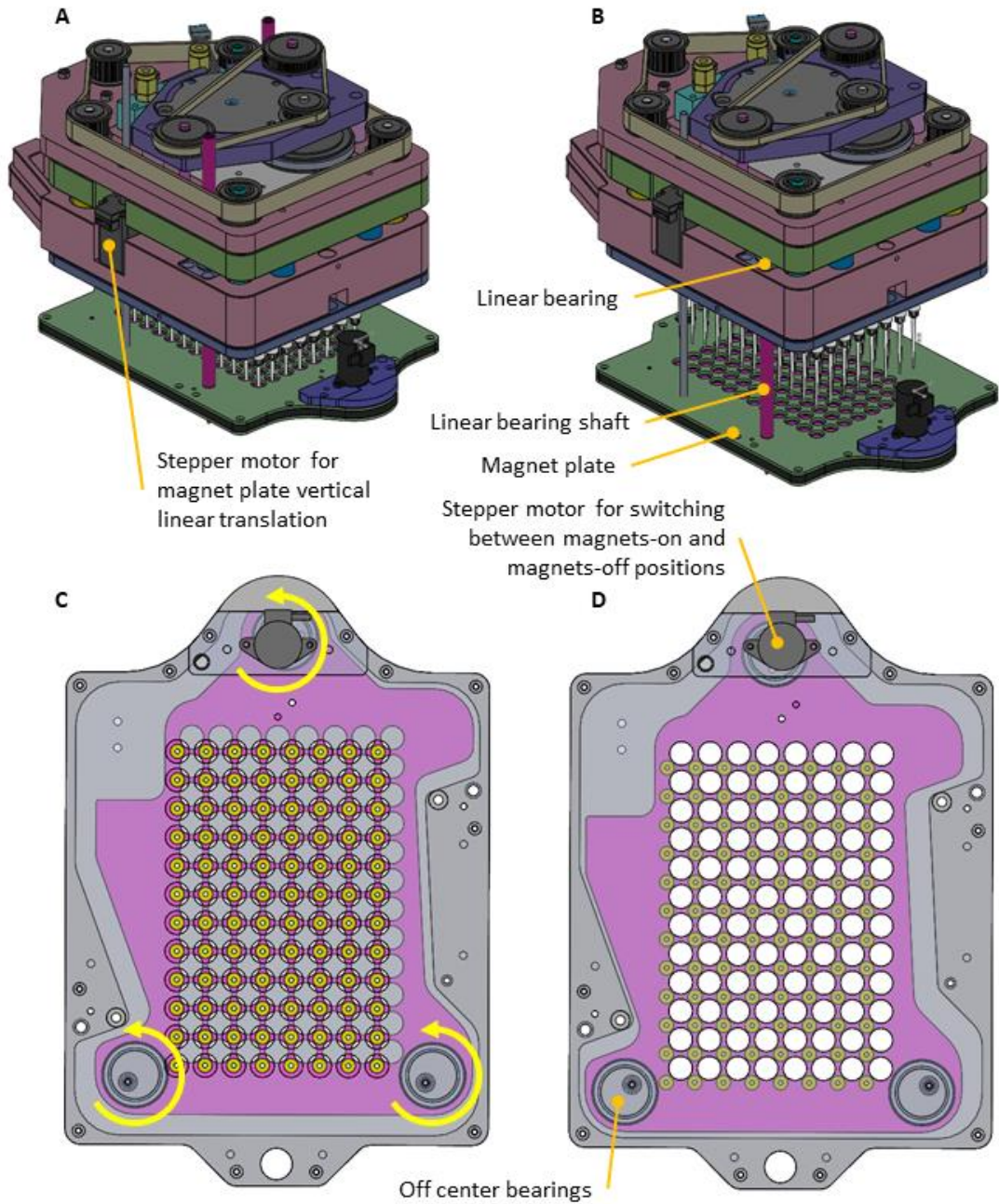


Figure 3.15: The magnet plate can move near the pipette tips (A) or disengage from the pipette tips and move downwards (B). While in this position, a stepper motor on the magnet plate can switch between magnets-on (C) or magnets-off position (D). The plate can then move up again with either the magnets or the through holes aligned to the pipette tips.

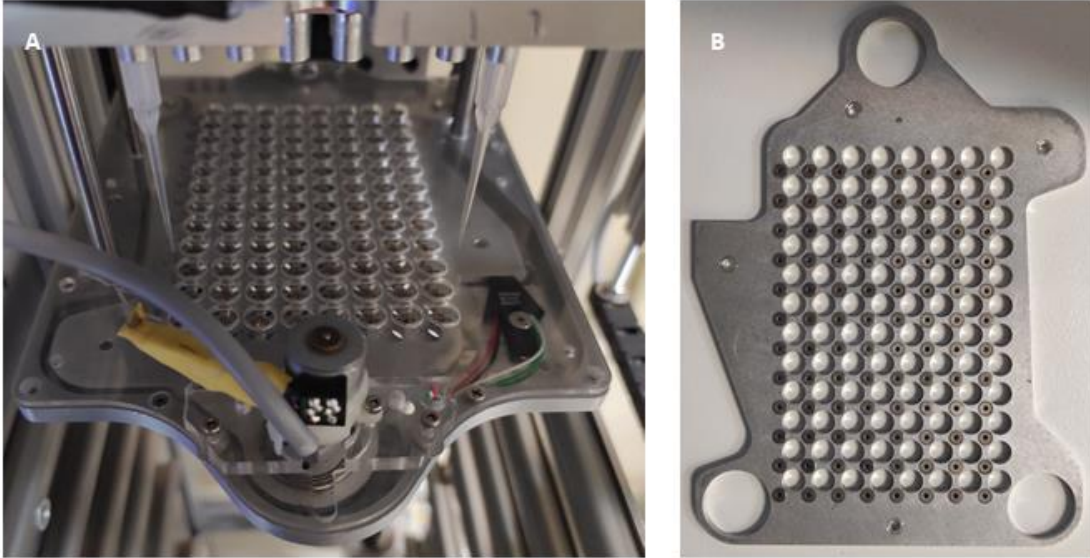


Figure 3.16: A prototype of the magnetic separation system. (A) The entire system assembled on the fluid handling head. (B) A magnet plate using ring magnets

FORCES ACTING ON A PARA/DIAMAGNETIC MICROBEAD

The theoretical foundation for the calculation of the forces acting on a superparamagnetic or diamagnetic microbead has been thoroughly explored in literature²⁴⁰⁻²⁴². For the case of superparamagnetic microbeads under the influence of a non-uniform magnetic field, the magnetic force can be calculated:

The general equation for a magnetic force acting upon a superparamagnetic bead^{243,244} is:

$$(1) \quad \vec{F}_m = (\vec{m} \cdot \nabla) \vec{B}$$

with \vec{m} being the magnetic moment of the bead and \vec{B} the external magnetic field affecting that bead. \vec{m} can be expressed as a function of the volume V and magnetization \vec{M} of the beads:

$$(2) \quad \vec{m} = \rho V \vec{M}$$

The magnetization of the beads is dependent on the initial magnetization of the material \vec{M}_0 and the effect of the external magnetic field. Breaking \vec{M} into these two components, (2) becomes:

$$(3) \quad \vec{m} = \rho V (\vec{M}_0 + \vec{M}(\vec{B})) = \rho V (\vec{M}_0 + \frac{\chi_b}{\rho \mu_0} \vec{B})$$

where χ_b is the initial magnetic susceptibility of the microbead, μ_0 is the magnetic constant and ρ is the material density. By substituting (3) into (1) we get:

$$(4) \quad \vec{F}_m = (\vec{m} \cdot \nabla) \vec{B} = \rho V (\vec{M}_0 \cdot \nabla) \vec{B} + \frac{V \chi_b}{\mu_0} (\vec{B} \cdot \nabla) \vec{B}$$

Expanding (4) into its components for cartesian coordinates we get:

$$(5) \quad \vec{F}_m = \rho V (\vec{M}_0 \cdot \nabla) \vec{B} + \frac{V \chi_b}{\mu_0} (\vec{B} \cdot \nabla) \vec{B} =$$

$$= \rho V \begin{pmatrix} M_{0x} \frac{\partial B_x}{\partial x} + M_{0y} \frac{\partial B_x}{\partial y} + M_{0z} \frac{\partial B_x}{\partial z} \\ M_{0x} \frac{\partial B_y}{\partial x} + M_{0y} \frac{\partial B_y}{\partial y} + M_{0z} \frac{\partial B_y}{\partial z} \\ M_{0x} \frac{\partial B_z}{\partial x} + M_{0y} \frac{\partial B_z}{\partial y} + M_{0z} \frac{\partial B_z}{\partial z} \end{pmatrix} + \frac{V \chi_b}{\mu_0} \begin{pmatrix} B_x \frac{\partial B_x}{\partial x} + B_y \frac{\partial B_x}{\partial y} + B_z \frac{\partial B_x}{\partial z} \\ B_x \frac{\partial B_y}{\partial x} + B_y \frac{\partial B_y}{\partial y} + B_z \frac{\partial B_y}{\partial z} \\ B_x \frac{\partial B_z}{\partial x} + B_y \frac{\partial B_z}{\partial y} + B_z \frac{\partial B_z}{\partial z} \end{pmatrix}$$

Assuming that the microbeads have no initial magnetization, we can again substitute (3) into (1) to get:

$$(6) \quad \vec{F}_m = (\vec{m} \cdot \nabla) \vec{B} = \frac{V \chi_b}{\mu_0} (\vec{B} \cdot \nabla) \vec{B}$$

Expanding (6) into its components for cartesian coordinates we get:

$$(7) \quad \vec{F}_m = \frac{V \chi_b}{\mu_0} (\vec{B} \cdot \nabla) \vec{B} = \frac{V \chi_b}{\mu_0} \begin{pmatrix} B_x \frac{\partial B_x}{\partial x} + B_y \frac{\partial B_x}{\partial y} + B_z \frac{\partial B_x}{\partial z} \\ B_x \frac{\partial B_y}{\partial x} + B_y \frac{\partial B_y}{\partial y} + B_z \frac{\partial B_y}{\partial z} \\ B_x \frac{\partial B_z}{\partial x} + B_y \frac{\partial B_z}{\partial y} + B_z \frac{\partial B_z}{\partial z} \end{pmatrix}$$

Eq. 7 is most frequently used in literature for the calculation of magnetic forces acting upon a superparamagnetic microbead. While eq. 4 is a more accurate form since it includes initial magnetization of the microbeads, the simplified form is a commonly used approximation and it will be used throughout this chapter.

Apart from the magnetic forces acting upon the microbeads, drag forces and gravitational forces are affecting the microbead behavior:

$$(8) \quad \vec{F}_d = 6\pi\eta R_{bead} (u_{particle} - u_{medium}) \text{ (Stokes' law)}$$

$$(9) \quad \vec{F}_g = V(\rho_{bead} - \rho_{medium})g$$

where \vec{F}_d and \vec{F}_g are the drag and gravitational forces respectively, η is the medium viscosity, $u_{particle}$, u_{medium} are the microbead and fluid medium velocities, R_{bead} is the bead radius, ρ_{bead} is the bead material density and ρ_{medium} is the medium density.

In order to explore the magnitude of these forces, we will assume a superparamagnetic polystyrene microbead of 6.5 μm in diameter with embedded iron oxide nanoparticles giving it an average density of 1.1 g/cm^3 . Let us also assume that this microbead is magnetically fixed on a barrier and it is resisting the flow of a medium of 1 mPa-s viscosity and 1 g/cm^3 density at a flow velocity of 10 mm/s. What becomes evident is that eq. 8 yields drag forces in the order of 10^{-10} N while eq. 9 yields gravitational forces in the order 10^{-14} N. In effect, gravitational forces are much smaller than fluid flow interaction forces and as such, they will not be considered when magnetic forces or drag forces are acting upon the microbeads. As such, in the general case of bead separation, the hydrodynamic drag and the magnetic attraction forces will be taken into account based on eq. (7) and eq. (8).

DEFINITION OF THE PROBLEM

The objective of a magnetic bead separation system is to be able to immobilize the beads while other process steps are taking place, for example washing. Additionally, it needs to be able to switch between bead immobilization and release positions. The immobilization is achieved using N48-N52 Nd magnets directly in contact with the pipettes. In Fig 6.9, a cross section of a row of pipettes can be seen. The magenta-colored part is where the magnets are located. As the pipette aspirates the solution which contains the microbeads, the flow goes through a cross section of the tip which has a diameter of 1000 μm where permanent magnets are positioned around the tip. In this way, when the microbeads go through the area encircled in Fig 3.17, they are immobilized by the magnets. We can define the aspiration volume of a pipette tip to be 20 μl and the time required to pipette this volume in and out of the tip (mixing) to be 4 sec with no dwell (so 2 seconds per each step). Based on these:

$$(10) \quad u_{medium_CS} = \frac{Vol_0}{A_0 t} = \frac{20 \text{ mm}^3}{\pi \left(\frac{1 \text{ mm}}{2}\right)^2 2 \text{ s}} \cong 12.7 \text{ mm/s}$$

$$(11) \quad F_{d_CS} = 6\pi\eta R(u_{particle_CS} - u_{medium_CS}) = 6\pi \cdot 1 \text{ mPa s} \cdot 6.5 \mu\text{m} \left(0 - 12.7 \frac{\text{mm}}{\text{s}}\right) \cong -15.6 \cdot 10^{-10} \text{ N}$$

where CS notation refers to calculations on the pipette cross section where bead immobilization is done, Vol_0 is the aspiration volume of the tip, A_0 is the required flow rate and t is the available time to complete the step.

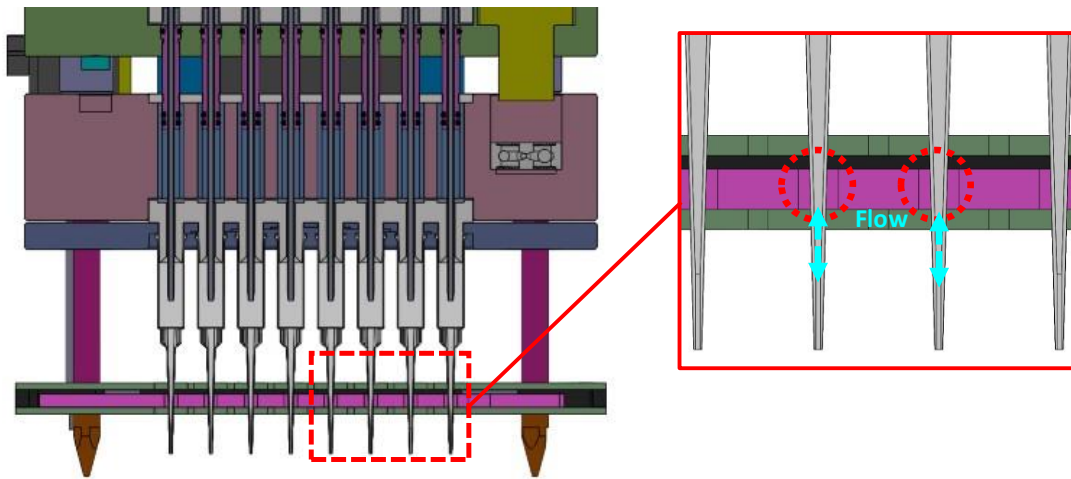


Figure 3.17: The objective of the magnetic separation system is to trap the microbeads within the pipette tips. This is achieved by retractable permanent magnets.

Using the theoretical background from the previous section, the appropriate type, shape and size of the magnet needs to be selected in order to overcome the drag force calculated in eq. 11. Since the magnet-carrying part needs to be able to switch between bead immobilization and release positions, both magnet positions and clearance holes for the pipettes exist and correspond to antipodal points in the motion profile of this part. This creates a geometrical constraint for the design of the magnets, since they need to fit in the space allowed by the pitch of the pipettes, which is predefined and equal to 9 mm for 96-well formats. As can be seen in Fig 3.18, the maximum space that can be used for the placement of magnets needs to be encircled within a diameter of 5 mm.

To maintain structural integrity of the magnet-carrying part, this is reduced to 4.5 mm. The inner diameter needs to be kept at or near 1.5 mm which is the outer pipette diameter at the middle of its functional length.

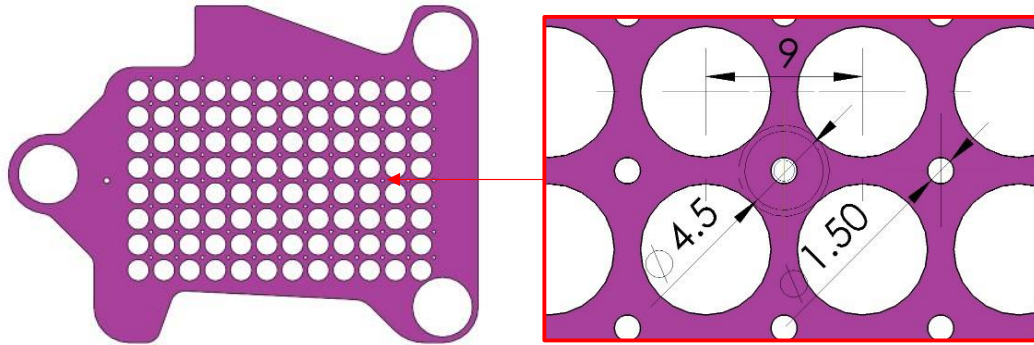


Figure 3.18: The main constraint of the separation module is geometrical. The permanent magnets need to be able to fit between the clearance holes which are used when magnetic trapping is undesirable. This leaves a maximum space of 4 mm in diameter in order to maintain the structural integrity of the magnet-carrying part

A secondary constrain is the requirement for the pipette tip to be able to reach a standard microwell bottom in both the bead immobilization and release positions. Particularly in the bead immobilization position, the maximum available space is 3 mm. However, to maintain structural integrity of the magnet-carrying part and in order to facilitate the magnet assembly, the total magnet height needs to be less than 3 mm (Fig 3.19).

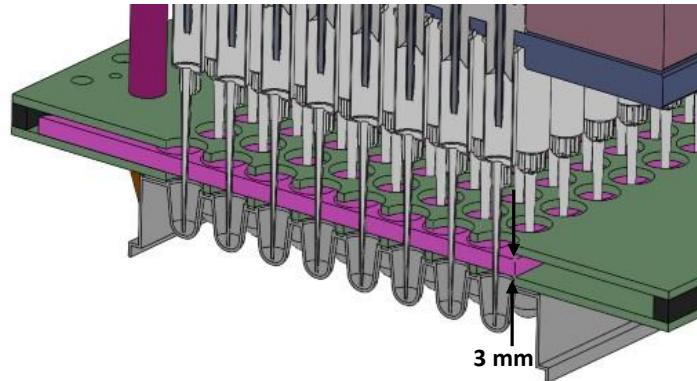


Figure 3.19: The magnet height is restricted by the total pipette tip length. The pipette needs to be able to reach the bottom of a standard microwell, so the maximum height of a separation magnet needs to be less than 3 mm.

In summary of this section, the design problem definition is the following:

- A permanent magnet arrangement is required to attract and immobilize superparamagnetic microbeads
- The magnetic trapping force needs to be able to overcome the drag forces of $\sim 13 \cdot 10^{-10} N$ exerted upon any microbead as a result of fluid flow
- The permanent magnets need to fit within a ring-shaped space of the following dimensions:
 - Outer max diameter= $\varnothing 4.5$ mm
 - Inner max diameter= $\varnothing 1.5$ mm
 - Height < 3 mm

FINITE ELEMENT MODELLING | RING SHAPED MAGNET

For the geometry of a pipette tip and a magnetic field caused by a permanent magnet, eq. 7 can be solved using a finite element model of a permanent magnet. Assuming we are using a ring-shaped magnet (Fig 3.20), the problem becomes axisymmetric. Additionally, we can make the following assumptions:

- The magnetic field of one tip position is not strong enough to affect other positions, each tip is modelled independently
- The rest of the materials in the assembly are not magnetic/ superparamagnetic and will be considered to have a relative magnetic permeability of $\mu_r = 1$
- It is assumed that bead immobilization will take place near the magnet
- The magnetic polarity will be coaxial to the flow direction

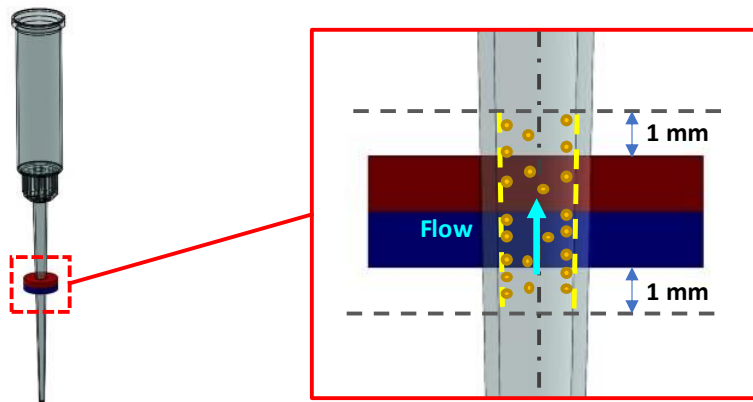


Figure 3.20: Using a ring-shaped magnet makes the trapping problem axisymmetric. The yellow dashed lines represent the bead immobilization zone, i.e. where the beads are expected to be trapped during aspiration/release steps

Based on these assumptions, an axisymmetric model can be built for each pipette individually. The following definitions are going to be used in the model:

The magnetic constant:

$$\mu_0 = 1.25664 \cdot 10^{-6} \text{ H/m}$$

The magnetic susceptibility of a superparamagnetic microbead²⁴³

$$\chi_b = 0.17$$

The volume of a MagPlex superparamagnetic microbead²⁴⁵ by Luminex:

$$V = \frac{4}{3}\pi r^3 = \frac{4}{3}\pi(6.5 \cdot 10^{-6})^3 = 1.44 \cdot 10^{-16} \text{ m}^3$$

The flux density of a neodymium N48 magnet in the direction of magnetization:

$$B_r = 1.38 \text{ T}$$

Using these parameters, a model is set up in COMSOL Multiphysics:

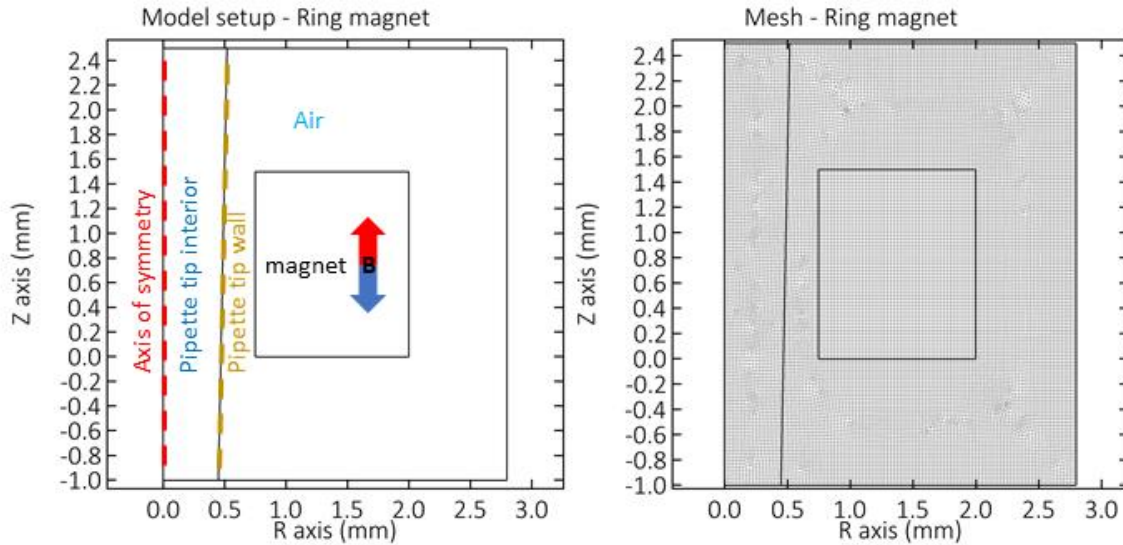


Figure 3.21: An axisymmetric model of bead separation within a pipette tip in COMSOL Multiphysics. On the left, the model setup. The microbeads are initially floating in the pipette tip interior. The magnet attracts and immobilizes the microbeads on the pipette tip wall. On the right, the mesh generation for the model.

The 2d model contains 3 boundaries: The magnet, the pipette interior and the free space. In effect, the pipette interior and free space have identical properties for this initial simulation. All domains are meshed using mapped quad elements. The model mesh size was selected by calculating the force upon a bead positioned at any length of the pipette tip wall. The mesh was refined until the force calculation converged to a smooth curve that would remain unchanged upon further refinement (Fig. 3.22)

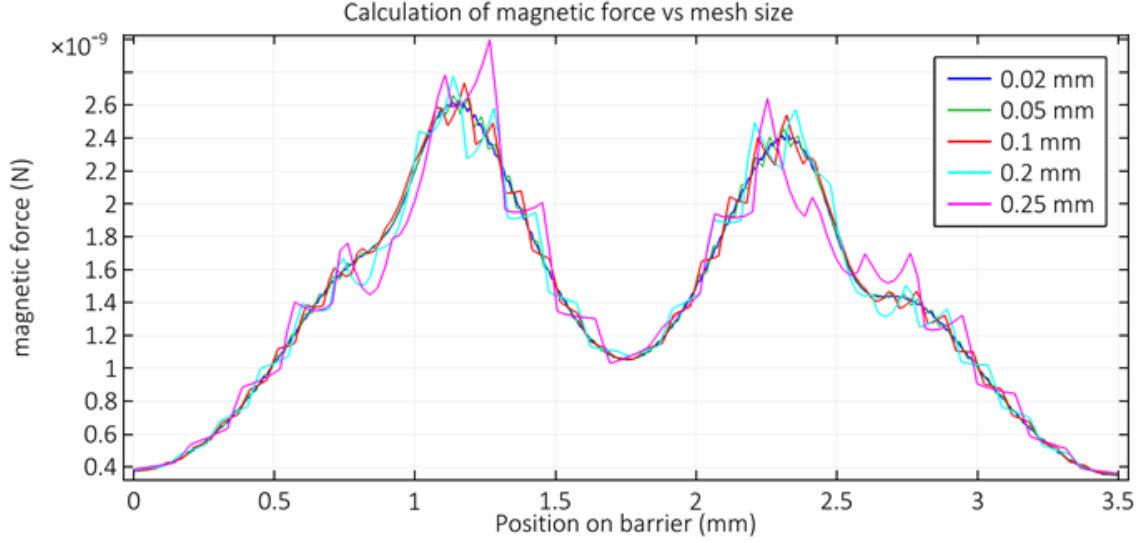


Figure 3.22: Mesh size was selected by refining the model until the force exerted upon a random bead on the pipette tip wall would converge and not change upon further mesh refinement

Solving a stationary study for these conditions gives the magnetic flux density $\vec{B} = (B_r, B_\theta, B_z)$ inside the pipette tip. Using Eq. 6 and \vec{B} the force \vec{F}_m can be calculated. Since the problem is axisymmetric, Eq. 6 needs to be written in cylindrical coordinates:

$$(12) \quad \vec{F}_m = \frac{V\chi_b}{\mu_0} (\vec{B} \cdot \nabla) \vec{B} = \frac{V\chi_b}{\mu_0} \begin{pmatrix} B_r \frac{\partial B_r}{\partial r} + \frac{B_r}{r} \frac{\partial B_r}{\partial \theta} + B_z \frac{\partial B_r}{\partial z} - \frac{B_\theta^2}{r} \\ B_r \frac{\partial B_\theta}{\partial r} + \frac{B_\theta}{r} \frac{\partial B_\theta}{\partial \theta} + B_z \frac{\partial B_\theta}{\partial z} - \frac{B_\theta B_r}{r} \\ B_r \frac{\partial B_z}{\partial r} + \frac{B_\theta}{r} \frac{\partial B_z}{\partial \theta} + B_z \frac{\partial B_z}{\partial z} \end{pmatrix}$$

Because of the symmetry around z , $B_\theta = 0$ and $\frac{\partial B}{\partial \theta}$ will also yield zero. Eq. 12 becomes:

$$(13) \quad \vec{F}_m = (F_{mr}, F_{mz}) = \frac{V\chi_b}{\mu_0} (\vec{B} \cdot \nabla) \vec{B} = \frac{V\chi_b}{\mu_0} \begin{pmatrix} B_r \frac{\partial B_r}{\partial r} + B_z \frac{\partial B_r}{\partial z} \\ B_r \frac{\partial B_z}{\partial r} + B_z \frac{\partial B_z}{\partial z} \end{pmatrix}$$

And the magnitude can be calculated for every point within the work area:

$$(14) \quad \|F_m\| = \frac{V\chi_b}{\mu_0} \sqrt{\left(B_r \frac{\partial B_r}{\partial r} + B_z \frac{\partial B_r}{\partial z} \right)^2 + \left(B_r \frac{\partial B_z}{\partial r} + B_z \frac{\partial B_z}{\partial z} \right)^2}$$

Using the flux density data which are calculated using the FEA model in Eq. 13 & Eq. 14, the force applied to a microbead by the permanent magnet can be calculated within the pipette tip (Fig. 3.23).

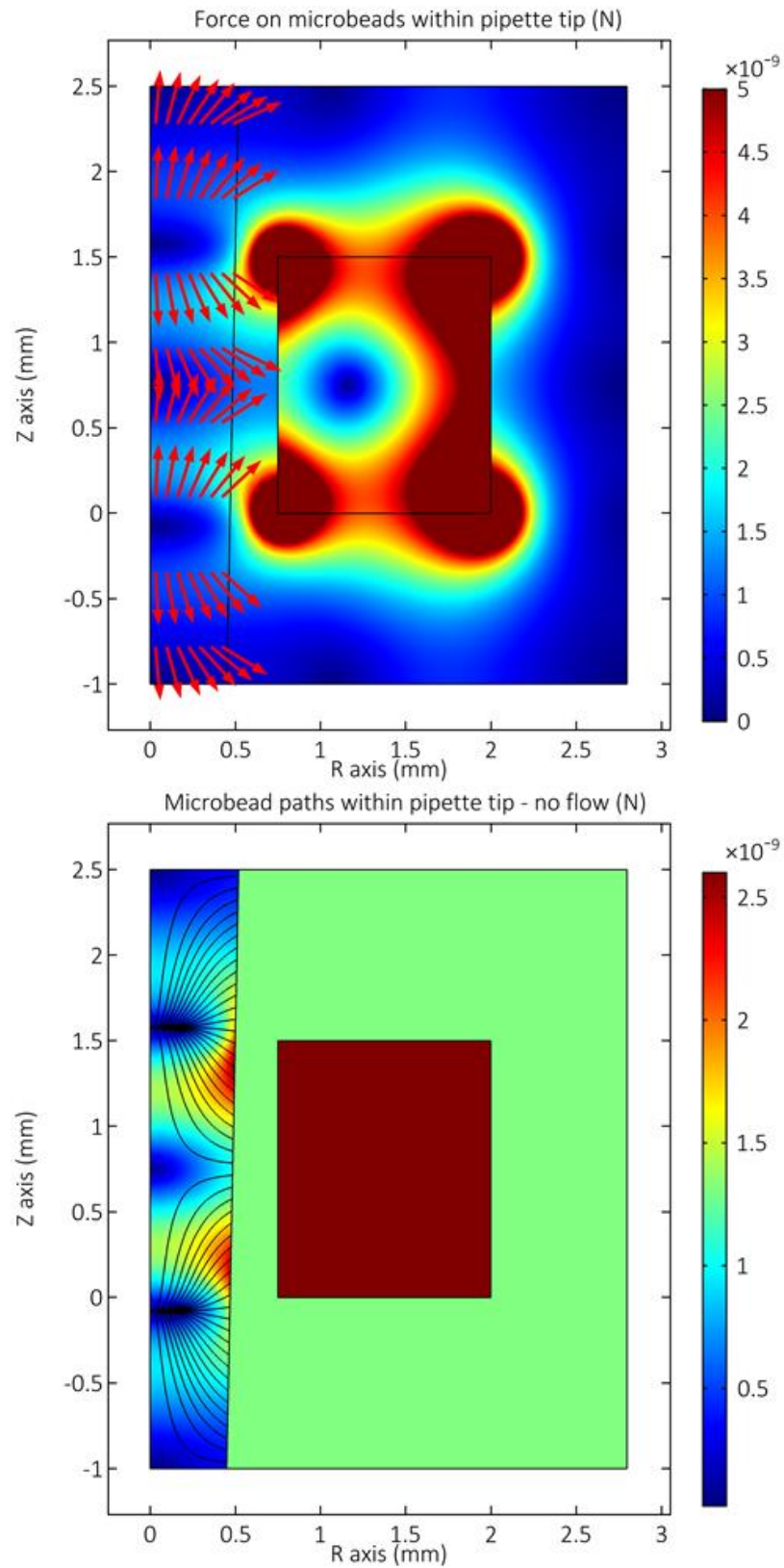


Figure 3.23: The magnetic force exerted on superparamagnetic microbeads by a ring-shaped magnet (up). Streamline plot to indicate microbead paths (down) (effects of fluid flow are ignored)

What can be seen in Fig 3.23 is that the force vectors indicate a movement of the microbeads towards the tip barrier where they will be immobilized. However, the force vectors above and below the magnet indicate that the microbeads will not be pulled towards the magnet but further away before they stop at the pipette tip wall. This can be better viewed in the streamline plot of Fig 3.23. While the starting point of the microbeads is near the upper or lower level of the magnet in the Z axis, they follow paths that move them towards the pipette tip barrier but away from the magnet. In a bead separation process, this could pose a challenge for the trapping efficiency since the microbead will move away from the magnet where the magnetic field is weak. In those positions, the drag force is likely to dominate over the magnetic immobilization force exerted by the magnet. So, if we were to use the magnetic immobilization technique as a flow through scheme for a binding assay, the microbeads could potentially be lost during an incubation or washing step.

The effect of the magnet size on the exerted force needs to be quantified to further explore the applicability of this solution. Since the endpoint of each microbead streamline is the pipette tip inner wall, it makes sense to calculate the force upon this barrier. The size range of the magnet has already been defined in the problem definition section. Solving the model for a range of magnet outer radiuses and heights gives the radial component of the magnetic attraction force which can be used for magnet sizing (Fig. 3.24). In the top part of this figure, the effect of the outer radius of a ring magnet on the magnetic force experienced by a microbead is calculated for different radiuses. The x-axis represents the position on the pipette's inner wall, starting from 1.5 mm over the top level of the magnet and moving 3 mm below the magnet bottom level. The inner radius and magnet height are kept at 0.75 mm and 1.5 mm respectively while the magnet top level corresponds to the 1.5 mm position on the figure's x-axis. What can be observed on the top part of the figure, is that the maximum outer diameter that can fit in this design, will also yield the maximum magnetic force. Additionally, there are 2 zones where the radial force is maximized, just below the magnet top level and just over the magnet bottom level. This can be seen by the double peak of each curve. On the bottom part of Fig. 6.16, the effect of magnet height is explored. Magnet heights ranging from 0.25 to 3 mm are used for the calculation, while the inner and outer radiuses are kept at 0.75 and 2 mm respectively. The magnet's top level again corresponds to 1.5 mm in the figure's x axis. In this case, the maximum attractive radial force occurs for a magnet height equal to 0.5 mm, while the force decreases both for smaller and larger magnet heights. Additionally, for the 0.25 & 0.5 mm magnet heights there is only one distinct trapping zone, while for the bigger magnets there are, again, two peaks. From these results, it can be deduced that the maximum attainable trapping radial force for a magnetic microbead at the pipette wall, will occur for the maximized outer diameter of a ring shaped magnet, which in this case is 4.5 mm, and a magnet height equal to 0.5 mm.

While the above provide an insight on the required magnet design for maximum trapping force on the pipette inner wall, the design of a microbead retention device cannot be fully described using this approach. The reason is that in this case, the design for maximum retention force on the pipette wall does not necessarily guarantee maximum radial force in positions further away from the tip wall. On the top of Fig 3.24, the magnetic forces on a microbead have been calculated for different magnet heights at the cross section in which the maximum trapping force was attained from Fig 3.23. However, what can be seen is that the magnet size with the highest trapping force on the pipette barrier ($h=0.5$ mm) is outperformed in positions closer to the pipette center by the magnet with $h=1$ mm. Additionally, the axial forces acted upon the microbeads in combination with the fluid flow within the tip will also affect the microbead orbit and its end position. In the bottom part of Fig. 3.25, the axial forces on a microbead have been calculated for different magnet heights in different positions of the pipette tip barrier. The results can be more easily visualized by also looking at the top part of Fig 3.25. The magnet with $h=1$ mm will give a magnetic force with a stronger z-component compared to the other magnets. But as can be seen in Fig 3.24, this component has the potential to either move the beads within the trapping zone or move them away over or under the magnet. This can result in inefficient trapping or even beads being lost.

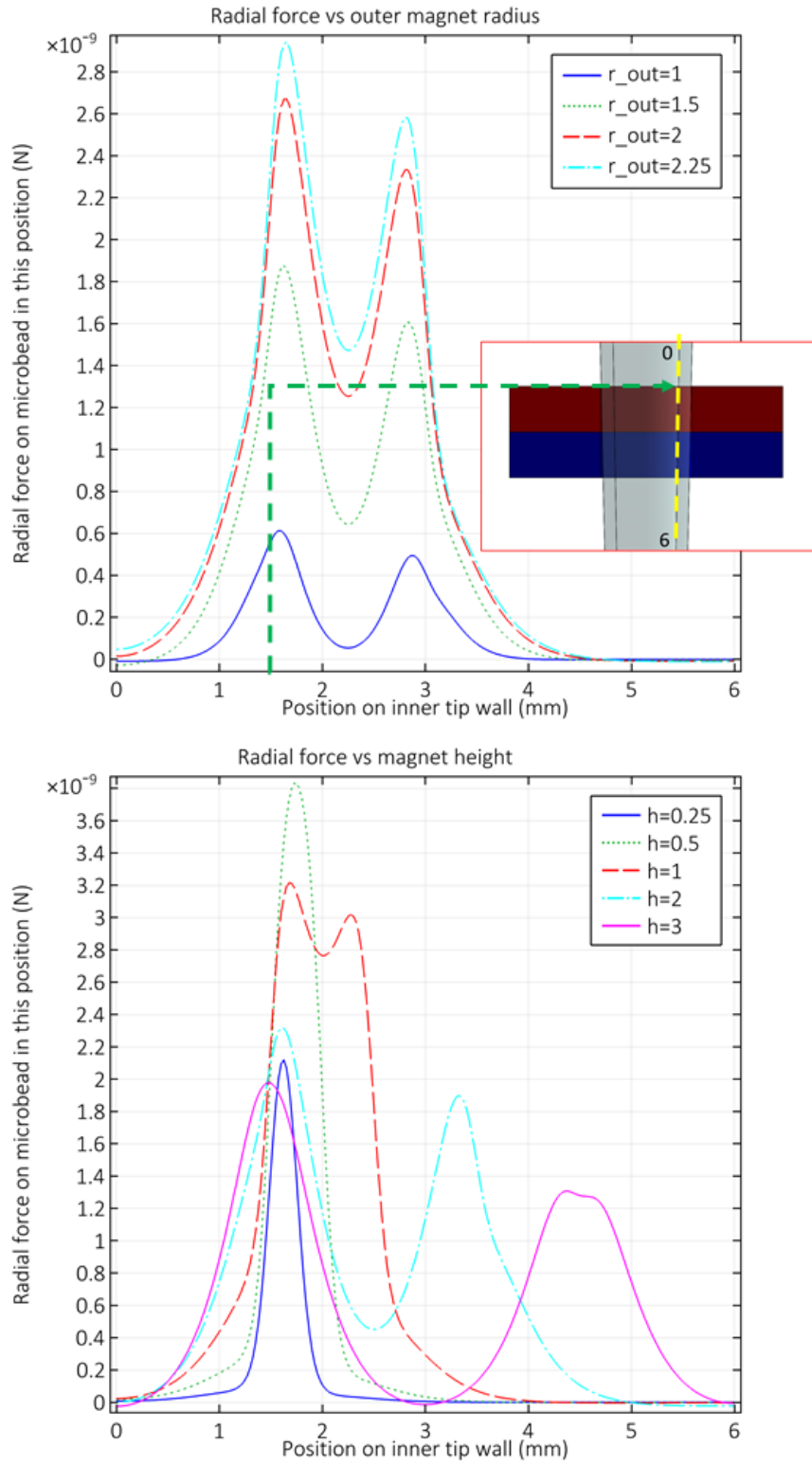


Figure 3.24: The radial component of the magnetic force on the pipette inner wall as a function of the magnet outer radius (top) and the magnet height (bottom)

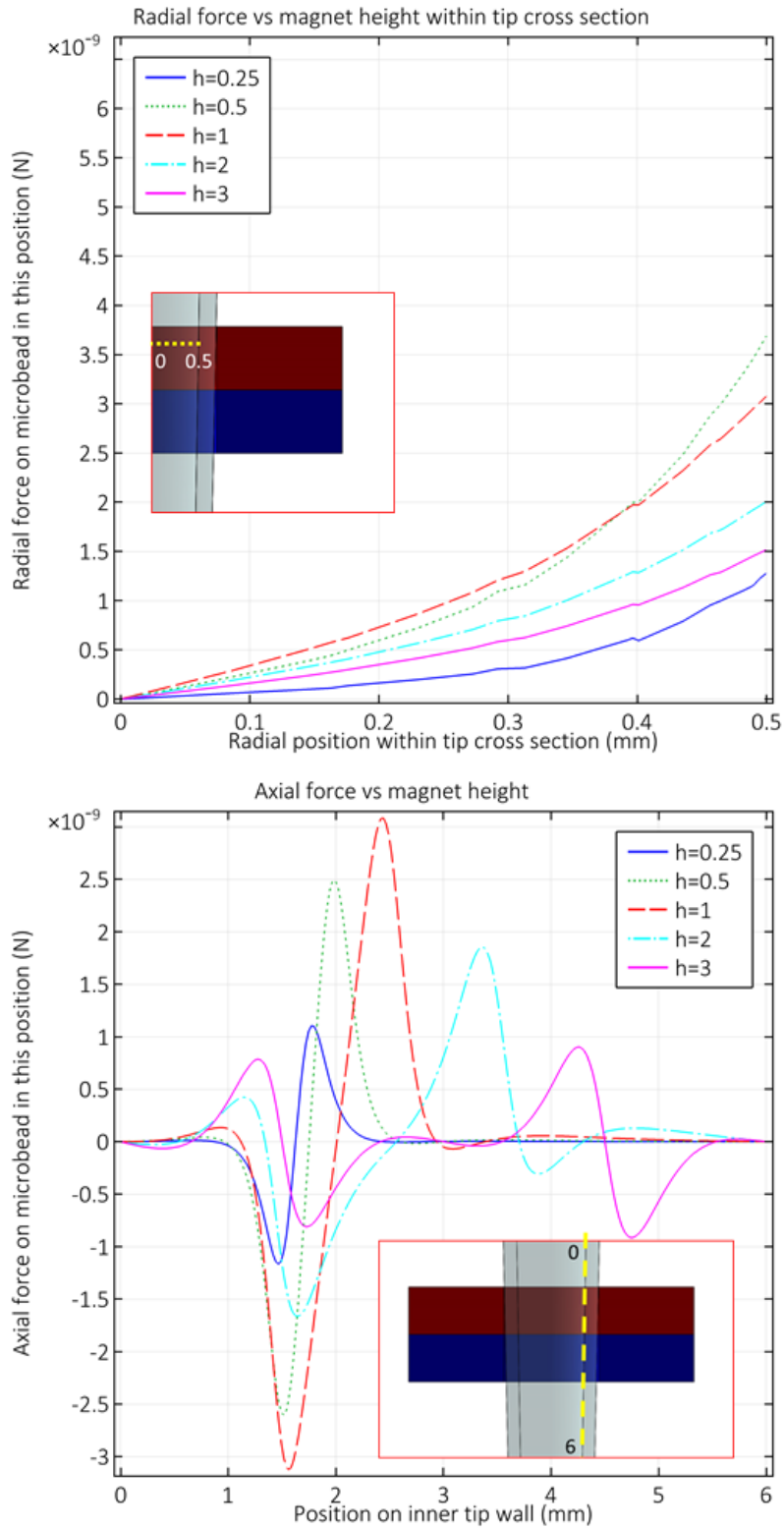


Figure 3.25: The radial component of the magnetic force within the cross section at the position of maximum trapping force(top) and the axial component of the magnetic force for different magnet heights (bottom)

PARTICLE TRACING | RING SHAPED MAGNET

In the previous section, the magnetic force components acting upon a microbead in various positions within a pipette tip have been shown. Different calculations have been made for different ring magnet sizes and the results have been shown for the pipette tip wall but also within a tip cross section. However, the existence of both axial and radial magnetic force components, the fact that there is fluid flow affecting the microbead orbit and the existence of multiple trapping zones -some of which may be undesirable-, necessitate a different approach that can model all of these conditions simultaneously and yield a result about the trapping efficiency vs the magnet size. Particle tracing is a straightforward way to evaluate the performance of a microbead retention mechanism.

In order to perform a particle tracing analysis for this problem, the following two vector fields need to be calculated:

- The magnetic forces acting upon a microbead in every position within the pipette tip
- The drag force due to the fluid flow velocity field within the pipette tip

The magnetic forces are calculated in the same way as in the previous section. In order to calculate the drag forces, we first define the required flow in and out of the pipette. Following the norm of the previous section, we can assume that for a mixing protocol, it is reasonable to aspirate and dispense a nominal volume of 20 μl in 4 seconds with no dwell time in between the steps. Therefore, each of the two steps will last 2 seconds. This corresponds to a mass inflow to the pipette tip equal to 10^{-5} kg/s. For a tip inner diameter of 840 μm , the average flow velocity will be $u_{avg} = 18$ mm/s. With these given, the Reynolds number for the flow within the tip can be calculated:

$$(17) \quad Re = u_{avg} \left(\frac{\text{mm}}{\text{s}} \right) \cdot \frac{Dh (\text{mm})}{\nu \left(\frac{\text{mm}^2}{\text{s}} \right)} = 18 \cdot \frac{0.84}{1} = 15.2$$

The Reynolds number indicates that the flow within the tip can be modeled as laminar, which is typical for applications near or in the microscale.

Using the same model as before, additional physics is added to the Comsol model:

- Laminar flow inside the pipette tip
- Particle tracing for fluid flow

For the laminar flow simulation we use an incompressible flow with no turbulence model. The bottom part of the pipette tip is set as an inlet with a condition of mass flow rate $\dot{m} = 10^{-5}$ kg/s and the upper part is set as an outlet. The pipette tip walls are modeled with a no slip boundary condition. The problem remains axisymmetric and the mesh remains the same for both the magnetic and fluid flow problems. The solution for the fluid flow problem can be found in the top part of Fig 3.26. The problem is solved to acquire a velocity vector field. Using this vector field and Stokes law (Eq.8) the forces acting upon a microbead due to fluid flow can be calculated for every position within the pipette tip.

For the magnetic force vector field, the model from the previous section as it was described by Eq. 12, is used here as well. In the bottom part of Fig 3.26, the force vector field acting upon a microbead can be seen. The arrows represent the force direction in different positions, while the color scale represents the force magnitude.

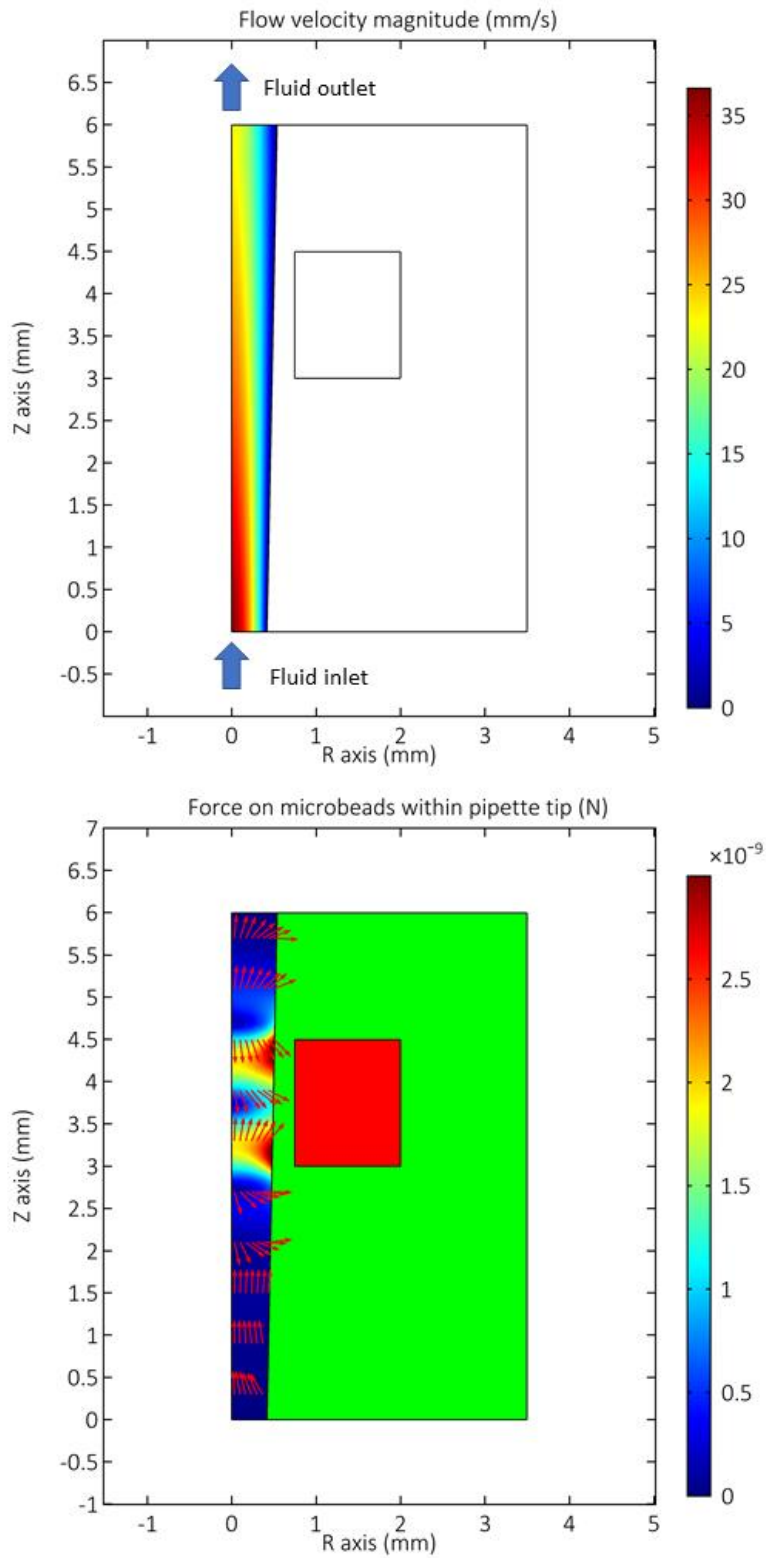


Figure 3.26: Two different physics models are required to model particle tracing: Fluid flow (top) for Stokes drag model on the microbeads and the magnetic forces on the microbeads (bottom) as described in Eq. 12

Having calculated the fluid velocity and the magnetic force on every position within the pipette tip, the particle tracing analysis becomes straightforward. The bead properties from the previous section are used here as well:

$$R_{bead} = \frac{6.5}{2} \mu m$$

$$\rho_{bead} = 1.1 \frac{g}{cm^3}$$

Based on the previous input, a time dependent model is built to simulate the behavior of 20 microbeads that are found on the pipette tip entry point at $t=0$ sec. The study duration is set at 1 second (defined by trial and error, may be different for some setups). The 20 microbeads are uniformly distributed at the inlet so that the dependence of the initial position can be effectively modeled. A time step of 0.01 seconds is defined for the model. The output is a sequence of positions for each microbead.

From the results of the previous section, a magnet outer radius $r_{out}=2.25$ mm and a magnet height $h=0.5$ mm were found to generate the stronger effect in terms of radial magnetic force. Using these parameters, the magnetic force field is calculated and the resultant microbead paths are recorded for each timepoint. In Fig. 3.27, the results of this simulation are presented in characteristic timepoints:

- $t=0.01$ s: The microbeads are still unaffected by the magnetic field and are following the parabolic flow profile
- $t=0.1$ s: The microbeads that initiated near the center of the pipette tip are now approaching the position where there the magnet's radial force peaks (See Fig 3.24)
- $t=0.2$ s: 10/20 microbeads have been immobilized at the position where the radial magnetic force peaks, 8/20 microbeads are approaching the magnet, but 2 microbeads have overshot the trapping position and will not be trapped
- $t=0.3 - 1.0$ s: The remaining 8 microbeads are immobilized, however not at the intended trapping position but at a position below the magnet where the radial force is much weaker

What can be deduced from the above analysis is that the maximization of the radial forces alone may not be enough to maximize the efficiency of the magnetic separation. The particle tracing analysis provides additional information, in particular the number of beads that is expected to overshoot the trapping position and the number of beads that may be immobilized in positions that are not intended for microbead trapping. It can be argued that the microbeads that overshoot the immobilization positions may again be trapped when the flow is reversed, i.e. during the dispending step. However, it is also possible that they will be immobilized at any position over the magnet, which could potentially cause them to be lost or affect subsequent process steps.

Additionally, while the position time series is an effective tool to display the effect of the magnetic field, only the end position of the microbeads is necessary to evaluate the trapping efficiency of the magnet.

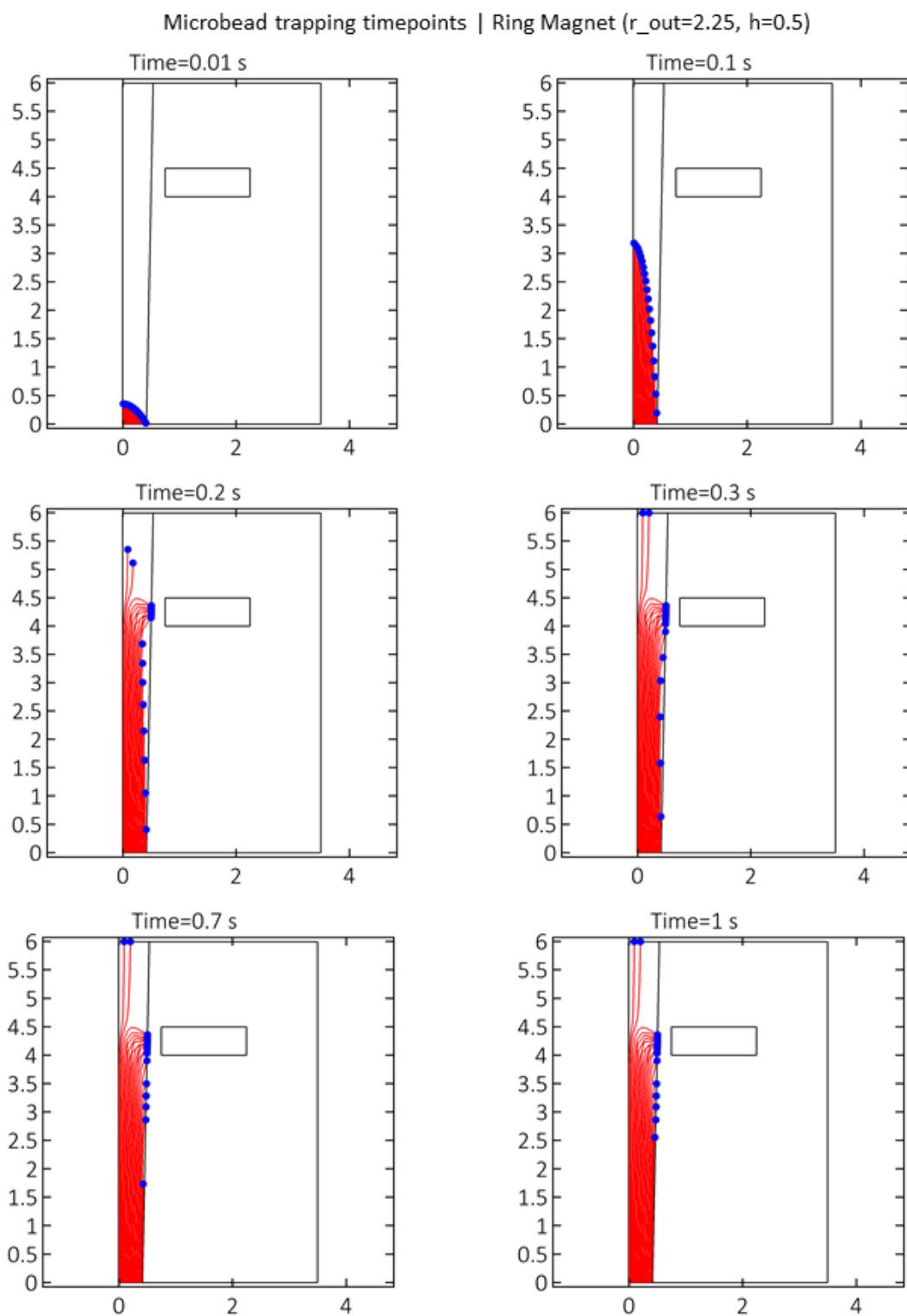


Figure 3.27: A time series displaying the effect of the magnetic field from a ring magnet on several superparamagnetic microbeads that are aspirated by the pipette.

Based on the previous, an effective way to optimize the magnet design would be to run a particle tracing analysis across the diameter and magnet height range. Using the same parameters as before, the magnetics model is solved for different magnet designs and a particle tracing analysis is done for each case. A compilation of the results can be seen in table 6.20 while the microbead paths per case can be observed in figures 6.21-6.24.

In table 3.2, the trapping efficiency of a range of ring magnet heights and outer radiuses combined is presented. A column for trapping (%) denotes the percentage of beads that were attracted by the magnetic forces and eventually ended up on the pipette tip wall. A column for overshoot (%) shows the percentage of beads that were not able to be trapped by the magnet and overshoot the magnet zone. A threshold is set at 95% trapping above which the solution is considered acceptable. However, some of the magnet designs are structurally undesirable. Designs with a magnet height of 3 mm and diameters equal or over 4 mm will weaken the magnet holding structure excessively as can be seen in Fig. 3.18. For this reason, 4 of the solutions are excluded from the selection as structurally undesirable.

Magnet height (mm)	Magnet outer radius (mm)	Trapping (%)	Overshoot (%)	Comments
0.25	0.5	40%	60%	Low efficiency
0.25	1.5	55%	45%	Low efficiency
0.25	2	60%	40%	Low efficiency
0.25	2.25	60%	40%	Low efficiency
0.5	1	55%	45%	Low efficiency
0.5	1.5	80%	20%	Low efficiency
0.5	2	90%	10%	Low efficiency
0.5	2.25	90%	10%	Low efficiency
1	1	65%	35%	Low efficiency
1	1.5	100%	0%	✓
1	2	100%	0%	✓
1	2.25	100%	0%	✓
1.5	1	65%	35%	Low efficiency
1.5	1.5	100%	0%	✓
1.5	2	100%	0%	✓
1.5	2.25	100%	0%	✓
2	1	60%	40%	Low efficiency
2	1.5	95%	5%	✓
2	2	100%	0%	✓
2	2.25	100%	0%	Structurally undesirable
3	1	55%	45%	Low efficiency
3	1.5	90%	10%	Low efficiency
3	2	100%	0%	Structurally undesirable
3	2.25	100%	0%	Structurally undesirable

Table 3.2: Trapping efficiency of different ring magnet size with varying magnet height and outer radius.

Microbead trapping paths vs magnet size 1

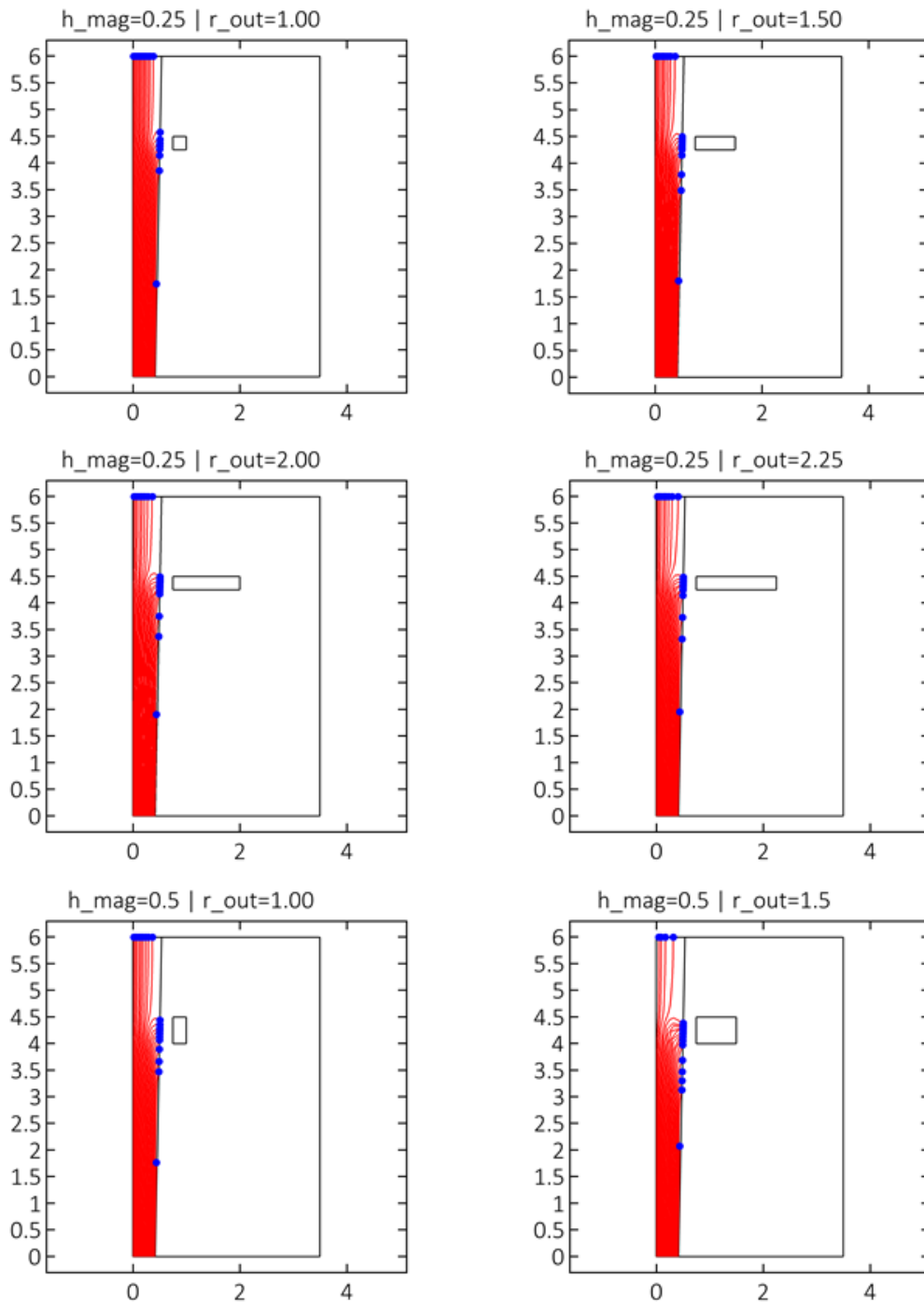


Figure 3.28: Paths and end positions of microbeads entering the pipette tip driven by a laminar flow under the influence of a magnetic field from ring magnets of different height (h_mag) and outer radius (r_out). Microbeads that appear to have reached the top of the pipette tip, are considered to have overshoot the trapping position.

Microbead trapping paths vs magnet size 2

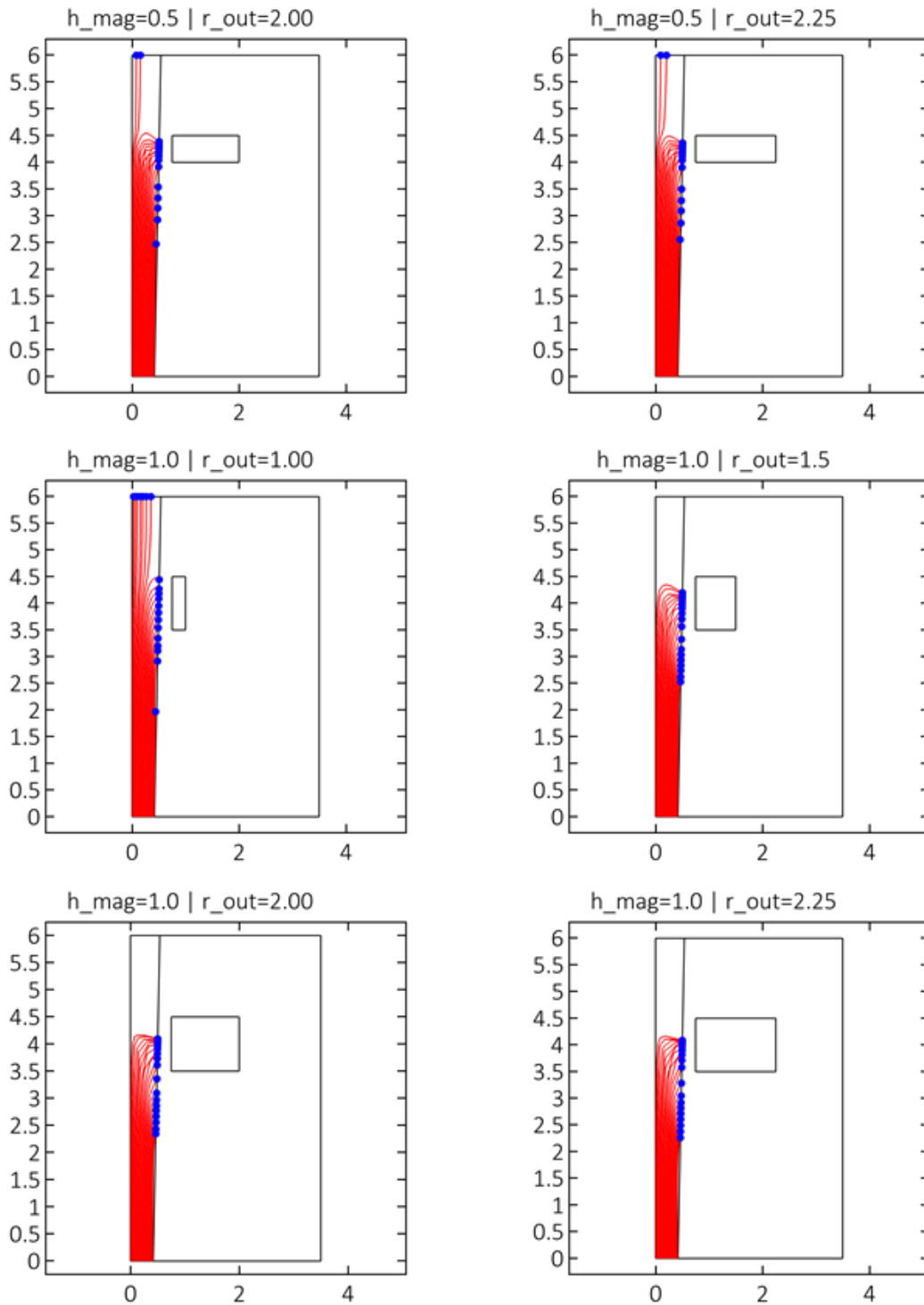


Figure 3.29: Paths and end positions of microbeads entering the pipette tip driven by a laminar flow under the influence of a magnetic field from ring magnets of different height (h_mag) and outer radius (r_out). Microbeads that appear to have reached the top of the pipette tip, are considered to have overshot the trapping position.

Microbead trapping paths vs magnet size 3

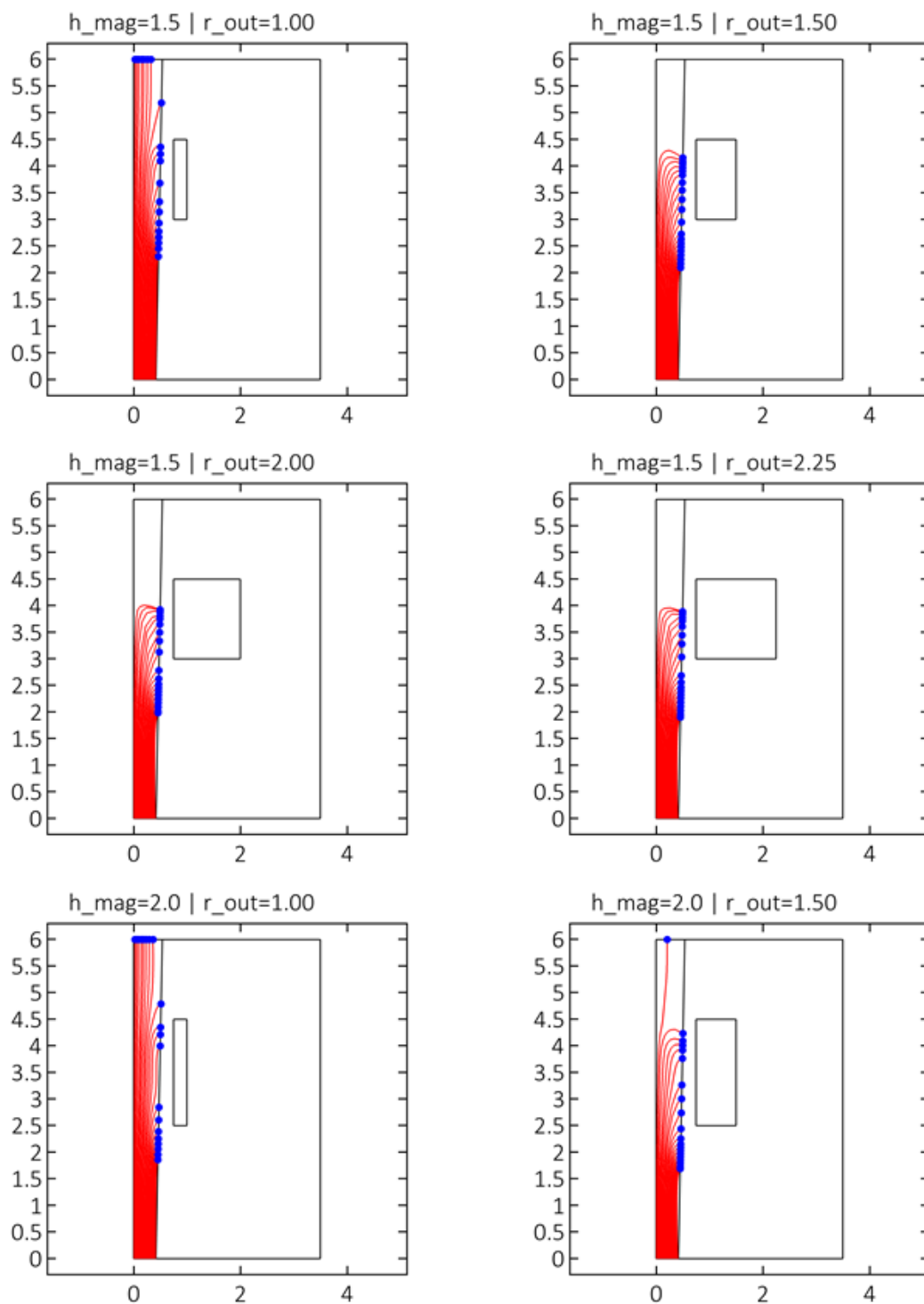


Figure 3.30: Paths and end positions of microbeads entering the pipette tip driven by a laminar flow under the influence of a magnetic field from ring magnets of different height (h_mag) and outer radius (r_out). Microbeads that appear to have reached the top of the pipette tip, are considered to have overshot the trapping position.

Microbead trapping paths vs magnet size 4

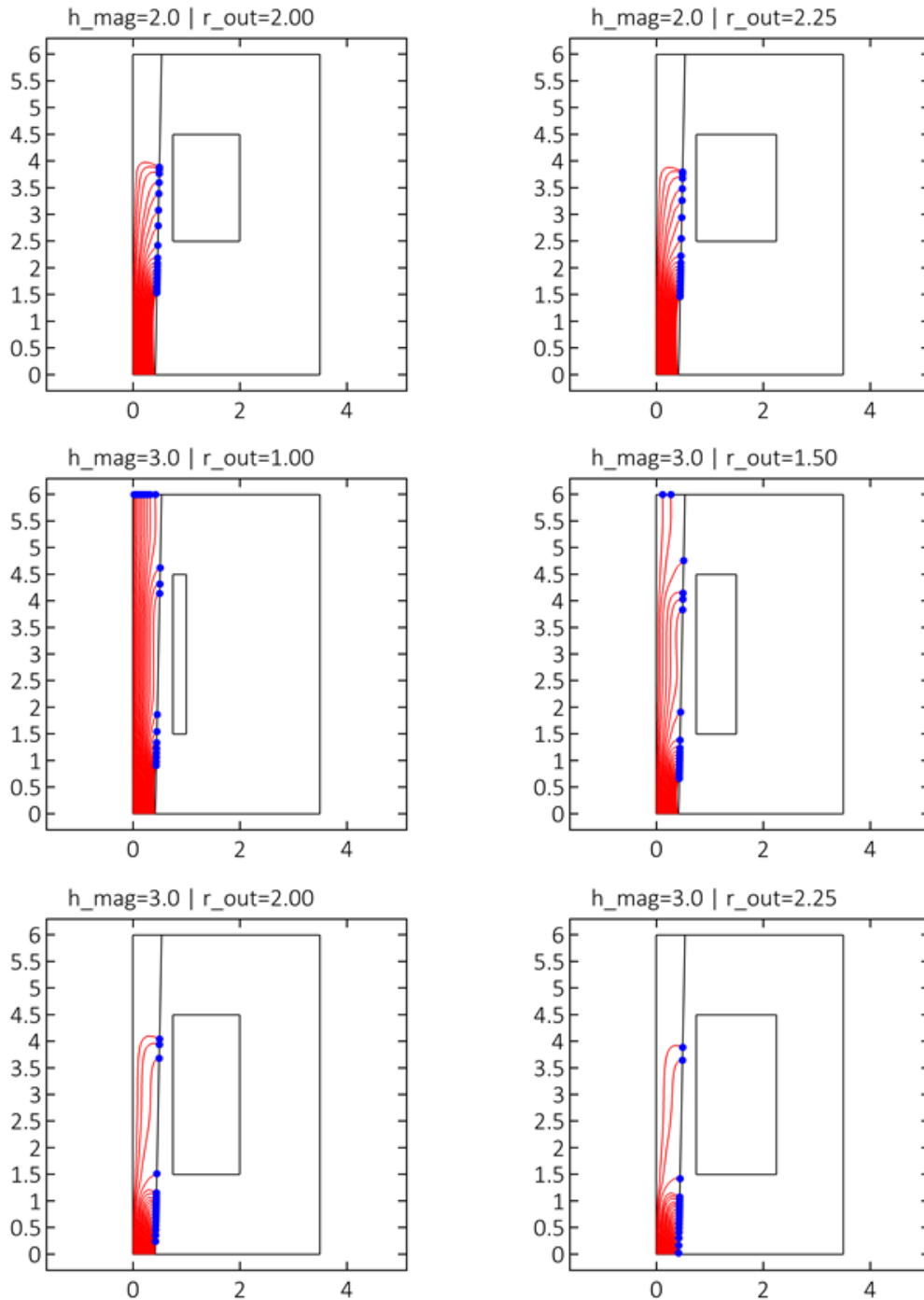


Figure 3.31: Paths and end positions of microbeads entering the pipette tip driven by a laminar flow under the influence of a magnetic field from ring magnets of different height (h_{mag}) and outer radius (r_{out}). Microbeads that appear to have reached the top of the pipette tip, are considered to have overshoot the trapping position.

Out of the 24 different combinations, 8 designs yield trapping efficiencies >95% based on the particle tracing model. Among these 8 designs, there are groups which share the same magnet height but a different magnet radius. As it has been shown in Fig 3.24, while the effect of the magnet height on the bead trapping may not be straightforward, larger outer radiuses result in an increase of the magnetic attraction. As such, out of the 8 designs we can assume that the three with the larger radius will yield the highest efficiency. This leaves 3 candidate combinations to be compared against each other:

Design No	Magnet height (mm)	Magnet outer radius (mm)
1	1	2.25
2	1.5	2.25
3	2	2

Table 3.3: Three different ring magnet designs are promoted from the particle tracing analysis as the more suitable design choices for efficient microbead trapping

One criterion which can be used as a comparison is the total force a microbead experiences near the pipette inner wall. Using as a calculation position a line within the pipette tip distanced 0.1 mm from the pipette wall, the magnetic attraction force towards the magnet can be estimated for microbeads in the pipette near the magnet. This is an indication of how strongly the magnet will affect particles that are near it. The results for the three promoted designs from the previous analysis can be seen on Fig. 3.32. The dashed yellow line represents the calculation position. The magnetic attraction force is calculated on this line starting from the top of the work area and moving downwards with the magnet upper level being at 1.5 mm. What can be seen is that the magnet design (1) with the smaller height has an advantage over the other two designs with the difference being smaller for the design (2) with $h_{mag}=1.5$ mm. The two peaks of the attraction force correspond roughly to the top and bottom level of each magnet and appear in different positions for each design due to the different magnet heights.

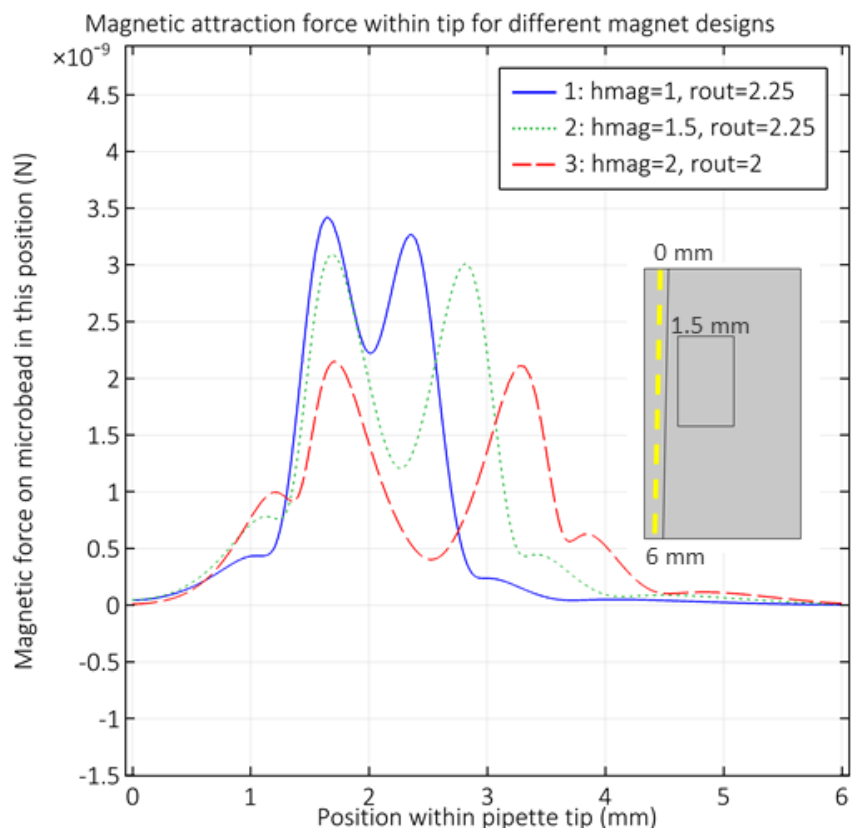


Figure 3.32: The total magnetic attraction force inside the pipette tip for the three different magnet sizes that were promoted from the analysis seen in table 6.20. This is an indication for the attraction of the different magnet designs in positions near the magnet.

A second criterion that can be used to evaluate the performance of the trapping system is the magnetic force on the pipette inlet. Since it is undesirable for the pipette to aspirate air, part of the liquid volume will remain on the bottom part of the pipette tip and will not be aspirated further upwards. For this volume, the particle tracing analysis does not provide any information. In order to achieve trapping, these microbeads will require a dwell step in which the liquid rests and the microbeads are left to move towards the magnet. This process step can be seen in Fig. 3.33. Starting at $t=0$ sec, a microbead-containing liquid volume has been aspirated by the pipette tip but the aspiration has stopped before these beads can reach the magnet level. The microbeads contained within this volume are left to float within the liquid buffer and approach the magnet due to the magnetic force alone. In the following time steps, the microbeads are seen to move towards the magnet following paths defined by the magnetic force vector field (Fig 3.33).

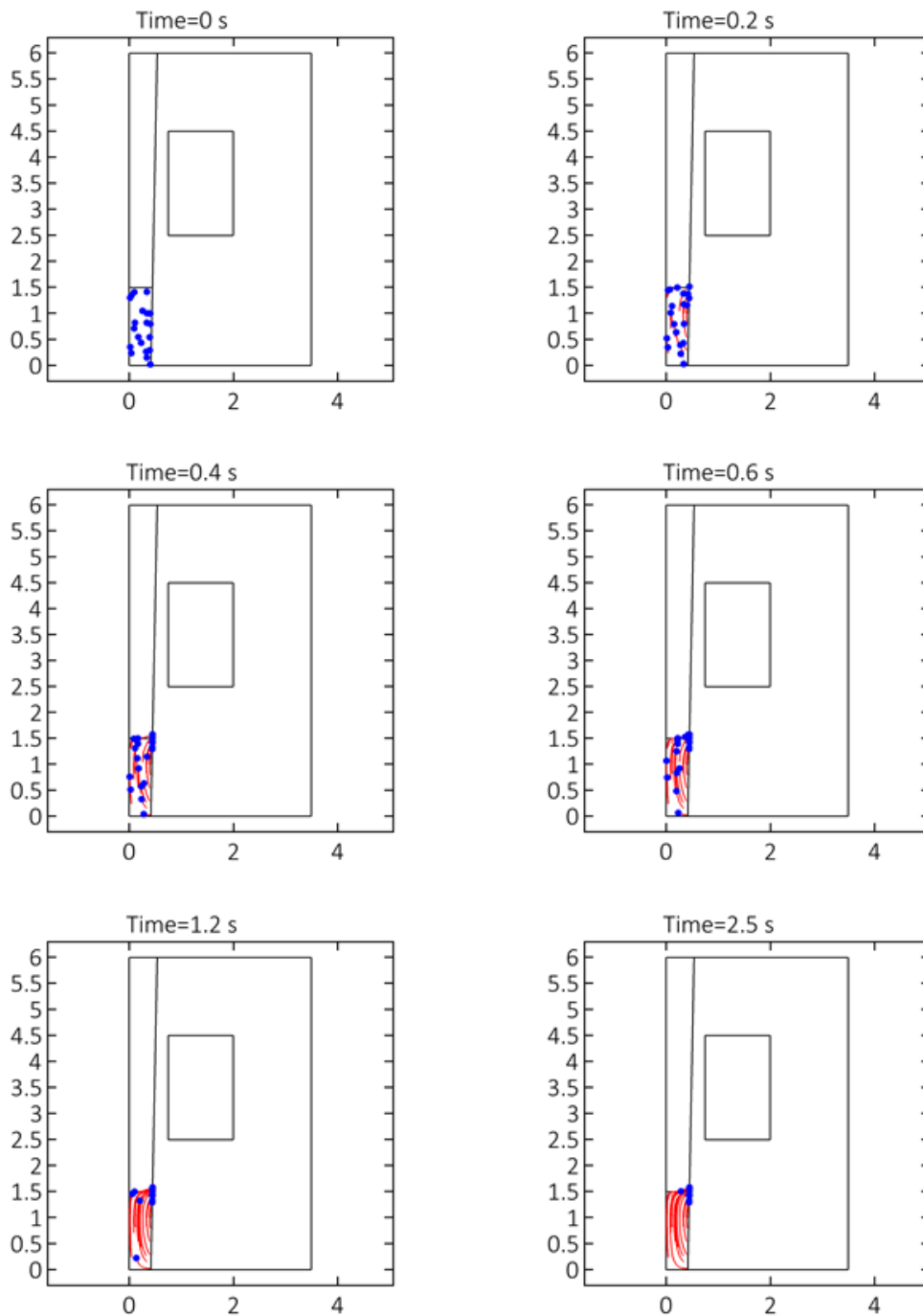


Figure 3.33: For microbeads that remain at the lower part of the pipette tip when the aspiration stops, the magnetic force alone needs to pull them towards the magnet so that efficient separation can be achieved

As seen during the analysis of Eq. 9, the effect of gravity in combination with buoyancy on the microbeads yield forces in the order of 10^{-14} N, while the magnetic forces at the most distant part of the working field are in the order of 10^{-11} N. As such, and in absence of a fluid velocity field, the magnetic forces dominate. Because of this, it makes sense that all three promoted designs will also result in the microbeads being trapped, although it would require different dwell times depending on their force vector throughout the capture paths. In order to compare the three designs as to their effect on microbeads further away from the magnet, the magnetic force for a pipette tip cross section at a lower position of the work area will be calculated. In Fig 3.23, a line crossing the pipette tip at $y=0.5$ mm is drawn and on this line the total magnetic attraction force is calculated for all three designs. The vector directions seen in Fig. 3.23 which are plotted again in 3.34, indicate that at further positions from the magnet level, the dominant component of the magnetic force is axial. This is the force acting upon the stationary microspheres that pulls them towards the magnet. What can be seen in Fig 3.34, is that the magnet design (3), which has the largest magnet height ($h_{mag}=2$ mm) yields the strongest magnetic force among the three designs. Design (1) -which gave the highest attraction force in positions near the magnet- yields the lowest force in this instance while design (2) is in between the other two.

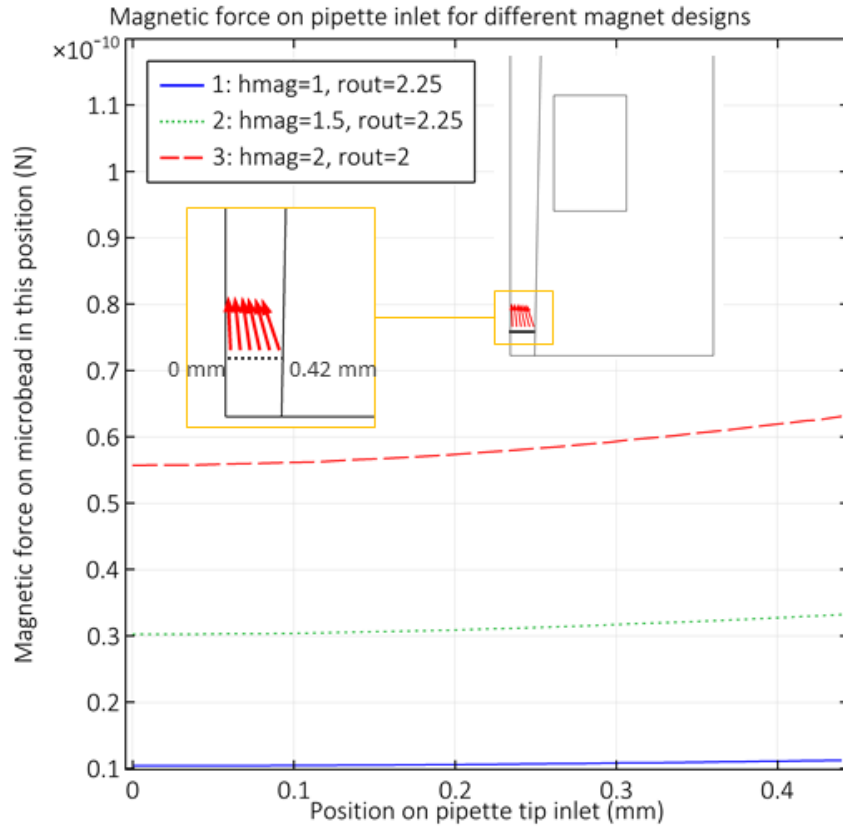


Figure 3.34: The total magnetic attraction force at the lower part of the pipette tip for the three different magnet sizes that were promoted from the analysis seen in table 3.2. The magnetic force at this distance from the magnet has a dominant axial component.

In summary, a particle tracing analysis resulted in the selection of 7 different ring magnet designs which would be expected to have an increased trapping efficiency over the rest. Because it was shown in Fig. 3.24 that ring magnets with larger diameters output larger magnetic forces, these 7 solutions were narrowed down to 3 solutions by excluding designs which had the same height but a smaller diameter than another promoted design. These 3 solutions were compared to one another using two different criteria: (A) The magnetic attraction in microbeads near the magnet and (B) the magnetic attraction in microbeads far from the magnet. In these final two analyses, design 1 yielded the best performance near the magnet but the worst far from the magnet. Design 3 yielded the best performance far from the magnet but the worst near the magnet. Design 2 had comparable results with design 1 near the magnet and was between the other two solutions far from the magnet. In all of these cases the inner magnet radius remains 1.5 mm and the calculations are made for an N48 neodymium magnet.

Overall, design 2 (height=1.5 mm , Outer radius=2.25 mm) yielded the most promising results as per its expected performance in a magnetic separation system for microbeads that is based on a ring magnet design.

FINITE ELEMENT MODELLING | QUATREFOIL MAGNET ARRANGEMENT

In the previous section, the trapping efficiency of a ring magnet placed around a pipette tip which is aspirating a solution containing superparamagnetic microbeads was modelled using finite elements and particle tracing. While the ring magnet is an intuitively obvious choice, a different arrangement can also be used which includes 4 symmetrically positioned cylindrical magnets around the pipette tip. The shape formed by the magnets can be seen in Fig. 3.35 and is known as a quatrefoil.

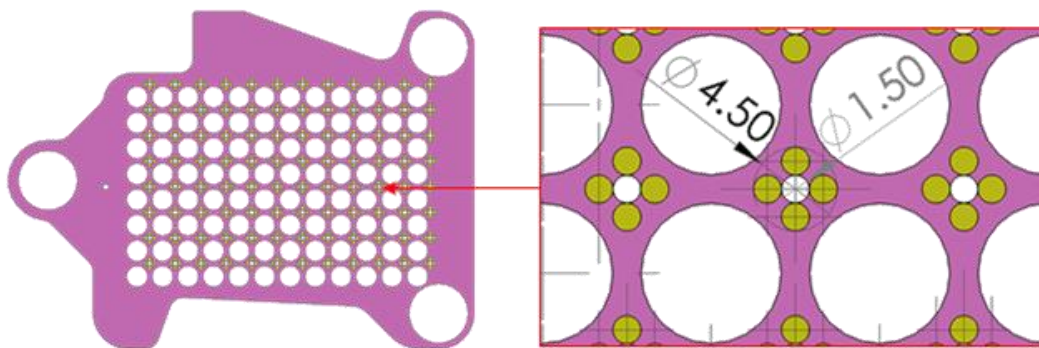


Figure 3.35: An arrangement based on 4 cylindrical magnets positioned around the pipette tip in order to trap microbeads within the pipette tip.

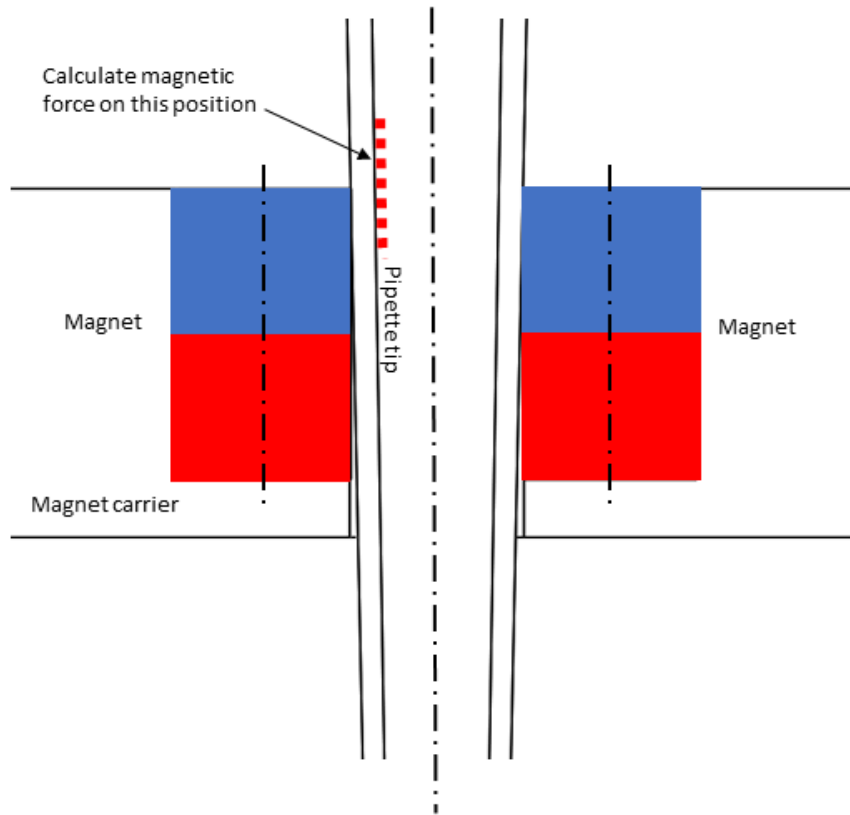
The potential benefit of this approach is that in this arrangement, larger magnets can be used without compromising the structural integrity of the magnet carrier as was the case with the ring magnets. In figure 3.35, four magnets have been placed within the area of a circumscribed circle of 4.5 mm in diameter. In the case of the ring magnet, solutions with a diameter of 4.5 mm and a height over 1.5 mm had to be rejected because they were structurally

undesirable. However, in this scenario, magnet heights of over 2 mm can be used since this arrangement does not weaken the part as much.

Since this arrangement is not axisymmetric, the cartesian space is more suited for the mathematical formulation. For this model, Eq. 7 will again be used for the calculation of magnetic forces within the pipette tip:

$$(7) \quad \vec{F}_m = \frac{V\chi_b}{\mu_0} (\vec{B} \cdot \nabla) \vec{B} = \frac{V\chi_b}{\mu_0} \begin{pmatrix} B_x \frac{\partial B_x}{\partial x} + B_y \frac{\partial B_x}{\partial y} + B_z \frac{\partial B_x}{\partial z} \\ B_x \frac{\partial B_y}{\partial x} + B_y \frac{\partial B_y}{\partial y} + B_z \frac{\partial B_y}{\partial z} \\ B_x \frac{\partial B_z}{\partial x} + B_y \frac{\partial B_z}{\partial y} + B_z \frac{\partial B_z}{\partial z} \end{pmatrix}$$

In terms of analysis, this scenario requires a 3D model with a quarter symmetry (Fig 3.36). Since this is a more demanding application computationally, the model was built with a coarse 0.3 mm mesh size of free tetrahedral elements applied across all domains. The metric used for the evaluation of the magnet size is the magnetic force on a microbead resting at the inner pipette tip wall adjacent to the magnet. This can be modelled as a line segment resting on the intersection of the plane generated by the pipette tip centerline and the magnet centerline and the inner pipette tip wall. This line can be seen in both parts of Fig 3.36. Since the evaluation of the magnetic force (Eq. 7) requires the calculation of derivatives across the magnetic flux density vector field, the results tend to be noisy and require a mesh refinement to better capture the magnetic flux density in the first place. For this reason, a refinement of 0.01 mm with a growth rate of 1.1 is used on the line of calculation (Fig 3.37). Using this model, the magnetics problem can be solved and the magnetic force acting upon a superparamagnetic particle can be calculated for the pipette tip domain. The magnetic material remains Neodymium N48 with a magnetization of 850 [kA/m] and every other material is considered to share a relative permeability equal to 1.



3D model with quarter-symmetry

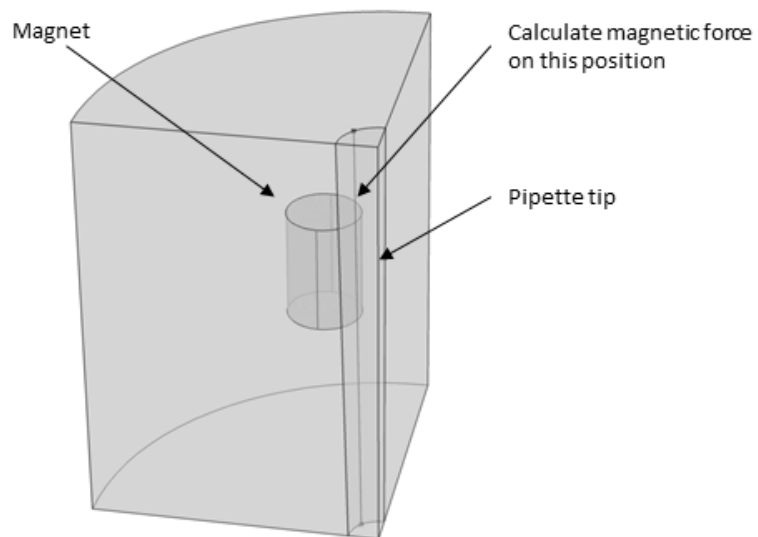


Figure 3.36: A 3D model of the quatrefoil magnet arrangement with a quarter symmetry. Calculations for the determination of the magnet size are done on the inner pipette tip wall on the line nearest to the magnet

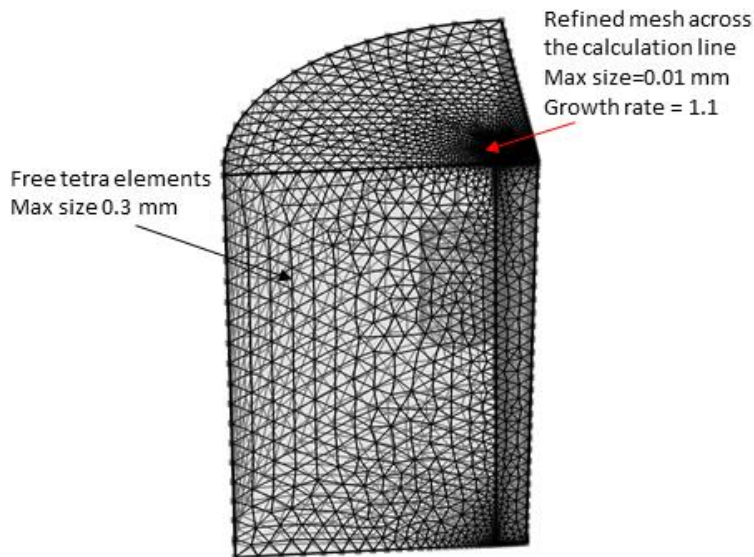


Figure 3.37: The model is meshed with a 0.3 mm element size across all domains and a refinement of 0.01 mm on the line where forces will be calculated

For the purpose of mapping the effects of different magnet geometric attributes, the model is solved (A) for magnets of a 1 mm diameter and heights ranging from 0.5 to 2.5 mm and (B) for magnets of 1.5 mm height and radiuses ranging from 0.25 to 0.75 mm. The results can be seen in Fig. 3.38. What is calculated is the radial magnetic force across the line of calculation which is used as a metric that indicates the trapping force of a microbead once that microbead has been immobilized on the pipette tip wall. This value is important because it indicates the ability of the system to retain trapped microbeads during assay operations. However, just like in the previous section, it cannot be the only criterion since it does not provide information about the ability of the system to capture the microbeads in the first place.

On the top part of Fig 3.38, the effect of different magnet heights is explored. The magnet radius is kept at 1 mm for all designs and the height is varied from 0.5 to 2.5 mm. What can be observed, is there is a small decreasing trend for the peak force of larger magnets, however the differences are within $\sim 10\%$ of the nominal value. Depending on the results of the particle tracing analysis that will follow, this difference could be unimportant.

On the bottom part of Fig. 3.38, the effect of different magnet radiuses is explored. The magnet height is kept at 1.5 mm for all designs and the radius is varied from 0.25 to 0.75 mm. What can be observed is that, just like with the ring magnets, the increasing diameter yields larger retention forces. This is an indication that larger diameters would most likely result in higher separation efficiency and retention ability.

Based on all the previous, for the case of the quatrefoil arrangement, a large magnet diameter appears to favor higher separation efficiencies, while the effect of the magnet height should be evaluated through a particle tracing study.

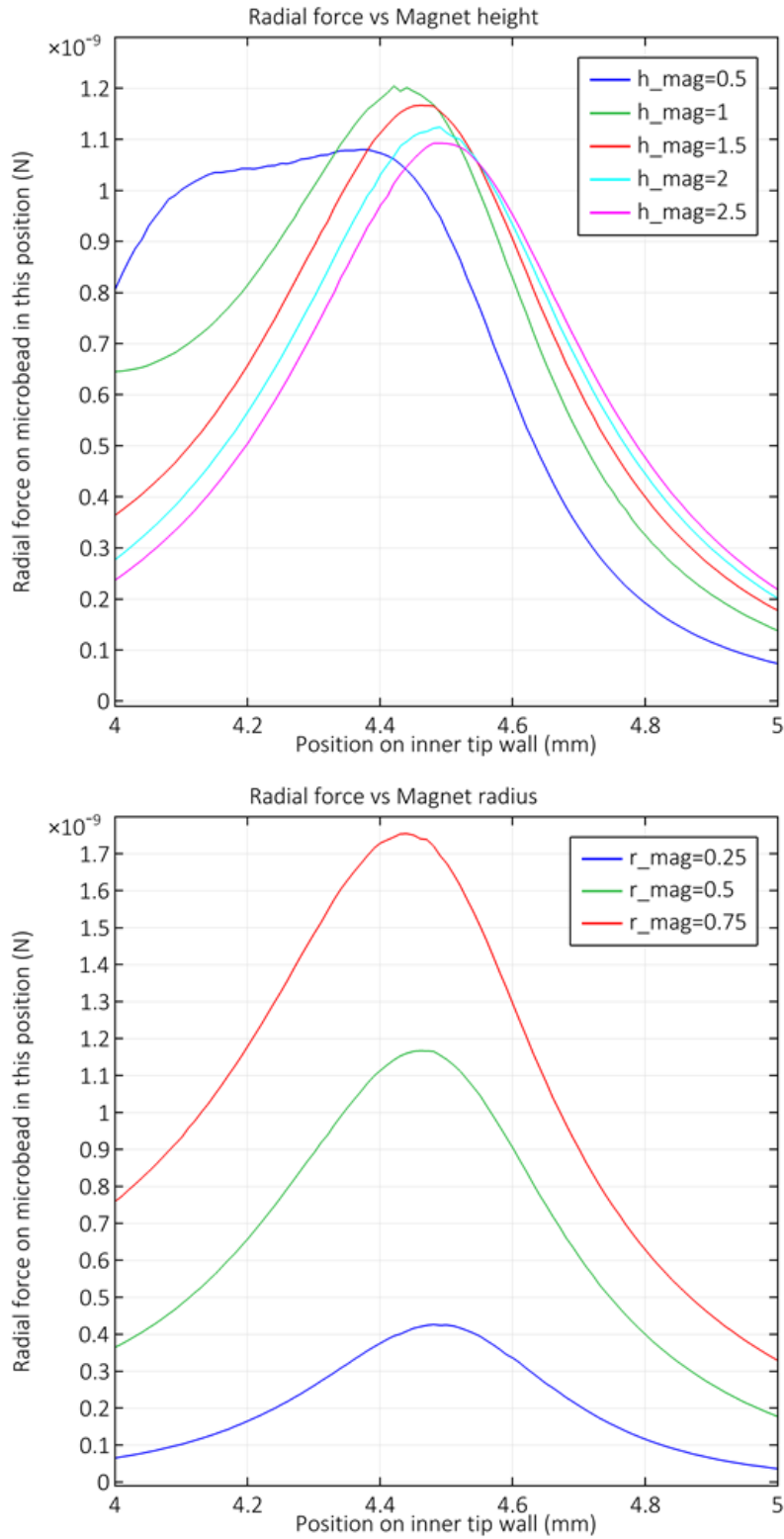


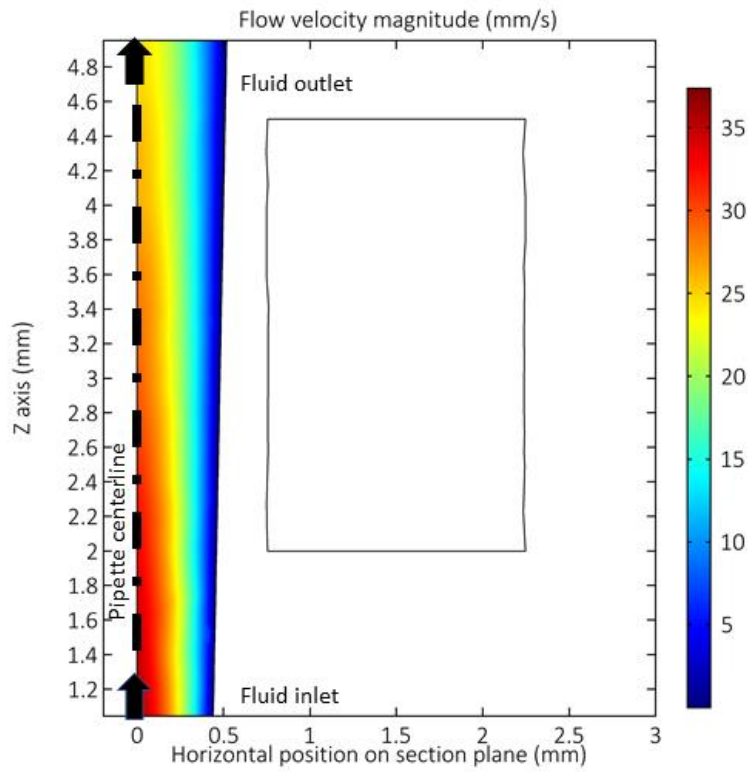
Figure 3.38: The effect of different magnet heights (top) and diameters (bottom) is explored independently for the quatrefoil magnet arrangement

PARTICLE TRACING | QUATREFOIL MAGNET

In the previous section, the magnetic force components acting upon a microbead in various positions within a pipette tip have been shown for the quatrefoil magnet arrangement. Different calculations have been made for different magnet sizes and the results have been shown for a microbead immobilized on the pipette tip wall. However, following the same rationale as in the ring magnet analysis, a particle tracing model is going to be used to assist in the design of the magnetic separation system.

As with the ring magnet, in order to perform a particle tracing analysis for this problem it is necessary to calculate the magnetic force vector field and the fluid flow velocity field within the pipette tip. Keeping the ring magnet conditions to produce comparable solutions, the mass inflow to the pipette tip is set to 10^{-5} kg/s. The pipette tip remains the same, thus the Reynolds number does not change. The force and fluid flow fields can be seen in Fig. 3.39.

On the top part, the velocity field during fluid aspiration is calculated for the 3D model using a laminar flow model. Just like in the previous section the model is set with a total fluid mass inlet of $\dot{m} = 10^{-5}$ kg/s, no-slip boundary condition at the pipette tip walls and no turbulence model. The results are identical to the axisymmetric model seen in the previous section which was expected. On the bottom part of Fig 3.39, Eq. 7 is solved for the magnet flux density vector field to yield the magnetic force acting on a superparamagnetic microbead in any position within the pipette tip. Only the force magnitude on the pipette wall is visible, however the field within the entire tip has been calculated to be used as input for the particle tracing problem.



Force on microbeads within pipette tip for quatrefoil magnet arrangement (N)

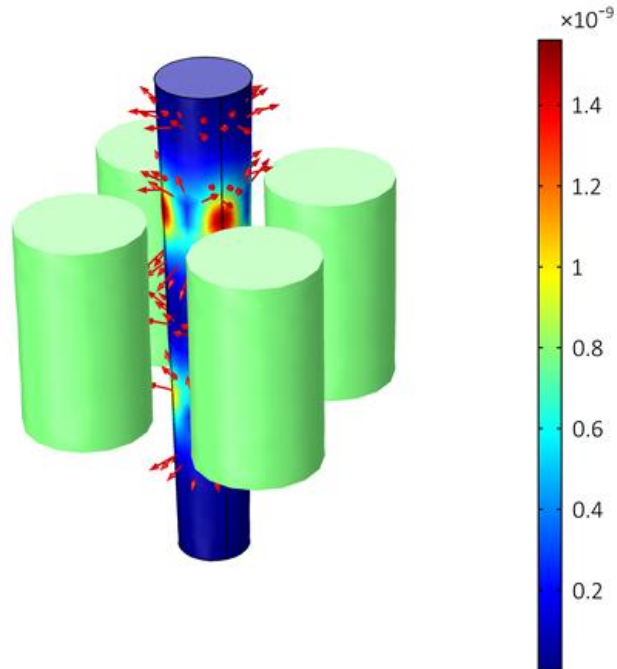


Figure 3.39: Two different physics models are required to model particle tracing: Fluid flow (top) for Stokes drag model on the microbeads and the magnetic forces on the microbeads (bottom) as described in Eq. 12

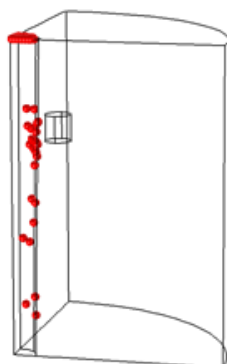
Using the two fields shown in Fig. 3.39, the 3D particle tracing problem is solved. The fluid inlet is set as a starting point for microbeads. The number of microbeads is set to 60 for each quarter section. The trapping efficiency of this arrangement has been compiled for all designs in Table 3.4 while each separate case can be seen in Fig. 3.40 – 3.42. Microbeads that overshoot the magnet position and flow towards the outlet of the model reduce the trapping efficiency of the magnet arrangement. Microbeads that are immobilized on the pipette tip wall are considered to be captured.

The results from this analysis (Table 3.4) show 4 magnet designs that yield trapping efficiency over 95%, the threshold over which a solution is considered acceptable. The promoted solutions include designs with the largest magnet radius (0.75 mm) and a range of magnet heights (1-2.5 mm)

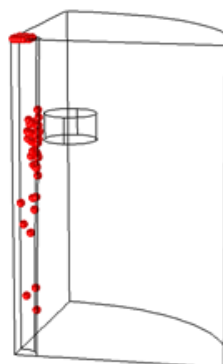
Magnet height (mm)	Magnet outer radius (mm)	Trapping (%)	Overshot (%)	Comments
0.5	0.25	47%	53%	Low efficiency
0.5	0.5	72%	28%	Low efficiency
0.5	0.75	83%	17%	Low efficiency
1	0.25	57%	43%	Low efficiency
1	0.5	83%	17%	Low efficiency
1	0.75	98%	2%	✓
1.5	0.25	57%	43%	Low efficiency
1.5	0.5	88%	12%	Low efficiency
1.5	0.75	100%	0%	✓
2	0.25	57%	43%	Low efficiency
2	0.5	87%	13%	Low efficiency
2	0.75	98%	2%	✓
2.5	0.25	57%	43%	Low efficiency
2.5	0.5	87%	13%	Low efficiency
2.5	0.75	98%	2%	✓

Table 3.4: Trapping efficiency of different magnet sizes in the quatrefoil magnet arrangement with varying magnet height and outer radius.

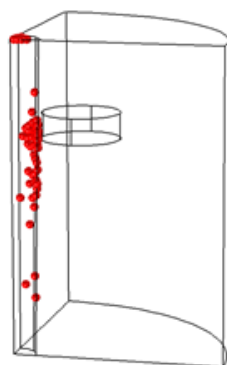
$h_{\text{mag}}=0.5, r_{\text{mag}}=0.25$ Time=1 s



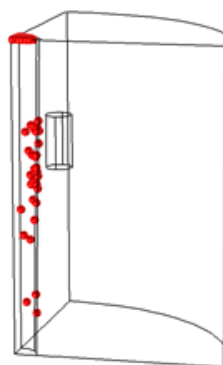
$h_{\text{mag}}=0.5, r_{\text{mag}}=0.5$ Time=1 s



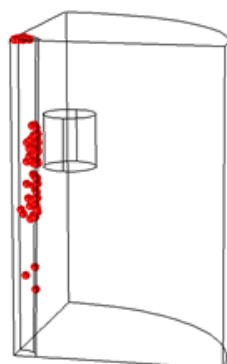
$h_{\text{mag}}=0.5, r_{\text{mag}}=0.75$ Time=1 s



$h_{\text{mag}}=1, r_{\text{mag}}=0.25$ Time=1 s



$h_{\text{mag}}=1, r_{\text{mag}}=0.5$ Time=1 s



$h_{\text{mag}}=1, r_{\text{mag}}=0.75$ Time=1 s

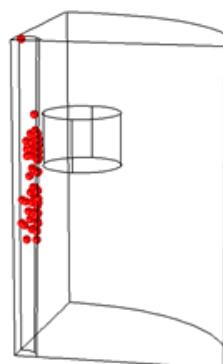
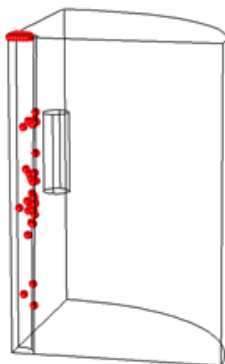
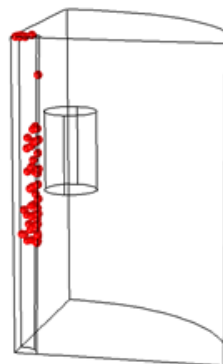


Fig 3.40: End positions of microbeads entering the pipette tip driven by a laminar flow under the influence of a magnetic field from a quatrefoil magnets arrangement with cylindrical magnets of different height (h_{mag}) and radius (r_{mag}). Microbeads that appear to have reached the top of the pipette tip, are considered to have overshot the trapping position.

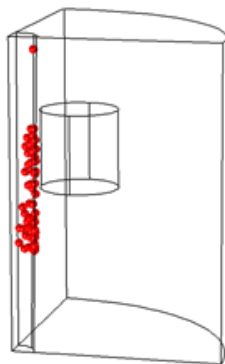
$h_{\text{mag}}=1.5, r_{\text{mag}}=0.25$ Time=1 s



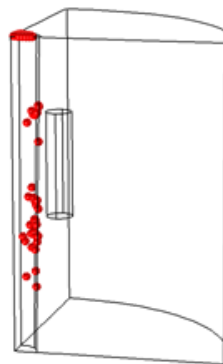
$h_{\text{mag}}=1.5, r_{\text{mag}}=0.5$ Time=1 s



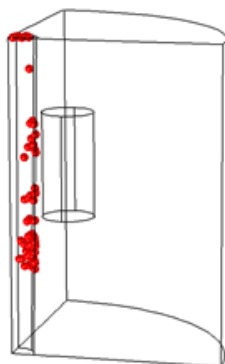
$h_{\text{mag}}=1.5, r_{\text{mag}}=0.75$ Time=1 s



$h_{\text{mag}}=2, r_{\text{mag}}=0.25$ Time=1 s



$h_{\text{mag}}=2, r_{\text{mag}}=0.5$ Time=1 s



$h_{\text{mag}}=2, r_{\text{mag}}=0.75$ Time=1 s

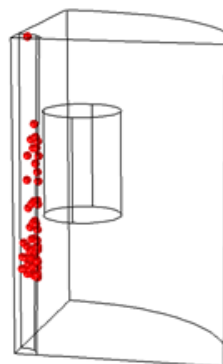
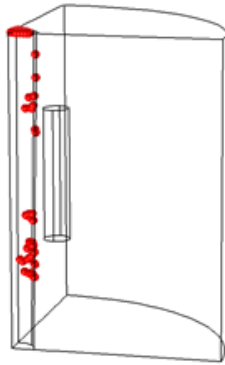
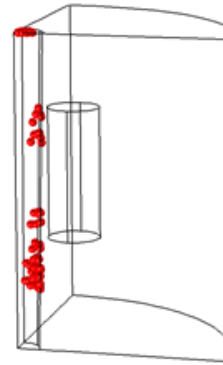


Fig 3.41: End positions of microbeads entering the pipette tip driven by a laminar flow under the influence of a magnetic field from a quatrefoil magnets arrangement with cylindrical magnets of different height (h_{mag}) and radius (r_{mag}). Microbeads that appear to have reached the top of the pipette tip, are considered to have overshot the trapping position.

$h_{mag}=2.5, r_{mag}=0.25$ Time=1 s



$h_{mag}=2.5, r_{mag}=0.5$ Time=1 s



$h_{mag}=2.5, r_{mag}=0.75$ Time=1 s

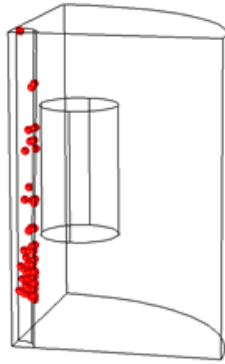


Fig 3.42: End positions of microbeads entering the pipette tip driven by a laminar flow under the influence of a magnetic field from a quatrefoil magnets arrangement with cylindrical magnets of different height (h_{mag}) and radius (r_{mag}). Microbeads that appear to have reached the top of the pipette tip, are considered to have overshot the trapping position

Following the previous analysis, there are 4 available solutions to be compared to each other (Table 3.5). In order to perform the comparison, the same methodology that was used for the ring magnet design will be used in this case too.

Design No	Magnet height (mm)	Magnet outer radius (mm)
1	1	0.75
2	1.5	0.75
3	2	0.75
4	2.5	0.75

Table 3.5: Five different magnet designs for the quatrefoil arrangement are promoted from the particle tracing analysis as the more suitable design choices for efficient microbead trapping

Using the same approach as in the ring magnet design, the following two criteria are explored in order to compare the different magnet sizes:

1. The total magnetic force within the pipette tip in an area near the magnet
2. The total magnetic force within the pipette tip in an area far from the magnet

The magnetic force within the pipette tip in an area near the magnet is an indication of the magnets ability to attract and trap microbeads that have been aspirated near the magnets level. In order to explore the effect of the different designs, a calculation line is drawn 0.1 mm from the pipette inner wall and the total magnetic force magnitude on a microbead is calculated on this line. The results can be seen in Fig. 6.38. The dashed yellow line is where the calculation is performed starting from the top of the work area and moving downwards. Just like in the ring magnet study, the promoted designs display a reverse correlation of the total magnetic force magnitude and the magnet height. Shorter magnets yield better performance for areas near the magnet. The double peaks present in most designs are again related to the magnet height and located roughly at the bottom and top plane of each magnet design. Design (1) with a magnet height of 1 mm yields the highest attraction force and design (4) with a magnet height of 2.5 mm yields the lowest attraction force.

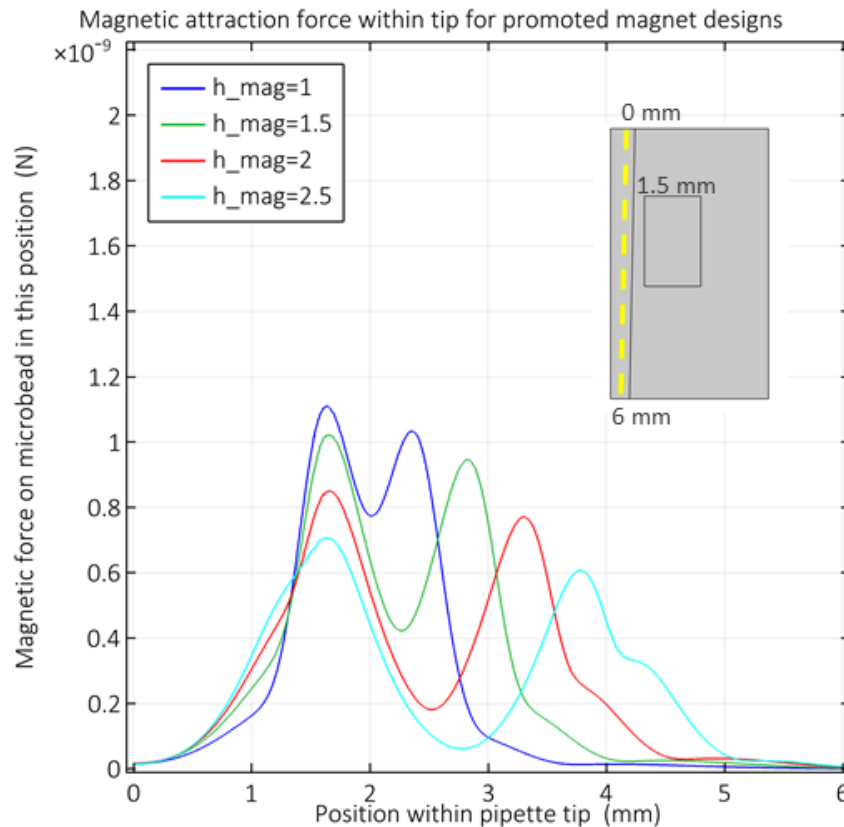


Figure 3.43: The total magnetic attraction force inside the pipette tip for the five different magnet sizes that were promoted from the analysis seen in table 3.4. This is an indication for the attraction of the different magnet designs in positions near the magnet.

The magnetic force within the pipette tip in an area far from the magnet is an indication of the magnets ability to attract and stationary microbeads that are not aspirated to positions near the magnet level. As described in the previous chapter, the entire liquid volume cannot be aspirated to the magnet level because this would result in air being drawn into the pipette tip which in turn could cause the formation in bubbles, an undesirable condition for fluidic and microfluidic assay systems. For this reason, the microbeads that remain into that liquid volume will need to move towards the magnet unassisted by fluid flow. The magnetic force in the lower positions of the pipette is the dominant force which will draw these microbeads into trapping positions. For this reason, magnetic forces are calculated at the position $y=0.5$ mm on a cross section of the pipette diameter. The results can be seen in Fig. 3.44. The dotted black line is the pipette tip cross section on which the calculation is performed. Just like in the ring magnet design, the larger magnets perform better on the far regions of the pipette tip compared to the smaller magnets. However, there is an overlap between designs 3&4 near the pipette tip centerline. The force vectors on the line of calculation point upwards and towards the magnet.

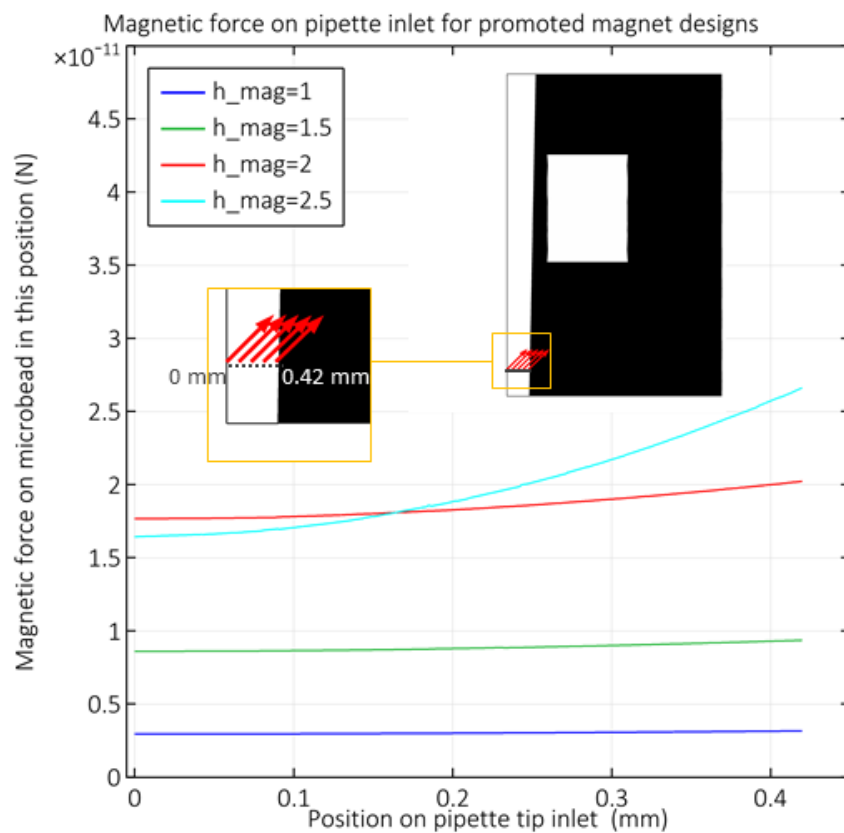


Figure 3.44: The total magnetic attraction force at the lower part of the pipette tip for the five different magnet sizes that were promoted from the analysis seen in table 3.4.

In summary, for the quatrefoil magnet arrangement, a particle tracing analysis resulted in the selection of 10 different cylinder magnet designs which are expected to have an increased trapping efficiency over the rest. Because it was shown in Fig. 3.38 that ring magnets with larger diameters output larger magnetic forces, these 10 solutions were narrowed down to 5 solutions by excluding designs which had the same height but a smaller diameter than another promoted design. These 5 solutions were compared to one another using two different criteria: (A) The magnetic attraction in microbeads near the magnet and (B) the magnetic attraction in microbeads far from the magnet. In these final two analyses, design 1 ($h=1$ mm) yielded the best performance near the magnet but a poor

result far from the magnet. Design 4 (h=2.5 mm) yielded the best performance far from the magnet but the worst near the magnet. Design 3 (h= 2 mm) displayed an average performance in both analyses. In all of these cases, the magnets re position so as to be tangent to a 1.5 mm tip radius and the calculations are made for an N48 neodymium magnet.

Overall, design 3 (h=2.5 mm , Outer radius=0.75 mm) yielded the most promising results as per its expected performance in a magnetic separation system for microbeads that is based on a quatrefoil magnet arrangement.

MAGNETIC SEPARATION SYSTEM DESIGN | SUMMARY

The purpose of the magnetic separation system is to retain superparamagnetic microbeads that are used as the primary antibody substrate in suspension immunoassays. The novelty compared to the state of the art is that the magnetic separation takes place within the pipette tip. This could potentially simplify and accelerate the assay process. In order to achieve effective separation, two different designs have been modeled using finite element analysis: A ring magnet separation system and a quatrefoil separation system. The two approaches have been explored as per their performance in correlation to different magnet sizes. The promoted solution from each approach is presented in table 6.40.



Design approach	Arrangement (cross section)	No of magnets	Magnet height (mm)	Magnet outer radius (mm)
Ring magnet		1	1.5	2.25
Quatrefoil design		4	2	0.75

Table 3.6: Two different magnet arrangements have been modelled and explored for magnetic separation systems. The dimensions that have been found to be optimal for each arrangement are summarized here.

3.3.4 MOTION SYSTEM

The fluid handling functionality and the bead trapping module have been presented in the previous sections. In order to automate the assay protocols, a motion system is used that is responsible for the manipulation of the fluid handling head, the microtiter plates and the loading and unloading of pipette tips. The motion system, as described in the system architecture section, includes a Z axis that is coupled to the fluid handling head as well as a Y axis that latches and manipulates microtiter plate carriers. In Fig 3.45 The main components of the motion system are shown.

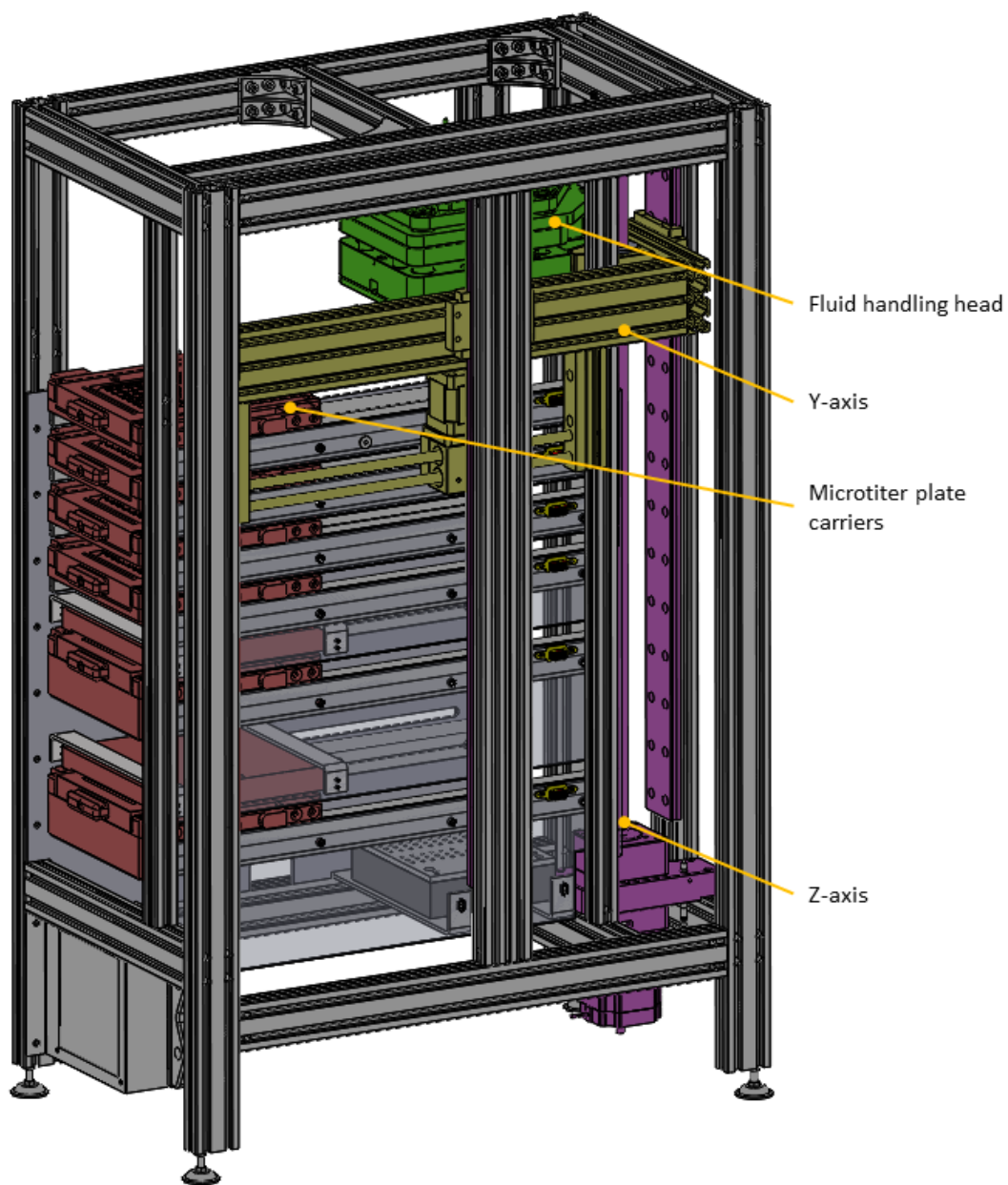


Figure 3.45: The motion system components of SampleX that are used for plate and head manipulation

Z axis motion is achieved using a ballscrew driven by a stepper motor with endstops at the terminal positions. The fluid handling head as well as the Y axis assembly are moved by the z axis leadscrew in the vertical direction while sliding on linear slides that are visible as part of the Z axis assembly of Fig. 3.45 are resting on the inner side of the back and side mid-positioned aluminum profile beams.

Y axis motion is achieved using a round rack and pinion motion transmission. The rack is stationary and the driving motor is the moving part. A stepper motor with endstops at the terminal position is again used for this axis. The end effector of the Y axis has a pear-shaped geometry and is responsible for latching onto the microtiter plate carrier so that the plates can be moved below the fluid handling head. The main components of the Y axis motion system can be seen in Fig. 3.46. By moving the Z axis downwards, the Y axis end effector couples into the plate carrier latch geometry. The plate can then move towards the fluid handling head using the Y axis rack and pinion drive.

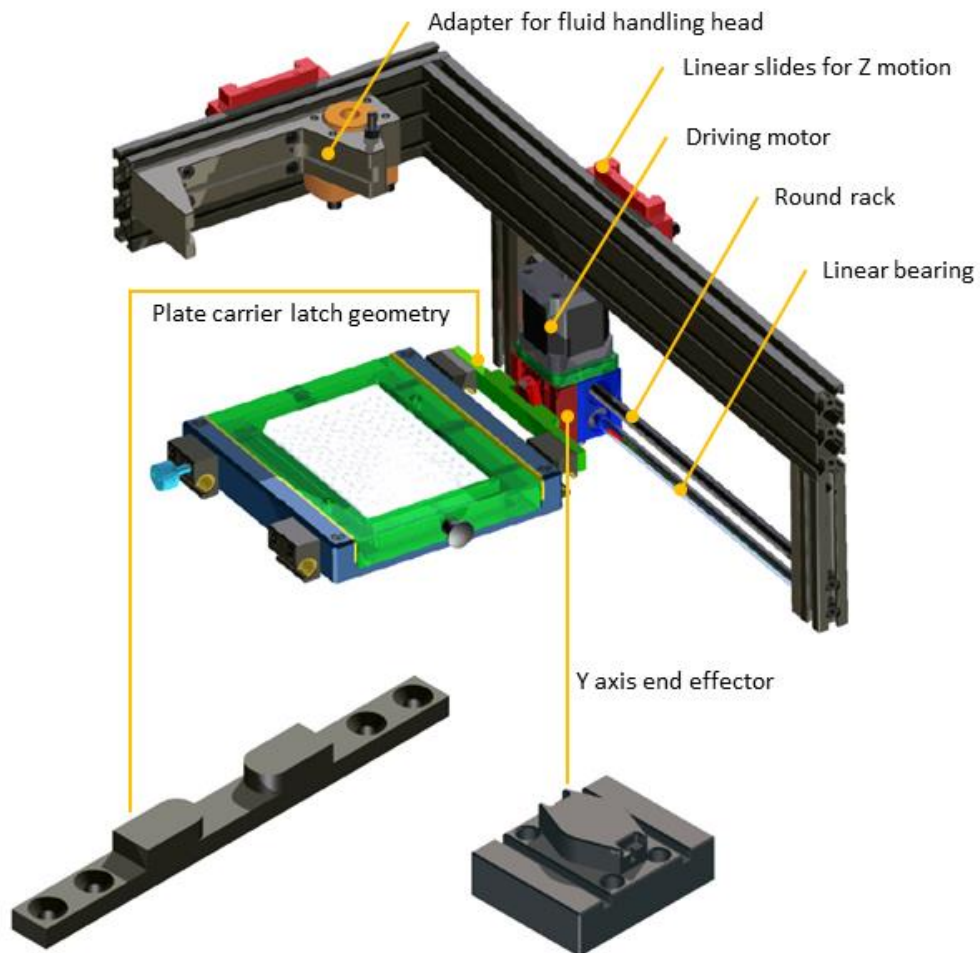


Figure 3.46: The Y axis motion system is used to bring the microtiter plates in and out of the working position of the fluid handling head

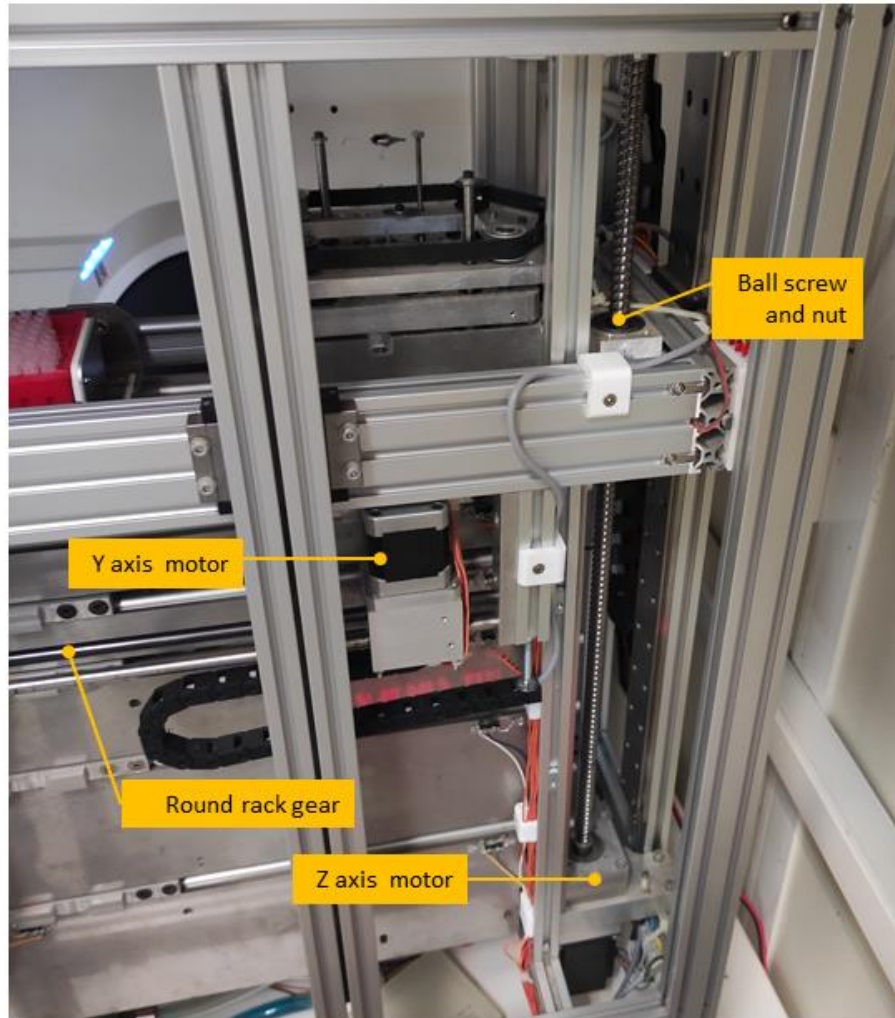


Figure 3.47: Part of the motion system of the SampleX platform

The microtiter plates are inserted into trays that assist in the alignment of the plate with the fluid handling head. The trays are placed on the plate carrier into which are aligned using ball plungers. The plate carriers are sliding on linear shafts using polymer linear guides and can freely move in the horizontal direction when they are not coupled to the Y axis end effector. The tray/carrier assembly as well as prototype plate trays can be seen in Fig. 3.48.

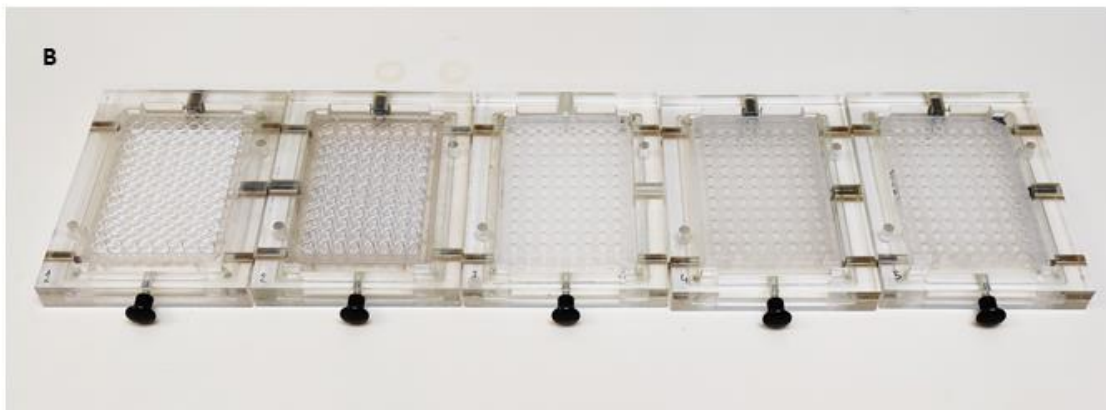
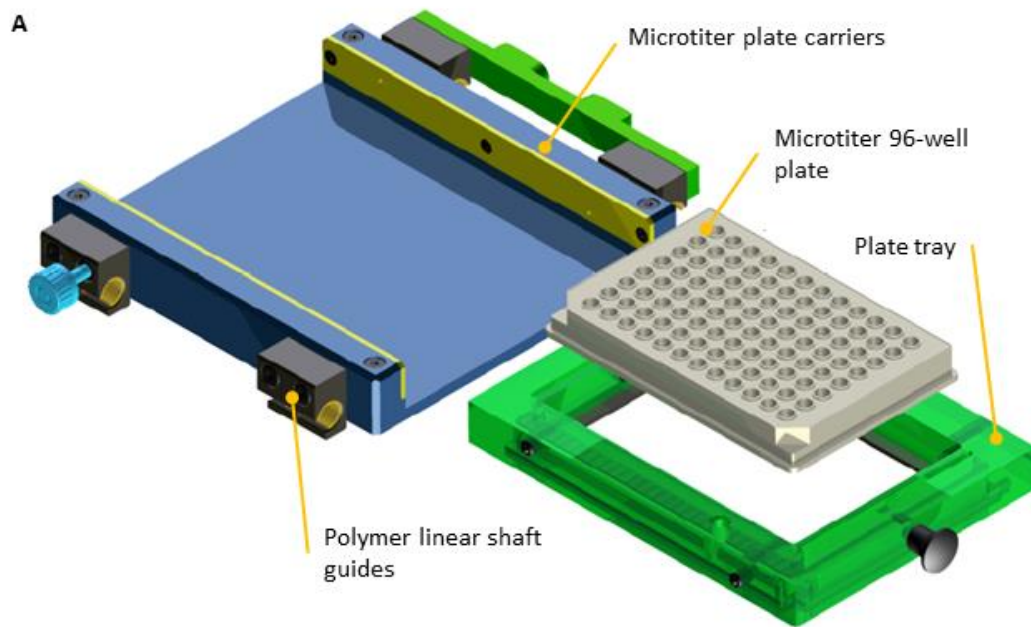


Figure 3.48: The microtiter plates are inserted into trays which are then placed in the plate carriers. (A) The tray assembly and carrier in exploded view. (B) Prototype plate trays with spring loaded plungers for plate alignment

3.3.5 ELECTRONICS AND SYSTEM PROGRAMMING

The SampleX system control relies primarily on open loop stepper motor actuators. There are 5 motors in total: Z axis motor, Y axis motor, stepping gearmotor for switching between magnets on and off position, linear stepping motor for the vertical translation of the magnet plate, pipetting motor and a stepper motor used for the unloading of pipette tips. The motors are controlled using TMC2209 trinamic drivers and a 32bit SKRV1.3 controller with an ARM Cortex-M3 processor. The open firmware for additive manufacturing *Marlin* is being used with a G-code interpreter. All protocols have been programmed using G-code subroutines and Pure Python to control stepper motion position sequences. Axes zeroing is performed using homing with terminal switches for Z,Y and pipetting

motors. Current control is applied on all motions to promptly sense machine crashes in order to activate an emergency stop.

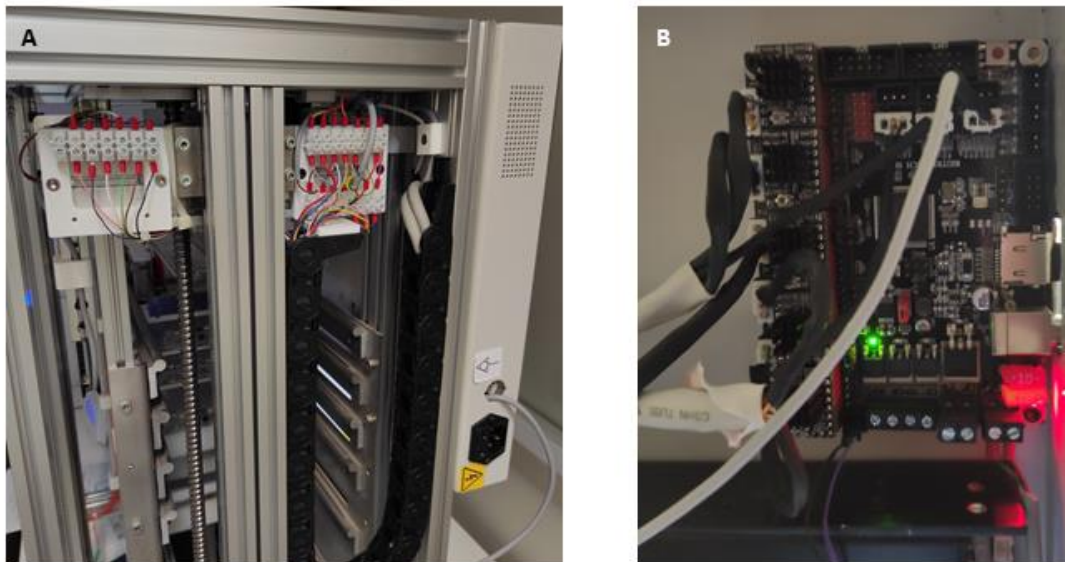


Figure 3.49: The electronics controlling the SampleX platform are based on the open source firmware Marlin. (A) The main electronic components are stepper motors and endstops, most of which are located on the moving Z axis. (B) The SKR V1.3 with on board stepper motor drivers.

3.3.6 IMMUNOASSAY PROCESS IN SAMPLEX

In the previous chapters, the fluid handling, microbead separation and motion systems have been presented. All of these systems combined can be used to perform a full immunoassay in a completely automated manner. In a bead-based sandwich ELISA, the required process steps are the following:

- Capture/ the microbeads
- Incubate with sample
- Incubate with secondary Ab
- Incubate with label
- Dispense microbeads for storage or reading

Between each of the previous steps, a washing process takes place to purge the microbeads from unbound reagents and prevent cross contamination. Incubations typically last several minutes or hours and they take place inside plate mixers. Each of these listed steps requires manual handling to be performed. The same process in SampleX requires the preloading of the plates with the necessary reagents and after that the immunoassay process is performed in an automated manner. In Figure 3.50, two different modes to perform immunoassays are shown.

In Fig. 3.50 A, each plate position is loaded with a different reagent. The fluid handling head performs each process step by loading the appropriate reagent plate. The two bottom plates are cooled using peltier elements to allow temporary storage of the more sensitive reagents (Secondary Ab) and to store the microbeads once the assay is complete for cases when the reading (the quantification of the assay results) is not done immediately, for example for assays that are completed overnight or during a weekend. For washing steps, either the flow-through system is used, or a plate is dedicated for washing buffer, or just below all plates there is a washing fluid container that can be used for aspiration of washing buffer.

In Fig. 3.50 B, all the reagents are loaded into a single plate. This is more convenient when less samples need to be processed. In a 96-well plate, up to 16 data points (samples) can be prepared from a single plate leaving two rows (16 positions) for microbead storage after assay completion and another two rows for assay buffer storage.

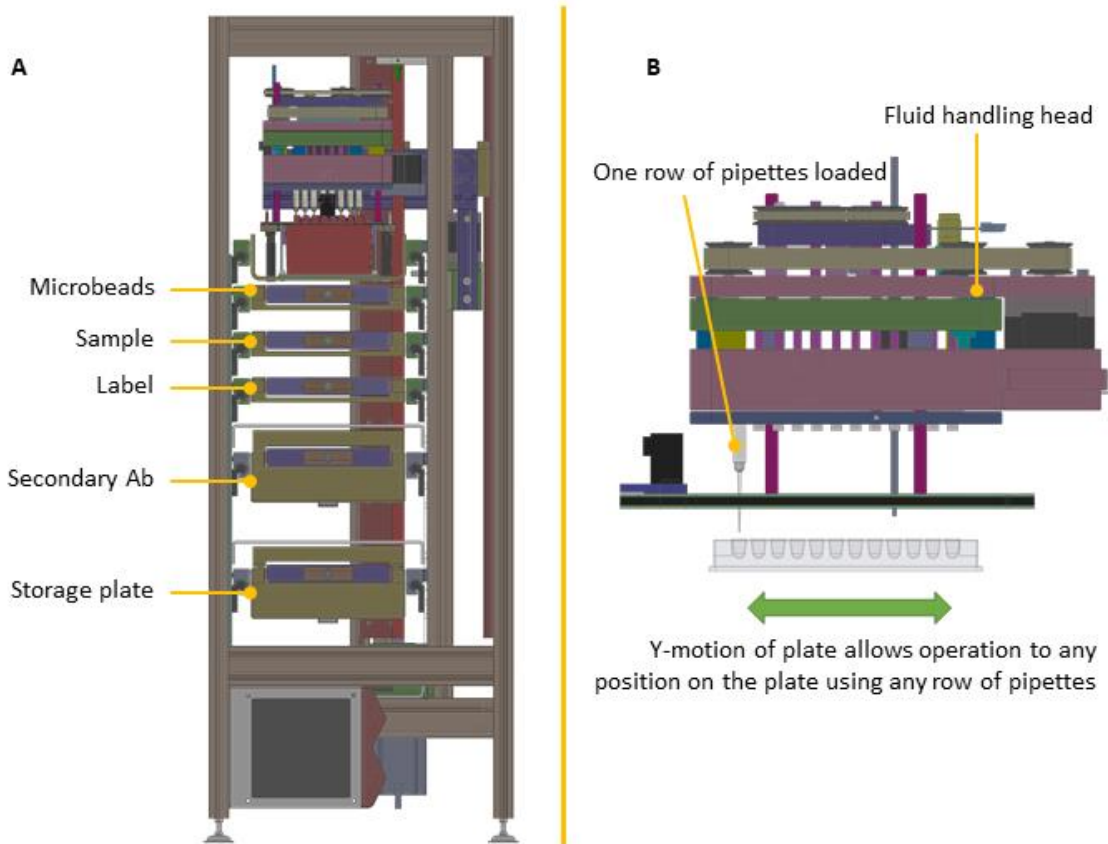


Figure 3.50: The immunoassay process in SampleX. (A) In the standard mode, each plate position holds a different reagent and the fluid handling head goes through all of them. (B) In the single plate mode, where only few data points are required, for example 8 or 16, all the reagents can be loaded in just one plate. SampleX will then use its Y-axis to align 1 or more rows of pipettes over the required positions of the plate, changing each time for the next process step.

Overall, this system has been designed to automate all the manual processes normally performed by laboratory personnel for sandwich ELISA assays. It could be used both as an assay development or as a clinical diagnostics tool, offering high throughput and versatility to the research and point-of-care setting.

3.4 RESULTS

3.4.1 MICROBEADS IN PIPETTE TIPS | MICROSCOPY

The finite element models presented in the previous sections were used to predict the end position of superparamagnetic microbeads that enter a pipette tip and are influenced by a permanent magnet's magnetic field. Two different arrangements have been examined, a ring magnet capture scheme and a quatrefoil shaped arrangement. In both designs, the model yielded the expected capture positions for microbeads the were entering the tip under the effect of a flow velocity field and when there was no flow in the tip. A useful tool to examine the separation method proposed in this work, is optical microscopy. An experimental setup to align a plunger driver pipette tip was used to allow the examination of the microbeads within the tip while under the influence of a magnetic field from a ring magnet. The magnet used is an N35 neodymium magnet with an external diameter of $\text{\O}4.5$ mm, an internal diameter of $\text{\O}1.5$ mm and a height of 1.5 mm. The experimental setup can be viewed schematically in Fig 3.51.

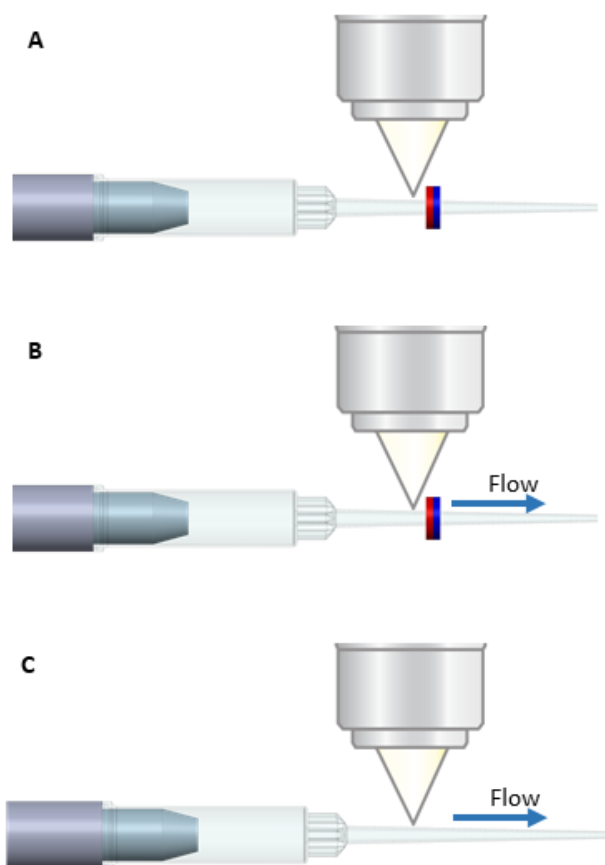


Figure 3.51: An optical microscopy setup to examine the behavior of paramagnetic microbeads under the influence of a magnetic field from a ring magnet. The scenarios examined are the following: (A) Captured microbeads are examined near the magnet without any flow (B) Captured microbeads are examined near the magnet while the liquid volume is dispensed (C) Captured microbeads are examined just after the magnet has been removed and while the liquid volume is dispensed

For the purpose of examining the behavior of microbeads, a pipette tip is positioned horizontally below a microscope objective lens. The ring magnet is already positioned on the tip and a microbead containing solution has been aspirated. In this setup, 3 different cases are examined: The already captured beads are seen in a position near the magnet (Fig 3.51-A), captured beads are seen in a position near the magnet while the pipette volume is dispensed (Fig 3.51-B), captured beads are seen in the same position after the magnet has been removed and while the pipette volume is dispensed (Fig 3.51-C). Each of these three is presented and discussed in the following figures.

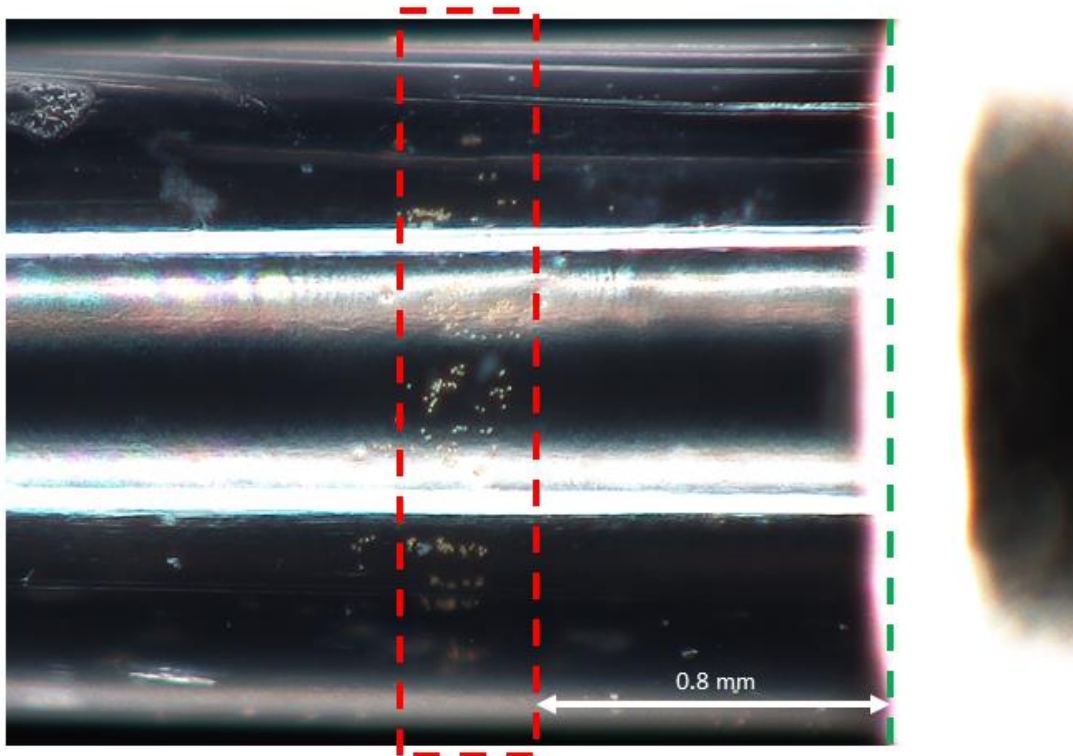


Figure 3.52: Captured microbeads inside the pipette tip. On the right side, the ring magnet can be discerned as an out of focus object. The beads are seen inside the red dashed rectangle.

In Fig. 3.52, captured microbeads within a pipette tip are seen. This is the case described in Fig. 3.51-A. The microbead solution was aspirated so that the average flow speed within the tip is approximately $u_{avg} = 18 \text{ mm/s}$. On the right side of Fig. 3.52, the ring magnet can be seen as an out of focus object. The microbeads have been captured at a position approximately 0.8 mm from the magnet's bottom plane. This is very close to the results obtained from the particle tracing model for $h_{mag}=1.5 \text{ mm}$ and $r_{out}=2.25 \text{ mm}$ which can be seen in Fig 3.30. While this observation does not provide any information on the capture efficiency of the method, it is evident that the beads are indeed being captured using the proposed method.

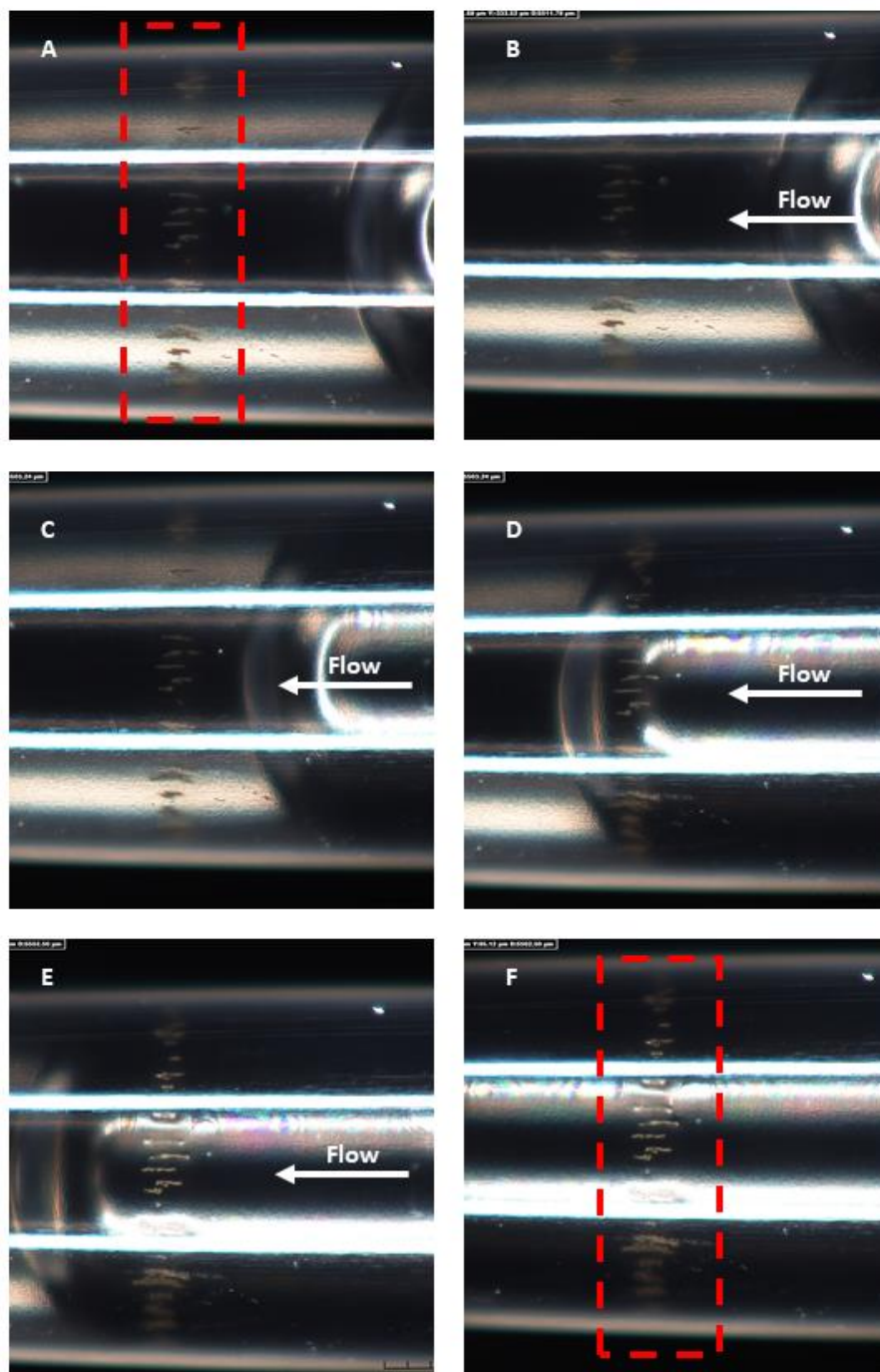


Figure 3.53: Captured microbeads inside the pipette tip under the influence of a ring magnet's magnetic field. The liquid solution is dispensed out of the tip but the microbeads remain trapped on the inner wall. The magnet (not seen) is located on the left side of the frames

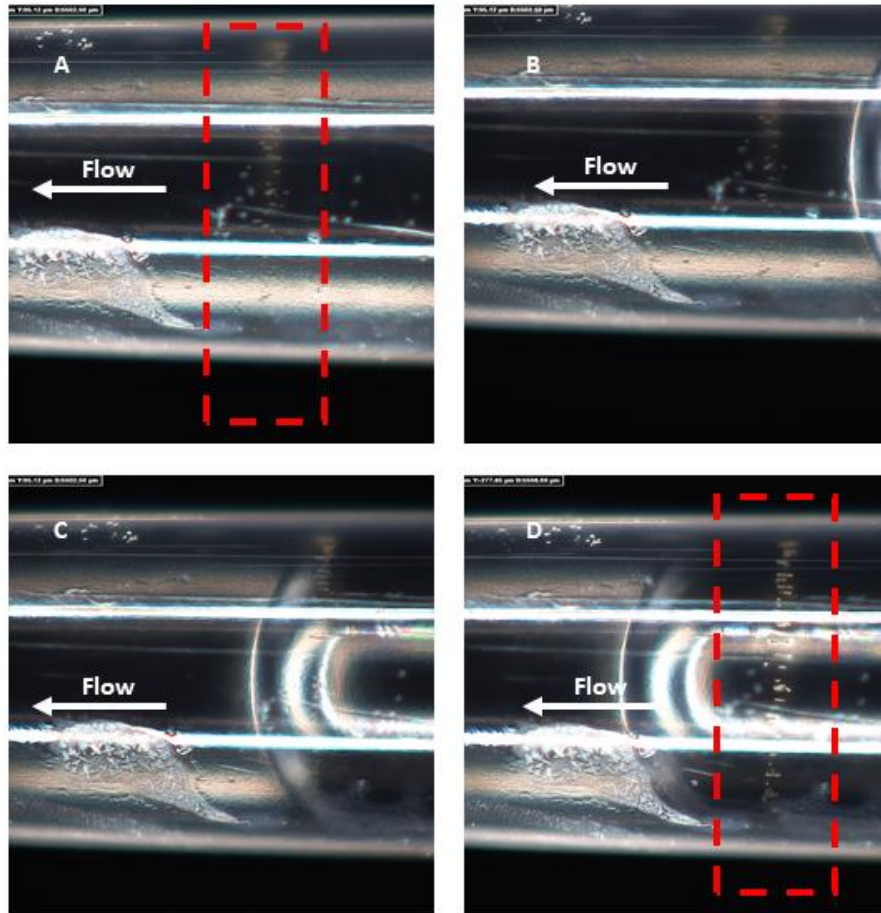


Figure 3.54: Captured microbeads inside the pipette tip under the influence of a ring magnet's magnetic field. The liquid solution is dispensed out of the tip but the microbeads remain trapped on the inner wall. The magnet (not seen) in this case is located on the right side of the frames

The second case as it has been described in Fig. 3.51-B, can be seen in Fig. 3.53. Captured microbeads within a pipette tip remain under the influence of a ring magnet's field while the liquid content of the tip is being emptied at an average flow speed of 2 mm/sec. The magnet is located on the left side of the picture (not seen in these frames), so these are beads that have been captured over the magnet's upper plane. Starting from 3.53-A and ending in 3.53-F, the liquid front is seen to go over the microbeads and move away from them while emptying the tip. In this figure, it can be observed that the captured microbeads remain captured even when the liquid content of the tip is dispensed. This is an important observation because it validates the proposed operating principle for the bead capturing displaying that the microbeads are not removed together with the liquid, but they remain immobilized under the influence of the magnetic field. The same process has been repeated for the case where the beads have been captured below the magnet's lower plane (Fig. 3.54). Again, it can be observed that the liquid is dispensed out of the tip but the microbeads remain immobilized on their initial positions. So, in both scenarios where microbeads are captured over or under the magnet, they remain captured after the liquid solution in the tip is dispensed.

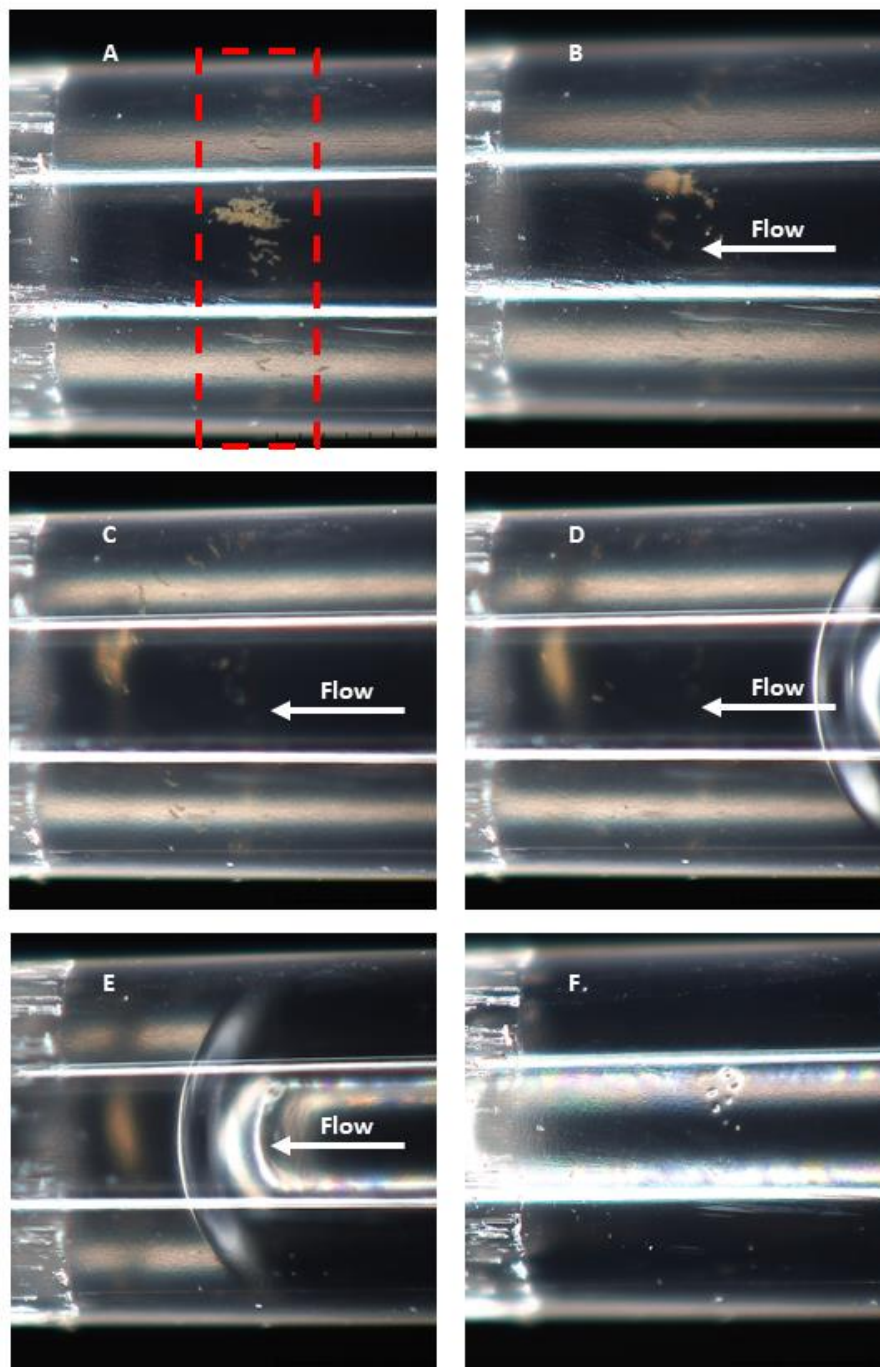


Figure 3.55: Captured microbeads inside the pipette tip just after the magnet has been removed. The liquid solution is dispensed out of the tip. The microbeads, in absence of the magnetic field, are removed along with the liquid content of the tip.

The third case as described in Fig 3.51-C, can be seen in Fig 3.55. A large number of microbeads previously captured by a ring magnet, are seen just after the magnet has been removed. Initially and in absence of any fluid flow, the

microbeads remain in position (Fig 3.55-A). However, immediately after a fluid flow (~ 2 mm/sec) is initiated, the microbeads drift away (Fig 3.55-B..F). While intuitively obvious, this experiment displays the ability of the proposed principle to capture microbeads when a magnet is present or release them by removing the magnet.

In summary, by optical observation of the captured microbeads within a pipette tip, the following have been shown:

- The microbeads are captured in positions very similar to the ones predicted by the particle tracing model
- Captured microbeads will remain captured under the influence of an appropriate magnetic field even after the liquid content of the tip has been dispensed
- In absence of a magnetic field, the microbeads will be dispensed along with the tip's liquid content

3.4.2 MAGNETIC SEPARATION EFFICIENCY

In order to evaluate the separation efficiency of the microbeads, a single step experimental process was created. For these experiments, 20 μl of a bead containing solution with a nominal concentration of 20000 beads/ml are placed into a v-bottom microwell plate. The plate is inserted into the SampleX and a separation protocol is executed. The captured microbeads are then suspended in a 40 μl reading buffer solution and are inserted into a Luminex MAGPIX system for counting. A control group on which no trapping tool place is also counted to monitor counting and fluid flow errors from the MAGPIX system or dispensing errors during experimental setup. Each experiment is repeated at least 4 times. The average bead count for captured and control wells is calculated, as well as the standard error for these counts. The average bead counts are used to calculate the separation efficiency of the protocol. The bead count standard errors are used to calculate the propagated standard error of the mean separation efficiency yielded by the protocol.

The setup used for these experiments includes a magnetic plate with the quatrefoil magnet arrangement in each of the 96 positions. Summarizing the results from the particle tracing analyses that were presented in the previous section, magnet designs for both the ring magnet and the quatrefoil arrangement were promoted. Initial testing showed that from a functionality perspective, the quatrefoil arrangement has some advantages over the ring magnet design:

- The ring magnets may have a tighter fit with the pipette tip than intended. This leads to the tip jamming onto the magnet. When the magnets are removed in order to release the microbeads, jammed tips are removed along with them. This issue is less frequent when using the quatrefoil arrangement presumably because the contact between the magnets and the tip is much more localized.
- The tip assembly onto the liquid handling adapter sometimes yields coaxiality problems because of the pipette tips sealing feature and often because the tip itself is curved. This sometimes leads to the tips crashing onto the ring magnet. This is less significant when using the quatrefoil arrangement because the magnets take up less space leaving more room for the tip to go through.

For the reasons seen above, among the two promoted solutions, priority was given to the quatrefoil arrangement. The optimal design as seen in the previous section included 4 magnets with a $h=2$ mm height and an $r=0.75$ mm radius. Due to reasons of component availability, an $h=2.5$ mm / $r=0.75$ mm magnet was used here instead. This design was also among the top performing ones in the particle tracing analysis of the previous section. The magnet type for these experiments is an SH45 gold plated neodymium magnet (1.32 T flux density).

In a first set of experiments, the microbead containing volume is aspirated at a rate of 16 $\mu\text{l}/\text{sec}$ which corresponds to an average velocity of ~ 20 mm/sec inside the pipette tip. The aspirated volume is left to rest for 4 mins to allow microbeads further away from the magnet to be drawn towards it so that they can be captured. The solution is released back into the microwell at a rate of 1.6 $\mu\text{l}/\text{sec}$ which corresponds to a velocity of 2 mm/sec inside the tip. The G-code used to generate the capturing processes is also included with the results to provide with a more concise form of the separation protocol. G1 denotes liner motion, Y2.8 is used to state that the motion concerns axis X (pipetting motor axis) which is to move to position 2.8 mm (the position at which 20 μl are aspirated). F100 is used to define a feed rate of 100 mm/min through which the flowrate can be calculated for a 3.5 mm plunger diameter. G4 is used for dwell operations and S240 defines the dwell time as 240 seconds. G1 X1 F10 dispenses the previously aspirated volume using a feed rate of 10 mm/sec. The results from the first set of experiments can be viewed in Table 3.7.

Experiment set number	1
Process description	Aspirate, dwell for 4 mins
Process code	G1 X2.8 F100 G4 S240 G1 X1 F10 G4 S0
Experiment repetitions	4
Control group bead count avg	151
Control group bead count standard error	35
Capture group bead count avg	106
Capture group bead count standard error	16
Separation efficiency	75%
Separation efficiency standard error	13%

Table 3.7: Experiment set 1, separation efficiency results

The calculated trapping efficiency for this protocol is 75% with a standard error of $\pm 13\%$. This is already a high separation efficiency when compared to standard protocols²⁴⁶ that require an initial quantity of 1000 beads in order to recover 50 for measurement. However, it is possible that during a multistep process there will be additional loss of microbeads. For this reason, it makes sense to improve the separation efficiency. Optical microscopy in this case has revealed microbeads that remain at the bottom of the microwell, potentially because of sedimentation. It is obvious that microbeads not entering the pipette tip will not be captured, for this reason a strategy to improve the separation efficiency could be to prevent microbead sedimentation during this process step.

In the second set of experiments, the dwell time is increased to 12 mins and a mixing step is added after each minute in which the plunger moves rapidly up and down to pipette $\sim 2.8 \mu\text{l}$ of solution in and out of the pipette. This is done to force beads that have settled at the bottom of the microwell to resuspend. The added dwell time is meant to allow time for resuspended microbeads to reach the magnet position. The results can be seen in Table 3.8.

Experiment set number	2
Process description	Aspirate, dwell for 12 x 1 mins, pipette up & down every 60 seconds
Process code	<pre> G1 X2.8 F100 !lim=12 !i1=0 !while i1<lim: !lim2=30 !i2=0 !while i2<lim2: G1 X2.5 F120 G1 X2.8 F120 !i2+=1 G4 S60 !i1+=1 G1 X1 F5 </pre>
Experiment repetitions	4
Control group bead count avg	199
Control group bead count standard error	29
Capture group bead count avg	187
Capture group bead count standard error	7
Separation efficiency	94%
Separation efficiency standard error	14%

Table 3.8: Experiment set 2, separation efficiency results

The separation efficiency is increased to 94%. Since this percentage is acceptable, a dwell time reduction is attempted to reduce the duration of unnecessarily long process steps. A duration of 8 minutes is set. The mixing process is extended to take place throughout the step duration so that the solution is not allowed to rest during the separation process. The results are presented in Table 3.9.

Experiment set number	3
Process description	Aspirate, dwell for 8 mins while continually pipetting up & down
Process code	<pre> G1 X2.8 F100 !lim2=480 !i2=0 !while i2<lim2: G1 X2.5 F120 G1 X2.8 F120 G1 X2.5 F120 G1 X2.8 F120 G4 S0.4 !i2+=1 G1 X1 F5 </pre>
Experiment repetitions	8
Control group bead count avg	192
Control group bead count standard error	12
Capture group bead count avg	174
Capture group bead count standard error	3
Separation efficiency	91%
Separation efficiency standard error	6%

Table 3.9: Experiment set 3, separation efficiency results

Reducing the dwell time to 8 minutes does not severely impact the separation efficiency of the process. Following this process, 91% of the microbeads are captured within the pipette tip. This is still an acceptable capture percentage for the purpose of a bead-based immunoassay protocol. The dwell time can be further reduced in order to optimize the separation process.

The results for a dwell time of 4 minutes can be seen in Table 3.10. The mixing process is again used continually during this process step. The separation efficiency yielded by this protocol step is 89%.

Experiment set number	4
Process description	Aspirate, dwell for 4 mins while continually pipetting up & down
Process code	G1 X2.8 F100 !lim2=240 !i2=0 !while i2<lim2: G1 X2.5 F120 G1 X2.8 F120 G1 X2.5 F120 G1 X2.8 F120 G4 S0.4 !i2+=1 G1 X1 F5
Experiment repetitions	4
Control group bead count avg	223
Control group bead count standard error	17
Capture group bead count avg	198
Capture group bead count standard error	2
Separation efficiency	89%
Separation efficiency standard error	7%

Table 3.10: Experiment set 4, separation efficiency results

Since an adequate separation efficiency has been obtained for a 1-step process, the ability to retain microbeads is examined for multi-step processes. In these tests, the beads are captured and then go through 10-minute incubation steps during which a liquid reagent is aspirated and released continuously to facilitate mixing. The experimental process includes aspiration from microwell positions, mixing with 3 reagents using alternating aspiration and release action, and releasing the beads in a separate microwell position. In Fig. 3.56, the plate arrangement for this experiment is shown. (B) denotes the position where the beads are initially located, (R) is reagent positions and (C) is where the captured beads are released.

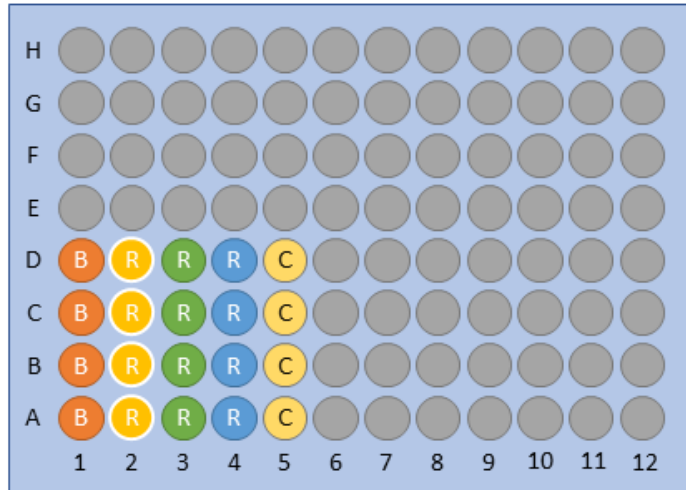


Figure 3.56: A three-step incubation assay is performed to evaluate the amount of microbeads lost during incubation steps. In column 1 is the initial position where the bead solution is stored. In 2,3 &4 the reagents are stored. In 5, the captured beads will be released at the end of the process.

Experiment set number	5
Process description	<ul style="list-style-type: none"> • Perform separation using process from exp. 5 (Col. 1) • Incubate with reagent 1 (Col. 2) • Incubate with reagent 2 (Col. 3) • Incubate with reagent 3 (Col. 4) • Release captured beads to storage position (Col. 5) • Measure remaining beads in all positions
Experiment repetitions	3
Initial position bead count average	90
Initial position bead count standard error	35
Reagent position 1 bead count average	0
Reagent position 1 bead count standard error	0
Reagent position 2 bead count average	0
Reagent position 2 bead count standard error	0
Reagent position 3 bead count average	31
Reagent position 3 bead count standard error	13
Capture group bead count avg	646
Capture group bead count standard error	59
Control group bead count avg	1116
Control group bead count standard error	84
Separation efficiency	58%
Separation efficiency standard error	12%

Table 3.11: Experiment set 5, separation efficiency results

The results of the previous experiment display reduced retention of microbeads after multiple process steps compared to the previous results. However, the final capture ratio is still quite high compared to the typical retention requirements of a clinical bead-based assay using a manual protocol. (~ 5%). Therefore, the bead capturing capabilities of the SampleX system can be assumed to be adequate for a full bead-based sandwich immunoassay, which will be presented in the following paragraph.

3.4.3 SARS-CoV-2 ELISA PROTOCOL IN SAMPLEX

In the previous paragraphs, the bead capturing abilities of the SampleX system have been investigated for an initial bead separation process and for consecutive incubation steps. In this paragraph, the results from an actual serological assay for SARS-CoV-2 IgG antibodies are presented. A research-use bead based sandwich ELISA assay was used by Prot-At-Once²⁴⁷. The assay has been designed to detect antibodies against coronavirus N, S1 and RBD antigens. The Nucleocapsid (N) protein is located in the viral core. It is not elicited by available SARS-CoV-2 vaccines at the time of writing of this work²⁴⁸. Therefore, an elevated measurement for this target during a clinical assay could indicate recent or past infection although this may not be highly specific to SARS-CoV-2²⁴⁹. S1 is a subunit of the SARS-CoV-2 spike protein and the least conserved among coronaviruses²⁴⁷. RBD is the receptor binding domain of S1 which binds onto ACE2, a protein found on the surface of many cells, and thus facilitates viral entry into the host cells.

ASSAY PRINCIPLE

The assay is based on the suspension array technology XMAP[®] developed by Luminex[®]. N, S1 and RBD antigens are immobilized onto the surface of superparamagnetic microspheres. The microspheres contain fluorescent dyes at different concentrations which allow the differentiation of each microsphere family by its emitted signal. The microspheres are suspended into a buffer solution. When diluted human serum is introduced to this solution, antibodies specific to the used antigens will bind to them. To facilitate the binding, an incubation step needs to take place during which the microbeads will be continuously mixed into with the diluted sample. Any unbound antibody will then be removed by washing the microbeads using a magnetic separation method. A secondary antibody mix will then be introduced to the now conjugated antigen-antibody pairs. The secondary Ab is a goat anti-human IgG coupled with a biotin molecule. The secondary Ab is incubated with the microbead mix allowing the binding to the anti-SARS-CoV-2 Abs. Excess Ab is then washed to purge the microbeads of unwanted reagents. In the next step, streptavidin-coupled R-phycoerythrin is incubated with the bead mix. The biotin of the secondary antibodies displays strong affinity with streptavidin which leads to the formation of Secondary Ab-Biotin-Streptavidin-R Phycoerythrin conjugates. Since R-phycoerythrin is a fluorescent molecule, its emission can be used to quantify the binding of the targeted antibodies to the microbeads. This quantification is done using specialized analyzers that are usually based on flow cytometry and fluorescent detection principles (See Ch. 1). The mean fluorescent intensity of the bead is correlated to the presence of the target antibody.

ASSAY REAGENTS AND REQUIRED EQUIPMENT

The following reagents are used to perform this assay:

Description	Comments
SARS-CoV-2 bead mix	3 bead families, one for each antigen: N, S1 & RBD. Each family is distinguished from the other by its red/IR emission when excited with a 611 nm radiation
Assay buffer	Used for washing and dilutions
Sample diluent buffer	Used to dilute the sample
SAPE (Streptavidin R-Phycoerythrin)	The fluorescent assay label. When excited with a green source, ex. a 532 nm laser, it emits light at 575 ± 10 nm
SARS-CoV-2 positive serum	The positive control for this assay
SARS-CoV-2 negative serum	The negative control for this assay

Table 3.12: Reagents used for a laboratory assay for SARS-CoV-2

In order to perform this assay in the laboratory, a plate shaker, a vortex mixer, a sonication bath, a magnetic plate separator, multi and single channel pipettes and optionally a plate washing station are required. For the quantification of the results, a Luminex analyzer such as a Flexmap 3D or a MagPix system are needed.

MANUAL ASSAY PROCESS

In order to perform the assay, a detailed process²⁴⁷ is followed by the user to prepare, mix, incubate and wash the microbeads in each step. A summary of the manual process is the following:

1. A microwell plate is prepared with the microbead solution in each tested position. 2500 beads per well are used.
2. The beads are separated from their original suspension solution and washed
3. The sample is diluted at 1:400 with sample diluent and mixed with the microbeads
4. The mixture is incubated for 2 hrs at room temperature while shaken at 900 RPM
5. The beads are separated and washed using a magnetic separator / plate washer
6. The secondary antibody is diluted and mixed with the microbeads
7. The mixture is incubated for 1 hr at room temperature while shaken at 900 RPM
8. The beads are separated and washed using a magnetic separator / plate washer
9. SAPE is diluted and mixed with the microbeads
10. The mixture is incubated for 30 minutes at room temperature while shaken at 900 RPM
11. The beads are separated and washed using a magnetic separator / plate washer
12. The beads are suspended in assay buffer and stored at 4°C until they can be loaded on an analyzer for testing

PROCESS AUTOMATION IN SAMPLEX

The automation of the process in SampleX required the definition of macros to perform tasks such as bead capturing, position switching and mixing. The approach for bead capturing has already been discussed in the previous experiments. Similarly, incubation and washing steps are performed by aspirating reagents or washing buffer and then releasing it back into the microwell plate. The concept in both cases is that the liquid reagent/buffer is aspirated into the pipette and then mixed by performing a plunger reciprocating motion continually for a multitude of times. The process lasts more for incubation steps that require time for the coupling of the protein sites to take place and

less for washing where the requirement is to wash away unbound reagents. During the incubation processes, some dwell times are placed in between mixing steps to allow microbeads that may have been detached during the reciprocating motion to move back to the magnet. For this assay, indicative processes for incubation and washing that were used are the following:

Incubation of Sample		Washing	
Description	Macros	Description	Macros
Go to height position for sample aspiration Aspirate 20 ul of sample	macro REASTART G1 Z133.7	Applies to all process steps	
	G1 Y2.6 F5	Repeat once	macro WASH !lim2=1 !i2=0 !while i2<lim2: !lim3=8 !i3=0 !while i3<lim3: G1 Y2.1 F10 G1 Y2.8 F10 !i3+=1 G4 S19.6 !i2+=1 M114
Repeat 120 times (2 hrs)	macro IN_SAMPLE !lim2=120 !i2=1 !while i2<lim2: !lim3=8 !i3=0 !while i3<lim3: G1 Y2.1 F10 G1 Y2.6 F10 !i3+=1 G4 S19.6 !i2+=1 M114	Repeat 8 times	
Repeat 8 times		Release 6 µl Aspirate 6 µl	
Release 6 µl Aspirate 6 µl		Wait for 19.6 sec	
Wait for 19.6 sec			macro REASTOP G1 Y1 F5
Release all the sample	macro REASTOP G1 Y1 F5		macro CLEAN G1 Y0 F5 G91 G1 Z-10 F300 G1 Y1 F30 G1 Z10 F300 G90
Dispense some air to make sure no reagent is left in the pipette.	macro CLEAN G1 Y0 F5 G91 G1 Z-10 F300 G1 Y1 F30 G1 Z10 F300 G90		

Table 3.13: Macros used to perform incubation of sample and washing in the SampleX platform.

For SampleX this assay translates to the following process steps:

1. Load pipettes
2. Activate magnets
3. Go to microbead position (plate 1, column 7)
4. Aspirate microbeads and perform trapping
5. Go to wash buffer position (plate 1, column 4)
6. Perform washing
7. Go to sample position (plate 1, column 1)
8. Incubate with sample for 120 minutes (macro sequence for sample incubation)
9. Go to wash buffer position (plate 1, column 10)
10. Perform washing

11. Go to secondary Ab position (plate 2, column 1)
12. Incubate with secondary Ab for 60 minutes
13. Go to wash buffer position (plate 2, column 4)
14. Perform washing
15. Go to SAPE position (plate 2, column 7)
16. Incubate with SAPE for 30 minutes
17. Go to wash buffer position (plate 2, column 10)
18. Perform washing
19. Go to storage position (plate 3, column 1)
20. Deactivate magnets
21. Dispense microbeads

The plate layout for this experiment can be seen in Fig. 3.57. The symbols for each well are described in a table in the same figure. In this assay, serum samples from 3 patients are tested for SARS-CoV-2 antibodies. The samples are tested in triplicates to obtain average measurements and if necessary exclude outlier values from sample contamination. The samples from each patient are denoted by the patient number: 1-3. Two more samples are included, a positive and a negative control to set the baseline for a positive and negative test result. Three plates with buffer only are used as a failsafe. The rest of the reagents are distributed between two plates as described in the process step sequence. For this assay both the standard operation mode and the single plate operation mode described in the previous section are used. The assay buffer is stored in the microwell plates. If the main washing buffer container of SampleX was used, the washing buffer positions could be avoided and the reagents could be merged in a single plate instead of two.

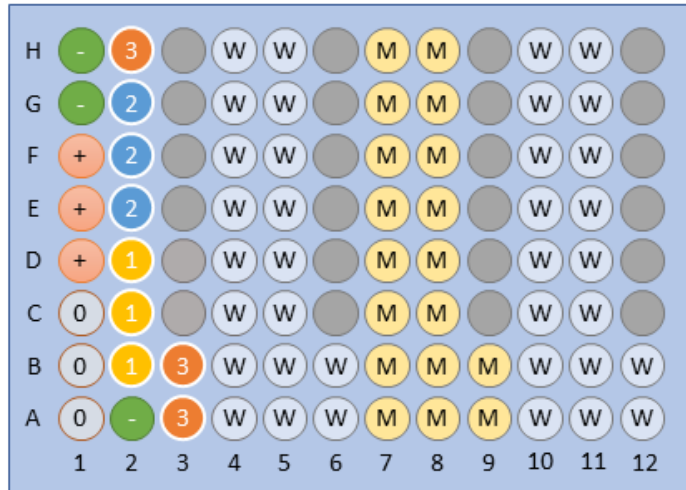


Plate 1

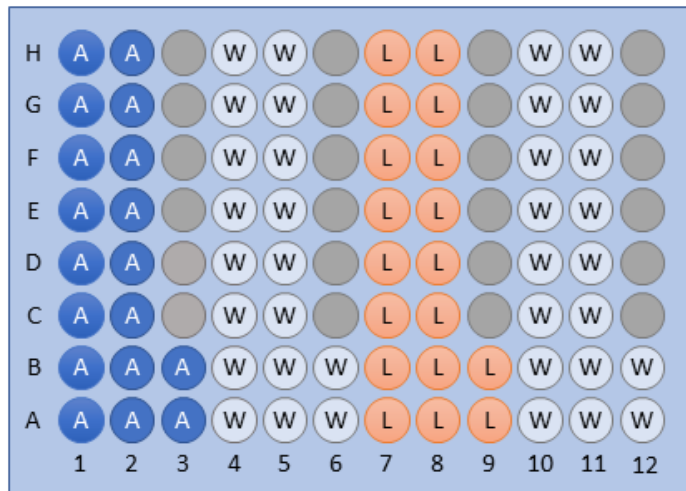


Plate 2

Symbol	Description
0	Buffer only, no sample
+	Positive control sample
-	Negative control sample
1	Sample from patient 1
2	Sample from patient 2
3	Sample from patient 3
W	Washing buffer
M	Microbead solution
A	Secondary antibody
L	Label (SAPE)

Figure 3.57: The plate layout for a SARS-COV-2 immunoassay for triplicates of 3 samples in SampleX

SARS-CoV-2 RESULTS FROM SAMPLEX

The serology assay for SARS-CoV-2 was performed both manually and using SampleX and the results were quantified using a Flexmap 3D analyzer. The results are summarized in Table 3.14 and in Figure 3.58. As notable events during the execution of these assay is a negative sample contamination due to user error for the SampleX protocol This resulted in excluding one of the three negative sample measurements from the analysis.

Manual Process	Mean Fluorescent Intensity					
Antibody	SARS-CoV-2 S1		SARS-CoV-2 RBD		SARS-CoV-2 N	
Sample	Average	CV	Average	CV	Average	CV
Blank	50.5	206.4%	190.5	407.1%	43.0	64.7%
Positive Ctrl	36028.0	0.5%	55495.5	1.0%	58185.0	1.6%
Negative Ctrl	1597.0	13.1%	1504.0	23.9%	1117.5	15.4%
Sample 1	58854	2.5%	58462	2.2%	5573	9.6%
Sample 2	51687.5	2.5%	60285	1.1%	4548.5	3.7%
Sample 3	58484.5	0.6%	59708	0.9%	1367.5	7.3%

SampleX	Mean Fluorescent Intensity					
Antibody	SARS-CoV-2 S1	CV	SARS-CoV-2 RBD	CV	SARS-CoV-2 N	CV
Sample	Average	CV	Average	CV	Average	CV
Blank	256.0	10.5%	648.0	10.3%	88.0	10.8%
Positive Ctrl	34312.0	9.3%	54931.0	4.0%	56789.5	7.3%
Negative Ctrl	1431.8	6.8%	1065.5	7.6%	918.8	8.1%
Sample 1	62574	3.6%	63140	1.6%	4774	3.6%
Sample 2	47773	5.7%	56074	2.3%	3427	2.0%
Sample 3	62077.5	0.7%	64548	1.6%	964	11.2%

Table 3.14: A comparison of assay results for processes performed manually and using SampleX

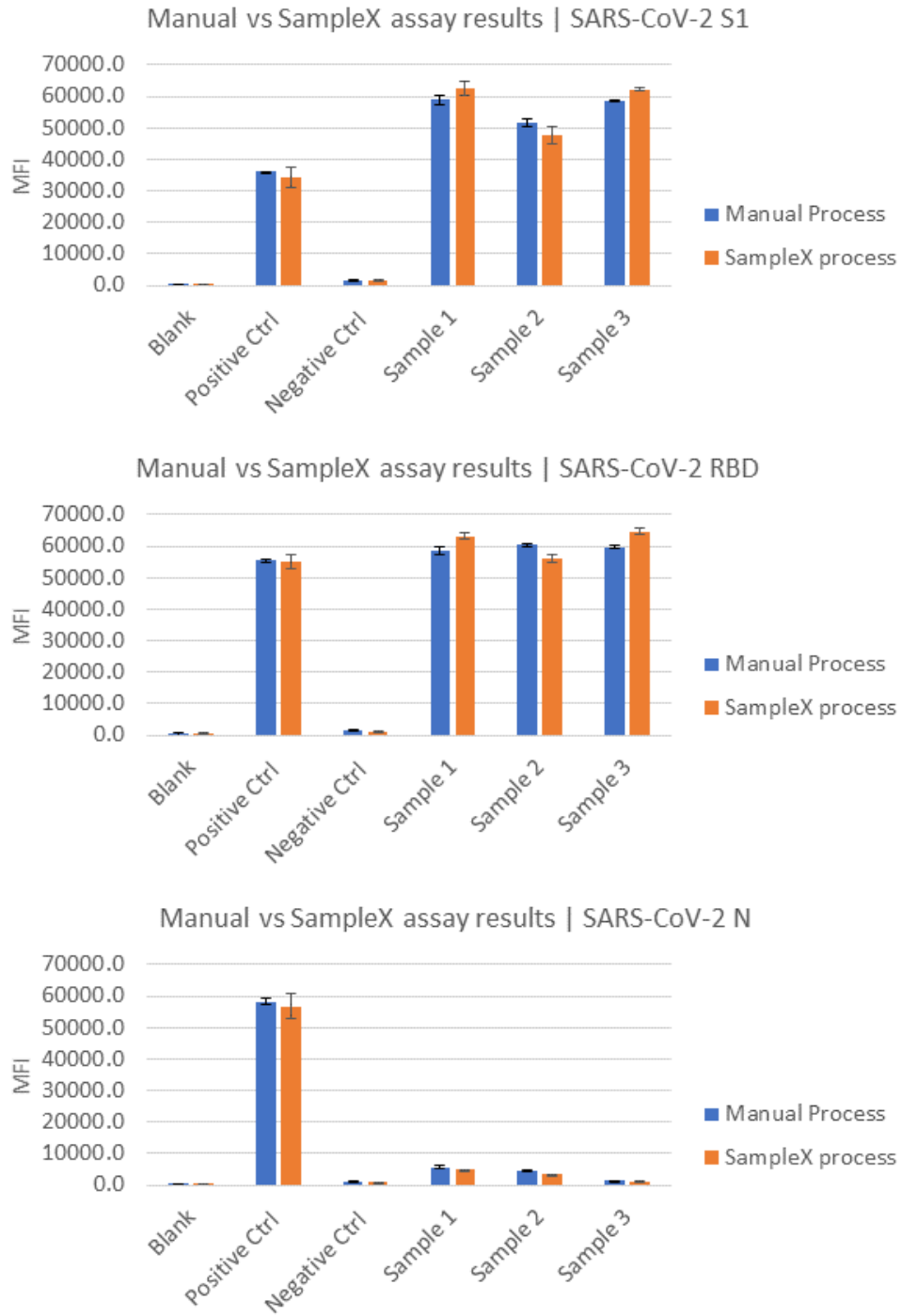


Figure 3.58: A comparison of assay results for processes performed manually and using SampleX in bar graph visualization

Several observations can be made from the comparison of the results of SampleX vs the manual assay. Firstly, the coefficients of variation for the two assays are comparable with the automated process presenting a more balanced performance than the manual one for most assay points. This indicates that the mixing approach used for the assay automation is at least comparable to the mixing performed by the plate mixer. Secondly, the measured values are close between the two tests considering that they have been performed in different occasions using different sample aliquots and reagents. Most SampleX measurement values are within 10% from the value obtained from the manual assay, which is close considering that the expected CV of a single test can be close to 10%. The highest percentage difference in the datapoints used for assay evaluation is at the negative control values which can be explained both by the high CV values of the manual assay and by the fact that a different negative sample aliquot is used in each case which can be affected by freeze-thaw cycles. Since different equipment may be used to quantify the results of an assay and the results themselves can be affected by reagent batch, metering errors, environmental conditions, sample aliquotes and other factors, one way to evaluate the test outcome is by extracting the ratio of any sample value against the negative control value. The results for this ratio are presented in Table 3.15:

Manual Process	Value-to-Negative control ratio		
Sample	SARS-CoV-2 S1	SARS-CoV-2 RBD	SARS-CoV-2 N
Blank	0.0	0.1	0.0
Positive Ctrl	22.6	36.9	52.1
Negative Ctrl	1.0	1.0	1.0
Sample 1	36.9	38.9	5.0
Sample 2	32.4	40.1	4.1
Sample 3	36.6	39.7	1.2

SampleX	Value-to-Negative control ratio		
Sample	SARS-CoV-2 S1	SARS-CoV-2 RBD	SARS-CoV-2 N
Blank	0.2	0.6	0.1
Positive Ctrl	24.0	51.6	61.8
Negative Ctrl	1.0	1.0	1.0
Sample 1	43.7	59.3	5.2
Sample 2	33.4	52.6	3.7
Sample 3	43.4	60.6	1.0

Table 3.15: A comparison of assay results for processes performed manually and using SampleX

What can be seen in Table 3.15 is that the positive signal ratios for the SampleX assay are larger than the ones calculated for the manual assay. This is mainly attributed to the lower negative signal values obtained by SampleX compared to the manual assay. The rule-based discrimination applied for this test is that any value that yields a signal stronger than 280% of the negative control signal can be considered positive. Using this rule, an identical diagnostic outcome from both processes is obtained, even for the N antibody of Sample 3 which yielded the highest CV among sample measurements in both assay methods.

In conclusion, the assay in both the manual and the SampleX process has yielded a positive result for the existence of vaccine elicited antibodies in all three samples and a negative result for N antibodies due to recent or past

infection in all three samples. While there were differences in the absolute values between the two tests, the measurements are close with comparable CVs between the two approaches.

3.5 CONCLUSIONS AND NEXT STEPS

In this chapter, an automated laboratory platform for the preparation of bead-based sandwich immunoassays has been presented. Its architecture is based on a fluid handling head, a permanent magnet bead separation system and a multi-axis motion system. The novelty of the development is that the bead capturing and the reaction with reagents happen inside pipette tips which are used as capillary reaction sites. The bead capturing system has been analyzed using finite element analysis for fluid flow and magnetism and the more promising setups have been outlined. The fluid handling system and the motion system have been presented. The platform was initially programmed to perform bead separation processes. Its ability to efficiently capture microbeads with retention ratios up to 94% for a single capture step and 58% for a 5-step process with incubation have been demonstrated. A full 3-plex bead-based immunoassay for SARS-CoV-2 S1, RBD and N antibodies has been performed using this platform with parity to laboratory performance results. Overall, the system is capable to perform fully automated bead-based immunoassays with applications ranging from life science to diagnostics.

Further steps would include the use of N52 magnets with the optimal characteristics discussed in the magnetic separation section to further improve bead capturing ratios during multi step protocols. Regarding fluid handling, the improvement of the flow-through washing system to operate with a positive displacement setup for each individual channel would reduce clogging and uneven flow issues and allow the use of this subsystem for bead washing which in turn would allow increased high throughput from using less microwells per data point. Regarding the assay optimization itself, decreasing incubation times and omission of washing steps would be a next step of the investigation to explore the possibilities of assay acceleration for PoC diagnostic applications. Towards the same end, the modification of the plate carriers to be compatible with 384 plates would quadruple the system's high throughput capabilities.

CHAPTER 4: LASER ACTIVATED MICROPUMPS

4.1 ABSTRACT

Lab on Chip technologies have enabled the possibility of novel μ TAS devices (micro Total Analysis System) that could drastically improve health care services for billions of people around the world. However, serious drawbacks that reside in fluid handling technology currently available for these systems often restrict the commercialization of such devices. This work demonstrates a novel fluid handling method²⁵⁰ as a possible alternative to current micropumping techniques for disposable microfluidic chips. This technology is based on a single use, low cost, thermal micropumping system in which expandable microsphere mixtures are activated by commercial grade laser diodes to achieve flow rates as high as 2.2 μ l/sec and total volumes over 160 μ l. With the addition of a volume dependent shut off valve, nanoliter repeatability is implemented. Pressure and heat transfer related data are presented. Finally, the possible prospects and limitations of this technology as a core element in unified optofluidic systems are discussed.

4.2 INTRODUCTION

4.2.1 MICROPUMP TECHNOLOGY

Microfluidic systems have grown to become a very important factor in the design of μ TAS, especially when the goal is the design for manufacturability (DFM) or the design for usability of a system. μ TA Systems add portability and accessibility in a large variety of protein analysis, genomic analysis, disease diagnostics, disease monitoring, environmental analysis and other procedures, while at the same time have the potential to reduce costs and increase assay sensitivity. However, from a plethora of proposed μ TAS technologies, few are finally realized in commercial systems since they are often hard to implement within the boundaries of industrial and commercial favorability.

Among many design considerations that need to be addressed, fluid handling inside a microfluidic system has proven to be quite challenging. As far as pumping is concerned, off-the-shelf components such as piston and peristaltic pumps suffer among other things from chip connectivity, cost, usability, modularity, dead volume and maintenance issues. For this reason, on-chip integration of fluid handling components has gained popularity over the last few years as an alternative to peripheral support equipment.

Several systems and methods for the partial or complete integration of active micropumps in microfluidic systems have been proposed, based on a variety of principles and technologies²⁵¹. The revolutionary Quake valve technology, based on pneumatic actuation, has been used to fabricate embedded micropumps²⁵². Peristaltic action has also been used with normally open²⁵³ or normally closed²⁵⁴ architecture for rectangular profile channels, while single stroke systems have been developed^{255,256} in an effort to reduce the number of actuators per micropump. Piezoelectric elements^{257,258} and Braille pins²⁵⁹ have been used as actuators in the same manner. Other technologies include electrochemical processes²⁶⁰, electroosmotic flow pumping systems²⁶¹, Acoustic systems²⁶², Magnetohydrodynamic micropumps²⁶³, Electrowetting²⁶⁴, PDMS gas permeation systems²⁶⁵, Optically driven thermoviscous expansion²⁶⁶, opto-electrical-thermal transduction²⁶⁷ and, of particular interest to this work, thermal micropumping that utilizes expandable microspheres embedded in a PDMS matrix²⁶⁸⁻²⁷⁰ and laser controlled wax microvalves and micropumps²⁷¹. While all of these methods have been successfully applied in laboratory environment, one common limitation is the inherent requirement of bulky and/or costly peripheral devices to support microfluidic functions. In other cases, integrated components often require complex manufacturing procedures that increase cost, or complex structures that introduce additional failure modes in the microfluidic operation.

This chapter presents a simple, fully integrated, on-chip liquid handling method in which a mixture consisting of expandable microspheres, an absorbance agent and a carrier liquid expand when heated by an infrared laser beam. Flow and pressure characteristics of the proposed micropumping method are evaluated as a function of the mixture composition. We introduce the placement of an ultraviolet laser diode which enables volume displacement control by inducing a photochemical process in a UV curing material. Finally, the pros and cons of this proposed method are discussed, as well as the potential that arises from this technology towards the development of reliable, low cost μ TA optofluidic platforms for *in vitro* diagnostics.

4.3 MATERIALS AND METHODS

4.3.1 EXPANCEL[®] EXPANDABLE MICROSPHERES

Expancel[®] microspheres (Nouryon, formerly AkzoNobel NV, Amsterdam, Netherlands) are microscale particles starting at a minimum unexpanded diameter of 5 μ m. They consist of a thermoplastic shell which encapsulates a pressurized hydrocarbon in liquid state. The thermoplastic shell is a mixture consisting mainly of acrylonitrile, methacrylate and acrylate polymers²⁷² while the hydrocarbon is liquid isobutane and constitutes²⁷³ 10-15% of the total particle mass. Isobutane has a boiling point of -11° C so it is already exerting pressure on the shell. When the particle is heated above the glass transition temperature of its shell material, the latter becomes soft and the particle expands due to the pressure of the liquid isobutane which vaporizes. The expansion can reach up to 40 times the original volume. When the temperature drops again, the shell rehardens but the isobutane remains at gas state. If the particles are heated over the point where the shell becomes too thin, the particles burst and the hydrocarbon is released. In between these states, there is a temperature where the particle expands significantly owing to the pliability of the shell and the pressure of the isobutane, however when the heat source is removed and the gas temperature drops, the particle loses some of its expanded volume.

Expancel[®] microspheres have numerous commercial applications²⁷⁴. They are used as additives in inks and pigments to add texturing, they are used as filler materials to produce low weight polymers or as blowing agents and they have been used as additives in a range of materials including concrete, coatings and food packaging. They are compatible with several thermal processing methods, notably injection molding, extrusion, thermoforming, blow molding and calendaring.

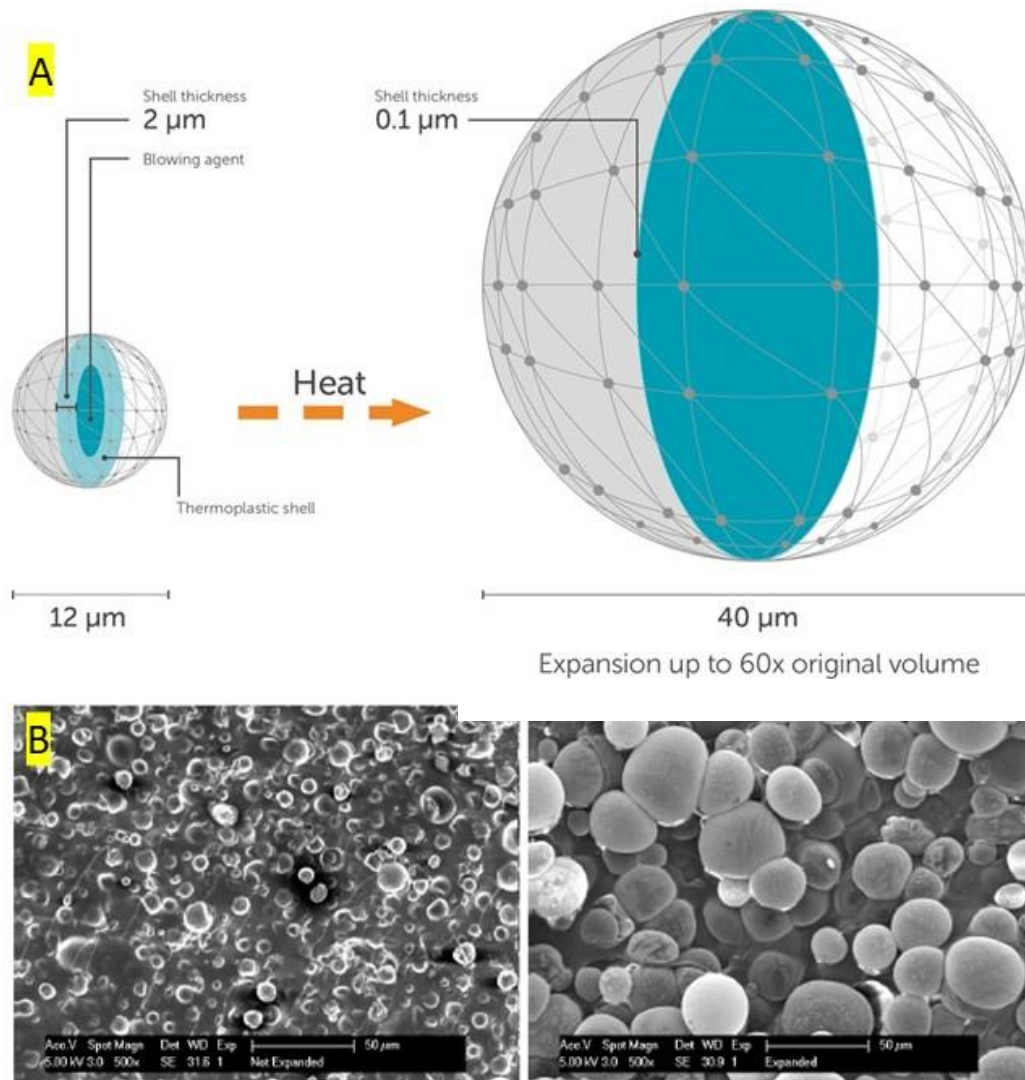


Fig 4.1 (A)²⁷⁴ The function of an expandable microsphere. When heated, the microsphere shell becomes pliable and expands from its pressurized content reaching up to 60X its original volume (B)²⁷³ SEM image of expandable microspheres prior (left) and after expansion (right)

4.3.2 PREPARATION OF LASER ACTIVATED EXPANDABLE MIXTURES

Since the materials of the microsphere shell present low absorbance in the near-IR spectrum, we designed a carrier that serves the purpose of bridging the expansion feature of the microspheres with a light activation scheme. In order to do this, the carrier must have high IR absorbance and additionally act as a sealant for any released hydrocarbon from the ruptured beads, thus preventing the gas from leaking into the microfluidic chambers. For this reason, Polydimethylsiloxane oil (PDMS) is used as a matrix material, while Acetylene black is used as an absorbance agent for near IR radiation. We tested various compositions of Expancel[®] particles, PDMS oil and carbon (acetylene) black particles mixed into a viscous composition. The specific type of product was DU 40 particles, which have an

expansion temperature of 80°C, the lowest among the different families of particles. PDMS oil was chosen because of its inert, non-toxic nature, its optical properties and its availability. Acetylene black was chosen because of its wide absorbance spectrum, its availability and cost. Overall, the mixture was designed for cost and for compliance with industry-friendly chip designs such as imprinted or molded polymer structures.

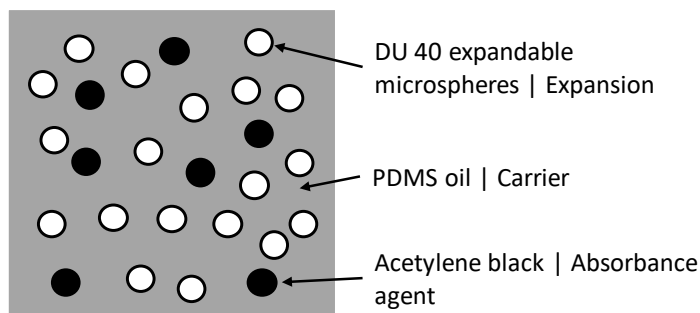


Fig 4.2 The expandable mixture consists of expandable particles, an absorbance agent for IR radiation and carrier liquid

4.3.3 CHIP DESIGN AND FABRICATION

The primary idea behind this work is to embed some quantity of the previously discussed expandable mixture into a microfluidic chip, which can at some point be activated (expanded) using an infrared laser source. Once the laser beam reaches the absorbant particles of the acetylene black, the later will increase in temperature thus transferring heat to their neighboring expandable particles. This will lead to the total mixture volume increasing and this could be used to displace liquid volumes of aqueous or other reagents which have been placed inline with the expandable mixture chamber. The Microfluidic chip structures were designed in order to facilitate the characterization of micropump performance in respect to total volume displacement, pressure capabilities and dosing precision. For volume displacement & pressure measurements, the design of Fig. 4.3 / 4.4-A was used. The chip embeds two round reservoirs (chambers 1&2) for the expandable particle mixture. Chamber 1 is primed with the mixture while chamber 2 is placed in line with the first one to receive the expanded volume after the pump is activated. After the two round chambers, a longer one is used into which the aqueous reagent is initially stored. After the pump activation, the mixture increases in volume and expands into the second chamber, thus forcing the reagent to flow into a meander-like channel which leads to a vented chip outlet port. The meander channel has been designed so that the chip has the required capacity to characterize the pump's displaced volume. The vented chip port is replaced with a pneumatic inlet port for pressure measurement experiments which is used to exert controlled pressure inside the chip circuit (Fig 4.4-C). However, in an actual application scenario, very often there is the need of "dosing", i.e. being able to displace specific volumes of a reagent from one reservoir into another. For this purpose, a different chip design is proposed (Fig 4.4-B) which utilizes a photopolymer material to achieve precise volume control. In this setup, chamber 2 is not empty but already primed with a photopolymer material. Upon laser activation, the photopolymer material flows inside a microfluidic channel of predefined volumetric capacity, at the end of which, a blue laser beam is constantly on. One the photopolymer fluid front reaches the blue laser beam spot, it solidifies and the expansion stops. In this way, precise volume displacement can be realized within a microfluidic chip without any need of pneumatic or mechanical connection to the chip itself, only by using external laser sources.

Microfluidic chip structures (channels and chambers), were fabricated using laser engraving and CNC milling machine for improved dimensional repeatability. The chip stocks were commercial grade PMMA 1x3 inches 2 mm thick slides. After fabrication, chips were washed in an ultrasonic bath and their pattern depth was measured in a microscope

using a 40X objective lens of $1\ \mu\text{m}$ depth of field and a precision dial gauge ($1\ \mu\text{m}$ resolution). Chips of varying depths were connected to a LabSmith® positive displacement microfluidic pump (LabSmith Inc, Livermore, CA) in order to find the correlation of the chip's volume capacity and the structure depth by incrementally pumping $0.05\ \mu\text{l}$ increments inside the microfluidic meander until it was full. The laser engraved structures had a depth of $364\ \mu\text{m} \pm 8.33\ \mu\text{m}$. The microfluidic channel profile and cross section, with a nominal width of $500\ \mu\text{m}$, were measured in a sample of chips to obtain a mean of variation coefficients equal to 5.5% in cross sectional area of each individual chip using a Matlab® pixel count algorithm and a calibration microscope slide. The machined structures had a mean depth of $511\ \mu\text{m} \pm 3.2\ \mu\text{m}$ and channel width equal to $1000\ \mu\text{m}$ in a semicircular profile. The chips were sealed with glass coverslips and optically clear UV adhesive where optical clarity or heat resistance was of the essence. Thick transparent adhesive membrane was used for less demanding chip positions. All reagents were injected manually into their respective positions using $500\ \mu\text{l}$ syringes and 30G hypodermic needles. The orifices created by the needles on the sealant were shut using UV curing photopolymer plugs.

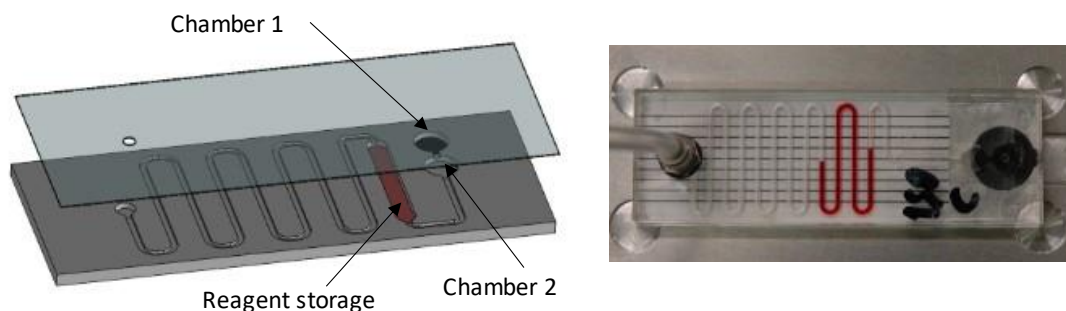


Fig 4.3 The experimental chip design for actuation without volume control. On the right, a setup with controlled circuit pressure is shown.

The fabrication methods used in this work were selected because they are suitable for prototyping. However, the designs and the actuation concept are both compatible with standard manufacturing processes for microfluidic chips such as injection molding, pressure molding or embossing. Additional features could be used in a production scenario such as ports to facilitate chip priming with the expandable mixture or inlets for aqueous reagents that would be used to reconstitute freeze dried or otherwise preserved components inside the chip. Such features were not used in this work in order to simplify chip fabrication.

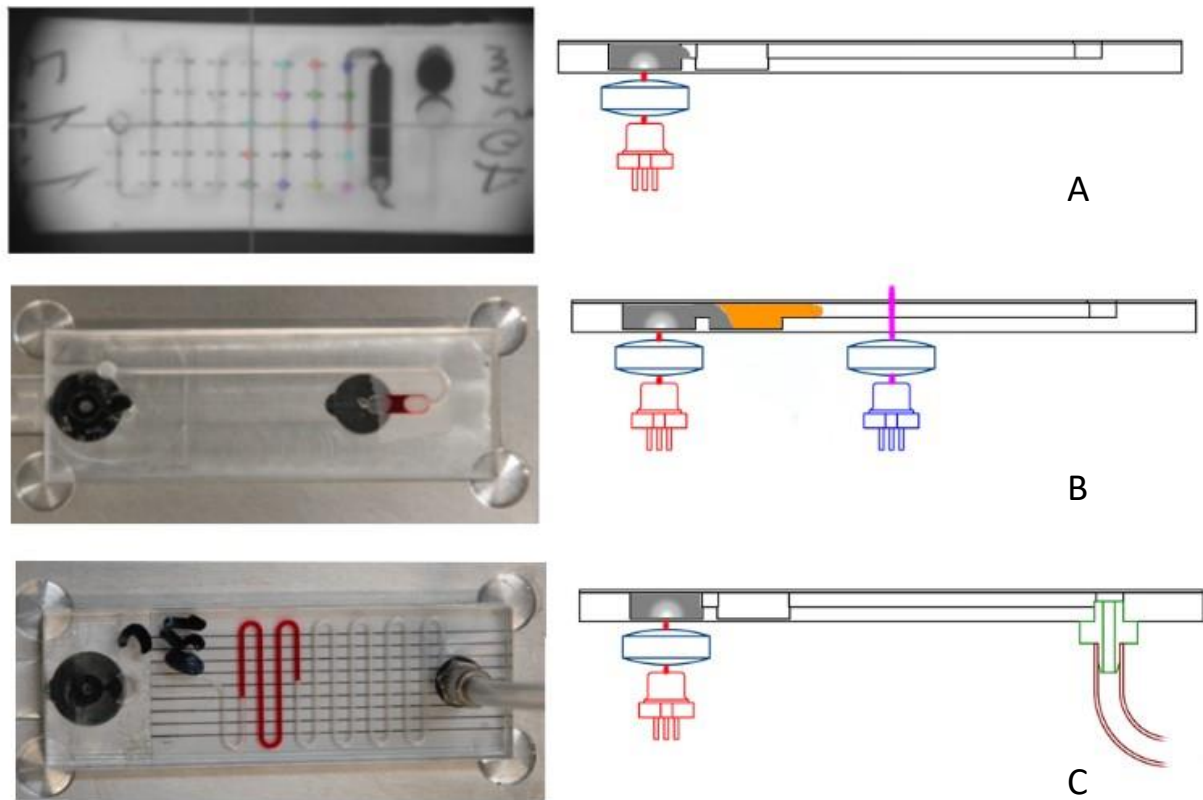


Fig 4.4 Three different chip designs for three different tests: (A) Total displaced volume tests (B) Predefined volume displacement tests where a photopolymer is used to stop displacement when the predefined volume has been reached (C) Pressure tests, where a precisely controlled back pressure is introduced to the chip in order to evaluate the pressure that can be reached using this type of micropump

4.3.4 EXPERIMENTAL SETUP

The experimental setup shown in Fig. 4.5 consists of a machined aluminum plate with a standard 3x1 in. slide seat. The plate has embedded openings for the pump activation laser and the photopolymerization laser. The setup is assembled on a micrometer XYZ stage which is used for chip measurements before testing. During testing, a CCD camera is secured over the chip with an infrared shortpass filter to avoid sensor damage from the IR laser beam. The experiments are recorded and the results are calculated based on the recordings using a video analysis script described below. Laser sources used were continuous wave commercial grade diode lasers. The sources used for activation were 980 nm diodes of 531 mW laser power, 15.2 % unit efficiency and 87 mW/mm² power density at an approximate 1.4 mm spot size at entry point. The sources used for displacement control (photopolymerization lasers) were 405 nm diodes of 62 mW laser power, 25.5 % unit efficiency and 78 mW/mm² power density. Focusing

was achieved using a collimator and a focus lens which were manually adjusted. A CCD camera placed on top of the microfluidic chips recorded all experiments to obtain relevant data with video analysis tools. Pressurizing of the chip outlet was achieved using an Elveflow® pressure generator (ELVESYS, Pépinière Paris Santé Cochin). The liquid reagent substitutes are red and blue water-soluble dyes. For the Set Volume Displacement experiments, the photopolymer used was a standard medical device UV adhesive by Loctite® (Henkel AG & Company, KGaA, Düsseldorf, Germany) with relatively low viscosity (300 cP) and fast curing time (ISO 4587, Fusion® D light source, 50 mW/cm², CT <5 sec). In heat flow experiments, images were acquired using a FLIR® T335 thermal imaging camera (FLIR GmbH, Frankfurt, Germany).

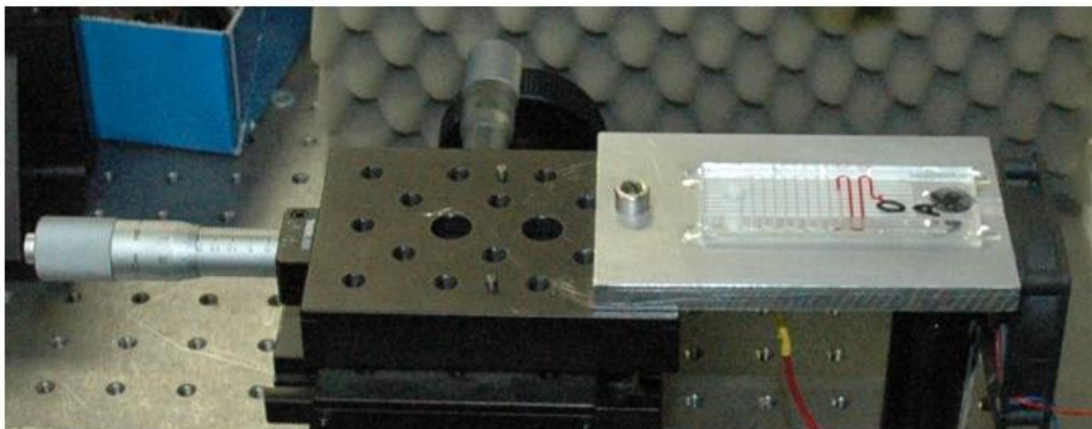


Fig 4.5 The experimental setup includes a machined aluminum plate with a standard 3x1 in. slide seat and two embedded laser sources for pump activation and photopolymer solidification.

4.3.5 VIDEO ANALYSIS TOOL

Custom video analysis tools were developed in Matlab®. The experiment recordings are used as input and the displaced volume is calculated against time. The algorithm identifies predetermined nodes along microfluidic channels that are tracked based on their color value in order to obtain displaced volume against time diagrams. The algorithm tracks the displaced volume continuously by overlapping a virtual fluid path on the microfluidic channel and quantifying color and intensity values versus time. The methodology is as follows:

1. The user inputs the zero timepoint which is the timepoint at which the laser is turned on
2. The user inputs the positions of the nodes and the meander channel is mapped by the algorithm using these nodes as interpolation points. Also, the user marks the position of the laser beam.
3. A mask is created that only includes the meander path and it is applied on each video frame.
4. A second mask is created that tracks the laser beam position
5. The algorithm goes through each video frame and records the fluid front progression and the status of the laser beam
6. Results for fluid volume displacement against time and laser beam status are recorded.
7. The data go through a Savitzky – Golay filter to smooth out the effect of the discretization from the video pixelation.

As post processing steps, the tool uses as a secondary input the specifics of each experiment, such as channel depth and trigger times of laser diodes, to provide with accurate diagrams on flow, volume displacement and segmentation of volume displacement into linear and nonlinear regions.

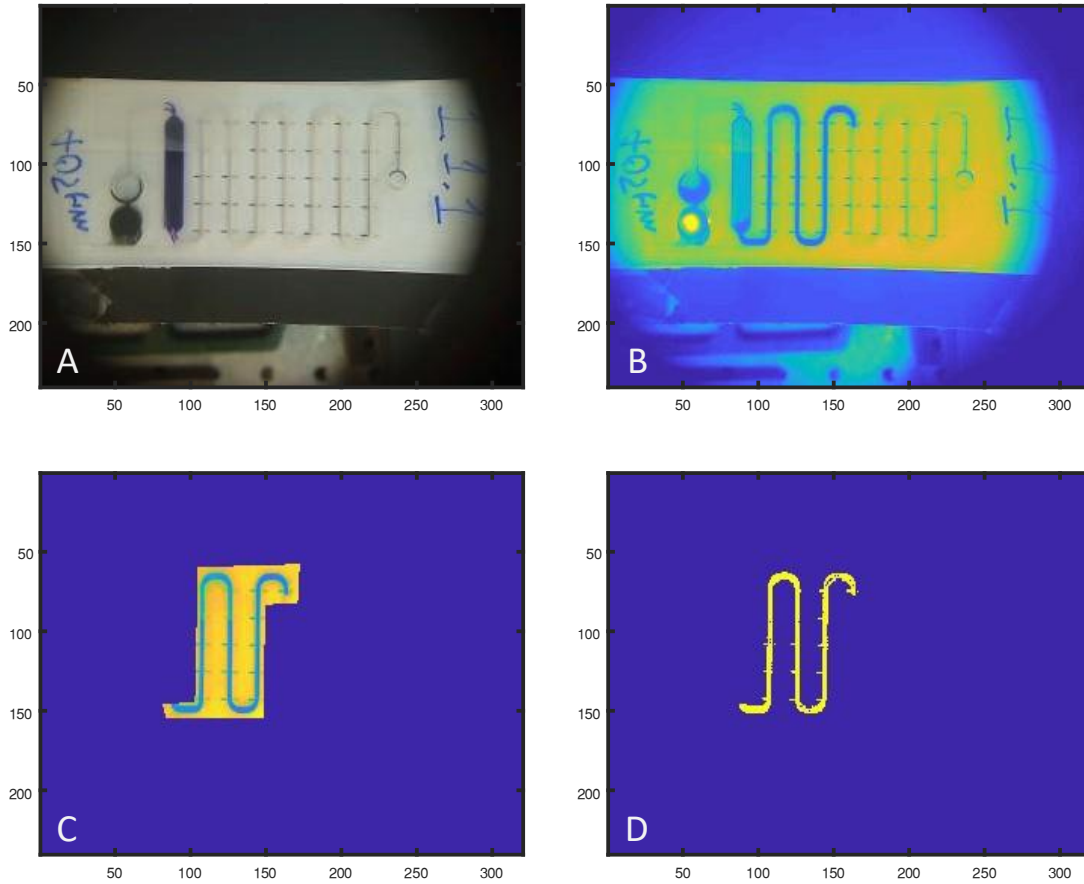


Fig 4.6 The displaced volume tracking is calculated throughout the meander channel. (A) The video recording is used as input (B) The frame with the maximum volume displacement is identified (C) A first mask is applied to remove the frame parts that contain no information (D) A second mask is applied that only keeps the pixels that contain the fluid path

4.4 RESULTS

4.4.1 SINGLE USE MICROPUMP DESIGN

The principle of operation for the developed micropump is shown in Figure 4.7. The mixture is placed in a chamber at one end of a microfluidic system enclosed laterally by optical windows that facilitate the entry of an infrared laser beam. The microfluidic system consists of two chambers, one filled with the microsphere mixture and one empty in line with a liquid filled chamber (Fig. 4.7). The empty chamber's purpose is to accommodate microsphere mixture being displaced due to the expansion. Upon activation of the laser diode (Fig. 4.7 B) heat is

added locally to the entry point of the beam and the first layer microspheres expand in volume thus pushing the unexpanded mixture into the empty cavity and the liquid reagent (aqueous dye solution) in line the microfluidic path. Subsequently, as temperature continues to rise locally, internal pressure builds up in the microspheres which eventually burst. The released hydrocarbon remains enclosed by the rest of the mixture (Fig. 4.7 C) creating a bubble transmissive to the infrared beam.

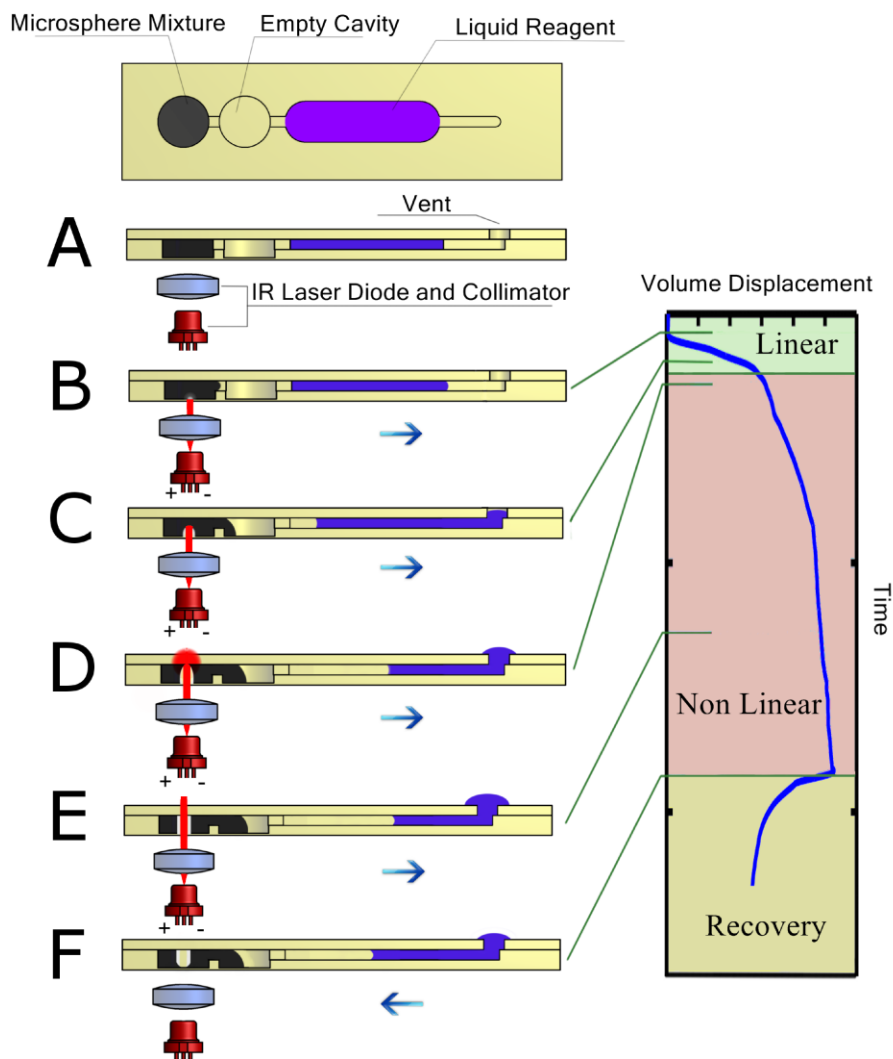


Fig 4.7 Top and cross-sectional views of the example microfluidic chip undergoing a mixture activation process. In the first curve section the displacement is linear in respect to time while in the second section nonlinear expansion takes place. F represents the deactivation of the laser after which there is partial retraction of the displaced volume.

This process allows for the laser beam to proceed through the mixture layer by layer and maximize expansion by only locally heating a percentage of the mixture at every given time. Until the peak of the beam profile reaches the upper level of the microsphere chamber, the expansion is linear, since the same amount of beads is available for activation at each layer. Once the beam starts exiting the chamber, the volume displacement rate drops (Fig. 4.7 D). When the beam has fully penetrated the mixture (Fig. 4.7 E) a region around the created orifice continues

to be excited by a lower power portion of the Gaussian profile laser beam. Some heat is still added to the mixture, but the expansion continues at a lower rate. Once the diode is deactivated, the heat input stops, causing a reduction of internal pressure, and part of the displaced mixture volume returns to the initial liquid containing chamber (Fig. 4.7 F). In order to characterize the proposed technology, we examined the key parameters of this method: flow rate and volume displacement, displaced volume repeatability (utilizing additional methods), pressure build-up capability and heat transfer from the pump to the reagents.

4.4.2 VOLUME DISPLACEMENT AND FLOW RATE EXPERIMENTS

In order to examine how the volume displacement and flow rate depend on the mixture composition, we performed experiments of mixture activation inside a microfluidic chip embodying a calibrated meander channel for volume tracking (Fig. 4.3) in line with the mixture and reagent chambers described in Section 3.1. Upon activation of the laser diode, the camera would start recording the volume displacement, during which the laser beam would cause the mixture to expand and act as a micropump for the liquid solution, pushing it into the meander channels.

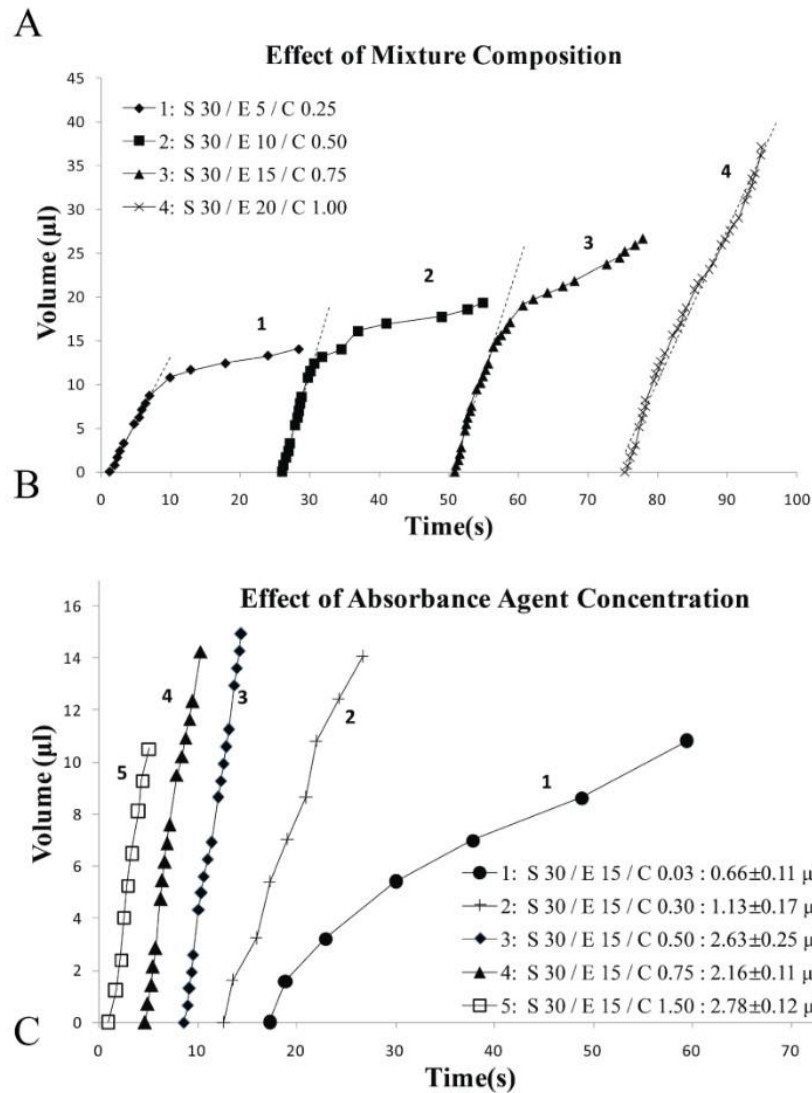
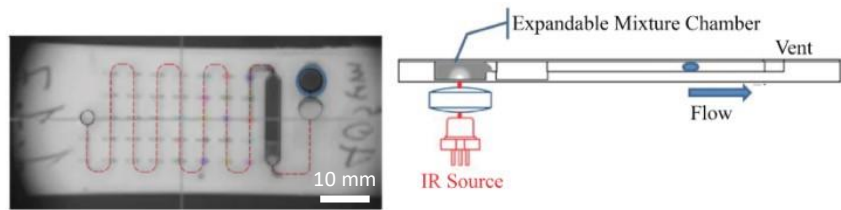


Fig 4.8 Micropump performance in correlation to the mixture composition. Presentation of sample curves. (A) The microfluidic chip used in the experiments, (B) Volume displacement for different expanding microsphere (marked : E) and absorbance agent concentrations (marked : C) in w/w (mass units) of Dimethicone (marked : S) as seen in the legends of the diagrams, (C) Volume displacement for different absorbance agent concentrations in fixed expanding microsphere content.

Various experiments were conducted in order to evaluate the effect of the expandable mixture composition. Four compositions were tested under the same conditions, starting from a less concentrated mixture of 5 gr of microspheres and 0.25 gr. of acetylene black in 30 gr. silicon oil medium, up to quadruplet quantities of

the active ingredients in the same amount of medium. What can be observed in Fig. 4.8-B is the presence of a linear and a non-linear curve segment in the expansion process, which was discussed in Section “single use micropumps design”. Specific data are shown in Fig. 4.9. Each experiment was conducted in 5 replicates. We define as Linear, the part of the curve for which a linear regression model can be applied with a coefficient of determination $R^2 \geq 0.99$. We define as “Linear flow rate” the flow rate acquired from the linear part of the curve, after which there is a drop in the micropump performance. The excitation laser diode has a power consumption that is independent to the micropump’s performance, so the linear section of the process yields maximum efficiency.

We observe that the linear flow rate appears to be relatively constant among compositions 2, 3 and 4 at about 2.22 $\mu\text{l}/\text{sec}$ and comparably repeatable (Fig. 4.9, Row 6), bearing in mind the error margin defined by the setup itself. Series 1, having the lowest content in microspheres and absorbance agent, has a lower linear flow rate. By increasing the content in microspheres and absorbance agent, the duration of the linear section (Fig. 4.9, Row 5), the Linear Volume Displaced (Fig. 4.9, Row 7) and the Total Volume Displaced (Fig. 4.9, Row 8) all increase.

		Mixture Composition			
Experiment series		1	2	3	4
Dimethicone Content		30	30	30	30
Expancel® Content		5	10	15	20
Absorbance Agent Content		0.25	0.50	0.75	1.00
Flow Characteristics	Duration of Linear section (s)	6.12 ±1.44	6.97 ±1.83	9.69 ±3.40	16.47 ±4.46
	Linear Flow Rate ($\mu\text{l}/\text{sec}$)	1.54 ±0.04	2.29 ±0.41	2.16 ±0.25	2.22 ±0.61
	Linear Volume Displaced (μl)	8.39 ±1.67	14.51 ±1.82	19.37 ±5.27	36.89 ±3.87
	Total Volume Displaced (μl)	18.46 ±4.04	37.36 ±2.19	74.78 ±2.62	161.54 ±3.53

Figure 4.9: Micropumping Characteristics vs. Mixture Composition. The error is represented by the standard deviation encountered during these experiments. Each experiment was conducted 5 times.

Examining the dependence of the Linear Flow Rate from the concentration of the absorbance agent separately (Fig. 4.9-C), we observe that for low concentrations, a rise in the agent content leads to a rise in the $\mu\text{l}/\text{sec}$ that can be achieved. However, there is a threshold after which an increase in the said content will not significantly affect the flow rate. In particular, the two lowest concentrations in absorbance agent yield an average of 0.66 and 1.13 $\mu\text{l}/\text{s}$ respectively, while the three consequent concentrations display 2.63, 2.16 and 2.78 $\mu\text{l}/\text{s}$ respectively. While moving from the lower to the higher concentrations of the absorbance agent we see an evident trend to increase the absorbed energy, there is a limit to how much energy can be absorbed given the current setup.

4.4.3 PRECISE VOLUME DISPLACEMENT

The proposed micropumping method so far utilizes an open loop control scheme to obtain a median value for each variable of interest within an error range. A limitation of this approach is that precise volume displacement is not possible. In order to overcome this, we developed a method of volume control in which a UV photopolymer is placed in line with the micropump so as to move along with the fluid reagent. In a predefined distance along the microfluidic channel, a 405 nm laser diode has been placed and is switched on along with the IR laser that causes the mixture to expand. When the photopolymer reaches the path of the laser beam, it rapidly increases its viscosity and eventually solidifies, thus isolating the pressurized part of the channel from the rest (Fig 4.10-A). This is done in attempt to define how much reagent is going to be pumped and also to cancel out the retraction feature of this method that has been mentioned in Section 3.1. The chip design consists of 2x40 μl chambers connected in line for the expandable mixture and the photopolymer respectively. A microfluidic channel of 500 μm depth and 1 mm width is placed after the photopolymer chamber. In a user specified distance along the channel, there is a flat end circular pocket acting as an optical window for the N-UV laser beam. The experimental procedure requires the activation of the expandable mixture by turning the IR laser diode on, while at the same time the N-UV diode is also activated. The expansion causes the photopolymer and the liquid reagent both to move forward in line until the photopolymer reaches the N-UV laser beam, at which point it solidifies and stops all flow in the circuit.

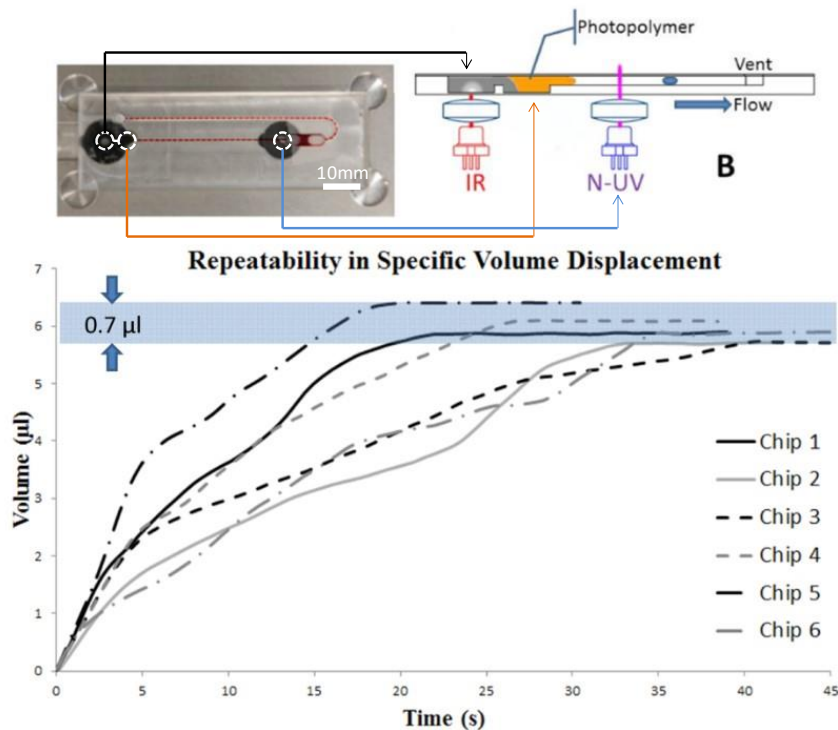


Figure 4.10: Experiments for the assessment of a method for predefined volume displacement. (A) The microfluidic chip design used for these experiments, (B) The volume displacement profiles of each repetition of the experiment, all concluding within a 0.7 μl wide zone around a nominal value after the solidification of the photopolymer.

The expandable mixture utilized in these experiments was a 30/15/1.5 w/w composition of Dimethicone, Expancel® DU 40 particles and acetylene black powder. We conducted six repetitions under the same experimental conditions in order to assess the repeatability of this method. Fig. 4.10 shows a significantly lowered flow rate

compared to the experiment results shown in Fig 4.8, due to the viscosity of the photopolymer utilized in this method. Nevertheless, the total displaced volume in all experiments falls within a $0.7 \mu\text{l}$ zone, having an average displaced volume equal to $5.94 \pm 0.27 \mu\text{l}$ (± 1 SD). It should be noted that the deviation from a nominal value in this experiment shows no correlation with the displaced volume quantity, but depends on the optical design and fabrication of the laser beam window, mainly because of scattering that affects the photopolymer before it reaches the polymerization spot. It should be noted that the results obtained from this experiment display higher deviations than the ones encountered in our previous experiments. A different experimental setup that was used here allows for expanded microspheres to move through the port connecting the mixture filled chamber and the empty chamber. This is a source of error that decreases travelling mixture homogeneity and consequently affects flow rate repeatability.

4.4.4 PRESSURE TESTING

In order to assess the functionality of the micropump when elevated pressure is encountered (i.e. when using viscous fluids or lengthy channels), a similar design to the one described in the previous sections was used. However this time instead of venting the outlet, it was connected to a pressure generator (Fig. 4.11-A). The experimental procedure of Section 4.4.2 was repeated using one composition of the expanding mixture (Dimethicone: 30 / Expandable Microspheres: 15 / Acetylene Black: 1.5 w/w) under back pressures ranging from 0 to 150 mbar relative to atmospheric. The micromachined chip embeds 2 chambers to facilitate the storage and expansion of the mixture, one chamber for the fluid reagent storage and a semi-circular profile channel of $500 \mu\text{m}$ radius for the displacement and tracking of the latter. The laser source was adjusted to output approximately half the power that was used in the previous experiments (531 mW reduced to 265 mW).

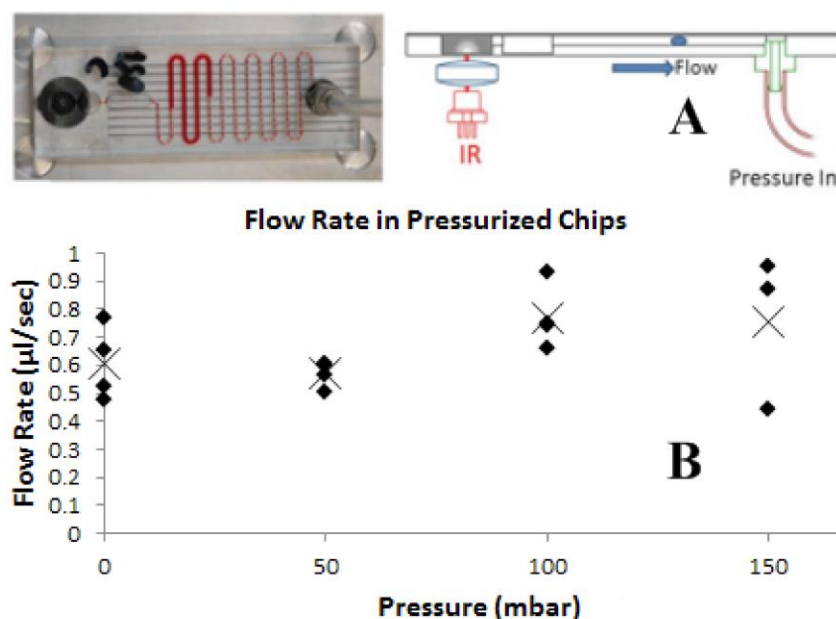


Figure 4.11: Flow rate in pressurized microfluidic channels. (A) The microfluidic chip design used for these experiments (B) Flow rates for the linear part of the expansion working against outlet pressure. (X) marks the mean values

Figure 4.12 shows no evident trend linking outlet pressures of this magnitude with the flow rate, however repeatability errors like the ones seen in the previous section are also present here. We believe that the apparent indifference of the pump performance towards the outlet pressure is due to the fact that the actual pressure needed to push the expandable mixture through channels is much higher than the 150 mbar that we apply on the outlet. This is to be expected if we consider that the expandable mixture is highly viscous ($\sim 10^5$ cP) and thus in need of high pressures to move across microfluidic chambers. The theoretical maximum pressure that can be countered by the proposed technology is the vapor pressure of the encapsulated hydrocarbon within the beads. This has been reported to be 16.2 bars at 90 °C [21] for the microspheres being used in this experiment. In a separate set of experiments that we conducted, the same expandable mixture was activated within chips that were fully sealed. The initial air volume was compared to the minimum (pressurized) air volume observed during 5 identical experiments to obtain a maximum generated pressure equal to 9.2 bar using the Van der Waals equation (Fig 4.12).

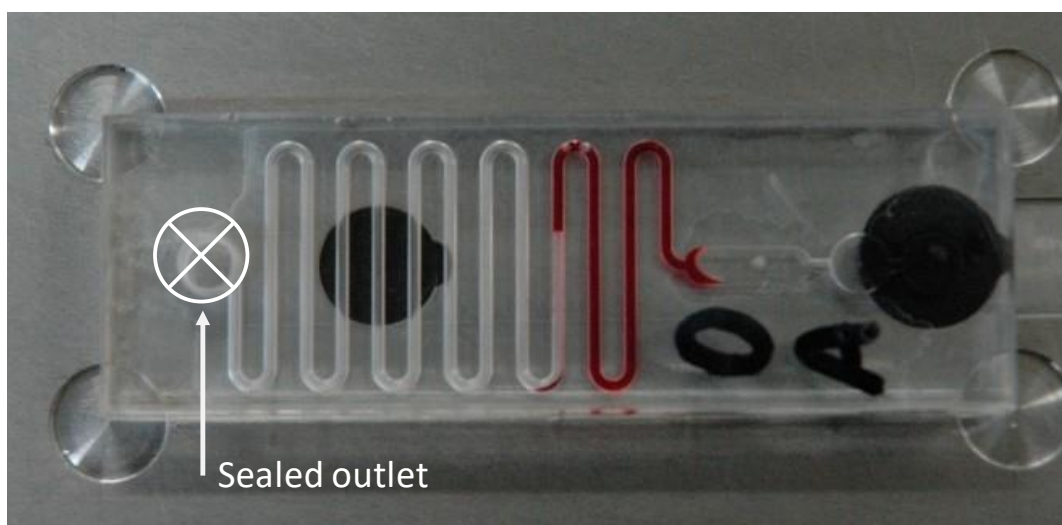


Figure 4.12: Experiments conducted in completely sealed chips showed that the mixture activation resulted in pressures equal to 9.2 bar

4.4.5 DEPENDENCY OF EXPANSION RATE FROM LASER POWER

While the expansion process in the proposed technology is governed by a multitude of parameters, the effect of laser power is of special interest. The ability to adjust the output laser power of the diode activating the micropump could potentially be used for dynamic flow rate adjustment, predefined time dependent flow profiles or even the ability to mix components by continuously changing the flow direction. In order to examine flow rate as a function of laser power, we conducted experiments identical to the ones described in the article's section 3.2 using a 808 nm continuous laser source with output (laser beam) power ranging from 224 mW to 488 mW. Each experiment was conducted 3 times. Flow rates that correspond to the linear part of the expansion were acquired using video processing algorithms. The results are presented in figure 1.

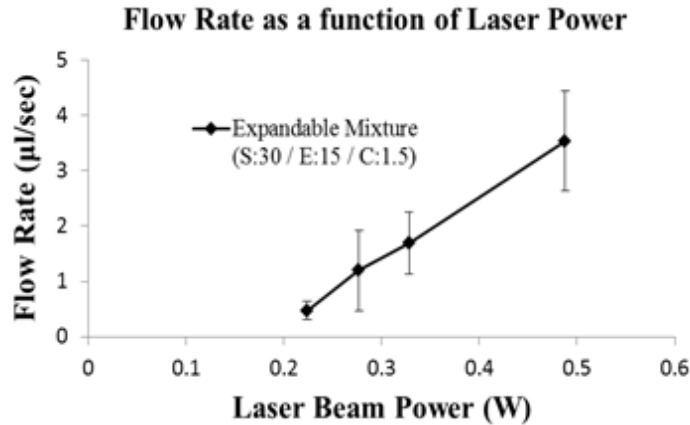


Figure 4.13: Investigation of the flow rate as a function of the diode’s laser power. The expandable mixture used had a content per weight of 30 units of dimethicone silicon oil against 15 units of expandable microspheres and 1.5 units of absorbance agent. The error bars represent $\pm 3 \times$ standard error to include 99.7% of scenarios.

As seen in 4.14, the flow rate appears to scale linearly with laser power in the range under investigation. However, the uncertainty of the median suggests that issues concerning the repeatability of the process should be addressed before any sound conclusions can be made regarding the usability of the proposed method in any scenario into which laser power modulation would be employed for flow rate adjustment.

4.4.6 HEAT TRANSFER | THERMAL IMAGING

An important consideration when designing a thermal micropump is the heat transfer from the pump to the reagents in nearby positions. As described in the previous sections, we employ layer-by-layer activation of the mixture through localized heating. In order to assess heat transfer during the expansion process, we repeated the experiment in Section 3.2 using a calibrated thermal imaging camera to quantify chip temperature.

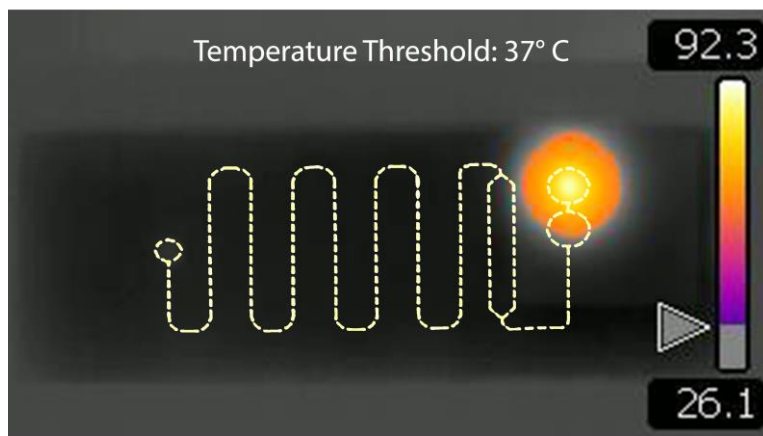


Figure 4.14: Thermal Imaging at the peak temperature with 37 °C threshold below which areas are presented in grayscale. Chip structure has been added in dashed lines for better representation.

Fig. 4.14 shows the temperature distribution just before the beam exits the mixture chamber, which is the peak temperature point during of the expansion process. We notice that the chamber and channels are near the temperature threshold boundary but remain under 37°C. The highest recorded temperature was 92.3°C at the center of the chamber. The lowest temperature was 26.1°C, the chip body temperature, which was cooled to 20°C prior to the experiment in order to be distinguishable from the environment in thermal images. It should be noted that the ambient temperature during the experiment was 31°C and that the test platform below the chip was a flat machined aluminum plate which does contribute to the heat transfer of the process through heat conduction from the chip to the environment. These results are significant because excessive heat could cause biological assays to suffer from denaturation and other temperature related processes. Additionally, they serve as an indication that the expansion is not due to liquid reagent evaporation or air expansion, but due to microsphere expansion and rupture.

4.4.7 HEAT TRANSFER | THE EFFECT OF CHAMBER SIZE

To evaluate the effect of chamber size on heat transfer in the chip, an FEA study of chips with diameter ranging from 2 to 8 mm was made (Figure 3). The region of interest is the IR irradiated chamber. The beam is assumed to have fully penetrated the expandable mixture, hence heat input is simulated using a virtual heat source of 500 mW at the circumferential area of the orifice seen in the center of the gradients as a small hole. A convection coefficient equal to 3 W/(m²·K) is assumed for all exposed surfaces. Both chambers are assumed to be filled with expandable paste with thermal conductivity equal to 0.1 W/m·K and heat capacity equal to 1370 J/kg·K. The chips have been assigned thermal conductivity equal to 0.21 W/m·K and heat capacity equal to 1500 J/kg·K which are characteristic values for acrylic materials. The analysis type is thermal transient with the heat source being active for 60 seconds. While the model is a very simplified version of what is actually happening within the chips during the expansion, the results in comparison to each other provide insight on the effect of the diameter of the mixture filled chamber on the heat diffusion inside the chip. From this particular analysis we can see that changing the diameter within the ranges specified does not significantly alter the thermal behavior of the microfluidic chip.

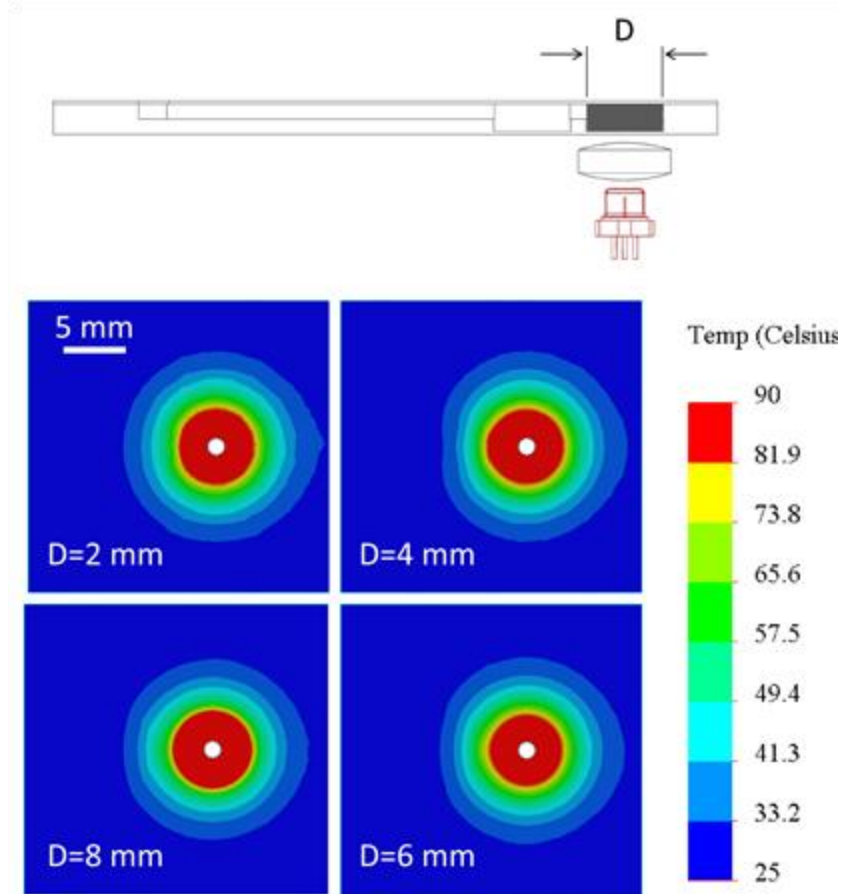


Figure 4.15: Transient thermal finite element study of chips with varying expandable mixture chamber diameter ranging from 2 to 8 mm. The snapshots represent temperature after 60 seconds of IR irradiation of the expandable mixture.. Results at or above 90 °C are presented in red. Ambient temperature is set at 25 °C. The chip design is identical to the one presented in figure 1 of the manuscript.

4.4.8 HEAT TRANSFER | THE EFFECT OF CHIP THICKNESS

Regarding the thickness of the chip itself, a similar FEA study was made, however this time the variable was the chip thickness H (Figure 4.16).

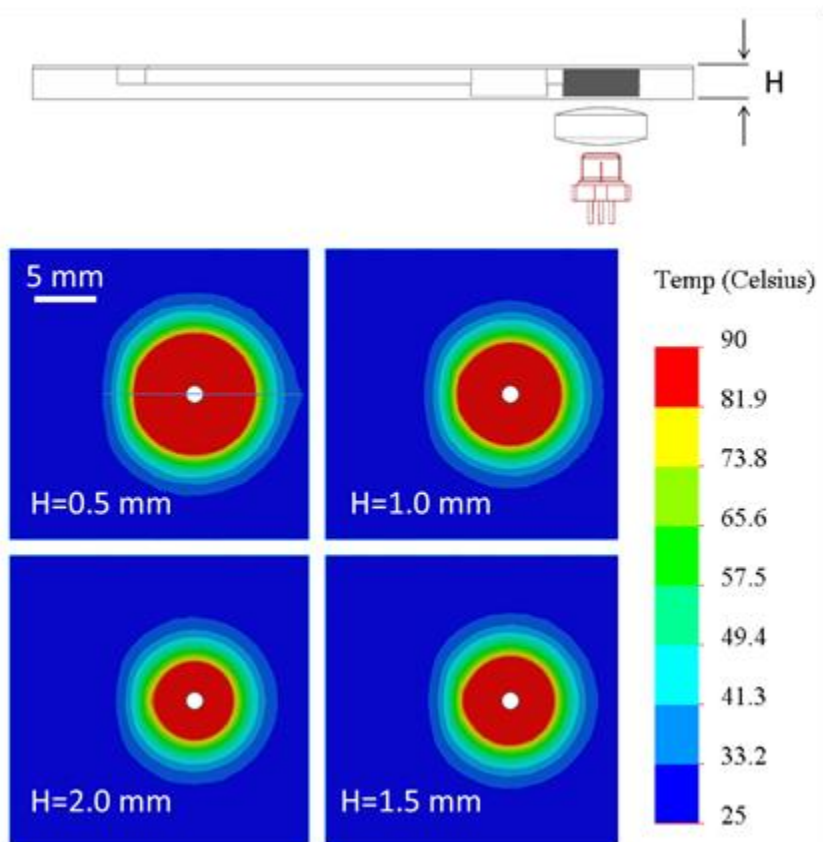


Figure 4.16: Transient thermal finite element study of chips with varying thicknesses (H) ranging from 0.5 to 2 mm. The snapshots represent temperature after 60 seconds of IR irradiation of the expandable paste. Results at or above 90 °C are presented in red. Ambient temperature is set at 25 °C. The chip design is identical to the one presented in figure 4.4 of the manuscript.

As can be seen in Figure 4.16, thinner chips present a wider heat affected zone than thicker chips for the same amount of energy input. The increase of the size of the zone over 37 °C when the laser is active is 24 % in radius comparing the 2 mm chip with the 0.5 mm chip. However even after the laser is switched off, the accumulated heat diffuses into the chip resulting in a maximum increase of 36 % in radius for the zone over 37 °C. This increase, though not extreme, could be an indication that in order to scale down the proposed method it would be necessary to further isolate the “hot spot” from the reagents, either spatially or by removing excess heat from the chip.

4.4.9 HEAT TRANSFER | USING A HEATSINK TO REDUCE THE SIZE OF HEAT AFFECTED ZONES

A possible way to further reduce the high temperature zone near the infrared laser spot is to implement a heat sink near the region. In figure 5, the use of an aluminum plate below the chip against natural convection to the environment is presented.

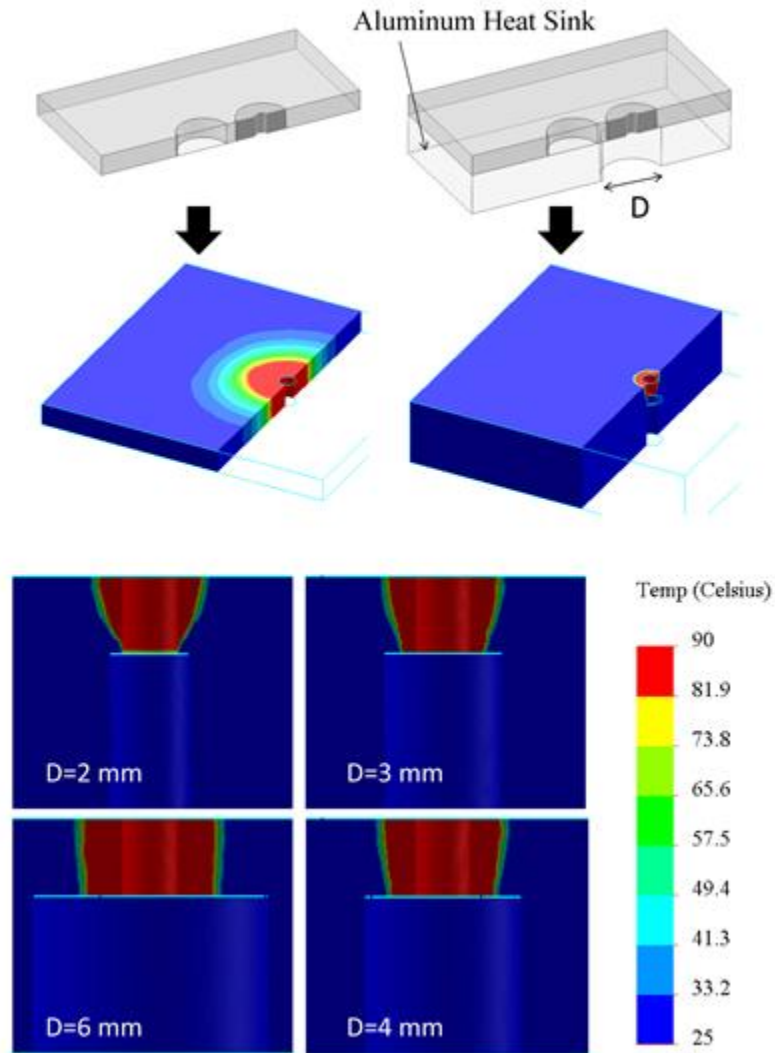


Figure 4.17: Transient thermal finite element study of chips with an aluminum heatsink embedding an aperture of diameter D to allow for laser irradiation of the chip. The snapshots represent temperature after 60 seconds of IR irradiation of the expandable paste in section views of the mixture chamber and the heatsink orifice right below it. On the top left the analysis is done without a heat sink. On the top right a heatsink is included. On the bottom, the heat diffusion is examined in correlation to the radius of the laser path aperture in the heatsink. Results at or above 90 °C are presented in red. Ambient temperature is set at 25 °C. The chip design is identical to the one presented in figure 1 of the manuscript.

As can be seen in Fig. 4.17, the addition of a heat sink reduces the radius of zones over 37 °C by more than 80%. This effect is enhanced as the laser path aperture of the heatsink is reduced in radius. Given that the proposed technology requires the use of a device into which the microfluidic chips are placed in order to perform assays, it is reasonable to say that the implementation of a heatsink is a cost effective and practical solution to further reduce heat affected zones within the chips.

4.5 CONCLUSIONS AND NEXT STEPS

We have demonstrated a prototype version of a single use micropumping system that requires only one laser source to achieve volume displacement. It has been shown that volumes over 35 μl can be easily displaced within a few seconds with a near-constant flow rate. The volume displacement has been shown to occur in two phases, a linear and a non-linear, out of which the first one yields maximum energy efficiency. The flow rate depends on the concentration of absorbance agent in the mixture, while the maximum volume that can be displaced depends on both the concentration of expandable microspheres and the volume of available mixture that is found along the laser beam path. We have shown that repeatability of less than 1 μl is possible by using a 405 nm laser source and a photopolymer, as a volume dependent shutoff valve. Additionally, it has been demonstrated that pressures up to 150 mbar will not affect the micropump's performance and that the heat transfer implications of the method can be contained so as not to affect active reagents on the chip. Finally, while it has not been investigated in depth, we have observed that after the expansion process, a recovery phase occurs. This phase could be used to enable liquid reagent aspiration from the environment to the chip.

This method is limited by the deviation of the measured flow rates and displaced volumes. This, we believe, is due to the dimensional deviations of the chips and the sensitivity of the method to the repeatability of the experimental conditions in respect to laser optics, i.e. beam power stability, focal point and transmittance of optical windows. Thus, optimization of these parameters is a necessary step for the improvement of repeatability. Another limitation is the energy consumption of this method ($>1.5 \text{ J}/\mu\text{l}$ moved) that is related to the efficiency of the laser sources and is also in need of optimization.

Possible applications of the proposed method are numerous in the fields of biology, medicine, point of care diagnostics and environmental research. Compared to the state of the art for fluid handling in microfluidics, the main advantages are four: (1) We identify the potential for a unified optofluidic technology in which fluid handling and detection are both done using only laser diodes or even just one laser diode. (2) The micropumping technology is embedded as a single use feature in the disposable microfluidic chips, thus removing the need for peripheral fluid handling hardware. (3) There is no need for tubing and tubing connectors, frequent sources of problems in microfluidic systems. (4) Even though it is not in an optimized state, this technology appears to already provide adequate performance for most applications at a small fraction of the cost.

The method can be easily scaled up by integrating multiple chambers, each performing a single task. In that way, multistep protocols such as ELISA assays can be realized in microfluidic chips powered by a single pocket-size device that need only contain a PCB assembly with embedded laser diodes and a camera or even a smartphone adapter. For more demanding applications that would make dedicated laser diodes an uneconomical solution, a device very closely modeled to a Blu-ray burner with appropriate firmware could also be used, since such devices often embed high power 405 nm laser diodes that could be used both for activation of the expandable

mixture and the photopolymer as well as for fluorescent marker excitation. In this case the microfluidic chip could be modeled to resemble the compact disk designs or simply fit in a CD shaped adapter. Such a solution would benefit from the Lab on a CD technology that has already been developed. The microfluidic chips themselves can be produced using simple molding techniques, since single layer structures suffice for this fluid handling method, thus making this technology advantageous for mass production.

The proposed method can be further optimized to reduce deviations in respect to flow rate and displacement precision and repeatability. Using this component, we believe that the fabrication of reliable no-moving-part PoC devices and single-diode high-throughput platforms for multistep assay preparation and detection is possible.

CHAPTER 5: POROUS HYDROPHOBIC MICROVALVES

5.1 ABSTRACT

The point-of-care (PoC) diagnostics system is one of the more sought-after applications of microfluidics and microelectromechanical systems (MEMS) both academically and commercially. The impact of decentralized diagnostics and health monitoring can be realized when examining the cases of actual application of such systems such as the ones presented in chapter 2 of this work. Glucose, β -hcG, Tp-I / CK-MB / Myoglobin are some of the most prominent diagnostic targets of PoC currently in commercial use with a great impact on healthcare. However, the common thing between these widely applied targets is that the diagnostic protocol for PoC applications is a single step process where the use wets a capillary or a lateral flow test with the sample, either directly or following a simple dilution step. When the diagnostic protocol necessitates a multiple step approach such as multiple mixing, incubation or washing, the implementation into a PoC device becomes much more complicated. While such devices do exist, they are not as widespread as LFIA or single step electrochemical sensing of glucose. Partially, this is because the elements of fluid handling that are necessary to perform multi-step analyses are not as easy to implement into disposable chips. One of these elements is the simple on/off valve which in this case is called a microvalve. In this chapter, the status of microvalves is reviewed and a brief categorization is presented. The benefits of passive valves over active elements in disposable lab-on-chip systems are discussed and a new type of microvalve is presented.

5.2 INTRODUCTION

5.2.1 MICROVALVE TECHNOLOGY

Microvalves are an essential element in microfluid chips where all but the simplest operations need to be performed. Their function is to switch, seal and regulate the flow within a microfluidic chip. There are several articles reviewing the status of microvalves^{251,275} and many different operating principles have been proposed and tested by research groups for these miniature elements. In general, microvalves can be either active or passive.

Active microvalves can be triggered on que and usually rely on a mechanism that is mostly independent of what is happening inside the fluidic circuit. The operating principles vary, but the most widely adopted implementation of the active microvalve includes some form of mechanical valving. These systems often rely on solid or more often flexible elements that deform and block the flow while driven by an actuator. Quake's group was the first to investigate pneumatically activated microvalves²⁵² which was an impactful discovery because it used soft lithography, a method already employed for the fabrication of microfluidic chips. Other principles²⁷⁵⁻²⁷⁷ for active microvalves include magnetic actuation, piezoelectric actuators, thermal and thermopneumatic valves as well as more elaborate applications. In all of these cases, the actuator can be either embedded in the chip which usually adds complexity and/or cost to the design, or it can be external which requires an interface to the chip, or split between the chip and an external device.

The second group of microvalves are called passive microvalves^{278,279}. These elements usually rely on the pressure of the microfluidic line, effectively operating like relief valves. In the most common case, the passive valve is restricting flow up until a burst pressure forces the fluid through. This can be achieved by introducing an abrupt enlargement to the channel which can be further treated to become hydrophobic. The capillary effect created by the combination of shape and hydrophobicity transforms this transition point into a relief valve with a predefined

burst pressure. For this reason, these elements are also called burst microvalves. Gyros protein technologies produces microfluidic immunoassays of the Lab on a Disk (LoaD) that embed burst valves as a necessary component.

Active and passive microvalves are two different approaches addressing the same problem, which is multistep fluid handling in a microfluidic chip. Because of their differences, they are more compatible with different chip architectures. Active components are more versatile and give overall higher control over microfluidic handling. However, they typically require assorted instrumentation to operate which is often undesirable in PoC applications. Passive components are more demanding as they require a specific burst pressure to operate and often the design of multistep processes is not straightforward. However, they require no instrumentation and are easier to manufacture and integrate into a microfluidic chip. This is significant advantage for PoC diagnostic applications and can be more easily adapted in commercial applications.

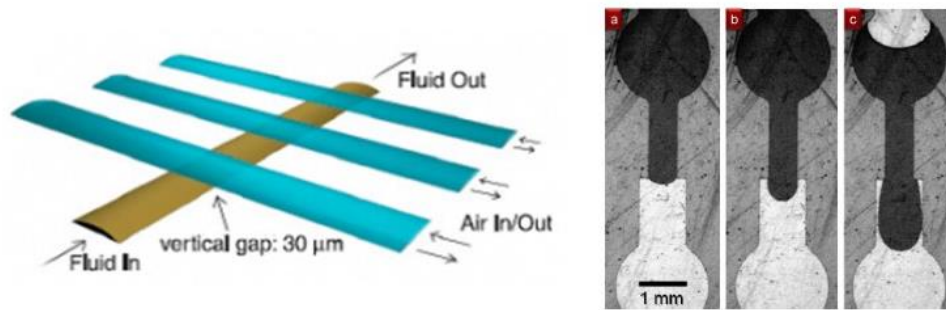


Fig 5.1 On the left image, the principle of the Quake pneumatically controlled microfluidic valve/pump configuration is shown²⁸⁰. On the right, a capillary valve is seen before, during and after burst²⁸¹.

5.2.2 BURST MICROVALVES - GEOMETRIC APPROACH

Microfluidic scaling laws make fluid behavior in the microscale much different than what is encountered in macroscale fluid mechanics. One of the most important distinctions is that in the microscale, capillary phenomena become dominant over forces that are dependent on volume or surface. This greatly amplifies the contribution of forces such as the Laplace force in the behavior of a fluid front. A steep increase in the width of a rectangular channel results in an increase of capillary pressure capable to stop an incoming flow. This is in effect a valving function, since to overcome this stop, energy is required as input. The theoretical principles behind this effect have been thoroughly described in published work^{282–284} both for fluid slugs and for a fluid stream. Assuming a rectangular microfluidic channel of width w and height h , where $w \gg h$ and a liquid sample introduced into this channel. The interfacial energy E of the channel-liquid-air system is described:

$$(1) \quad E = A_{sl}\gamma_{sl} + A_{sa}\gamma_{sa} + A_{la}\gamma_{la}$$

A_{sl}, A_{sa}, A_{la} are the interface areas between the solid-liquid, solid-air and liquid air, while $\gamma_{sl}, \gamma_{sa}, \gamma_{la}$ are the corresponding surface energies. Since the solid-liquid and solid-air surface energies are not easy to measure, Young's equation can be used:

$$(2) \quad \gamma_{sa} = \gamma_{sl} + \gamma_{la}\cos\theta$$

where θ is the contact angle of the liquid with the channel walls. Eq (1) now changes into:

$$(3) \quad E = A_{sl}(\gamma_{sa} - \gamma_{la}\cos\theta) + A_{sa}\gamma_{sa} + A_{la}\gamma_{la}$$

$$= (A_{sl} + A_{sa})\gamma_{sa} - A_{sl}\gamma_{la}\cos\theta + A_{la}\gamma_{la}$$

Due to the small size of the microfluidics channel, capillary forces are going to dominate the flow and the sample is going to be drawn forward by a pressure P described in Eq (4) :

$$(4) \quad P = -\frac{dE}{dV}$$

where V is the fluid volume inside the microfluidic channel

By substituting (3) into (4) we get the following expression:

$$(5) \quad P = -\frac{dE}{dV} = \gamma_{la}(\cos\theta \frac{dA_{sl}}{dV} - \frac{dA_{la}}{dV})$$

The rate of change of $(A_{sl} + A_{sa})\gamma_{sa}$ is zero since $A_{sl} + A_{sa}$ is a constant sum equal to the entire channel area. Expression (5) is now a function of measurable quantities and can be calculated for the case of a microfluidic channel.

In the case of microfluidic capillary valves, the objective is to create the appropriate geometry so that the pressure switches to negative values, hence acts like a valve. This can be accomplished by the abrupt enlargement of a microfluidic channel either by width or height. Let us assume the following structure: A channel of height h and width $w \gg h$ expands with angle β to form an enlarged cross section (Fig. 5.2). Since the liquid is drawn into the channel, a meniscus that can be simplified to be a circular arc of angle 2α will correspond to the equilibrium contact angle θ while the liquid is drawn into the channel. Once the liquid meets the expanded section, the meniscus angle will change in order to satisfy the contact angle equilibrium at the point where the geometry changes. If the geometry change is done with a sufficiently steep angle β , the meniscus will change curvature to negative α values and energy input is going to be required to further advance the fluid. Man et al²⁸⁴ have shown that at the critical angle $\beta = \frac{\pi}{2} - \theta$ the pressure becomes zero and for larger β values the curvature is inversed and the pressure becomes negative. The pressure in this case can be calculated using the following formula proposed by Man et al. ²⁸⁴⁻²⁸⁶.

$$(6) \quad \Delta P = 2\frac{\gamma}{h} \left(\frac{\cos\theta - \frac{\alpha}{\sin\alpha} \sin\beta}{\cos\beta + \frac{\sin\beta}{\sin\alpha} \left(\frac{\alpha}{\sin\alpha} - \cos\alpha \right)} \right)$$

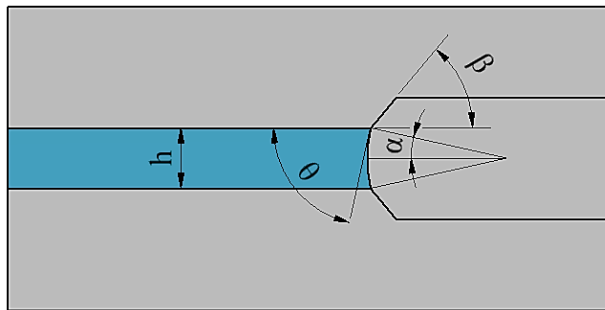


Figure 5.2: A basic design for a geometrical microfluidic valve

For a typical microfluidic chip made from a hydrophobic material, embedding an aqueous solution and assuming the following values $\theta = 90^\circ$, $\gamma = 72.8 \frac{mN}{m}$, $h = 50 \mu m$, $\beta = 90^\circ$, formula (6) would yield a pressure requirement of $\sim 12.6 kPa$ for the fluid to flow through the valve.

For circular capillary valves of diameter r , an analytical expression for the estimation of the burst pressure is proposed by Glière et al²⁸⁶:

$$(7) \quad \Delta P = 2\gamma \left(\frac{\cos(\beta + \theta)}{r} \right)$$

For a capillary diameter expansion described by the following parameters $\theta = 90^\circ$, $\gamma = 72.8 \frac{mN}{m}$, $r = 25 \mu m$, $\beta = 90^\circ$, formula (7) would yield a pressure requirement of $\sim 5.8 kPa$ for the fluid to flow through the valve

Both previous models approximate a geometric valve which is not commonly encountered in a commercial chip. The valve proposed by Man et al requires a microfluidic channel with a depth much larger than its width while the opposite relationship between these two parameters usually holds true due to manufacturing reasons. The round capillary valve is not easily implemented in a microfluidic chip, again due to manufacturing reasons. The most common design for a geometric burst valve would include a rectangular, trapezoidal or semicircular microfluidic channel with a width comparable or larger than its height and a polymer cover that seals off the valve from the top. Bauer et al.²⁸² have proposed an analytical model that takes into account the standard form of a geometric burst valve:

$$(7) \quad \Delta P = \gamma \left(\frac{\cos\theta_R}{H} - \frac{\cos\theta_A}{h} + \frac{\cos\Psi_R}{H} - \frac{\cos\Psi_A}{h} + 2 \left(\frac{\cos\theta_R}{Wc} - \frac{\cos\theta_A}{w} \right) \right)$$

$\cos\theta_R$: The fluid slug's receding front contact angle with the structure material

$\cos\theta_A$: The fluid slug's advancing contact angle with the structure material

$\cos\Psi_R$: The fluid slug's receding front contact angle with the sealant material (top layer, not shown)

$\cos\Psi_A$: The fluid slug's advancing front contact angle with the sealant material (top layer, not shown)

H : Fluid chamber height

h : Microfluidic channel height

Wc : Fluid chamber width

w : Microfluidic chamber width

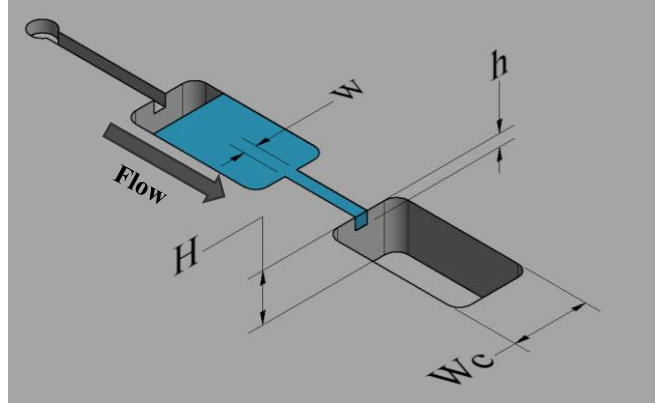


Figure 5.3: A 2D structure to be used as a geometrical burst valve. On top of this structure, a thin adhesive film is typically used to seal off the microfluidic circuit.

For a typical geometric burst valve on a polycarbonate chip with a top adhesive sealing film and $h=50\ \mu\text{m}$, $H=500\ \mu\text{m}$, $w=400\ \mu\text{m}$, $W_c=2000\ \mu\text{m}$, $\theta_R = 23^\circ$, $\theta_A = 96^\circ$, $\Psi_R = 23^\circ$, $\Psi_A = 123^\circ$ ²⁸² the pressure required for an aqueous solution (ex. saline solution) to flow through the valve is $\sim 1.3\text{kPa}$.

While geometric burst microvalves present a simple solution for fluid handling and they have been widely investigated and used by several research groups, they also have restrictions²⁸². Minor imperfections of the channel/valve inner surface can significantly affect the valve performance. More to that, for the geometry of a molded component, which would most likely be the case in a commercial microfluidic chip, very sharp edges cannot easily be achieved in the interface between a channel and a valve. The rounding of the valve geometry also affects its performance. Another important factor that would weight in in the case of a commercial microfluidic chip is that especially in the case of centrifugal systems, there are two main approaches for the chip manufacturing: Either the chip is injection molded and sealed with an adhesive membrane or fused with a second injection molded part. In the general case, each discreet structure will be only imprinted on one of the two parts. This is important because it implies that the other part (the seal) will also come in contact with the liquid and this will affect the valve performance. In order to further explore the expected performance of such a valve in a centrifugal system (Lab on a Disk, LoaD) we need to compare the burst pressure of a geometrical burst microvalve with the pressures induced in a LoaD system:

The pressure of a liquid slug in a centrifugal system is due to the centrifugal force induced by the disk rotation and can be calculated using the following formula²⁸⁷:

$$(8) \quad \Delta P = \frac{1}{2} \rho \omega^2 (r_2^2 - r_1^2)$$

where ρ is the density of the fluid inside the channel, r_1, r_2 the radiuses of the fluid receding and advancing levels respectively, and ω is the rotational frequency of the centrifugal system (Fig 5.4)

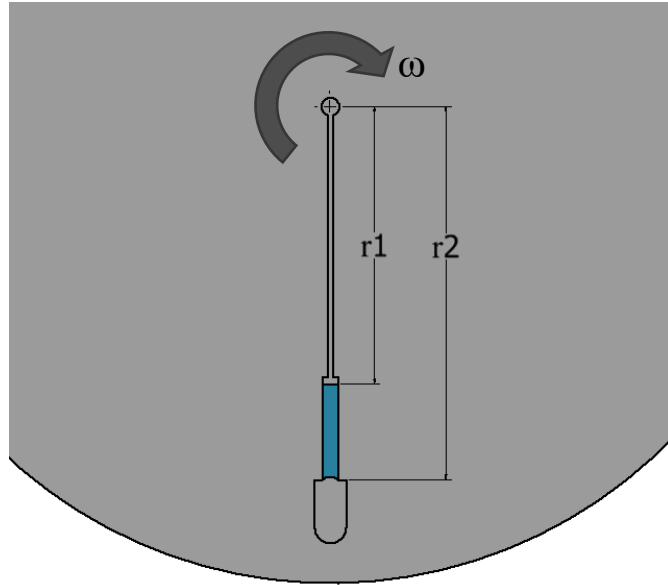


Figure 5.4: A fluid slug that has advanced to the barrier of a geometrical burst valve inside a centrifugal microfluidic disk

We could assume the following case study to examine the expected performance of a burst microvalve in a lab on a disk system: A polycarbonate disk of 100 mm in diameter and 2 mm in thickness is the macroscopic chip design. The chip is assumed to be injection molded, which is a typical manufacturing process for point of care microfluidics. Using this technique, rectangular or trapezoidal channels in which the width is comparable or larger to the height would be typical. We can also assume that a channel width of 100-400 μm is reasonable for such a chip design²⁸⁸⁻²⁹⁰. This is not to say that much smaller channels are not possible in a laboratory environment or even in a mass production scenario. It is however a reasonable size limit to avoid clogging issues and to facilitate manufacturability. Additionally, it is assumed that the chip will be sealed using a membrane with pressure sensitive adhesive. In this case it would be reasonable to keep channel depths over 50 μm to avoid accidentally blocking the channel with the sealing film. We also assume a valving scheme just like the one seen in Fig. 5.2 with the following parameters as described in Eq. 7: $H = 500 \mu\text{m}$, $W_c = 2000 \mu\text{m}$, $\theta_R = 23^\circ$, $\theta_A = 96^\circ$, $\psi_R = 23^\circ$, $\psi_A = 123^\circ$. For the selected channel size range and these parameters, using Eq. 7, we can calculate the expected microvalve burst pressure (Fig. 5.5)

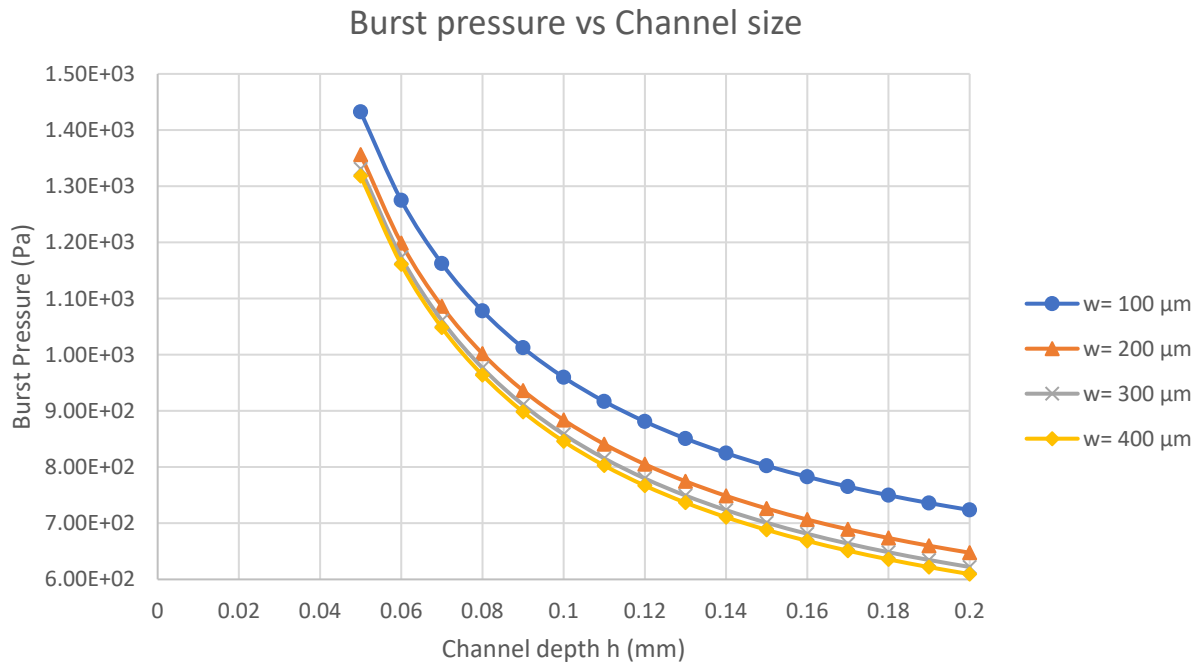


Figure 5.5: The burst pressure for different channel widths and depths

As expected, the smaller structures favor higher burst pressures. If we now place one of these components inside a centrifugal system like the one described in our case study, we could calculate the required rotational frequency in order to open one of these valves. For a disk of 100 mm in diameter, we could assume an advancing front before the valve barrier to be at $r_2 = 29 \text{ mm}$ and the receding front, which in this case would be inside the inlet tank, to be at $r_1 = 14 \text{ mm}$. The resultant burst pressure for a range of rotational frequencies can be seen in Fig 5.6

Exerted pressure vs Rotational frequency

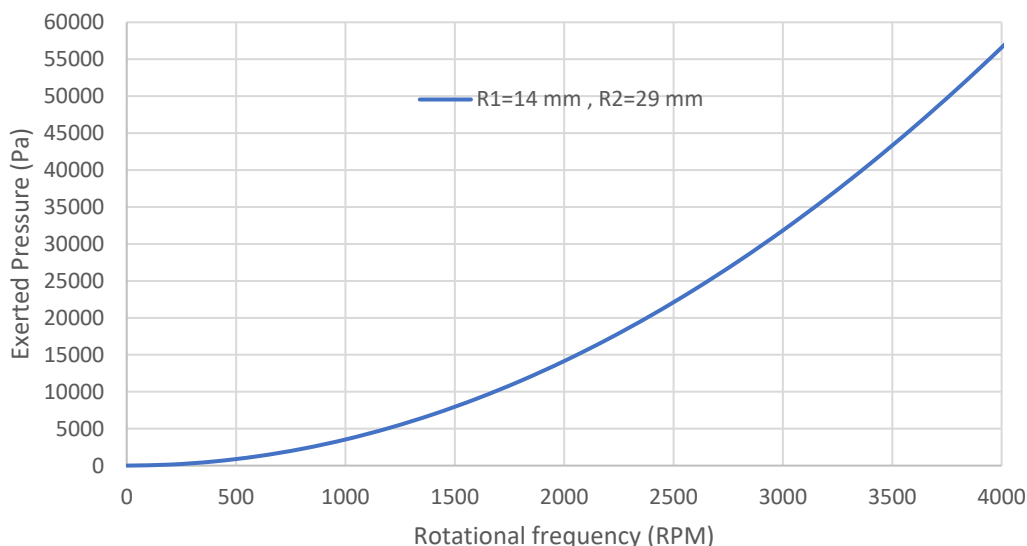


Figure 5.6: The exerted pressure of a fluid slug between $r_1=14$ mm and $r_2=29$ mm inside a spinning centrifugal system

What can be observed in the previous two figures, is that the geometric valve burst pressures could potentially be too low to use in an actual PoC system. As described in Chapter 2, centrifugal microfluidics are based on an artificial gravitational field which is created through the rotation and keeps reagents and solutions in their respective chambers. Low rotational frequencies in the order of 600 RPM are often reported^{291,292} as baseline or aliquoting frequencies. In our case study, since the chip and seal material are hydrophobic, frequencies in this order could be necessary just for the chip priming. Finally, assuming a point of care system in which the sample would require centrifugation before any other operation, for example for the extraction of plasma from blood, it would not be possible to have valves that are activated at pressures as low as 0.01 bar because they would all be activated during sample centrifugation. Therefore, a need exists to create burst valves that operate at higher burst pressures.

HYDROPHOBIC VALVES

One solution that is frequently used for the creation of microvalves is the hydrophobic barrier^{279,293–295}. In this approach, a hydrophobic patch is created at the valving point. Once the liquid front reaches the valving point, the contact angle shift prevents it from moving further until the burst pressure is met. This method has been thoroughly investigated and applied commercially^{296–298}. The key factor in this valve is the transition from the hydrophilic to the hydrophobic surface region, referred to as “break”²⁹⁸. This can be achieved by applying a hydrophobic patch on a hydrophilic base material, for example a perfluorinated hydrocarbon or silicone containing species.

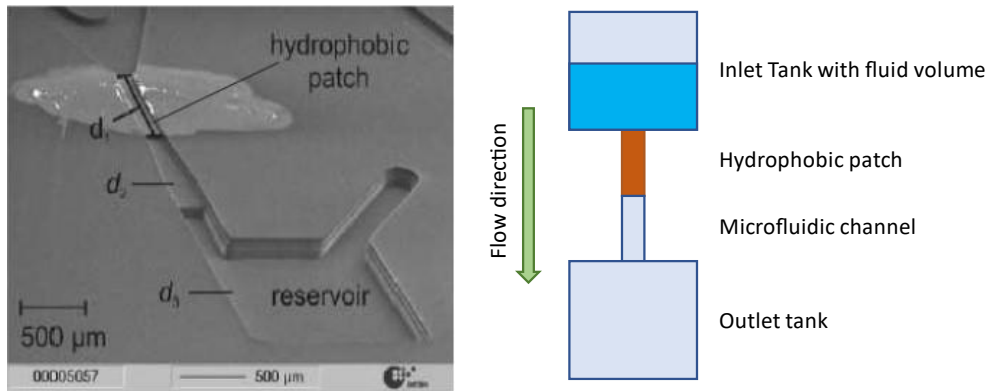


Figure 5.7²⁹⁹: Modifying the contact angle of a constriction point is a valving method frequently employed in research but also in commercial PoC applications

This method provides a better control over the performance of the microvalve and increases the burst pressure which facilitates chip design. For a channel of 200 μm width and 100 μm in depth, changing the contact angle of the advancing front with the barrier material can greatly affect the valve burst pressure. Keeping the rest of the parameters the same as in Fig 5.5, the expect valve behavior can be calculated using Eq. 7 for hydrophobic to superhydrophobic materials (Fig 5.8).

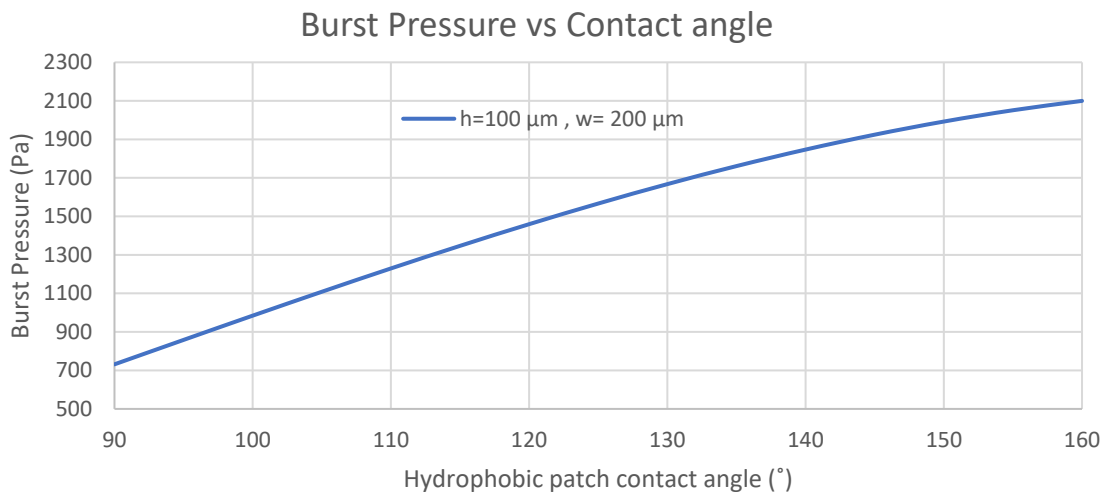


Figure 5.8: Modifying the contact angle of a constriction point is a valving method frequently employed in research but also in commercial PoC applications

However, doing this will require some kind of material deposition or other treatment such as plasma treatment²⁷⁹ or surface modification³⁰⁰. While these have been thoroughly investigated and there are both laboratory and industrial processes to apply them, avoiding them in some cases would simplify and speed up the manufacturing process. For example, a fluoropolymer patch will need to be precisely positioned into the constriction point in order to avoid adhesion failure with the sealing film. This could be avoided by using plasma etching/deposition with appropriate masking elements in order to create hydrophobic structures. However, these processes may require several minutes per batch of chips. Additionally, geometric imperfections of the microfabricated form could affect

the valve performance. Thus the need for a simple valving scheme based on an easy to integrate component is recognized as a step towards low cost, simple and reliable PoC systems.

ASSEMBLED HYDROPHOBIC MICROVALVES

What is proposed in this work is a novel kind of microvalve which is inserted into the chip instead of requiring a special modification or deposition. The valve consists of a hydrophobic or superhydrophobic porous component with one dimension in the microscale and two dimensions large enough to be processed in a component assembly scenario. This approach allows for a modular chip design in which the valve is an external component which is inserted at the required position. The intention behind this approach is to simplify the chip design and manufacturing process. A drawing of the valve assembly can be seen in Fig 5.9. The valve component is inserted in a pocket of appropriate size within the chip and sealed using the chip sealing membrane. In the following chapters, the prototyping method for such chips is described and the valving scheme is tested using a centrifugal test setup.

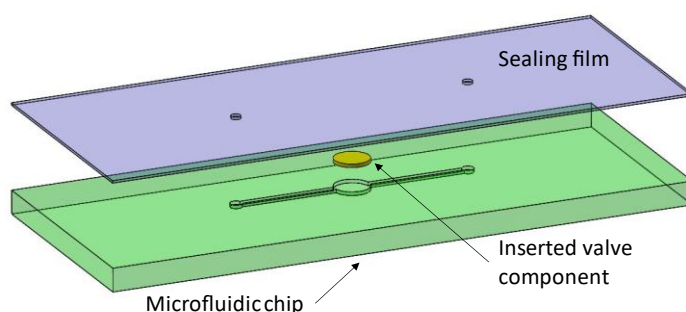


Figure 5.9: The proposed valving scheme includes a hydrophobic porous component which is inserted in the microfluidic chip

5.6 METHODS

5.6.1 VALVING ELEMENT FABRICATION

In order to create a superhydrophobic water-permeable element, a porous material and a hydrophobization agent are employed. As a porous material, a glass microfiber Whatman filter of 700 nm porosity was chosen. The borosilicate material makes this component suitable for use in a point of care system because of its inertness. Additionally, filtration elements have controlled porosity which ensures consistent structure and behavior. Regarding the hydrophobization agent, there is a large number of commercially available hydrophobization solutions for textiles and porous materials using different technologies³⁰¹. For this study, a solution of 100 nm SiO₂ particles by NanoProm was used. The fabrication process was the following:

- Circular pieces of glass microfiber filter are cut out of the sheet using a 3 mm biopsy punch
- The circular filters are soaked in the SiO₂ solution for 10 minutes
- The wet filters are removed from the solution and are left to dry for 24h in room temperature

After this process, the filter surface becomes superhydrophobic and can be used as a valving element. Measurements in a contact angle goniometer display contact angles of 149° for the hydrophobization process.

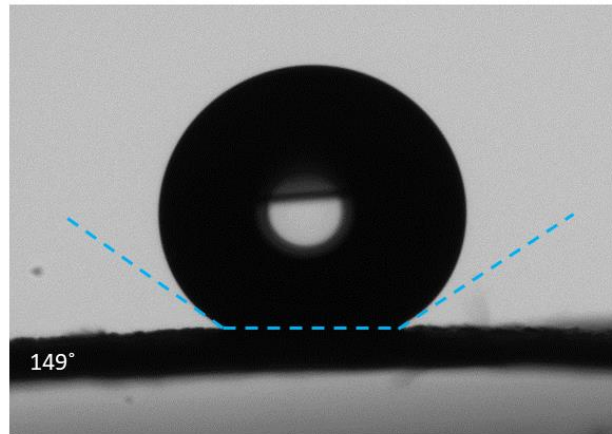


Figure 5.10: The contact angle of a water droplet on the processed filter was measured at 149°

5.6.2 CHIP DESIGN AND FABRICATION

In order to test the principle of the superhydrophobic valving element, two different designs were realized. The first design is a simple tank-valve-tank sequence based on 2.5D structures (Fig. 5.11). The chip is made from 3 mm commercial PMMA sheets which were laser cut into shape. The channels have a width of $900\ \mu\text{m}$ and a depth of $270\ \mu\text{m}$ with a circular segment profile of $1000\ \mu\text{m}$ diameter. The valving element position has a depth of $300\ \mu\text{m}$ and a diameter of $3000\ \mu\text{m}$. When the chip is primed, the receding front is at $R1=14\ \text{mm}$ while the advancing front, which is in contact with the valving element, is at $R2=29\ \text{mm}$. Both the top & bottom surface of the chip are sealed using microtiter plate sealing films which are cut into shape manually.

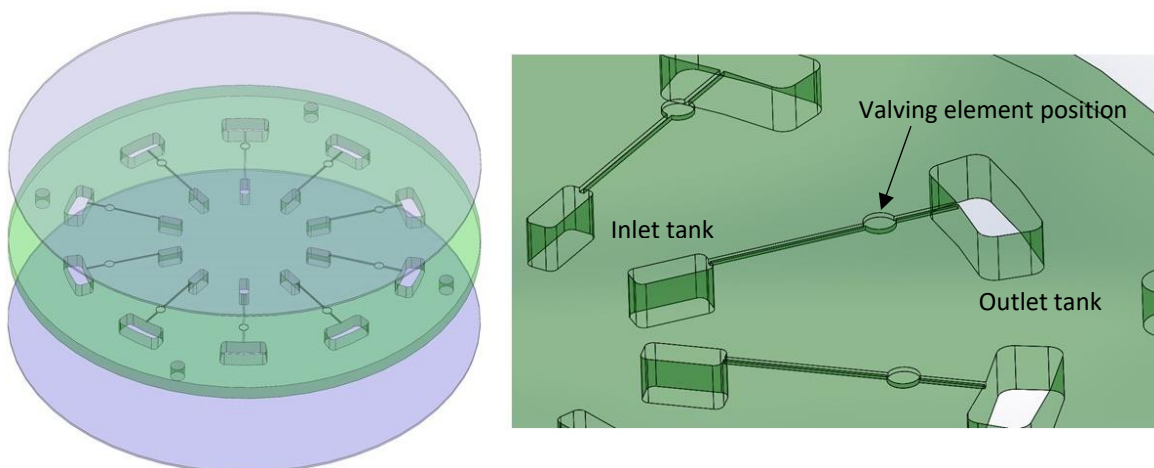


Figure 5.11: Standard valve implementation. Chip is sealed using top & bottom adhesive films

Both the inlet and outlet tanks were cut through the chip during the laser cutting process. The connecting channels and the valving element position were machined in a subsequent step using an alignment jig into a cnc milling machine (Fig. 5.12). While the methods used here are suited for prototyping, the chip design is compatible with mainstream mass production methods such as injection molding or embossing³⁰². The implementation of this valving element would only require a cylindrical pocket of controlled depth and diameter into which the hydrophobized filter would be inserted. Additionally, the sizes used here are such that coarse machining methods and manual assembly are not impairing the device's functionality. Using automated assembly and mass production methods, the valving element could be further miniaturized.

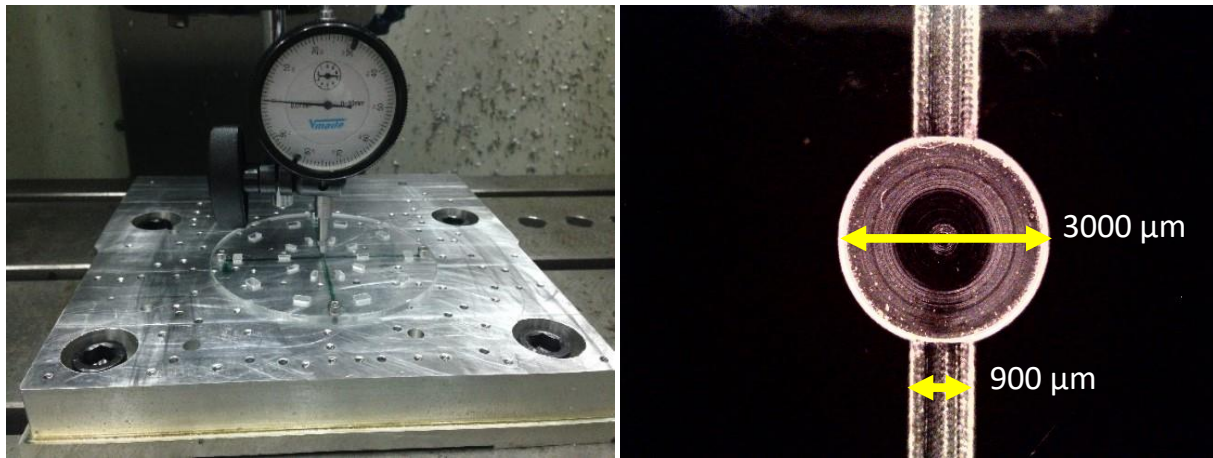


Figure 5.12: The chip channels and valve positions are machined using a jig and the depth is verified on site.

After the chips structure is complete, it goes through a degreasing, rinsing and drying process. Once the chip is completely dry, the valving elements are manually inserted in the respective positions and the chip is sealed. Before the chip is used, the inlet tanks are pierced and primed with 20 μl of colored aqueous solution.

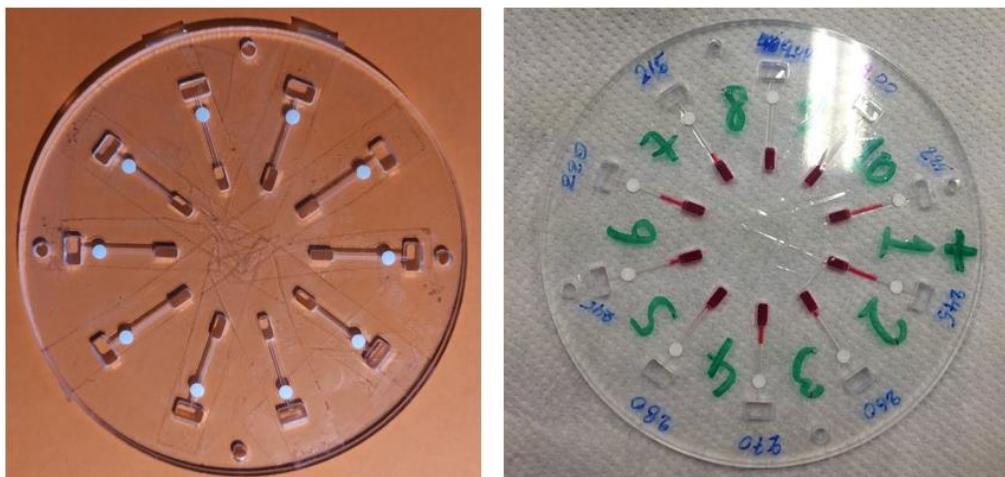


Figure 5.13: The chip and valves are assembled and then primed with 20 μl of colored solution

The second chip design is based on a radial implementation of the operating principle described here, in which the valving element of cylindrical profile is inserted into a circular radial channel (Fig 5.14). A threaded hollow plug locks the 300 μm thick circular hydrophobized filter (valving element) into position and seals off the circumference. This way it is ensured that the fluid can only go through the valving element and avoid leaking around it.

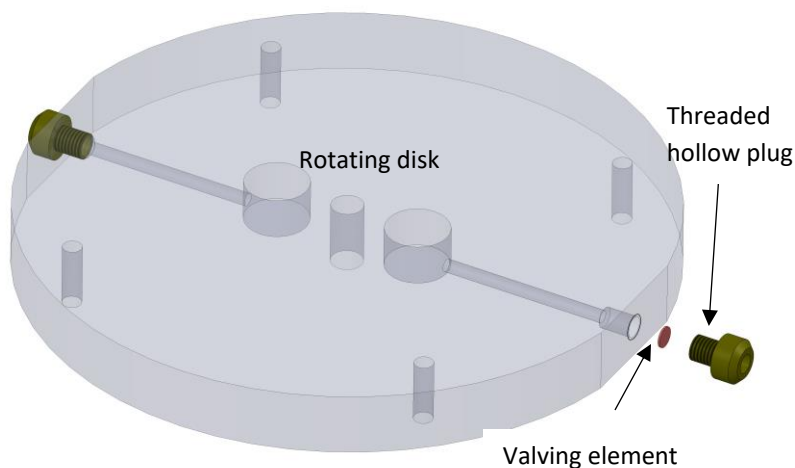


Figure 5.14: Radial valve implementation. Chip is sealed using an adhesive membrane (not shown)

This chip design is manufactured using conventional tooling. An 8 mm PMMA disk is machined to form an inlet tank with an outlet circular channel towards the disk circumference. The circular channel has a diameter of 2 mm on the end of which the valving element is secured using an M4 plug with a hollow center that allows air and liquid to flow through outside the chip once the valve is burst (Fig 5.15). In this application, both the channel size and the method of fabrication are untypical of what would be used in a PoC setting. The reasoning behind this chip design is that the burst pressure in this instance is going to be dependent only on the hydrophobization of the valving element and not on the shape of the filter or the interface between the chip and the valving element. In this sense, it is an ideal situation which would demonstrate what the highest attainable burst pressure would be for this material.

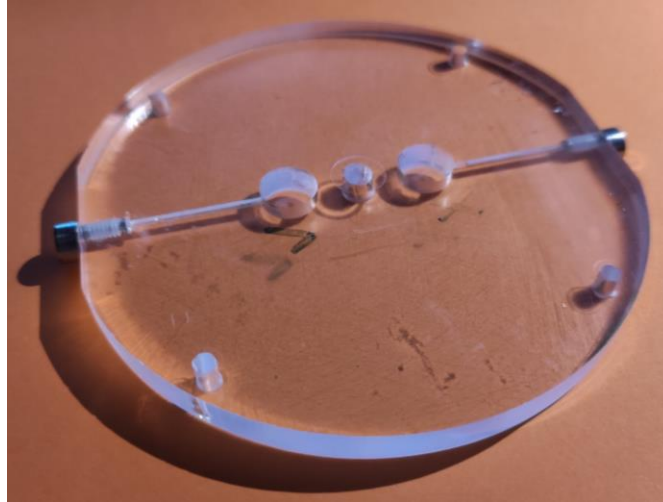


Figure 5.15: Radial valve test chip.

5.6.3 EXPERIMENTAL SETUP

The evaluation objective for these valving elements is the fluid pressure which is required to burst open the valve in a centrifugal setup. For this purpose, a test setup was developed which allows adjustable angular frequency up to 9000 RPM and it includes a strobe illumination which enables the evaluation of the valve performance during the experiments (Fig 5.16)

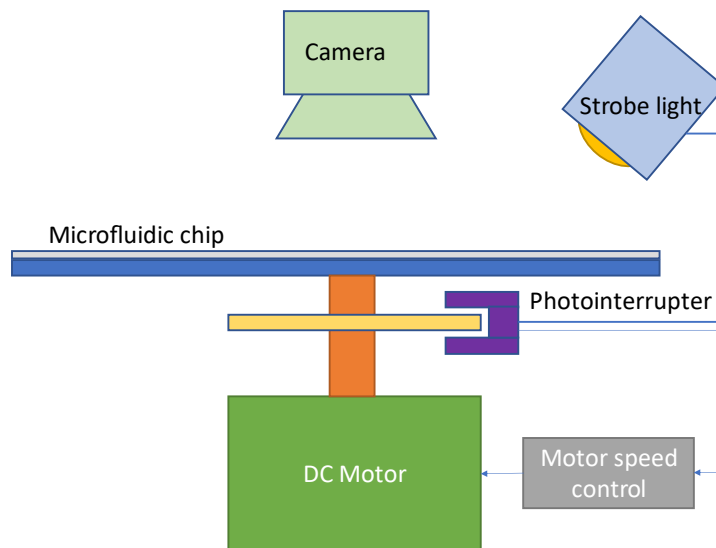


Figure 5.16: Experimental setup for the evaluation of the valve performance

The photointerrupter was also used as a feedback signal for the adjustment of the DC motor speed through a commercial Arduino microcontroller. The setup was installed inside a metal enclosure for safety reasons. More information about the setup can be found in ³⁰³.

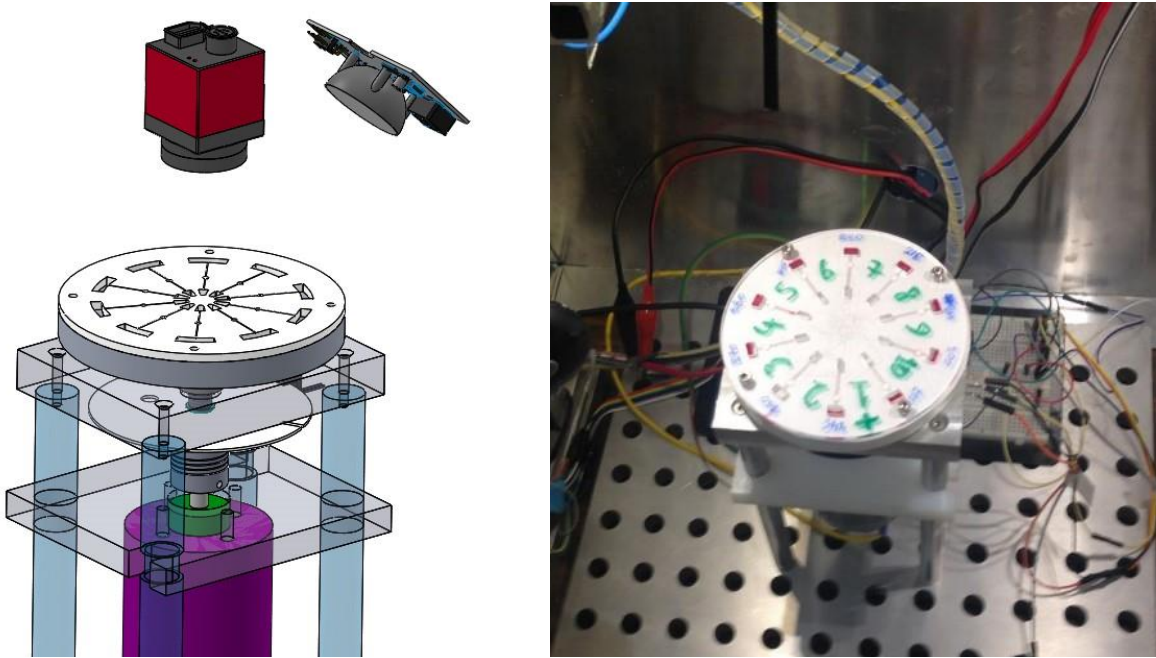


Figure 5.17: Design and implementation of the experimental setup for the evaluation of the valve performance

EXPERIMENTAL PROCESS

The tests protocol for the burst frequency evaluation of each valve design starts by mounting the chip on the device and then running the rotor to a minimum frequency that has been seen to always be below the expected burst frequency of the valving elements. While the rotor is spinning, the valve behavior is recorded to be used later for the evaluation of the valve performance. The speed is increased by increments of 35 RPM and remain in each set point for 120 s. The burst pressure is evaluated by visual observation of the spinning disk with stroboscopic illumination. In Fig. 5.18, part of a valve test recording is presented in snapshots. At the 0.000 time point, the rotor is starting to spin. At 0.601 s, the channels are primed with the colored aqueous solution. At 2.5 s, the valve has burst and there is flow from the channel towards the outlet tank. Within ~10 s, the entire inlet tank has emptied into the outlet tank.

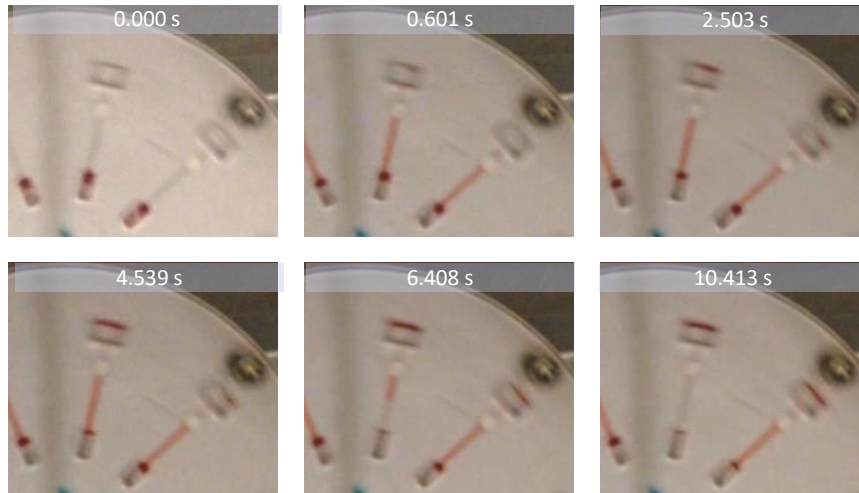


Figure 5.18: Recording of the valve performance using stroboscopic illumination. The valve is primed at 0.601 s. At 2.503 s the valve has been burst while at 10.413 the entire fluid volume has gone through it.

5.7 RESULTS

5.7.1 STANDARD CHIP DESIGN

Using the standard chip design, 10 experiments were conducted. The chips were primed with 20 μl of coloured aqueous solution and inserted into the testing platform. In nine of these experiments the valve functioned as intended, while in one experiment the valve sealing failed and the reagent flew through at minimum frequency. The advancing front was measured to be at $r_2=29$ mm while the receding front was at $r_1=17$ mm. Again, the frequency of the rotation was gradually increased and the chip response was recorded using a camera and a strobe illumination synchronized to the rotational frequency. The resulting burst points were obtained and are presented in Fig. 5.19 & 5.20.

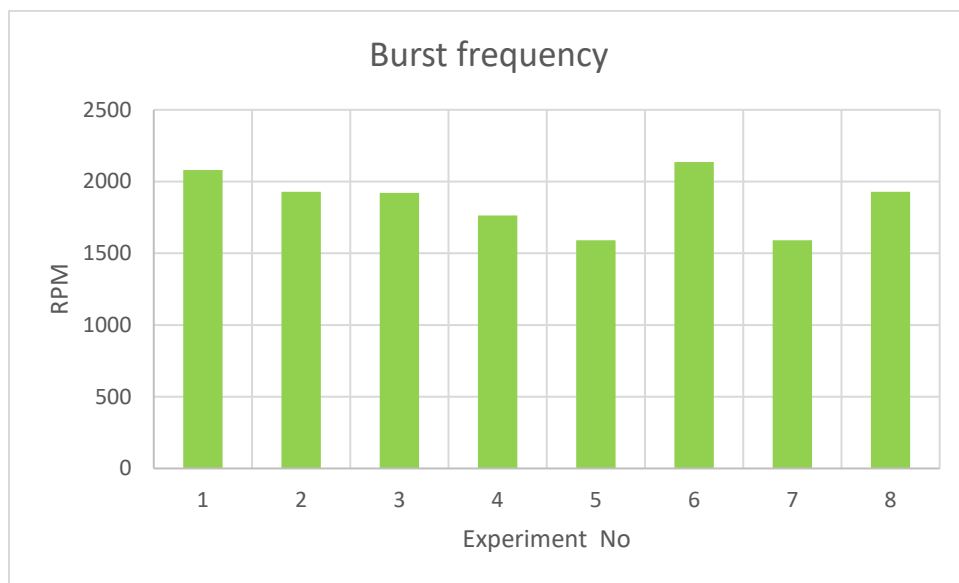


Figure 5.19: Standard chip design, burst frequency

These measurements are linked to the advancing and receding front positions. Using Eq. 9, the equivalent burst pressures are calculated in Fig. 5.20.

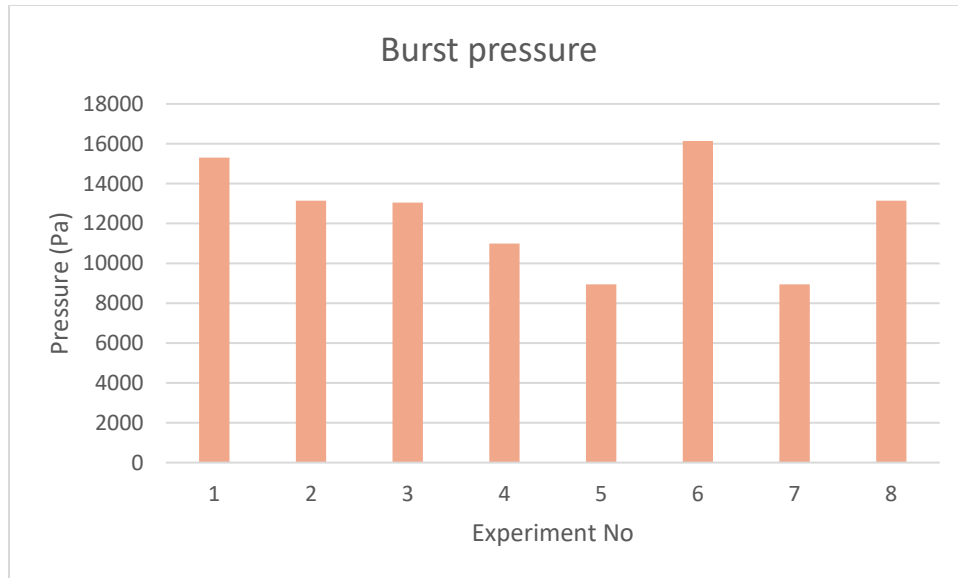


Figure 5.20: Standard chip design, burst pressure

For the radial chip design, the following results were obtained:

	Rotational Frequency (RPM)	Pressure (Pa)
Average burst point	1867	12457
Standard deviation	204	2667
Minimum burst point	1590	8941
Maximum burst point	2136	16136

Table 5.1: Burst frequency and pressure for hydrophobic valves.

What can be observed in Fig. 5.20 is the consistently high burst pressures compared to geometric and standard hydrophobic valves. The lowest pressure observed is more than 4 times higher than the pressures seen in the geometric valve examples in the theory and applications section of this work. However, there is significant variability between the burst pressures encountered during the experiments. This can be explained by the observation that after the burst valves were only wetted on their outer surface. The fluid volume appears to bypass the filter core and flow through the outer layers of the filter, near the interface of the chip/sealing membrane. While the filter has been wetted, it is evident that the rest of the chip components, i.e. the main chip body and the membrane play an important role in the valve performance. This could be verified by using the radial chip design in which the circumference of the filter is sealed and thus prevents the liquid volume from flowing around it.

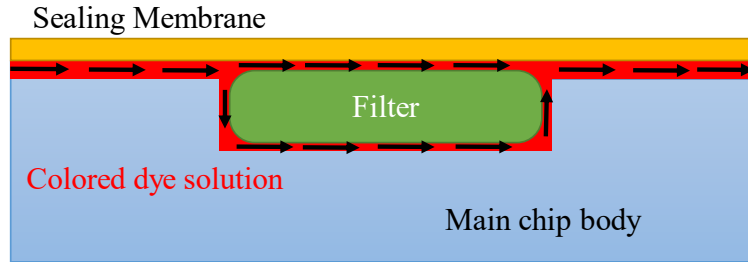


Figure 5.21 : Incision on the burst filter revealed that the reagent may bypass the core of the valve and flow through the outer layers

5.7.2 RADIAL CHIP DESIGN

Using the radial chip design, a total of 12 experiments were conducted. The chips were primed with 45 μl of colored aqueous solution and inserted into the testing platform. The advancing front was measured to be at $r_2=40$ mm while the receding front was at $r_1=17$ mm. The frequency of the rotation was gradually increased and the chip response was recorded using a camera and a strobe illumination synchronized to the rotational frequency. The burst frequencies and equivalent pressures that were observed are presented in Fig. 5.22 & 5.23.

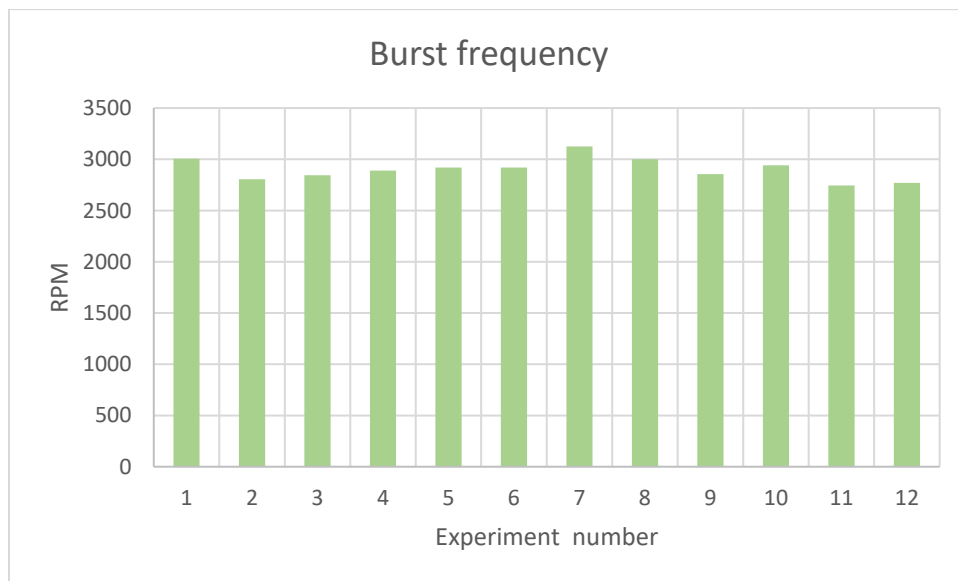


Figure 5.22: Radial chip design, burst frequency

The above measurements are entirely linked to the advancing and receding front positions. Using Eq. 9, the equivalent burst pressures are calculated in Fig. 5.22

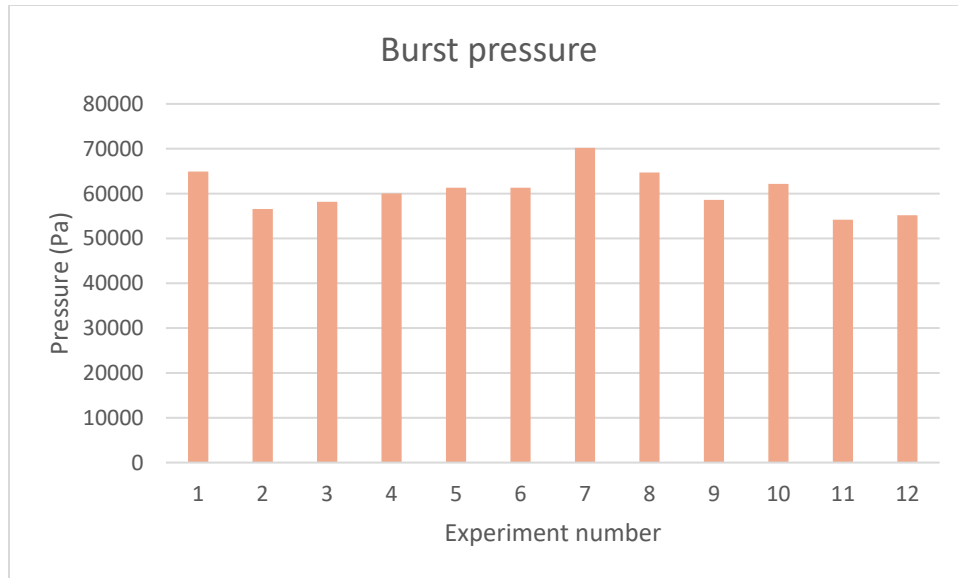


Figure 5.23: Radial chip design, burst pressure

For the radial chip design, the following results were obtained:

	Rotational Frequency (RPM)	Pressure (Pa)
Average burst point	2902	60604
Standard deviation	108	4558
Minimum burst point	2745	54164
Maximum burst point	3125	70199

Table 5.2: Burst frequency and pressure for superhydrophobic valves in a radial chip design

In these tests we notice even higher burst pressures than before with more consistent behavior. This supports the claim that the lower pressures encountered in the previous tests were a result of the fluid interaction with the filter/chip/sealing film interfaces. What is evident here is that by forcing the fluid volume to go through the filter, much higher pressures can be attained with better consistency. An additional observation during this test was that once the hydrophobic filters were wet, they remained in that state and as such they no longer functioned as valves.

5.8 DISCUSSION

The need for a valving method which is simple and modular has been put to focus. An approach for producing such a valving method has been presented. An insertable hydrophobized component has been used as a valving element. Two different chip designs have been tested, one that is more compatible to standard chip manufacturing techniques and one that uses a radial channel design to demonstrate the expected performance of the proposed method if the effect of the valve interfaces with the rest of the chip materials was minimized.

The tests on the radial chip design displayed an average burst pressure of 60.5kPa which is significantly higher than typical burst pressures encountered in capillary and hydrophobic valving schemes. This could enable a series of on chip functions to be performed at lower rotational frequencies, for example aliquoting or siphoning, while higher RPM regions could be reserved for valve activation to release a reagent or a washing buffer. The tests on the standard chip design yielded burst pressures of 12.5 kPa which is lower than the pressures seen in the radial design, but still higher than most other approaches. In the standard chip design, a large variability was observed with the standard deviation being at 2.7 kPa. This is a point which would require optimization and appears to be connected to the interaction of the fluid volume with the chip and sealing material at the valving position. In an actual centrifugal platform with a fluid volume between a receding and advancing front at 14 and 29 mm respectively, all of the valves of the standard chip design could be activated by using a 2200 RPM rotation and none of the valves would be activated for frequencies below 1500 RPM. This defines a range of frequencies which could be dedicated to the activation of these valves, while all frequencies below that could be used for other chip operations. Overall, this appears to be a promising technology which could enable fast and low-cost microfluidic chip development and fabrication.

CHAPTER 6: POINT OF CARE CONCEPTS

6.1 ABSTRACT

In this chapter, different centrifugal microfluidic concepts for bead-based immunoassays are presented that make use of the micropumps and microvalves discussed in the previous chapters. A microfluidic disk using both microvalves and micropumps is presented along with basic components that would need to be embedded on a PoC device to use this disk. A variation of the laser activated micropump for increased modularity is presented and some concept immunoassay applications based on this variation are discussed.

6.2 INTRODUCTION

In the previous chapters of this work, a vision for bead-based modular immunoassay PoC systems has been described. A high-throughput, automated immunoassay system has been presented along with a diagnostic application. Two different methods, one for on-chip micropumping and one for microvalving have been proposed. It has been argued that these methods are steps towards the creation of modular microfluidic chips, since they can be implemented by assembling or injecting already prepared components into the circuit. In an effort to describe how these contributions could be used for the development of modular PoC immunoassays, two concept microfluidic disks for centrifugal systems are described with variations and initial steps towards their development are discussed.

6.3 CONCEPT 1: LAB-ON-A-DISK BASED ON MODULAR MICROPUMPS AND MICROVALVES

In this first concept, a LoAD concept is presented. The concept is based on the micropumping and microvalving concepts that were presented in the previous chapters and is targeted towards bead-based sandwich ELISA immunoassays.

The on-chip immunoassay process is presented on Fig. 6.1. A microfluidic disk has an inlet port at its center which leads to a reaction channel. The reaction channel is shaped as an arc of a circle concentric to the disk. When a liquid reagent is placed at the center of the disk and the disk is spun, the centrifugal force causes the liquid to move outwards and into the reaction channel. For a bead-based immunoassay, the first step would be the introduction of the bead solution. Since the microbeads have a larger density than the aqueous solution, they will move to the outer portion of the reaction channel under the influence of a centrifugal force (Fig. 6.1 B). The reaction channel is also connected to a waste chamber using a siphon structure (see Ch. 2). When additional volume is added into the inlet port (for example, washing buffer) and the liquid flows over the siphon, the entire content of the reaction channel will empty into the waste chamber. A geometric valve is also included in the siphon structure to avoid liquid flow due to capillary forces when the disk is stopped. However, note that the microbeads will not flow towards the waste chamber, but they will remain on the outer wall of the reaction channel.

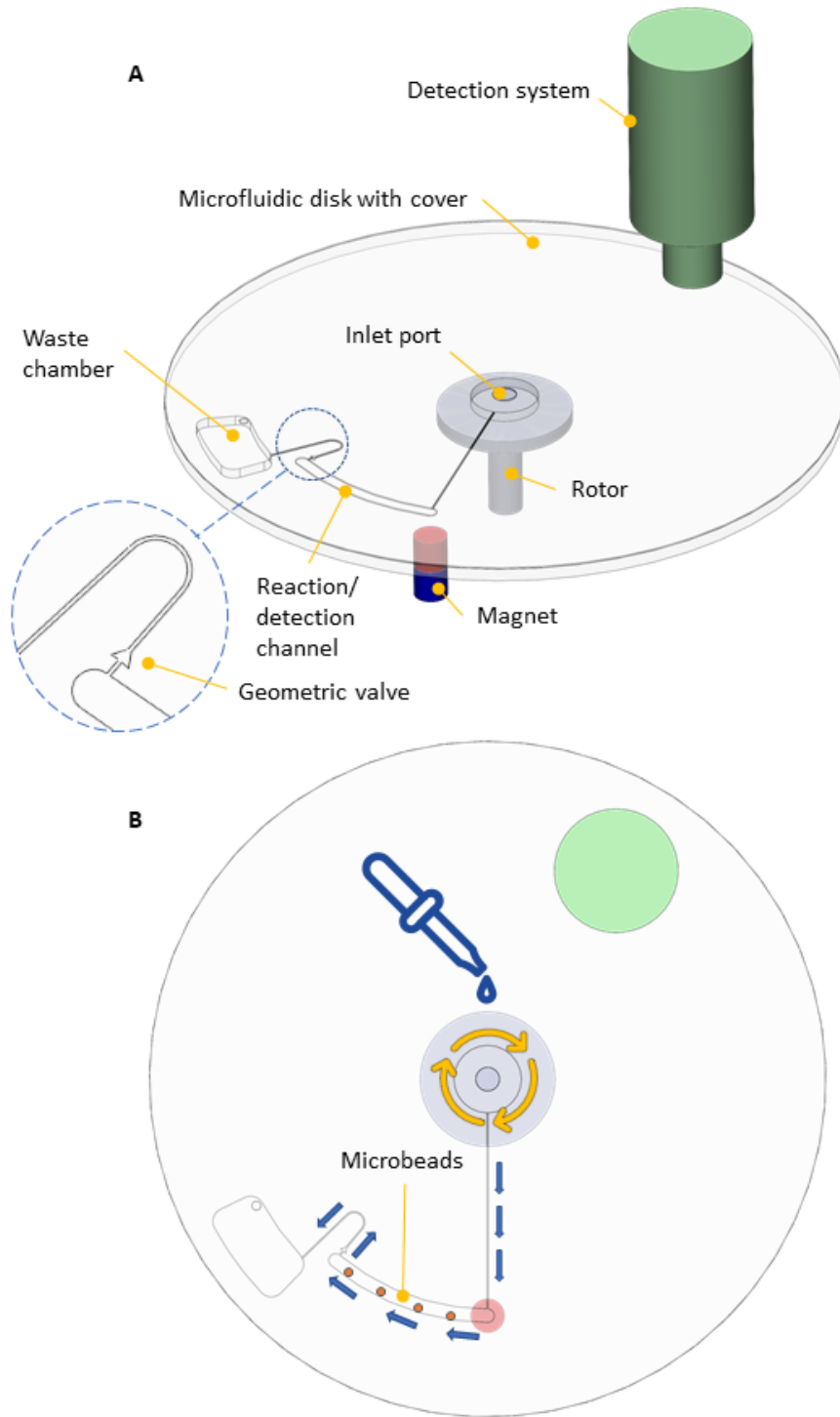


Figure 6.1: The principle of concept 1 for the realization of an on-disk immunoassay. Liquid samples and reagents are inserted from the inlet port to move to the reaction channel due to centrifugal force. When excessive volume is inserted, for example washing buffer, the siphon structure empties the chip contents to the waste chamber

Comparing the functionality of this disk with the process of a sandwich ELISA assay as it has been described in Ch. 1, this can be viewed as one of the microwells used in the lab with the ability to separate the beads from a liquid solution. The magnet below the disk, can be used to mix the beads with the liquid content of the reaction channel by hovering the chip over the magnet and rotating back and forth so that the beads can move from the one end of the channel to the other. Once the entire process is complete, the microbead signal can be quantified using an optical detection system which can be located on another position over the disk.

So far, this concept does not follow the PoC principles described in Ch. 1, since it requires user input for every assay process step. In order to create a concept that describes a complete PoC system, an automated way to insert the different reagents and sample would be required. For this, the micropumps and microvalves described in the previous chapters of this work could be used.

In Fig. 6.2, a more complete concept is presented. This is a double-sided disk. In this figure, the top side is shown. This disk contains (1) an inlet port, (2) hydrophobic porous microvalves, (3) lyophilized/dried reagents on disk, (4) laser activated micropumps and (5) a waste chamber. The first step into the immunoassay protocol would be to reconstitute all the lyophilized reagents and prime the disk with buffer solution. Following the ASSURED criteria, this should be ideally a 1-step process that does not require any special training. In the disk of Fig. 6.2 the following steps take place:

1. The user is required to dispense buffer solution into the center of the disk using a pre-filled syringe or a Pasteur pipette (Fig 6.3 A)
2. The disk spins at lower RPM than what is required to collapse the superhydrophobic microvalves (Fig 6.3 B)
3. The buffer solution fills the metering chambers under the influence of the centrifugal force
 - Excess volume is drained through a channel at the end of the aliquoting structure
 - When excess volume is drained, the aliquoting channel empties and only the metering chambers remain full (Fig 6.3 C)
4. The disk spins at higher RPM to collapse the superhydrophobic valves
 - The metered volumes go through the valves into the lyophilized reagent chambers
 - The reagent chambers are filled and the lyophilized reagents are resuspended in the solution (Fig 6.3 D)
 - Now each chamber is connected to its own individual laser activated micropump
5. The disk stops and the laser activated pump connected to the first reagent that needs to be used (ex. a buffer solution for microbead reconstitution) is positioned below an infrared laser source
6. The infrared laser source activates the micropump and the volume is pushed forward and into an orifice that leads to the other side of the chip (Fig. 7.4 A)
7. The liquid reagent moves through a channel into the other side of the chip where lyophilized microbeads are positioned near the reaction chamber (Fig. 7.4 B).
8. The infrared laser source is deactivated and the expansion stops
9. The disk spins at low RPM to force the buffer solution to go through the lyophilized microbeads, resuspend them and fill the reaction chamber
10. The following steps are similar to this sequence using the rest of the micropumps.

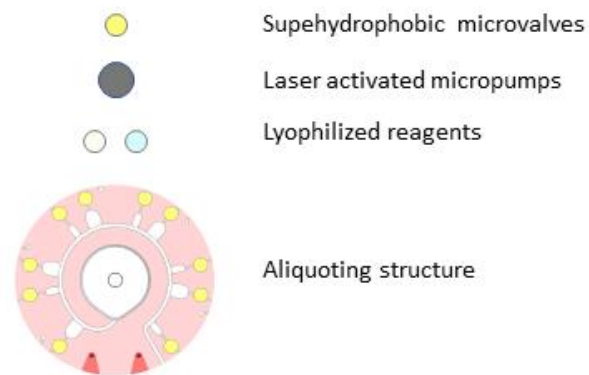
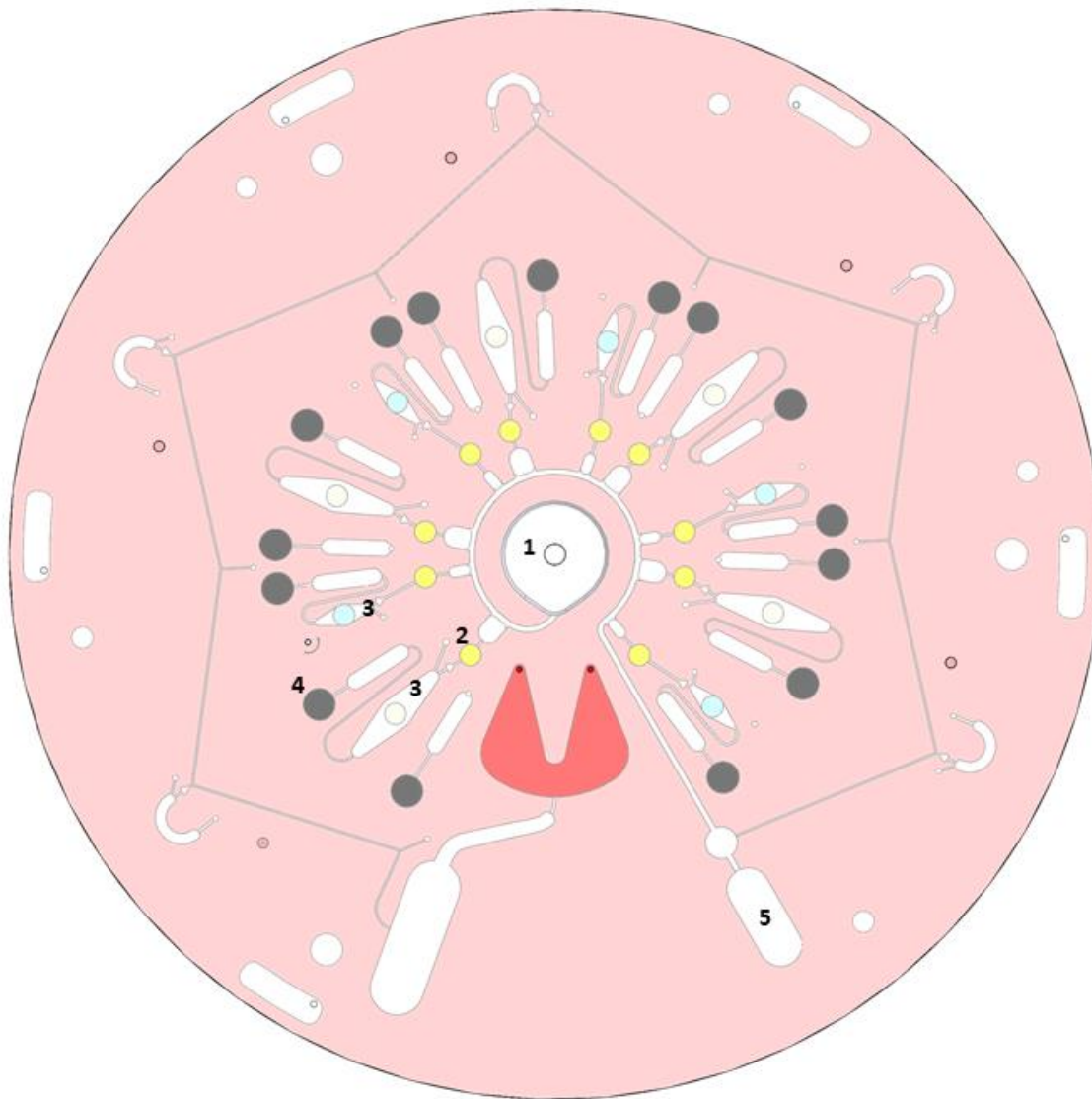


Figure 6.2: A microfluidic disk designed to perform sandwich immunoassay protocols with resuspension and metering of lyophilized reagents

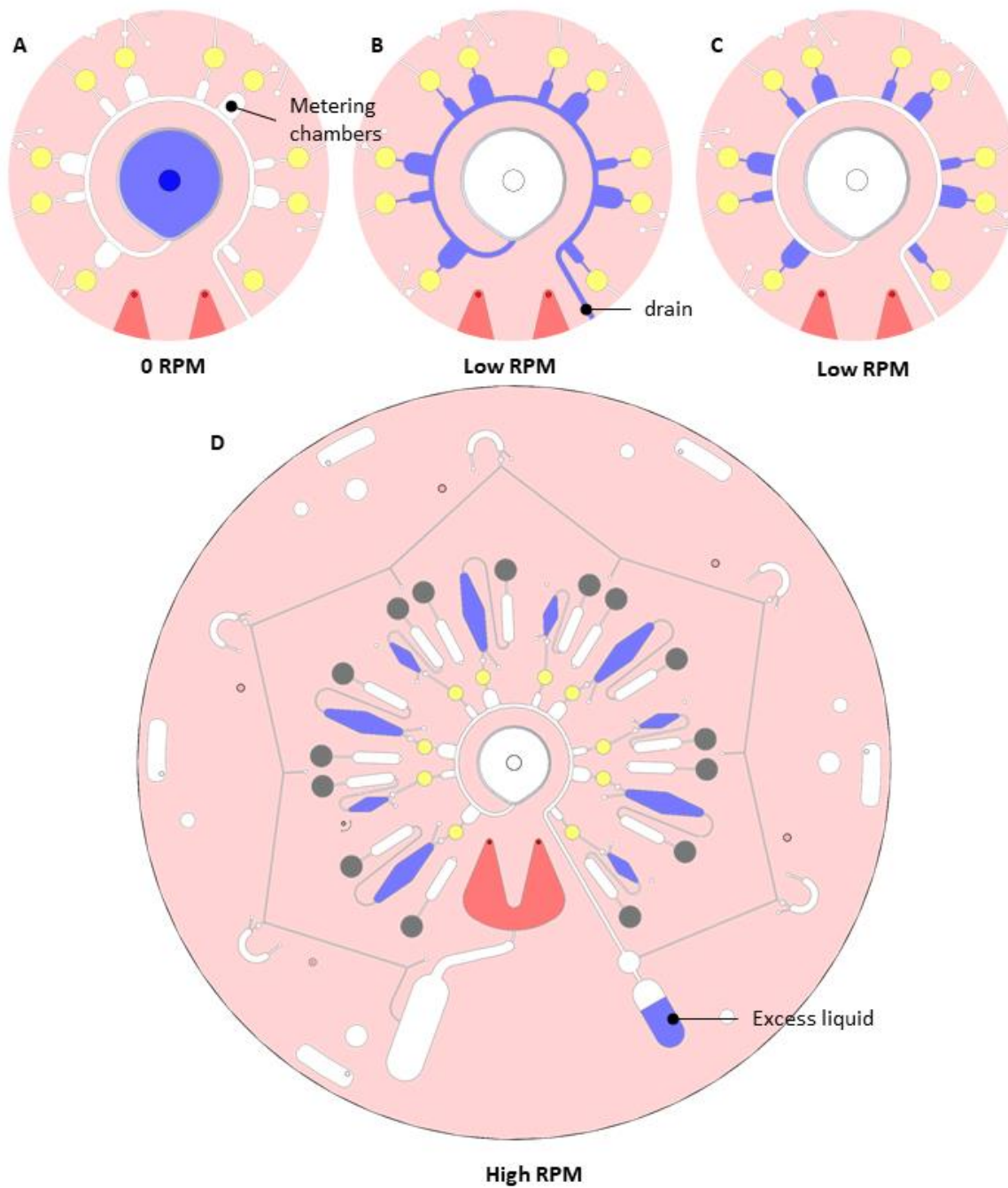


Figure 6.3: The reagent resuspension aliquoting structure is based on superhydrophobic microvalves like the ones described in Ch. 5

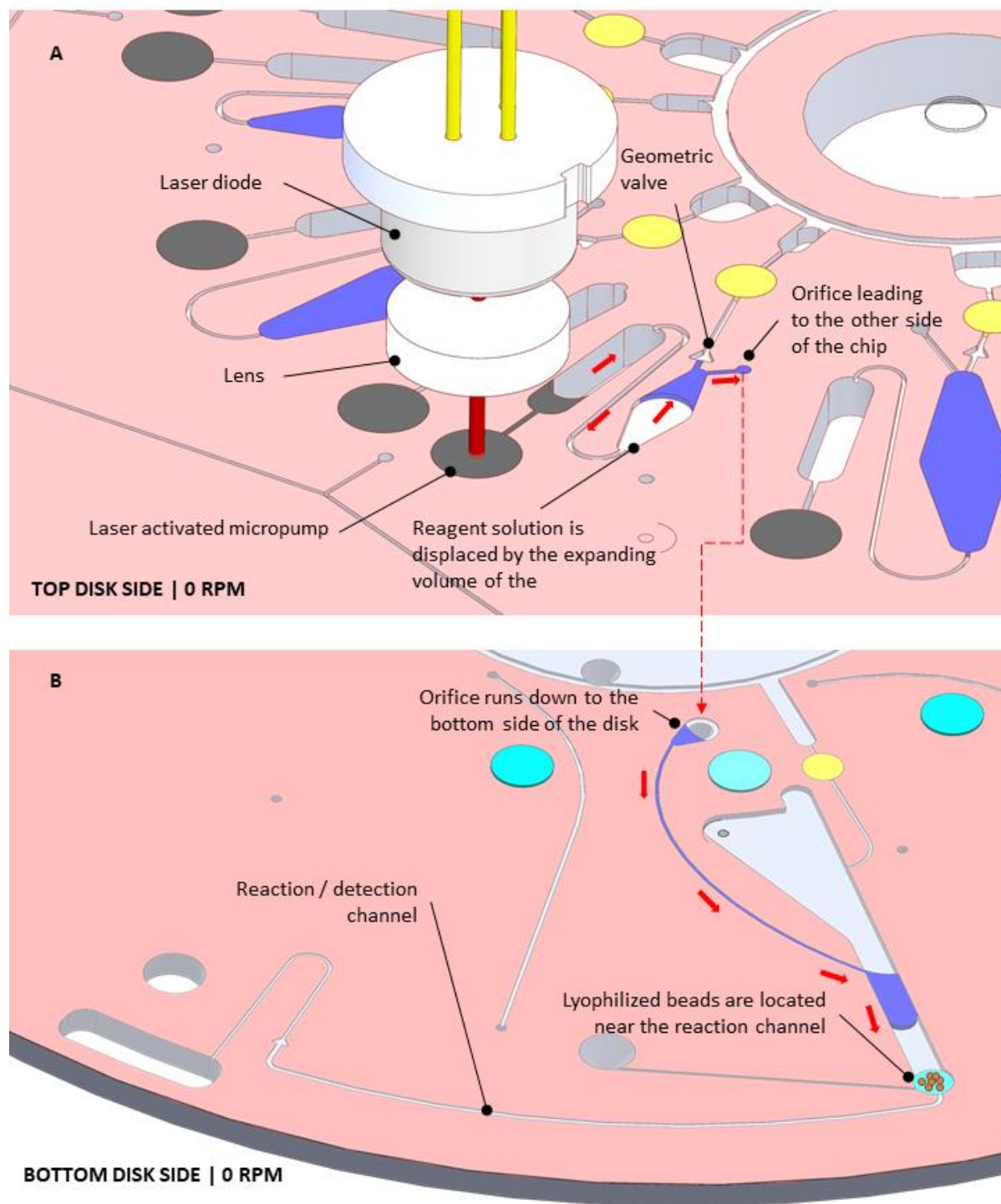


Figure 6.4: The on-demand dispensing of any reagent contained on the chip is based on laser activated micropumps like the ones described in Ch. 4

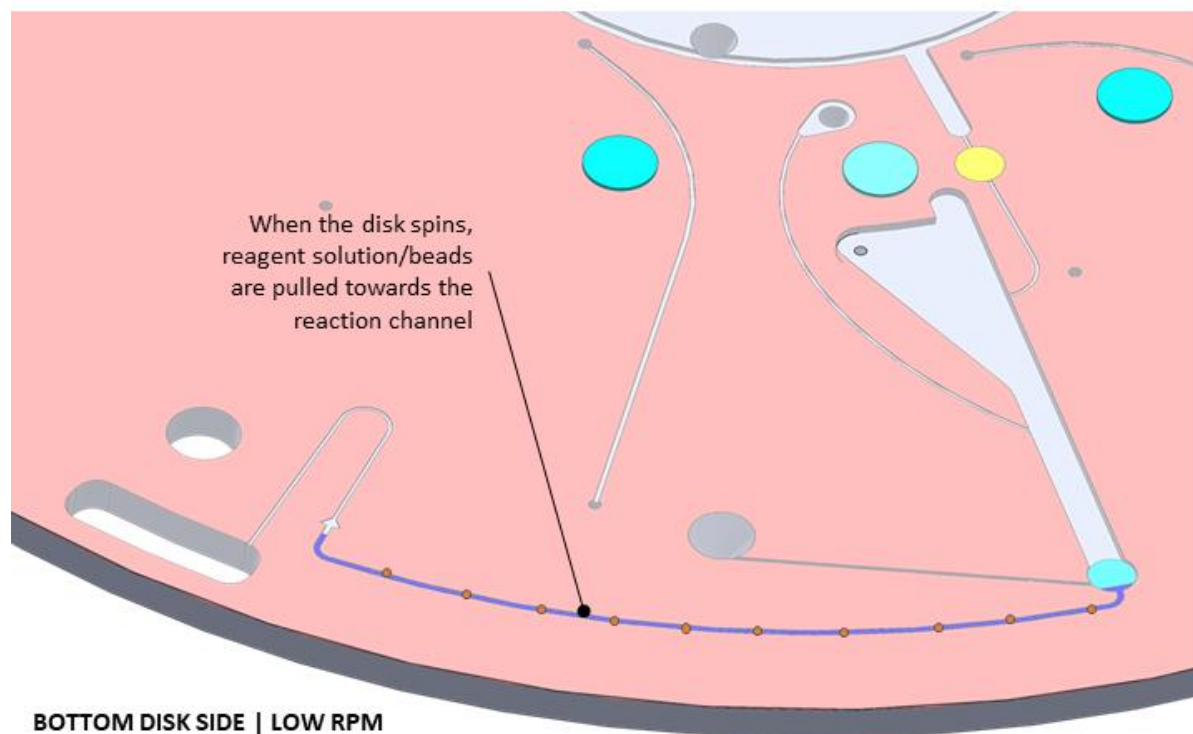


Figure 6.5: After the laser activated pumps finish expanding, the disk spins so that the displaced reagent volume or bead solution are pulled into the reaction channel

The above description and figures describe an embodiment of a sandwich immunoassay-based disk that makes use of the micropumps and microvalves that have been described in the previous chapters. An indicative setup which would be required to perform an immunoassay using this disk can be seen in Fig. 6.6 A&B. A motor rotates the disk for positioning and centrifugation and three stationary components, a magnet, an IR laser and a detection system are used to perform magnetic trapping and mixing, fluid actuation and assay results quantification. More components may be required such as additional magnets to cover more positions on the chip, indexing features or additional laser sources if a micro pumping method with volume control needs to be used (see Ch. 4).

The modularity concept can be seen in Fig. 6.6 C. The consumable can be made by composing the disk, seals, micropumps, microvalves and lyophilized components together. Especially the lyophilized/dried reagents and microbeads can be initially placed in plastic plugs such as the ones seen in Fig. 6.6 C so that lyophilization or drying is not required to be done on the disk.

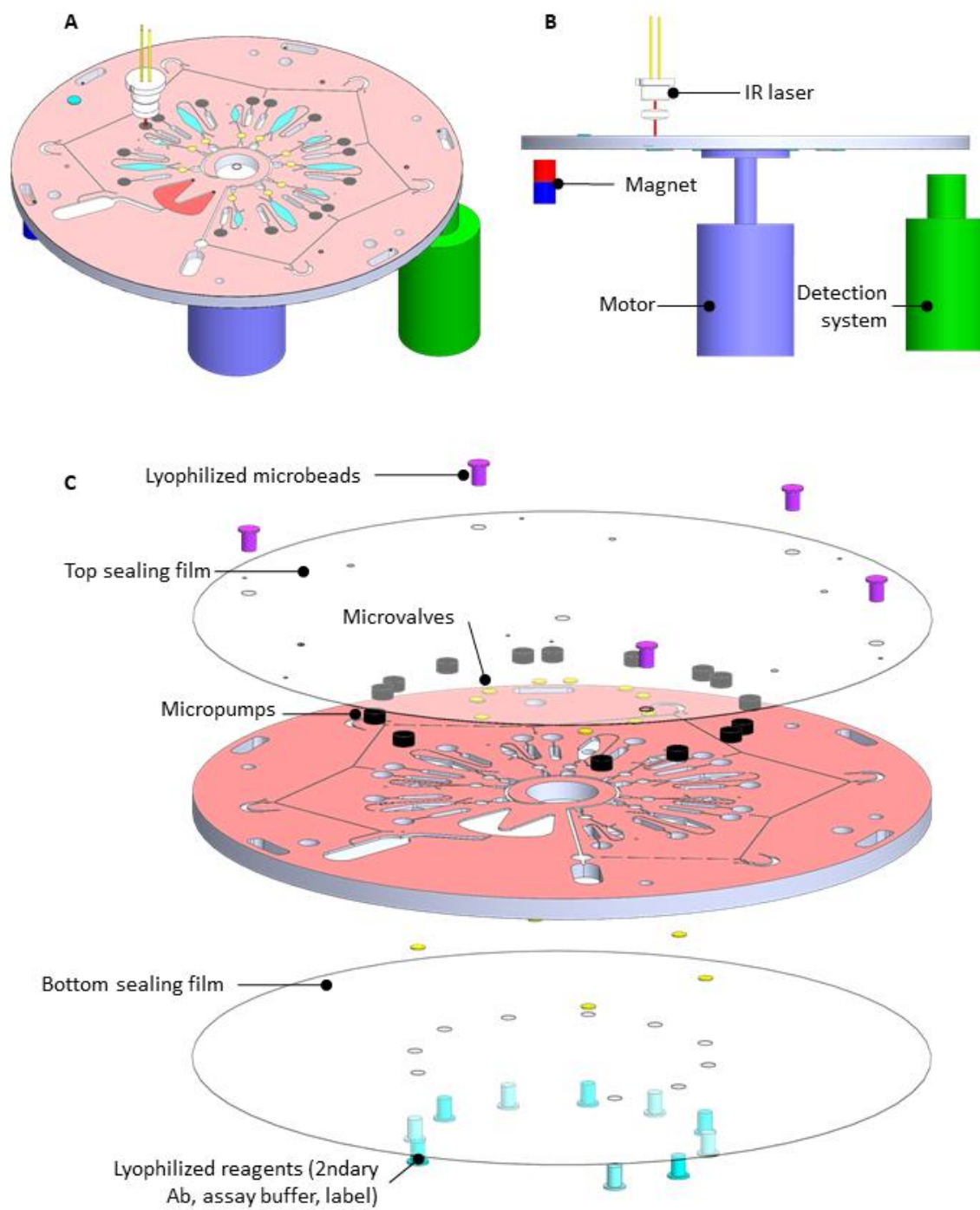


Figure 6.6: Assorted device (A&B) and exploded view of the proposed microfluidic disc (C)

The benefits that this concept presents compared to the current state of the art are the following:

- It can replicate laboratory process steps for a bead-based immunoassay
- The consumable is modular and can be produced by composing different elements together
- No post processing or special deposition methods are required for the disk
- All micropumping and microvalving is done in a contactless method that does not require interfacing with external devices
- It is a generic approach that can be used for multiple immunoassay applications
- Centrifugal technology has the following advantages:
 - It works very well with microbeads as it inherently has the ability to separate them from a suspending solution.
 - It is compatible with tests that use blood samples since centrifugation is used to extract plasma.
 - It is the only microfluidic technology that does not suffer from bubbles and air entrapment issues.
- The positioning of a stationary permanent magnet is a very low cost and robust method to manipulate microbeads by moving the disk over it.

Regarding the drawbacks, it is a complicated design that would require significant development to counter common failure modes such as sealing problems or poor optical properties of the chip and sealing films. Additionally, the design of the detection system requires the selection of optical components that can provide the required sensitivity (for example dichroic mirrors and dielectric filters) but can also fulfil the affordability requirement of the ASSURED criteria. Lastly, the motion system requires simultaneously a centrifugation mode at multiple thousand RPM and a positioning mode that can achieve resolution of 0.02° to capture a $6.5 \mu\text{m}$ microbead at a radius of 20 mm. The component selection to cover this requirement as well as size and cost specifications is not straightforward.

6.4 CONCEPT 2: LAB-ON-A-DISK BASED ON SELF-CONTAINED REAGENT INJECTORS

The previous concept is based on the micropumps and microvalves of Ch. 5&6 as they were described and used to prove their operating principle. This next concept was made as a variation to the micropump design that was already presented, with a focus towards reducing the chip complexity and increasing its modularity. The main idea is that a laser activated micropump could also be fitted into a glass capillary tube (Fig. 6.7 A). In this modified version of the micropump, the reagents could also be included in the capillary in order to create a self-contained injection component. A version with displaced volume control could also be realized with an intermediate layer of photopolymer (Fig. 6.7 B). In both cases, each layer should be separated from the others using thin seals that would break or move when the micropump is activated. This could be realized by replacing the silicon oil matrix of the micropump material with a photopolymer and exposing this photopolymer to a short amount of UV/ blue radiation, enough to cause a polymerization of only the outer layer of the mixture. This would be aided by the presence of the absorbance enhancer (See Ch. 5) which prevents the radiation from penetrating further into the mixture.

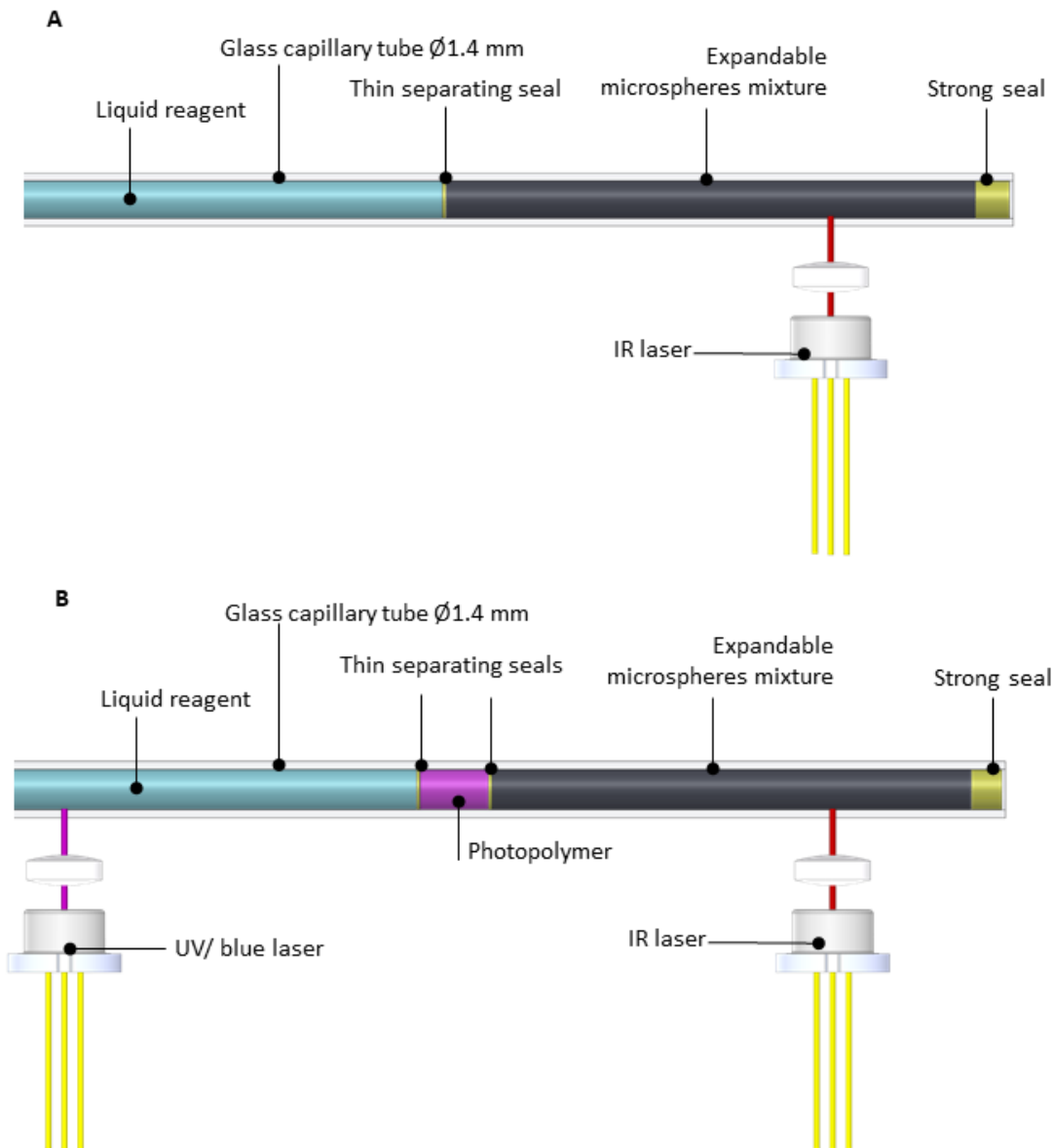


Figure 6.7: The concept of self-contained reagent injectors based on laser activated micropumps. (A) An injector containing an expandable portion and a liquid reagent (B) An injector containing an expandable portion, a photopolymer and liquid reagent.

A concept microfluidic disk based on the micropump variation of self-contained injectors can be seen in Fig. 6.8. In this design, each of these injectors contains a component necessary for a bead-based sandwich immunoassay. The injectors are activated using laser irradiation, and their content flows towards the reaction channel since it is the only vented channel in the microfluidic circuit. When a new injector is activated, the contents of the reaction channel are pushed towards the waste chamber by the incoming fluid. The injector contents and the sequence for a sandwich ELISA using the notation of Fig. 6.8 could be the following:

Injectors:

- s: sample micropump
- 1: Microbead solution with primary Ab
- 2: Sample diluent
- 3: Secondary Ab
- 4: Label
- w1-4: Wash solution

Process steps:

1. Insert sample (blood) into sample chamber and close port
2. Centrifuge to separate plasma from blood cells
3. Position magnet over 1 to pull microbeads towards the end of the channel
4. Activate 1 to push microbeads into the reaction channel
5. Centrifuge to purge channels, notice that excess liquid will flow back into sample chamber and 1
6. Position reaction channel over magnet to capture microbeads
7. Activate w1 to perform a washing step
8. Centrifuge, excess liquid will flow back into sample chamber, 1 & w1
9. Activate s to inject sample into reaction channel
10. Activate 2 using volume control to inject the required amount of diluent in reaction channel while simultaneously displacing part of the sample volume
11. Centrifuge to purge channels
12. Incubate using magnet and oscillating disc motion
13. Position reaction channel over magnet to capture microbeads
14. Activate w2 to perform a washing step
15. Activate 3 to inject secondary Ab into reaction chamber
16. Centrifuge to purge channels
17. Incubate using magnet and oscillating disc motion
18. Position reaction channel over magnet to capture microbeads
19. Activate w3 to perform a washing step
20. Activate 4 to inject label into reaction chamber
21. Centrifuge to purge channels
22. Incubate using magnet and oscillating disc motion
23. Position reaction channel over magnet to capture microbeads
24. Activate w4 to perform a washing step
25. Centrifuge to purge channels
26. Perform detection

As described in these process steps and as can be seen on the disk design of Fig. 7.8, centrifugation in this concept is used for purging the channels after an injector has been activated as well as for sample preparation. The main fluid actuation tasks are performed by the injectors. The activation sequence is important since during centrifugation, the backflow from the channel will be distributed between the injectors in front of the last one activated including the last one activated. In order to avoid cross contamination, the injectors should be activated on a clockwise sequence in which case excess liquid will end up on injection positions that have already been used.

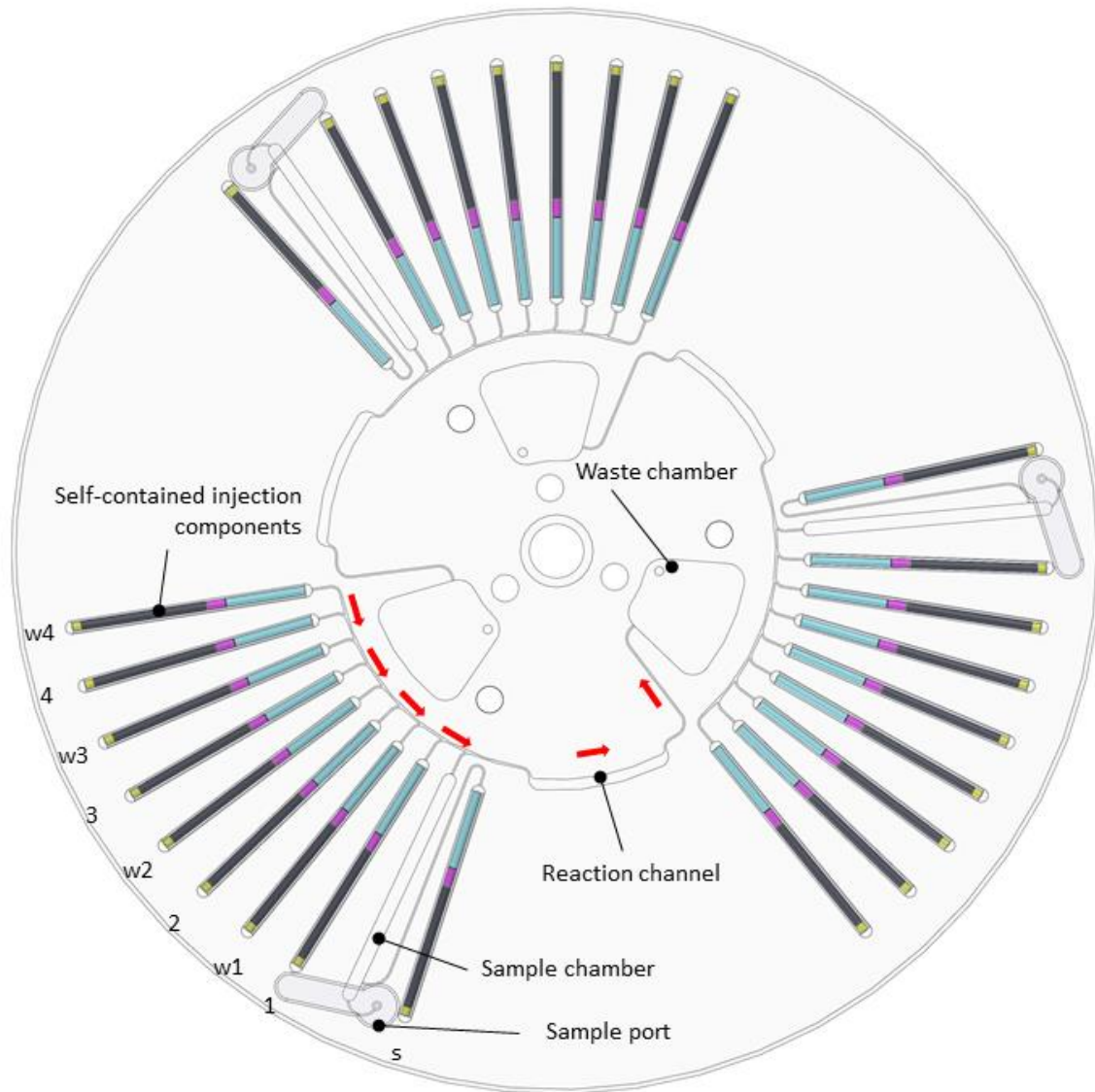


Figure 6.8: A microfluidic immunoassay disc based on self-contained injectors. The disc has three identical and independent circuits.

An indicative setup which would be required to perform an immunoassay using this disk can be seen in Fig. 6.9 A. A motor rotates the disk for centrifugation and positioning. A stationary infrared laser is used to activate the injectors. A UV/blue laser diode is used to control the displaced volume as per the method described in Ch. 5. The UV/blue laser diode can be positioned using a linear axis motion system to accommodate different volume requirements especially for different sample dilutions. Permanent magnets are used for microbead separation. A plurality of magnets could be required to accommodate all different positions that the disk can assume during injector activation. A detector system would be required to perform signal reading at the end of the immunoassay.

In Fig. 6.9 B, an exploded view of the consumable disk can be seen. The injectors are placed inside disk cavities that are directly connected with the microfluidic channels. The assembly is sealed with a film that is perforated in positions that venting or sample inlet are required. The sample ports need to be sealed after the sample is inserted using an on-chip seal.

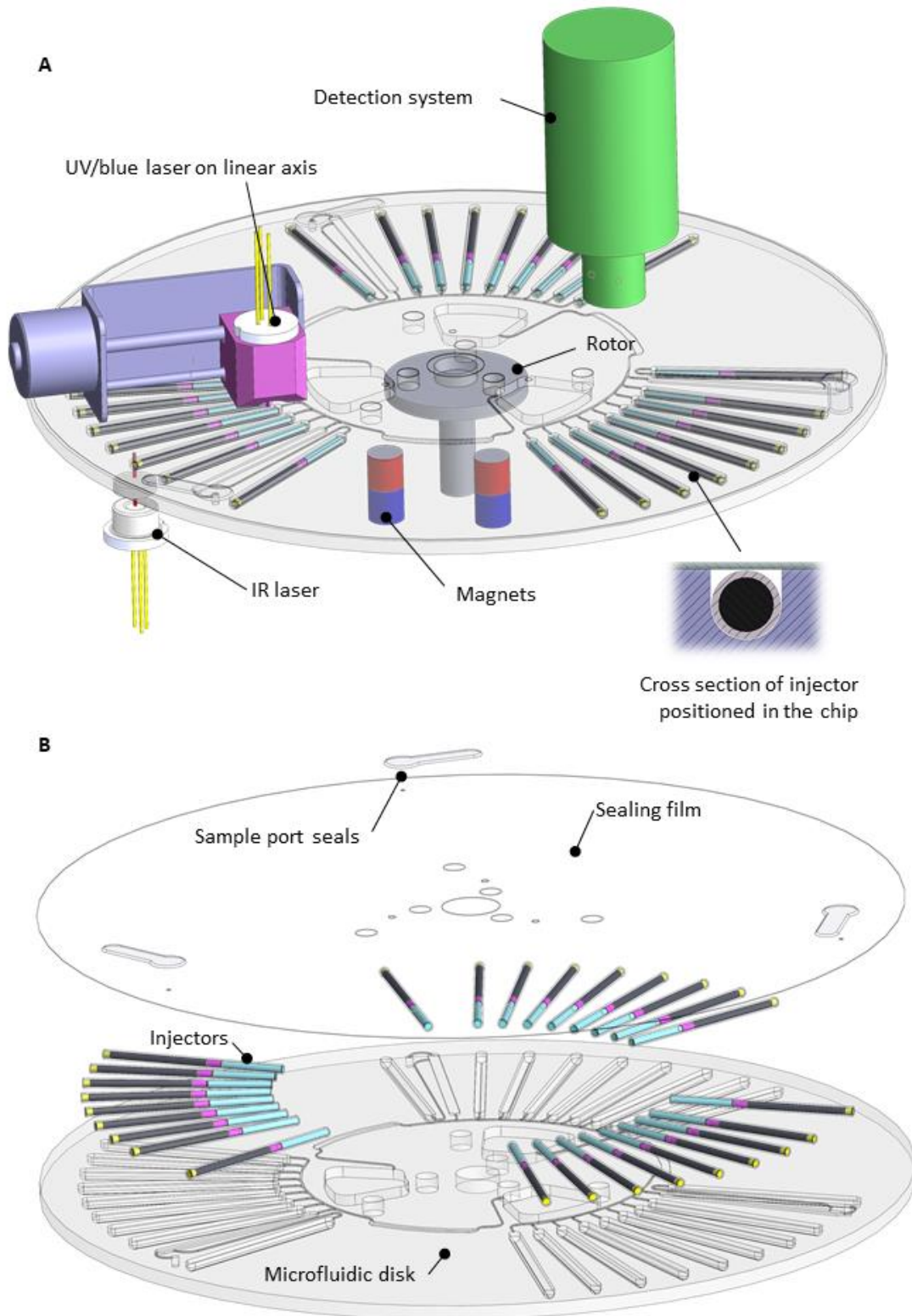


Figure 6.9: The injector-based disc assorted device components (A) and an exploded view of the consumable (B)

The benefits that this concept presents compared to the previously presented disk are the following:

- It is a simpler design with less on-chip components
- It requires less space, a one-sided chip may suffice
- Increased modularity

One drawback of this design is that reconstituted reagents cannot be stored for long periods of time. From a technical standpoint, the main drawback of this design is the sealing of the injectors into the disk cavities. In a scenario where manufacturability is of importance, the injectors would be inserted from the top of the chip. Looking at the cross section in Fig. 6.9 A, the space between the injector and the disk cavity needs to be sealed off otherwise the displaced volume can flow inside the cavity instead of into the microfluidic channel. In Fig. 6.10 A, a prototype disk based on this design was fabricated using laser processing in a VLS 3.50 laser cutter and micromachining in an LPKF S63 milling/drilling station. The stock material was 2.5 mm thick PMMA (acrylic). Injectors were fabricated using $\varnothing 1.4$ mm micro haematocrit capillary tubes. The tubes were primed with a composition of expandable mixture described in Ch. 4 and a red colored aqueous solution. The injectors were activated using a 530 mW 980 nm laser source. In Fig. 6.10 B-C the activation process can be seen. Although the volume expands as per the results of Ch. 4, only a portion of it flows into the microfluidic circuit because of the inability to completely seal the interface between the capillary tube and the microchannel.

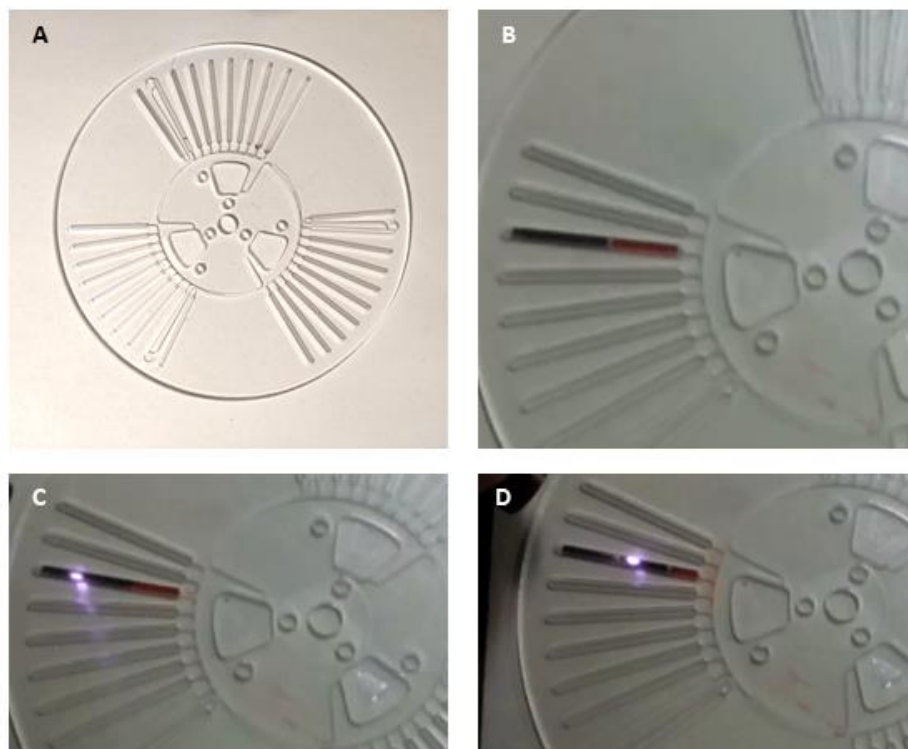


Figure 6.10: A prototype of the injector disk during preliminary testing with an IR laser. (A) the PMMA disc (B) An injector with a colored solution inserted in the disc (C) The injector is activated (D) The colored solution flows through the circuit

To counter sealing challenges, a different approach into embedding the injectors into the disk is required. A variation of the injector approach in which the injectors are placed into a cartridge is shown in Fig. 6.11 A. Using an

elastomer cartridge, the injectors could be assembled in a way that no empty space remains within the sealed area. Sealing features can be added onto the cartridge (Fig 6.11 B) to assist in interfacing the external component with the microfluidic circuit.

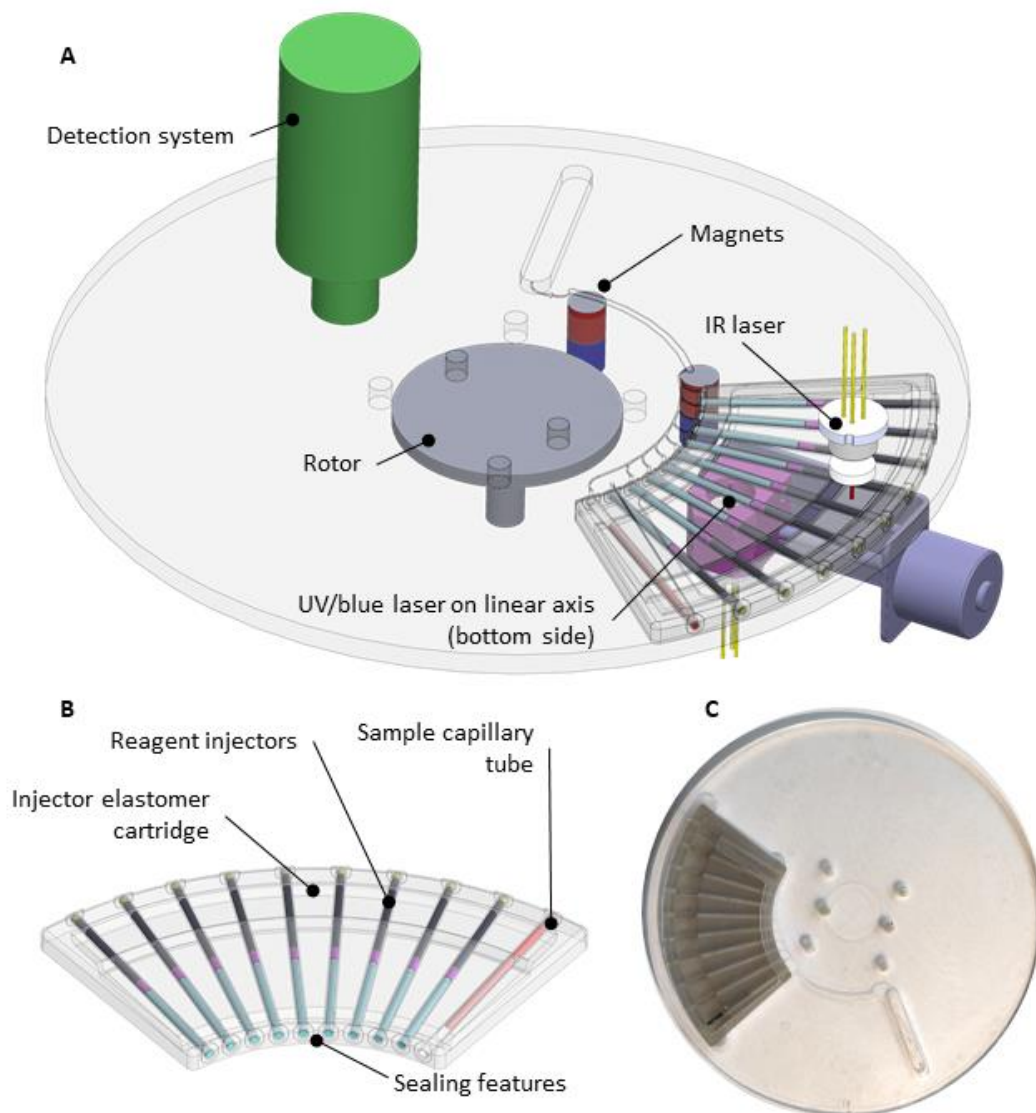


Figure 6.11: A variation of the proposed injector-based design in which the injectors are placed in an elastomer cartridge. (A) the disc in its assorted device (B) A cartridge including injectors (C) a prototype disc

A prototype disk has been fabricated based on this concept (Fig. 6.11 C). The disk has been manufactured using the same methods as in the previous prototype. The cartridge was fabricated using VAT polymerization additive manufacturing with a photocurable resin with elastomer-like properties (FLGR-01-P1). The Form 1 printer was used by FormLabs. Although the sealing condition was improved, during initial testing there was some leakage, especially during centrifugation. Managing consistent sealing in these concepts is a requirement and would be one of the tasks during the development of a system based on these disk designs.

6.5 CONCLUSIONS AND NEXT STEPS

Two different concepts for bead-based immunoassays have been presented that are based on laser activated micropumps and porous microvalves. The objective of this chapter was to display how the proposed methods could be used to develop modular PoC microfluidics. In both concepts, no special processing for the consumable is required (ex. plasma treatment, on-chip lyophilization, precise positioning or fabrication of special on-chip elements) and all the disk's components (micropumps, microvalves, reagents, sealing films and ports) are assembled to produce the final product. The components (micropumps, microvalves) can be produced in bulk and they do not require costly and precise operations like lithography or micromachining. The merits of modularity, apart from increased manufacturability, also include simplicity into adaptation in different applications and the ability for rapid deployment of PoC systems.

The challenges of the presented concepts, partially seen through initial prototyping, include sealing of modular components with the main disk and the development of a lyophilization/storage method for insertable reagent plugs. Additionally, the detection and motion systems for these concepts would need to be developed based on the specs of bead-based immunoassays and challenges. Initial steps towards these last two directions can be found at the supplementary material of this work.

CHAPTER 7: CONCLUSIONS AND FUTURE WORK

7.1 ABSTRACT

In this final chapter, a review of the directions and findings of this work is presented. The contributions from each chapter are discussed along with the constraints of the proposed methods. A laboratory automation system for bead-based immunoassays has been proposed for which a prototype has been developed and tested. The results are promising and support the value of such a system for life science and diagnostic applications. A new type of micropump and a new type of microvalve for on-chip operations have been presented. Their performance has been investigated and their results indicate that these methods contribute to the current state of the art, although further research is required to enhance the repeatability of these methods. Based on the developed components, some concept microfluidics are discussed. Future steps towards modular PoC systems are proposed.

7.2 SUMMARY

In this work, components that enable the development of modular point of care systems have been pursued. The research has been focused on systems that perform immunoassays for diagnostics, either for the laboratory or the clinic setting. To establish the start of the art, existing PoC systems and their diagnostic targets have been reviewed with a focus on their core technologies. It has been shown that for immunoassays, two distinct trends have been formed: The lateral flow immunoassay, with the most prominent example being the SARS-CoV-2 rapid test, and the device-based immunoassay systems. While rapid tests focus on simplicity and low cost, device-based immunoassays aspire to bring quantification and sensitivity to PoC systems. Aligning to this goal, we identify suspension arrays based on superparamagnetic microbeads as a candidate technology for modular immunoassay systems. Discerning such systems into larger, laboratory devices and smaller, autonomous clinic devices, we establish that in the former the problem that needs to be solved is one of automation, while in the later, one of the core problems is the on-chip fluid-handling. Developmental efforts were thus directed towards these two goals: Creating the automation needed for laboratory bead-based immunoassays and providing technical solutions for the transfer of the same immunoassay technology to chip based devices. The development and findings of this work are summarized in the following points:

- A method to perform bead-based immunoassays in a fully automated way has been displayed. An automated system that performs such assays has been presented and analyzed
- A bead - based immunoassay for the detection of SARS-CoV-2 antibodies testing has been performed using the developed automated platform with results displaying its capability for life science and diagnostic applications
- A method to perform fluid handling using a new type of laser activated micropumps has been demonstrated and its potential and limitations have been explored
- A method to perform liquid handling using a new type of porous burst microvalve has been demonstrated and its strength and constraints have been discussed
- Based on the previous developments, concept designs of lab-on-a-disk systems that embed bead-based technology combined with laser activated micropumps and porous microvalves have been demonstrated

7.3 CONCLUSIONS

7.3.1 A LABORATORY DEVICE FOR IMMUNOASSAY PROTOCOLS

In the third chapter of this work, the development of an automated laboratory immunoassay platform was presented. The platform makes use of superparamagnetic microbead technology, with the novelty being that the biochemical processes take place inside the disposable pipette tips. The main subsystems, notably the fluid handling head, the magnetic manipulation unit and the motion system of the platform were presented. This approach towards bead-based immunoassays was shown to have the following key benefits compared to the current state of the art:

- A novel method that allows the automation of bead-based immunoassays has been proposed
- A platform has been developed which can be used both for assay development and for diagnostic applications
- The platform has a small footprint and does not require the use of auxiliary systems such as shakers and magnetic plates, making it self-contained
- The method of operation bypasses the problems associated with handling small reagent volumes, since the platform handles the microbeads and not the liquid volumes
- The platform itself is modular and could be scaled up or down depending on the application requirements

This system was used to perform an immunoassay for the detection of SARS-CoV-2 antibodies S1, RBD and N in three vaccinated patients. The results displayed good correlation with the laboratory assay with low CVs across the different measurements and better repeatability in the lower measurement regions compared to the manual assay. The assay was performed as a three-plex, meaning that all three antibodies were tested simultaneously in each sample using different microbead families.

The constraints of the platform are the following:

- The prototyping of the device has revealed manufacturing challenges that should be addressed in future implementations, such as the ability to reliably load multiple pipettes and ensure sealing during assay operations
- From a design standpoint, the platform's motion system could be made more space-efficient and fail-proof by replacing the individual plate carrier stations with a single plate handling system that can operate in different plate positions.
- The platform's flow through washing system is prone to clogging and unequal flow rates. In subsequent versions, a different design should be employed that is based on positive displacement pumping for the washing buffer in each pipette tip.

7.3.2 LASER ACTIVATED SINGLE-USE MICROPUMPS

In the fourth chapter of this work, a new type of micropump for fluid handling in microfluidic chips was presented. The micropump is based on a mixture of expandable microspheres that increases in volume when irradiated with an infrared laser source. The ability to displace volumes over 35 μl with near constant flow rate has been displayed. Pressures up to 150 mbar have been achieved using this method. Additionally, a variation of this micropump which can achieve displacement repeatability of $<1 \mu\text{l}$ has been presented. This variation is based on an additional blue laser source that is used to cure a photopolymer inside the microfluidic channel and stop the flow when a predefined volume has been displaced.

The proposed micropump brings the following benefits compared to the state of the art:

- This is a novel, contactless approach for on-chip fluid handling
- The method requires no chip processing or special microfluidic components
- The proposed approach enables truly modular design of microfluidic chips for PoC applications as the micropump itself is a microfluidic component that can be embedded in any chip design, where required and in numerous instances.
- The micropump does not require physical interfacing with the external device but is triggered using an IR laser, while no peripheral equipment is needed. This simplifies the external device design and reduces the failure modes from auxiliary components
- A single IR laser could be used to activate multiple micropumps.
- This micropump design could bring additional functionality in lab-on-a-disk PoC systems, since the inherent ability to rotate the chip can be used to align multiple micropump positions with a stationary laser source. This implementation would require only the addition of a laser source to the external device and the micropump building blocks to the microfluidic chip.

The constraints of the proposed micropump are the following:

- The simple embodiment of this micropump in which no volume control feature is used can yield displaced volume variations which may be unsuitable where precision dosing is required. When precision volume displacement is required (<1 μl repeatability), the variation using photopolymerization of an advancing photopolymer front should be used or a metering application using aliquoting structures in a lab-on-a-disk format.
- The method may be unsuitable for completely mobile applications due to its high energy requirements (> 1.5 J/ μl)
- The use of this micropump in centrifugal systems would require the optimization of the mixture matrix and the photopolymer density so that they are compatible with centrifugation process and they don't separate during the assay steps
- The storage of the components that constitute the micropumps in a microfluidic chip should also be evaluated per their stability during transportation or temperature variations.

7.3.3 POROUS MICROVALVES

In the fifth chapter of this work, a new type of microvalve was presented that is based on hydrophobization of a porous component and the use of that element as a pressure-driven flow control element. The preparation of test chips with superhydrophobic porous microvalves is presented in two different chip designs. In the first design, the microvalve is assembled from the top of the microfluidic circuit while in the second design the microvalve is assembled radially. Among the two designs tested, the first one is much easier to implement in a microfluidic device. The microvalve burst pressure is tested using a centrifugal platform. Burst pressures of 12.5 kPa on average are reported for the first design and 60kPa for the second design. The proposed microvalve brings the following benefits compared to the state of the art:

- A novel superhydrophobic burst micropump is proposed
- The proposed method enables modular chip design since the microvalve is an external component that is assembled onto the chip

- The fluid handling approach does not require processing of the microfluidic chip to render parts of it hydrophobic and is not dependent on microfabrication of structures or geometric valve forms
- The burst pressures reported are higher than pressures attained using geometric valves or hydrophobic barrier structures on comparable channel sizes.

The constraints of the proposed microvalve are the following:

- The burst pressure standard deviation of the first chip design is high. Although this is not necessarily a constraint for applications where it is permitted to use all micropumps at a specific burst pressure range, it could become a constraint if it would be of interest to create micropumps with different burst pressures to use sequentially
- An inherent constraint of the proposed component is that it also acts as a filter. This could be beneficial for some applications (ex. filtration of debris or unwanted particles from samples) but it could also be restrictive when particles or microbeads need to be moved within the microfluidic circuit.

7.3.4 MODULAR POC CONCEPTS

In the sixth chapter of this work, two PoC concepts based on the presented fluid handling components were proposed. The first concept is a centrifugal disk embedding both laser activated micropumps and porous microvalves for sandwich immunoassays. An approach for the on-chip assembly of lyophilized reagents is theorized. The second and the third concept are based on an adaptation of the laser activated micropump described in Ch. 4 into self-contained injectors. The reagent solutions in this version are assumed to be stored inside the injectors. There are two variations for this concept: One in which the injectors are directly assembled on the chip and one on which the injectors are assembled on a cartridge which is in turn assembled on the chip. The proposed concepts could add to the state of the art in the following ways:

- The implementation of multi-step protocols could be realized using centrifugal microfluidics on a simple device
- The modular design of the consumable disks would allow fast development, flexibility into revisions and easy manufacturing
- The combination of assay development using SampleX and easy adaptation of that assay in the centrifugal microfluidic concepts would allow the rapid deployment of immunoassays

Some of the constraints of the proposed concepts would be the following:

- The storage of liquid reagents in contact with the micropump materials would need to be investigated and perhaps methods to isolate one from another would be required
- The long-term storage of liquid reagents for immunoassays is not always possible as often cryopreservation or lyophilization is necessary
- Interfacing the injectors and the cartridge with the microfluidic chip is a challenging task and could introduce failure modes

7.4 FUTURE WORK

In the introduction of this work, the concept of a modular bead-based PoC immunoassay has been presented and the concept of a shared technology between laboratory and PoC instruments has been discussed. Key parts of this concept have been outlined, in particular laboratory systems, on-chip fluid handling, detection methods and on-chip reagent storage. In the scope of this work, laboratory systems and on-chip fluid handling have been developed and their potential has been presented. To enable the implementation of functional modular PoC microfluidics, more steps need to be taken in each of these fields:

7.4.1 LABORATORY SYSTEMS

An automated immunoassay system for laboratory and diagnostics use has been presented. As a future step, this system could be optimized for faster and more precise assay performance. In particular:

- Reduction of incubation times to accelerate assays
- Explore whether the omission of washing steps significantly affects the assay performance using a flow-through approach.
- Develop an optimized washing system that is based on positive displacement of buffer volumes in the pipette tip to solve clogging and uneven flow constraints
- Develop a modification of the system architecture to be able to operate on 384-well plates

7.4.2 ON-CHIP FLUID HANDLING

A new micropump and a new microvalve have been presented. Their contributions and limitations have been discussed. Future steps on these topics would include the following:

LASER ACTIVATED SINGLE-USE MICROPUMPS

- Further optimize the laser activated micropump to reduce variability in flow rate and displaced volume. Potentially use injection molded microfluidics or PDMS prototypes to achieve optical quality for the laser window.
- Develop compositions of controlled matrix density to make this micropump fully compatible with centrifugal platforms
- Explore the replacement of the mixture matrix with a photopolymer to facilitate volume control with a single composition
- Further explore the integration of micropumps into self-contained injectors as per their displacement capacity, repeatability, fabrication, storage and compatibility with liquid reagents.

POROUS MICROVALVES

- Optimize the porous microvalve chip integration to reduce variability in burst pressure. Potentially use injection molded microfluidics or PDMS prototypes to achieve low surface roughness and improved chip-valve sealing
- Explore different superhydrophobic treatments, for example various dilutions of the SiO₂ suspension to achieve variable burst frequencies for sequential multi step valve actuation using centrifugation

7.4.3 MODULAR POC CONCEPTS

Two different concepts for the modular design of lab-on-a-disk consumables have been presented. The implementation of these concepts and the integration of the developed components would be the next step for this work. In particular:

- Optimization on the sealing of self-contained injectors in microfluidic disks
- The development of the lyophilization of reagents on plastic inserts that can be assembled on chip would be a necessary step towards modular microfluidic diagnostics
- The development of a low cost, sensitive and robust detection system for centrifugal bead-based immunoassays

SUPPLEMENTARY MATERIAL

CHAPTER 4

A DISCUSSION ON THE SCALABILITY OF THE PROPOSED MICROPUMP DESIGN

An important aspect in any proposed methodology for embedded microfluidic systems is the ability to scale according to the needs of the application. While in the current investigation only very similar chips have been tested, some conclusions have been drawn in regard to the scalability of the proposed micropumping method.

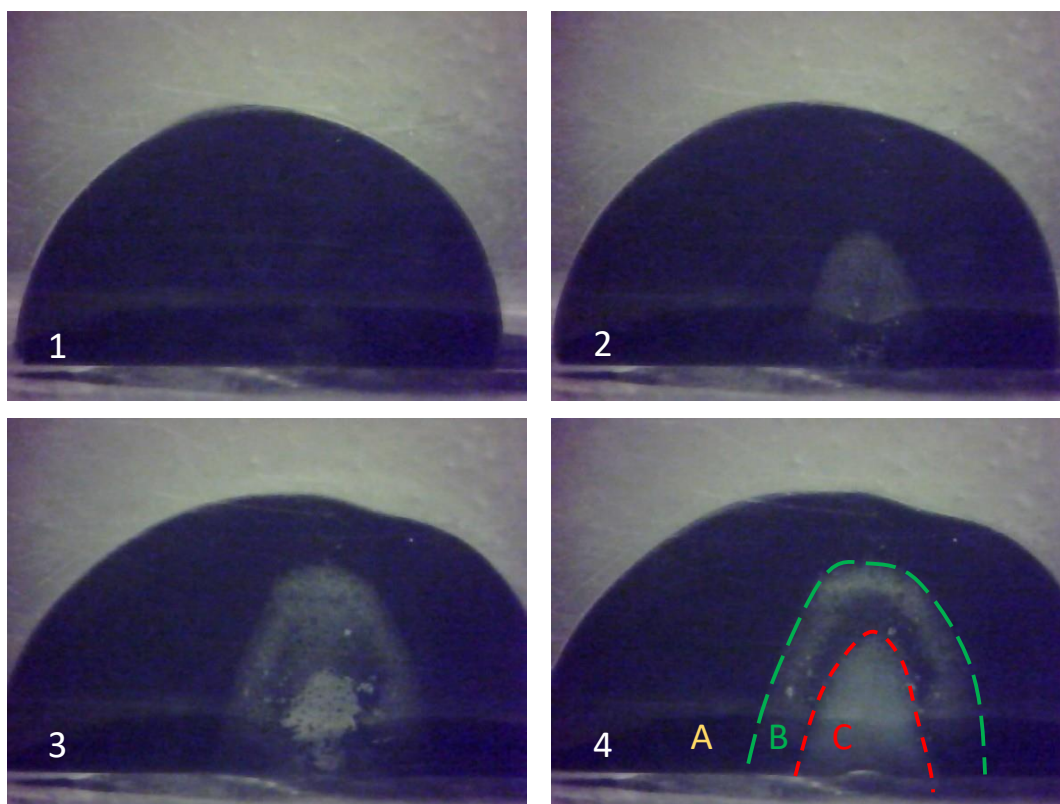


Figure S.1: Section view of a microsphere mixture undergoing expansion when exposed to an infrared laser beam. Zone A consists of unexpanded mixture, Zone B consists of expanded microspheres and Zone C is gaseous hydrocarbon from ruptured microspheres. The laser beam is represented by the red arrow.

The first observation is that only the mixture volume that lies in the laser beam's path will eventually participate in the expansion process while the rest will remain unexpanded. As can be seen in Fig. S.1, there are 3 distinguishable zones in a section view of the micropump. In zone A, outside the laser beam path the mixture remains

unexpanded. In zone C, close to the axis of the laser path which includes the higher energy portion of the beam, the microspheres burst releasing their encapsulated hydrocarbon. This is the main source of linear expansion which starts at the entry point of the laser point and ends at the other end of the chamber. In zone B, which surrounds zone C, microspheres expand but do not rupture. This zone could be of special interest during the design process since it essentially consists of gas-filled microspheres and hence functions as a thermal insulator for the rest of the chip. Considering the above, two rules that could possibly be of use are:

- A.** The portion of mixture that will participate in the excitation process depends on the size of the laser beam spot, not the full capacity of the chamber into which the mixture is stored.
- B.** The chamber height, i.e. the length at which the laser beam will encounter microbeads affects the maximum displaced volume that can be achieved. Larger chambers in height will result in larger volume output.

As far as the size of the microspheres themselves is concerned, a typical expanded microsphere could have a size of 50 μm . At that size they could clog chamber interconnections and microfluidic channels if the design allowed microsphere migration from one chamber to another. Consequently, a third rule that could be relevant to the design procedure that implements this micropumping technology is:

- C.** The expanded particle size ($\sim 50 \mu\text{m}$) is a measure by which chamber sizes and channels through which expandable mixture moves should be designed in order to avoid clogging and maintain continuous rheological behavior during expansion. Smaller structures may result in full clogging or discontinuities in flow due to partial clogging.

Regarding the ability to separate the liquid reagents from heat affected zones within the chip in correlation with chip scaling, we identify 3 parameters as the most crucial ones: **I.** Expandable mixture chamber size, **II:** Chip thickness and **III:** The presence of a heat sink.

MATLAB VIDEO ANALYSIS TOOL FOR DISPLACEMENT RESULTS EXTRACTION

```
%% Video analysis tool for laser activated single use micropumps experiments
%%

clearvars;

%choose video name
videoname=uigetfile('*.avi');
vidprocess=VideoReader(videoname);
info = mmfileinfo(videoname)
% vidprocess=vision.VideoFileReader(videoname);

%get no of frames and frame rate
nframes=vidprocess.NumberofFrames;
nframerate=vidprocess.FrameRate;
```

```



```

```

%get one random frame to do some processing
sampleframe20=read(vidprocess,20);
gframe20=rgb2gray(sampleframe20);
%get the area of laser exit
imshow(gframe20);
ses=roipoly(gframe20);

%get the maximum displacement frame
motionframe=read(vidprocess,FMaxim);

%get the area of masking procedures
hold on
methcolor=zeros(1,1);
mfgray=rgb2gray(motionframe);
intrack=roipoly(mfgray);
%get the nodes using lines%%
hold off
imagesc(mfgray);

%get the trackpoints
title('Horizontal Lines, Up to Down')

for i=1:nohor
    mline=imline;
    posl=wait(mline);
    linh(i,1)=posl(1,1);
    linh(i,2)=posl(1,2);
    linh(i,3)=posl(2,1);
    linh(i,4)=posl(2,2);
    clear mline,posl
end

title('Vertical Lines, Left to Right')
for i=1:nover
    mline=imline;
    posl=wait(mline);
    linv(i,1)=posl(1,1);
    linv(i,2)=posl(1,2);
    linv(i,3)=posl(2,1);
    linv(i,4)=posl(2,2);
    clear mline,posl
end

xs1=zeros(nohor,2);
ys1=zeros(nohor,2);
xs2=zeros(nover,2);
ys2=zeros(nover,2);

%get the trackpoints from intersections and arrange them

for i=1:nohor
    xs1(i,:)=[linh(i,1),linh(i,3)];
    ys1(i,:)=[linh(i,2),linh(i,4)];

```

```

end

for j=1:nover
    xs2(j,:)=[linv(j,1),linv(j,3)];
    ys2(j,:)=[linv(j,2),linv(j,4)];
end

ij=0;
xint = zeros(nohor*nover,1);
yint = zeros(nohor*nover,1);
for j=1:nover
    for i= 1 : nohor
        ij = ij + 1;
        %         if mod(j
        [xint(ij),yint(ij)]=polyxpoly(xs1(i,:),ys1(i,:),xs2(j,:),ys2(j,:));
        %         ij=ij+1;
    end
end
[xint_sorted, idxX] = sort(xint);
yint_sorted = yint(idxX);
xyint_sorted = [xint_sorted,yint_sorted];
for j = 1 : nover
    idxs = (j-1)*nohor+(1:nohor) ;
    if mod(j,2)==1
        xyint_sorted(idxs,2) = sort(xyint_sorted(idxs,2), 'descend');
    else
        xyint_sorted(idxs,2) = sort(xyint_sorted(idxs,2), 'ascend');
    end
end
figure(3);clf;
imagesc(mfgray)
title('Numbered Trackpoints Detected, Click to Continue')
% hold on
for i =1:length(xyint_sorted)
    text(xyint_sorted(i,1),xyint_sorted(i,2),sprintf('%i',i))
end
kk=waitforbuttonpress;
close
h1 = image(mfgray);
geth1x=get(h1, 'XData');
geth1y=get(h1, 'YData');
[nrows,ncols] = size(get(h1, 'CData'));

imagesc(mfgray);
colormap('jet');

%get the trackpoint in order, get color values
[c,r,pixelcol]=impixel(geth1x,geth1y,mfgray,xyint_sorted(:,1),xyint_sorted(:,
2));
maskedim=mfgray.*uint8(intrack);
methcolor=mean(pixelcol(:,1));
colormask=roicolor(maskedim,methcolor-45,methcolor+45);

xyint_sorted=xyint_sorted(1:novalid,:);

trackdims=xyint_sorted;

```



```

pixx=round(axes2pix(ncols, geth1x, xyint_sorted(:,1)));
pixy=round(axes2pix(nrows, geth1y, xyint_sorted(:,2)));

sqhaa=3;
sqwaa=5;

sqh=(sqhaa-1)/2;
sqw=(sqwaa-1)/2;
[mm,nn]=size(pixx);
trackmask=zeros(size(mfgray));

[mx,nx]=size(mfgray);
chpoint=zeros(mx,nx,50);
checkpoint=zeros(mx,nx,50);

%create the tracking mask
for ii=1:mm
    checkpoint(:, :, ii)=zeros(size(mfgray));
    for ij=1:sqhaa
        for jj=1:sqwaa
            trackmask(pixy(ii,1)+sqh-ij,pixx(ii,1)+sqw-jj)=1;
            checkpoint(pixy(ii,1)+sqh-ij,pixx(ii,1)+sqw-jj,ii)=1;
        end
    end
    chpoint(:, :, ii)=gframe20.*uint8(checkpoint(:, :, ii));
    aga=chpoint(:, :, ii);
    startval(ii)=sum(aga(:));
    aga=0;
end

negtrackmask=1-trackmask;
imagesc(negtrackmask);
justtocheck=mfgray.*uint8(negtrackmask);
imagesc(justtocheck);

hold off
c=zeros(size(ses));
meantime=zeros(1,nframes);
time=zeros(1,novalid);
timef=zeros(1,novalid);
ii=1;

%tracking procedures
for i=1:nframes
    vfr=read(vidprocess,i);
    vfrgray=rgb2gray(vfr);
    c(find(ses))=vfrgray(find(ses));
    meantime(i)=(i-1)/nframerate;
    meanval(i)=sum(c(:));
    tracksel=vfrgray.*uint8(colormask);

    nowim=vfrgray.*uint8(checkpoint(:, :, ii));

```

```

nowval(i)=sum(nowim(:));
'outer loop';
i;
'nowval';
nowval(i);

if ii<=mm
    if nowval(i)<startval(ii)/1.1
        'innerloop'
        ii
        time(ii)=(i-1)/nframerate;
        timef(ii)=i;
        ii=ii+1;
    end
end
meantrack(i)=sum(tracksel(:));
clear vfr vfrgray c tracksel;

end
close all

%user validates point tracking
for i=1:novalid
    hold off

    vfg=read(vidprocess,timef(i));
    kk=waitforbuttonpress;
    imagesc(vfg);
    title ('User Validation of point Tracking, click to continue')

end
close

hold on

plot(meantime,25*meanval/(max(meanval)), 'color', 'black') ;
plot(time,vols(1:novalid), 'color', 'r');
title('Results processed and unprocessed')
xlabel('Time (seconds)')
ylabel('Volume (microliters)')

filname1=strcat(videoname, '.mat');
save(filname1);

varstr=videoname;
varstr=strrep(varstr, '.', '');
varstr=strrep(varstr, 'avi', '');
varstr=strrep(varstr, '_', '');
varstr1=strcat(varstr, 'var1xxx');
varstr2=strcat(varstr, 'var2xxx');
varstr3=strcat(varstr, 'var3xxx');
var1=genvarname(varstr1);
var2=genvarname(varstr2);
var3=genvarname(varstr3);

```

```

eval ([var1 '= [meantime; meanval];']);
eval ([var2 '= [time; vols(1: novalid)];']);
eval ([var3 '= allinp;']);
clearvars -except -regex xxx$
save('fullresults.mat', '-append');

```

CHAPTER 7

LAB-ON-A-DISK FLUORESCENCE DETECTION SYSTEM

In Ch. 7 of this work, two different concepts for a centrifugal microfluidic bead-based immunoassay systems were discussed. Centrifugal microfluidic systems have an inherent compatibility with bead-based assays, because through centrifugation the microbeads can be collected against an arced channel, while by using stationary permanent magnets they can be mixed with a reagent solution by moving the centrifugal disc in an oscillating manner. In Fig. S.1 A, the key concept of a reaction/detection chamber is shown isolated from the rest of the microfluidic circuit. A microfluidic channel is designed as an arc around the center of the disc. When the disc spins, the microbeads will accumulate on the edge of the channel. With the microbeads now located at a specific radius from the center of the circle, a detection method (quantification of the bead signal) can be envisioned where a detector is located at a stationary point located below the position where the microbeads are positioned. Still, the detection method itself may not be straightforward.

In Fig. S.2 B-D, different detection methods for microbeads are presented. For simplicity, it is assumed in all cases that a green source is used for excitation and that the emission from the microbead is at the red wavelengths. In B, a classic epifluorescence method is presented in a simplified manner. Epifluorescence is based on the existence of a dichroic mirror, i.e. a component that will transmit light of some frequencies and reflect light of the rest of the frequencies. An excitation source emits light at a wavelength which is reflected by the dichroic mirror towards the microbead. The light is focused on the microbead, whose fluorescent label is excited and emits a fluorescent signal at a frequency that is transmitted by the dichroic mirror. Fluorescence goes through the mirror towards the detector, which can be a camera, a photodiode or a photomultiplier. This method is commonly used in microscopy. One of the key concerns when designing a detection system is that the emission wavelength does not interfere with the detection signal. This can be challenging, especially when laser sources are used for excitation.

In Fig. S.2-C, a detection system based on flow cytometry principles is shown. The microbeads run through a sheath flow channel in which they are centered and passed through a laser excitation source one after another. A detector, typically a PMT, is located laterally to the optical path of the laser beam. The detector captures the emission signal of the fluorescent labels as the microbeads go through the detection position one by one. This can be used for fluorescent labels but also for fluorescent tags to differentiate bead families from one another by adding laser sources of different wavelengths in other positions of the sheath flow channel. This is the most common detection system used for Xmap technology bead-based immunoassays.

In Fig. S.2-D, A detection system based on a LED excitation source and a CCD/CMOS camera is shown. The bead tags and labels are excited using LEDs and their emission is recorded by a camera through appropriate dielectric filters. This simplified technology is used by Luminex MagPix system.

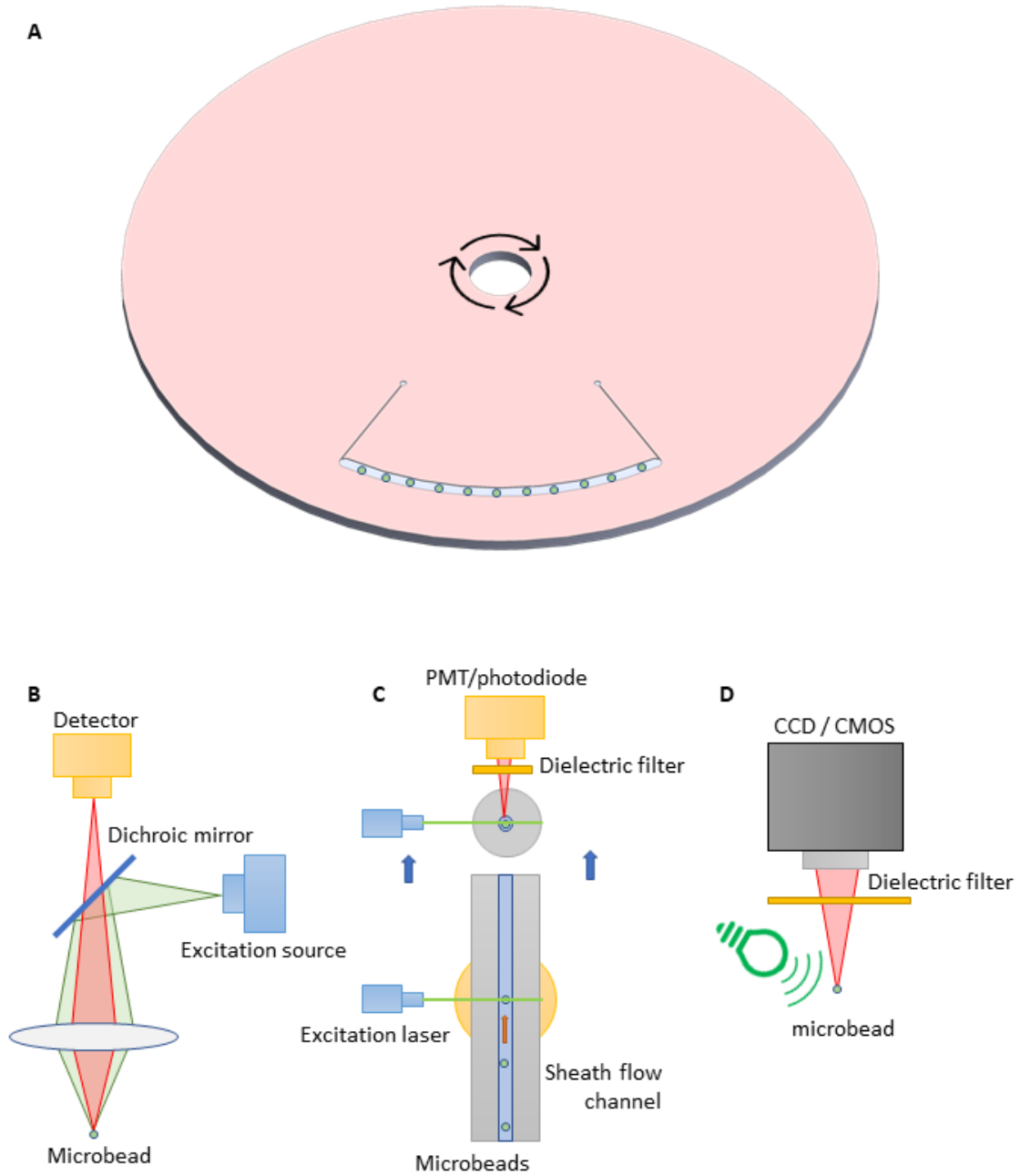


Figure S.2: The arrangement of microbeads in a detection channel of a centrifugal microfluidic and different common approaches towards fluorescence detection. (A) Microbeads in an arced channel inside a microfluidic disk (B) Epifluorescence, (C) Flow cytometry-based detection (D) LED / camera arrangement

In the context of a microfluidic circuit, the detection system design needs to follow ASSURED criteria. In this case the challenge is to keep the system low cost and compact. An additional challenge for fluorescent detection systems is the need to use a high intensity source tuned for the excitation wavelength of the label, for example a laser diode, but be able to isolate the incident excitation wavelength from the sensor. Considering that dichroic mirrors and spectral filters are not 100% efficient in reflecting or blocking the unwanted bands, the excitation beams need to be diverted away from the detector. Notice that in all of the approaches described in Fig. S.2 , the incident beams are not directed towards the detector. This principle needs to be followed in fluorescent detection systems. Looking at each individual approach, they all have merits and constraints. The epifluorescence approach is compatible with different sources and detectors, but it has a large footprint and requires high quality optics. The flow cytometry-based approach is the gold standard for bead-based immunoassays because of its ability to align microbeads one behind the other. Additionally, the laser beam forms a 90° angle with the optical path of the detector thus isolating the PMT from incident excitation beams. However, it requires sheath flow and a cuvette which is difficult to implement in a microfluidic disk. Moreover, because exposure time is constrained by the flow velocity, very sensitive detectors are required, for example photomultipliers. The camera/LED option is a simplified approach, but it requires a sensitive CCD/CMOS sensor with high quantum efficiency which makes this option quite expensive to integrate in a PoC system.

As part of the device/microfluidic concepts of this work, the prototype for a microfluidic bead-based immunoassay detection system was created. The idea behind it was to combine the benefits of a flow cytometry system with the format of a microfluidic disk (Fig. S.2). The concept, which can be seen in Fig. S.3-A, is based on lateral excitation of the detection channel using a collimated laser beam. The beam is reflected on 1 or two mirrors and enters the disk from the side. It travels through the disk to go through the detection channel in which the microbeads reside. The labels attached on the secondary antibodies, fluoresce as a result of the excitation beam, but at a different wavelength. Focusing optics below the disk drive the fluorescent signal into a detector, which can be a camera or even a photodiode, provided that the microbeads are perfectly aligned from centrifugation. The signal is thus recorded. Since the detection channel is arced, scanning can be achieved simply by rotating the disk. This approach has the following benefits compared to standard detection methods:

- A lateral laser excitation, just like in the flow cytometry systems, protects the detector from noise coming from the excitation beam.
- Unlike in flow cytometry systems, the beads can remain stationary which allows larger exposure times. A photomultiplier could potentially be substituted with a lower cost photodiode in this case.
- Multiple beams/detectors can be integrated into a single device to be able to detect both label and tag signals from microbeads.

The main drawbacks of this approach are the following:

- The disk needs to be thick enough to be used as a beam propagation material
- Beam misalignments can cause interference from the disk sealing film or even total internal reflections in the disk
- The disk material may itself have some fluorescent properties that can affect the reading of the detector

In Fig. S.3-B, a prototype for this detection system is displayed. The laser source is positioned below the right mirror assembly. A 532 nm laser beam is focused on the detection channel and then reflected towards a beam termination unit which is located below the left mirror. In the photo, the detection channel is empty and the laser beam can be seen diffusing onto the channel wall.

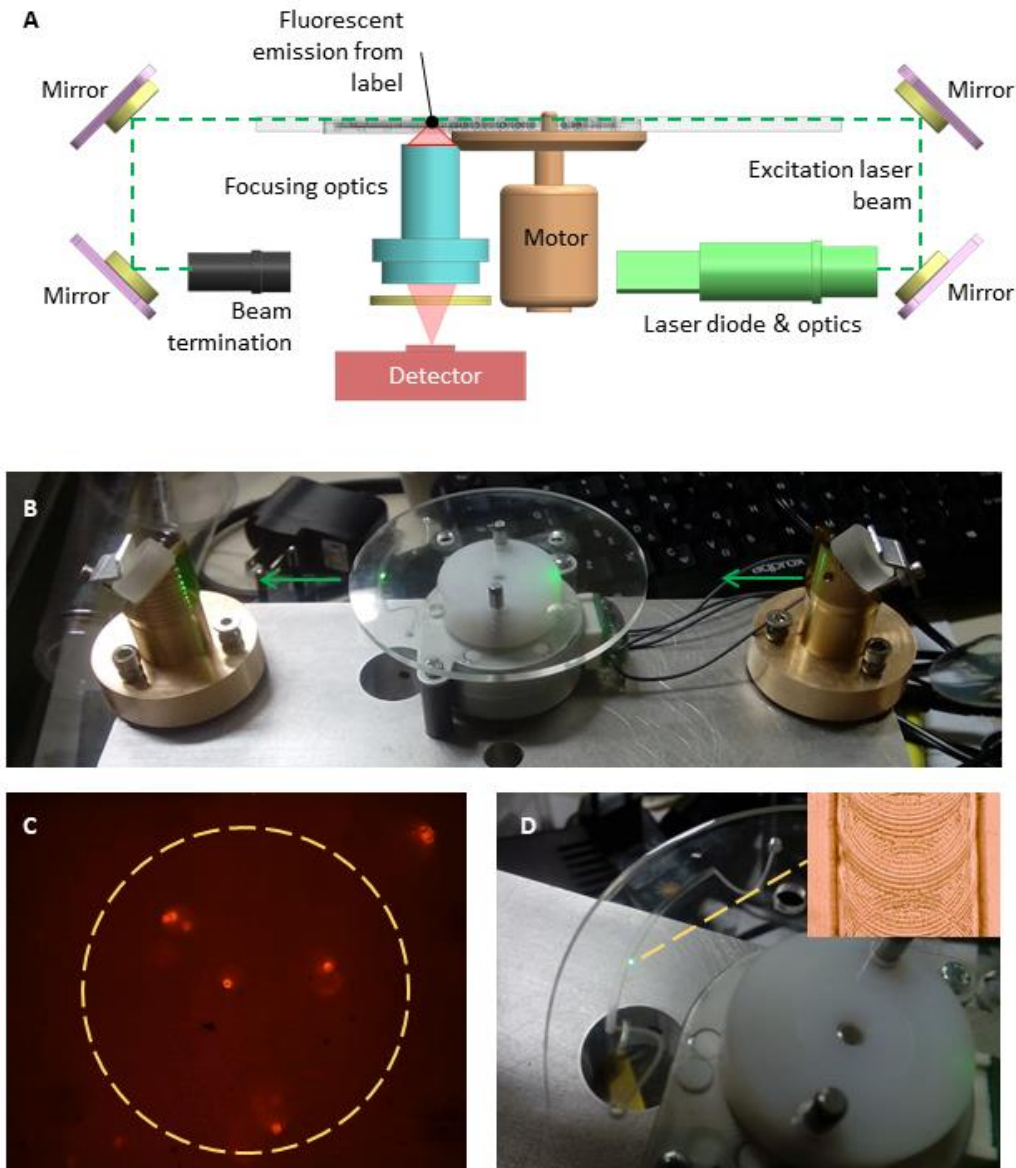


Figure S.3: An approach towards bead-based immunoassay detection on chip, which is consistent with the concepts presented in Ch. 7 (A) The optical paths of the excitation laser and the fluorescent emission signal from the bead label (B) A prototype system that is based on this principle (C) A microscopy image from microbeads acquired using this excitation signal and a dielectric longpass filter (D) a microscopy image of the detection channel machined surface

In Fig. S.3-C, an image acquired from this system is shown. The excitation signal in this case is a 532 nm laser diode which is used on microbeads coupled with a phycoerythrin label to acquire peak fluorescent emission at 578 nm. A longpass filter is used to filter out the excitation wavelength and the image is acquired using a CCD camera and a 20X objective lens. While the excitation concept does work, there are aberrations from the lateral illumination and significant background noise. This is attributed to the prototyping method of the disk which is machined (Fig S.3 D). The surface roughness and machining marks of the prototyping process result in significant light scattering, which in turn creates background noise in the detection system. Injection molded or PDMS disks would need to be fabricated in order to evaluate this approach further

LAB-ON-A-DISK MOTION SYSTEM

Different concepts have been proposed in this work on a microfluidic disk that could be used for bead-based immunoassays. One challenge that we encountered when creating prototypes for the detection systems, is that a detection system, especially when it is based on photodiodes, would need to have very high spatial resolution to be able to be used with 6.5 μm microbeads. The reason is that the detector would need to be able to focus on a single microbead, or at the least be able to achieve a continuous rotary motion with very low RPM to be able to acquire signal from each microbead. Assuming that the microbead detection channel is at a radius of 55 mm from the center of the disk, that the required exposure from each microbead is 50 ms and that each microbead is 6.5 μm in diameter, the rotation speed required is $0.0065/0.050=0.13$ mm/sec, which corresponds to ~ 0.023 RPM. Since this would be used for detection, this rotation would need to be performed smoothly without stepwise motion or faster/slower sections within the rotation, as all of these would affect the measurement of individual microbeads. However, for the centrifugation mode, rotational speeds of 3000 RPM are not uncommon, as seen in Ch. 5 of this work. One challenge that may be encountered during the development of a scanning bead-based PoC device, is that both high speeds, very low smooth speeds and high resolution may be required from the motion system. While sophisticated servomotor solutions with high resolution encoders may exist that can cover this specification, they may not be suitable in the context of a low cost PoC device.

A proposed solution for a low-cost system with high resolution and high-speed capabilities can be seen in Fig. S.4-A. The motion system consists of one DC motor and two stepper motors with a gearbox. The stepper motors are driving sectioned rollers which are engaging via friction with a disk. From each roller, a section of $\sim 90^\circ$ has been removed. Two terminal switches for indexing of the stepper motors have been included. The motion concept can be seen in Fig. S.4-B. When both rollers are disengaged (1), the DC motor can run freely at several thousand RPM for centrifugation operations. When high resolution or very low speed is required, the two steppers first assume a 180° phase shift (2), and then they are moved simultaneously. Because of the 180° shift and the 90° cut-out, there is always at least one roller engaged with the disk (3&4). In a device implementation, the disk would be used to mount a centrifugal microfluidic consumable. With this setup two modes can be achieved: a high-resolution mode when the stepper motors are engaged, and a high-speed mode when the DC motor runs freely.

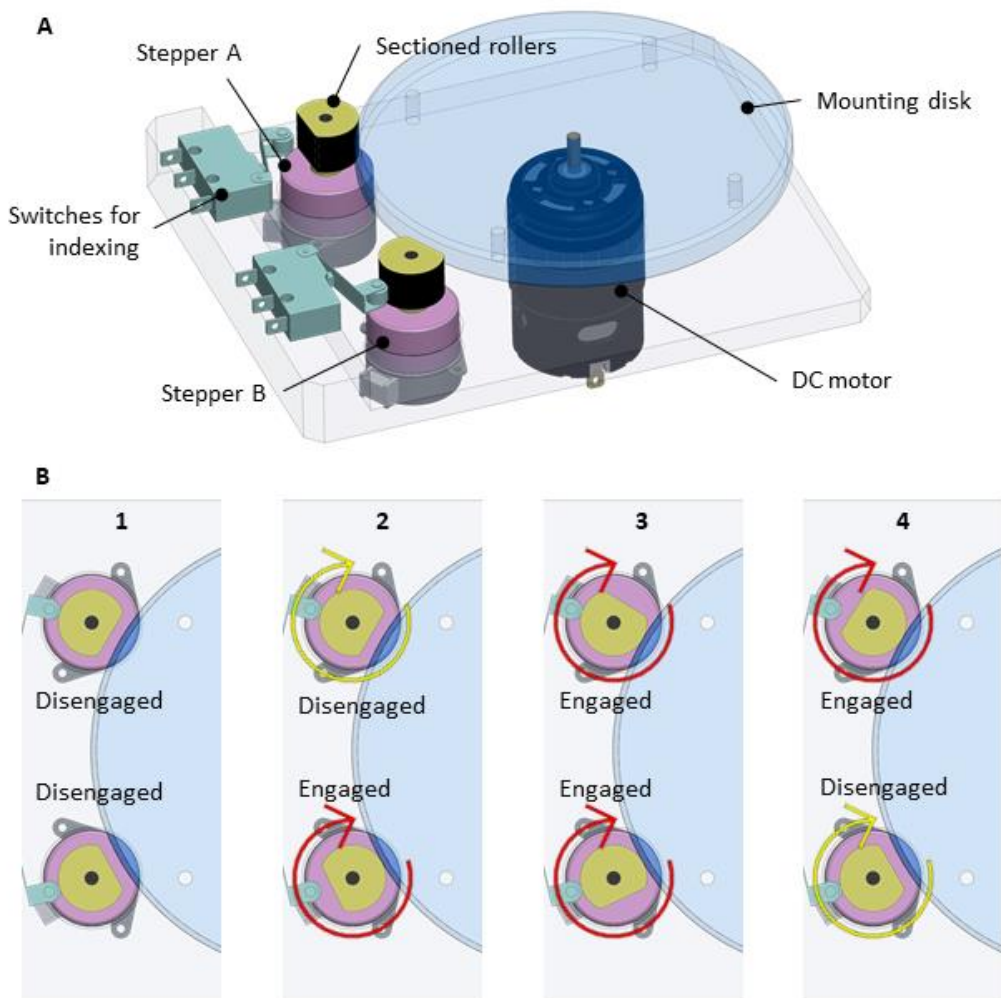
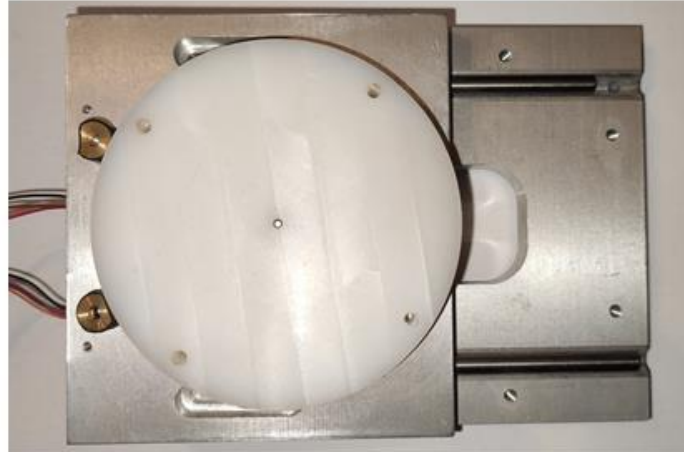


Figure S.4: A proposed motion system for a centrifugal PoC device that requires both scanning abilities with high resolution and high-speed rotation for centrifugation operations. (A) System components (B) Different positions of stepper motors during device operation

A prototype for the proposed system can be seen in Fig. S.5. The 80 mm plastic disk is driven by two stepper gearmotors with an 18° deg step and a 1:100 reduction ratio. The centrifugation drive is a small brushed 5V DC motor (below the disk). In Fig. S.5-B, the angle step of the mounting disk has been measured against full steps from the stepper motors working in parallel. To measure the stepping angle, a target (white line on black background) was mounted on the disk. For each step taken, the target image was captured using a microscope. Using image analysis in Matlab, the incremental movement of the disk was calculated from the captured frames. The stepping angle was found to be 1.19 arcmin with a standard deviation of 0.14 arcmin for $N=35$. This corresponds to a resolution of ~ 18200 steps/rev. For comparison, in a closed loop servo application, a 14-bit encoder would give ~ 16400 steps/rev which makes this open loop implementation an interesting alternative.

In summary, a low cost motion system has been presented and evaluated at an initial level to yield a high resolution which could be used for scanning and centrifugation in a lab-on-a disk device.

A



B

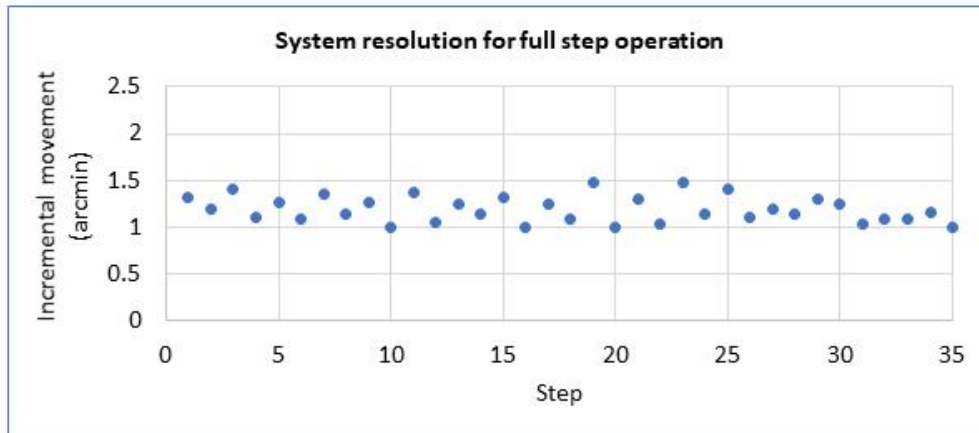


Figure S.5: A prototype of the motion system and initial evaluation (A) A photo of the system (B) Consecutive measurements of the angle step of the disk for one full step of the stepper motors.

ΚΕΦΑΛΑΙΟ 1: ΕΙΣΑΓΩΓΗ

1.1 ΚΙΝΗΤΡΑ ΕΡΕΥΝΗΤΙΚΗ ΕΡΓΑΣΙΑΣ

Η ανάγκη διάγνωσης, παρακολούθησης ή αποκλεισμού μιας παθολογικής κατάστασης όπου και όταν χρειάζεται εξακολουθεί να είναι μια σημαντική πρόκληση στον τομέα της υγείας. Η έγκαιρη διάγνωση παθήσεων, όπως οι νεοπλασματικές ασθένειες ή ο ιός της ανθρώπινης ανοσοανεπάρκειας (HIV), συσχετίζεται με βελτιωμένη πρόγνωση για τον ασθενή^{1,2}. Σε περιπτώσεις μολυσματικών ασθενειών, η έγκαιρη διάγνωση βοηθά στον περιορισμό της εξάπλωσης της νόσου. Στην πρόσφατη περίπτωση του SARS-CoV-2, προέκυψε η ανάγκη για φορητά και ευαίσθητα διαγνωστικά εργαλεία⁸ τόσο για τον έλεγχο της εξάπλωσης του ιού, όσο και για την αποφόρτιση των διαγνωστικών εργαστηρίων.

Ωστόσο, για τους περισσότερους διαγνωστικούς στόχους, ο έλεγχος εξακολουθεί να περιορίζεται σε κεντρικές εργαστηριακές δομές, όπως εργαστήρια κλινικών ή διαγνωστικά κέντρα. Αυτές οι δομές είναι εξοπλισμένες με αυτόματους εργαστηριακούς αναλυτές μεγάλου μεγέθους, που παρέχουν δυνατότητες ελέγχου πολλαπλών δειγμάτων. Παρότι η προσέγγιση του κεντρικού εργαστηρίου έχει πολλά οφέλη, συχνά συσχετίζεται με μεγάλους χρόνους αναμονής από τη δειγματοληψία μέχρι το πόρισμα της εξέτασης¹⁰. Η ανάγκη να μεταφέρονται δείγματα και ασθενείς από απομακρυσμένες τοποθεσίες στο κεντρικό εργαστήριο, αυξάνει περαιτέρω τις καθυστερήσεις και επιδεινώνει την ποιότητα ζωής των ασθενών συχνά αποθαρρύνοντάς τους από το να υποβληθούν σε απαραίτητες εξετάσεις.

Για τους παραπάνω λόγους, η ανάπτυξη τεχνολογιών για την παροχή αποκεντρωμένων υπηρεσιών διάγνωσης συνιστά μια ερευνητική κατεύθυνση ωφέλιμη για την κοινότητα. Παρότι τα παραπάνω αφορούν μια σειρά από ιατρικούς ελέγχους, στην παρούσα εργασία οι ερευνητικές προσπάθειες επικεντρώνονται στην ανάπτυξη τεχνολογιών για παρακλινικά συστήματα ανοσολογικών δοκιμών.

1.2 ΑΝΟΣΟΛΟΓΙΚΕΣ ΔΟΚΙΜΕΣ ΓΙΑ ΔΙΑΓΝΩΣΗ ΚΑΙ ΕΡΕΥΝΑ

Οι ανοσολογικές δοκιμές είναι βιοχημικές μέθοδοι ανίχνευσης αντισωμάτων ή αντιγόνων μέσα σε ένα δείγμα. Όταν ένα μακρομόριο, για παράδειγμα μια πρωτεΐνη, έχει διαγνωστική αξία, συχνά χρησιμοποιείται μια ανοσολογική δοκιμή για την ανίχνευση/ποσοτικοποίησή της. Μια κοινώς χρησιμοποιούμενη μέθοδος ανίχνευσης πρωτεϊνών είναι η ELISA (Enzyme Linked Immunosorbent Assay). Στη μέθοδο ELISA, η πρωτεΐνη-στόχος προσδένεται σε ένα ακινητοποιημένο αντιγόνο ή αντίσωμα, διαχωρίζοντάς την από τις υπόλοιπες πρωτεΐνες που βρίσκονται μέσα στο δείγμα. Το σύμπλοκο αντιγόνου/αντισώματος σηματοδοτείται, συνήθως με τη χρήση κάποιου ενζύμου που παράγει ένα ανιχνεύσιμο σήμα, όπως χρώμα ή φθορισμό. Με τη μέτρηση αυτού του σήματος γίνεται η ποσοτικοποίηση ή απλά η επιβεβαίωση/αποκλεισμός της ύπαρξης της πρωτεΐνης-στόχου μέσα στο δείγμα. Υπάρχουν πολλές παραλλαγές τις τεχνικής ELISA, μια εκ των οποίων είναι η χρήση υπερπαραμαγνητικών σφαιριδίων ως υπόστρωμα για τη δοκιμή. Σε αυτή την παραλλαγή, η ακινητοποίηση των αντισωμάτων/αντιγόνων γίνεται πάνω σε μικροσφαιρίδια διαμέτρου ~6 μm τα οποία περιέχουν νανοσωματίδια οξειδίου του σιδήρου. Επίσης, κάθε οικογένεια μικροσφαιριδίων περιέχει φθορίζουσες χρωστικές που τη διαφοροποιούν από τις υπόλοιπες οικογένειες μικροσφαιριδίων. Λόγω αυτών των χαρακτηριστικών, οι ανοσοδοκιμασίες με τη χρήση μικροσφαιριδίων επιτρέπουν πολυπλεκτικές μετρήσεις (πολλοί στόχοι σε ένα μόνο δείγμα), τη χρήση μαγνητισμού για την διαχείριση των μικροσφαιριδίων και τη χρήση συστημάτων βασισμένων σε κυτταρομετρία ροής για την ταχεία ποσοτικοποίηση των παγιδευμένων πρωτεϊνών-στόχων.

1.4 ΕΛΕΓΧΟΣ ΣΤΟ ΣΗΜΕΙΟ ΦΡΟΝΤΙΔΑΣ

Έλεγχος στο σημείο φροντίδας ή παρακλίνιος έλεγχος (Point-of-care testing) είναι ο όρος που χρησιμοποιείται για να περιγράψει διαγνωστικά τεστ που δεν πραγματοποιούνται αυστηρά στο εργαστήριο, αντ' αυτού διενεργούνται στο σημείο και στον χρόνο που είναι απαραίτητα. Σημαντικές προσπάθειες σε ακαδημαϊκό και βιομηχανικό επίπεδο επικεντρώνονται στην ανάπτυξη τεχνολογιών και συστημάτων που μπορούν να παρέχουν διαγνωστικές λύσεις για το σημείο φροντίδας. Ο Παγκόσμιος Οργανισμός Υγείας έχει καταρτίσει μια λίστα οδηγιών για την ανάπτυξη τέτοιων συστημάτων με το ακρωνύμιο ASSURED²². Οι οδηγίες αυτές προτείνουν πως ένα παρακλίνιο διαγνωστικό σύστημα πρέπει να έχει χαμηλό κόστος, να είναι ευαίσθητο και ειδικό, να είναι απλό στη χρήση, γρήγορο, αξιόπιστο, κατά το δυνατόν αυτοτελές και να είναι διαθέσιμο σε αυτούς που το χρειάζονται.

Μια μέθοδος κατηγοριοποίησης των παρακλίνιων συστημάτων ελέγχου είναι με βάση το σημείο και τη χρήση για την οποία προορίζονται. Με βάση αυτά τα κριτήρια, μπορούμε να διακρίνουμε 3 κατηγορίες συστημάτων: Τις μικρές φορητές συσκευές (lateral flow tests, συσκευές μέτρησης σακχάρου), τα μικρά επιτραπέζια συστήματα (μικρορευστονικά κυκλώματα μιας χρήσης, Lab-on-a-Disk) και τα εργαστηριακά συστήματα μεγαλύτερης κλίμακας. Συσκευές που ανήκουν στις παραπάνω κατηγορίες διαφοροποιούνται ως προς την τεχνολογία της ανοσοδοκιμασίας, ως προς την μέθοδο διαχείρισης ρευστών και ως προς τις τεχνικές ανίχνευσης του σήματος. Ωστόσο, η δημιουργία συστημάτων που ακολουθούν τα κριτήρια ASSURED έχει προκλήσεις σχετιζόμενες μεταξύ άλλων με την διαχείριση των ρευστών σε πρωτόκολλα πολλαπλών βημάτων, με την ενσωμάτωση επενεργητών και συναφών υποσυστημάτων μέσα στις συσκευές και τελικά με την ίδια την προσαρμογή των πρωτοκόλλων ανοσοδοκιμασιών στις δυνατότητες τις εκάστοτε συσκευής.

1.5 ΕΥΕΛΙΚΤΟΣ ΣΧΕΔΙΑΣΜΟΣ ΓΙΑ ΣΥΣΤΗΜΑΤΑ ΠΑΡΑΚΛΙΝΙΩΝ ΑΝΟΣΟΛΟΓΙΚΩΝ ΔΟΚΙΜΩΝ

Στόχος αυτής της εργασίας είναι η διερεύνηση τεχνολογιών που επιτρέπουν την διενέργεια πρωτοκόλλων ανοσοδοκιμασίας σε επίπεδο εργαστηριακών και μικρών επιτραπέζιων συσκευών. Η εργασία εστιάζει στη χρήση υπερπαραμαγνητικών μικροσφαιριδίων, στην ανάπτυξη ενός επιτραπέζιου εργαστηριακού συστήματος για τη διενέργεια αυτοματοποιημένων ανοσοδοκιμασιών και στην ανάπτυξη τεχνολογιών για την αυτοματοποιημένη διαχείριση ρευστών σε μικρορευστονικά κυκλώματα. Η σύνθεση όλων αυτών θα μπορούσε να οδηγήσει στη δημιουργία παρακλίνιων συστημάτων ανοσοδοκιμασιών που μοιράζονται την ίδια τεχνολογία με τα εργαστηριακά ανάλογά τους.

ΚΕΦΑΛΑΙΟ 2: ΑΝΑΣΚΟΠΗΣΗ ΠΑΡΑΚΛΙΝΙΩΝ ΔΙΑΓΝΩΣΤΙΚΩΝ ΣΥΣΤΗΜΑΤΩΝ

Σε αυτό το κεφάλαιο⁷² γίνεται μια ανασκόπηση των τύπων, τεχνολογιών και διαγνωστικών στόχων που χρησιμοποιούνται σε παρακλίνια διαγνωστικά συστήματα (PoC systems). Ως αφετηρία χρησιμοποιούνται 105 κατασκευαστές PoC συστημάτων. Η λίστα αυτών των κατασκευαστών καταρτίστηκε με βάση τη συμμετοχή τους σε διεθνείς εκθέσεις⁸², συνέδρια και αναλύσεις αγοράς⁸³.

2.1 Η ΤΕΧΝΟΛΟΓΙΑ ΤΩΝ ΠΑΡΑΚΛΙΝΙΩΝ ΔΙΑΓΝΩΣΤΙΚΩΝ ΣΥΣΤΗΜΑΤΩΝ

Κατηγοριοποιώντας τα PoC συστήματα με βάση την τεχνολογία τους, προκύπτουν 4 βασικές κατηγορίες: Τα συστήματα lateral flow γνωστά και ως rapid tests, τα φυγοκεντρικά PoC συστήματα, τα συστήματα ηλεκτροχημικής ανίχνευσης και τα συστήματα ανίχνευσης νουκλεϊκών οξέων. Πλέον αυτών των κατηγοριών, υπάρχουν και ιδιαίτερες περιπτώσεις συστημάτων που συναντώνται σπανιότερα.

2.2 ΤΕΣΤ LATERAL FLOW

Τα συστήματα lateral flow είναι ίσως η πιο χαρακτηριστική κατηγορία PoC συστήματος. Σε αυτή την κατηγορία χρησιμοποιείται τεχνολογία sandwich ELISA με μικροσφαιρίδια latex ή κολλοειδή χρυσό για να παραχθεί ένα ορατό σήμα ενδεικτικό της ανίχνευσης της πρωτεΐνης-στόχου. Η ιδιαιτερότητα αυτής της μεθόδου σε σχέση με την εργαστηριακή ELISA, είναι πως τα αντιδρώντα βρίσκονται σε στερεή μορφή σε διαφορετικά σημεία πάνω σε μια λωρίδα ενός πορώδους, υδρόφιλου μέσου. Το διάλυμα που περιέχει το δείγμα εισάγεται στη μία άκρη αυτής της λωρίδας και ωθούμενο προς την άλλη, συμπαρασύρει τα αντιδρώντα για να δημιουργήσει τελικά ορατές γραμμές που σηματοδοτούν την εγκυρότητα του τεστ και την ανίχνευση ή μη του στόχου. Τυπικά τεστ lateral flow είναι το τεστ για SARS-CoV-2 Ag, τεστ HIV και το τεστ hcG. Η τεχνολογία lateral flow είναι μια έξυπνη προσαρμογή ενός εργαστηριακού ανοσολογικού πρωτοκόλλου σε ένα απλό αναλώσιμο τεστ μιας χρήσης. Ωστόσο, το κόστος αυτής της προσαρμογής είναι η μειωμένη ευαισθησία ή/και ειδικότητα αυτών των τεστ²⁵. Επίσης, τα lateral flow τεστ εν γένει δεν παρέχουν δυνατότητες ποσοτικοποίησης του στόχου και περιορίζονται σε εφαρμογές όπου η ανίχνευση ή μη του στόχου επαρκεί.

2.3 ΦΥΓΟΚΕΝΤΡΙΚΑ ΡΟC ΣΥΣΤΗΜΑΤΑ

Τα φυγοκεντρικά PoC συστήματα, γνωστά και ως Lab-on-a-Disk (LOAD) εκμεταλλεύονται τη φυγοκεντρική δύναμη για την υλοποίηση μικρορευστονικών κυκλωμάτων σε περιστρεφόμενους δίσκους. Συνδυάζοντας τα τριχοειδή φαινόμενα που εμφανίζονται σε μικρορευστονικές διατάξεις με τη φυγοκεντρική δύναμη που ασκείται στο ρευστό εντός του κυκλώματος και με εναλλαγή υδρόφιλων και υδρόφοβων επιφανειών, σύνθετα πρωτόκολλα μπορούν να υλοποιηθούν χρησιμοποιώντας την τεχνολογία LOAD. Λόγω αυτής της ευελιξίας, τα διαθέσιμα LOAD συστήματα στην κλινική πράξη διαφοροποιούνται μεταξύ τους ως προς τους διαγνωστικούς στόχους και τη διάταξη των κυκλωμάτων^{124–129}, ^{130–133}. Κοινά στοιχεία ανάμεσα στα συστήματα είναι πως σε όλα χρησιμοποιείται ένα μικρορευστονικό κύκλωμα εντός ενός πλαστικού αναλώσιμου δίσκου. Ο δίσκος τοποθετείται σε συσκευή όπου και περιστρέφεται σε 100s - 1000s RPM. Με εναλλαγές στην περιστροφική ταχύτητα, τα αντιδρώντα αραιώνονται, δοσομετρούνται, αναμιγνύονται και τελικά με τη χρήση κάποιας οπτικής μεθόδου ανίχνευσης γίνεται η ποσοτικοποίηση του στόχου. Στα φυγοκεντρικά PoC συστήματα υλοποιούνται εκτός από ανοσολογικά πρωτόκολλα και αιματολογικές μετρήσεις καθώς και μετρήσεις αερίων αίματος και ηλεκτρολυτών.

2.4 ΗΛΕΚΤΡΟΧΗΜΙΚΑ ΡΟC ΣΥΣΤΗΜΑΤΑ

Τα ηλεκτροχημικά PoC συστήματα χρησιμοποιούν την αλληλεπίδραση ηλεκτροδίων και αντιδρώντων για την ποσοτικοποίηση ενός στόχου. Χρησιμοποιούνται διαφορετικές αρχές λειτουργίας, όπως αμπερομετρία, βολταμετρία και μέτρηση αγωγιμότητας για να μετρηθεί ένα ηλεκτροενεργό προϊόν το οποίο είναι συνήθως άμεσα συνδεδεμένο με την ύπαρξη ενός ενζύμου-καταλύτη. Τα ηλεκτροχημικά PoC συστήματα συνήθως εμπεριέχουν ένα μικρορευστονικό κύκλωμα, είτε παθητικό (μετρητές γλυκόζης) είτε με κάποια ενεργητικά στοιχεία^{170,171}. Τα ηλεκτροχημικά PoC συστήματα χρησιμοποιούνται ευρέως για τη μέτρηση γλυκόζης, χοληστερόλης, αιματοκρίτη, αερίων αίματος, ηλεκτρολυτών και χρόνου προθρομβίνης.

2.5 ΣΥΣΤΗΜΑΤΑ ΑΝΙΧΝΕΥΣΗΣ ΝΟΥΚΛΕΪΚΩΝ ΟΞΕΩΝ

Τα PoC συστήματα για την ανίχνευση νουκλεϊκών οξέων σε ένα δείγμα χρησιμοποιούνται κυρίως για την ανίχνευση DNA/RNA ιών και βακτηρίων σε δείγματα με στόχο την επιβεβαίωση/αποκλεισμό μόλυνσης, ή την ανίχνευση γνωστών γονιδίων σε ένα δείγμα με στόχο την αναγνώριση μια γενετικής προδιάθεσης για κάποια νόσο. Όπως και στα εργαστηριακά μοριακά συστήματα, το όφελος είναι η δυνατότητα πολλαπλασιασμού των αλληλουχιών που έχει ως αποτέλεσμα την αυξημένη ευαισθησία της μεθόδου. Η μέθοδος που χρησιμοποιείται πιο συχνά είναι η αλυσιδωτή αντίδραση πολυμεράσης (PCR) που απαιτεί τη χρήση θερμικών κύκλων. Άλλες μέθοδοι είναι η LAMP και η NEAR που είναι ισοθερμικές τεχνικές πολλαπλασιασμού. Η μέθοδος ανίχνευσης συνήθως περιλαμβάνει

μέτρηση φθορισμού. Διαγνωστικοί στόχοι για συστήματα νουκλεϊκών οξέων περιλαμβάνουν τον SARS-CoV-2, τους ιούς της γρίπης και γνωστά ογκογονίδια.

2.6 ΣΥΜΠΕΡΑΣΜΑΤΑ

Σε αυτό το κεφάλαιο αναλύονται οι διαφορετικές τεχνολογικές προσεγγίσεις για την υλοποίηση PoC συστημάτων. Η τεχνολογία των lateral flow test συγκεντρώνει το μεγαλύτερο ενδιαφέρον σε αριθμό συστημάτων, διαγνωστικών στόχων και εταιριών. Τα πιο σύνθετα συστήματα διακρίνονται σε φυγοκεντρικά με οπτική μέθοδο ανίχνευσης του στόχου, σε ηλεκτροχημικά με μικρορευστονικό κύκλωμα είτε παθητικό είτε ενεργητικό και σε συστήματα ανίχνευσης νουκλεϊκών οξέων. Κάθε μια από αυτές τις προσεγγίσεις εξυπηρετεί διαφορετικές ανάγκες και διαγνωστικά σενάρια. Το ζήτημα της διαχείρισης των πρωτοκόλλων σε μικρορευστονικό επίπεδο καθώς και η προετοιμασία του δείγματος φαίνεται να είναι σημαντικοί παράγοντες στον σχεδιασμό του συστήματος.

ΚΕΦΑΛΑΙΟ 3: ΕΝΑ ΕΡΓΑΣΤΗΡΙΑΚΟ ΣΥΣΤΗΜΑ ΓΙΑ ΑΝΟΣΟΛΟΓΙΚΑ ΠΡΩΤΟΚΟΛΛΑ

Σε αυτό το κεφάλαιο παρουσιάζεται ένα εργαστηριακό σύστημα που αναπτύχθηκε για τη διεξαγωγή ανοσολογικών πρωτοκόλλων με χρήση τεχνολογίας υπερπαραμαγνητικών μικροσφαιριδίων. Αναλύονται τα επιμέρους υποσυστήματα και παρουσιάζονται δυνατότητες και οι περιορισμοί. Χρησιμοποιώντας το σύστημα διεξάγονται ανοσολογικά πρωτόκολλα με διαγνωστικό στόχο αντισώματα έναντι του ιού SARS-CoV-2. Τα αποτελέσματα συγκρίνονται με τα αντίστοιχα εργαστηριακά.

3.1 ΤΕΧΝΟΛΟΓΙΑ ΑΝΟΣΟΛΟΓΙΚΩΝ ΔΟΚΙΜΩΝ ΜΕ ΜΙΚΡΟΣΦΑΙΡΙΔΙΑ

Οι ανοσολογικές δοκιμές για την ανίχνευση αντισωμάτων ή αντιγόνων είναι βασικό εργαλείο της διαγνωστικής και της έρευνας για την ανίχνευση βιοδεικτών. Η τεχνολογία μικροσφαιριδίων παρέχει δυνατότητες πολυπλεκτικότητας και αυξημένης ευαισθησίας καθώς και αυξημένη ευελιξία στην διεξαγωγή τέτοιων δοκιμών. Για τη διεξαγωγή ανοσολογικών δοκιμών με μικροσφαιρίδια, χρησιμοποιείται εργαστηριακός εξοπλισμός όπως δοσιμετρικές πιπέτες, συστήματα ανάδευσης και πλύσης μικροπλακών και συστήματα παγίδευσης μικροσφαιριδίων. Για τη διεξαγωγή μικρού αριθμού δοκιμών, τα πρωτόκολλα εκτελούνται χειροκίνητα. Για τη διεξαγωγή πολλαπλών πειραμάτων έχουν αναπτυχθεί ρομποτικά συστήματα γενικής χρήσης που μπορούν να εκτελέσουν μέρος ή ολόκληρο το πρωτόκολλο. Ωστόσο, υπάρχουν περιορισμένες λύσεις για την διεξαγωγή πρωτοκόλλων με τη χρήση μικροσφαιριδίων και οι συσκευές είναι συνήθως μεγάλου μεγέθους, γενικής χρήσης εργαστηριακές πλατφόρμες αυξημένης πολυπλοκότητας. Στα πλαίσια αυτής της εργασίας έγινε προσπάθεια ανάπτυξης ενός επιτραπέζιου συστήματος προσαρμοσμένου στην τεχνολογία μικροσφαιριδίων, που μπορεί να χρησιμοποιηθεί για διαγνωστική και για έρευνα.

3.2 ΜΕΘΟΔΟΙ

Το σύστημα αποτελείται από 3 κύρια υποσυστήματα: Την κεφαλή διαχείρισης υγρών και μικροσφαιριδίων, το σύστημα κίνησης και τους φορείς μικροπλακών.

Η κεφαλή ενσωματώνει 96 παράλληλα έμβολα για τη διαχείριση υγρών. Η αναρρόφηση, διανομή και ανάμιξη γίνεται με τη χρήση εμπορικών ρυγχών πιπετών. Η διάταξη επιλέχθηκε ώστε να είναι συμβατή με τυποποιημένες φόρμες μικροπλακών (8x12, 16x24). Επίσης στην κεφαλή ενσωματώνεται ένα σύστημα διαχείρισης μικροσφαιριδίων που αποτελείται από μόνιμους μαγνήτες που μεταφέρονται σε ενεργές ή ανενεργές θέσεις σε σχέση με τις πιπέτες. Η διαφοροποίηση της λειτουργίας του συστήματος σε σχέση με υπάρχουσες λύσεις, είναι πως η διαχείριση και ο διαχωρισμός των μικροσφαιριδίων γίνεται εντός των πιπετών. Με αυτή την προσέγγιση απλοποιείται το πρωτόκολλο διεξαγωγής ανοσολογικών δοκιμών και αίρονται ζητήματα διαχείρισης μικρών

ποσοτήτων ρευστού σε βοθρία μικροπλακών, καθώς όλες οι αντιδράσεις λαμβάνουν χώρα μέσα στα πλαστικά ρύγχη.

Ο σχεδιασμός της διαχείρισης μικροσφαιριδίων έγινε με χρήση προσομοίωσης με πεπερασμένα στοιχεία της επίδρασης του μαγνητικού πεδίου και του πεδίου ταχύτητας του ρευστού σε εναιώρημα μικροσφαιριδίων. Δύο διατάξεις δοκιμάστηκαν, ο δακτυλιοειδής μαγνήτης και η διάταξη τετραπλού μαγνήτη περιφερειακά του ρύγχους. Βρέθηκαν λύσεις συμβατές με τις απαιτήσεις του προβλήματος και από τις δύο προσεγγίσεις. Η χρήση τετραπλού μαγνήτη είχε κατασκευαστικά και λειτουργικά πλεονεκτήματα και επιλέχθηκε για τη διεξαγωγή των πειραμάτων αξιολόγησης του συστήματος.

Το σύστημα κίνησης και οι φορείς μικροπλακών είναι τα βοηθητικά υποσυστήματα που μεταφέρουν τα διαφορετικά αντιδρώντα και τα υγρά πλύσης σε θέσεις που να μπορεί να τα επεξεργαστεί η κεφαλή διαχείρισης. Πλέον αυτών, στην πλατφόρμα ενσωματώνονται δύο θέσεις κρυσυντήρησης με στοιχεία peltier για την προσωρινή αποθήκευση ευαίσθητων αντιδρώντων και αυτοματισμοί για την φόρτωση/εκφόρτωση πιπετών. Η ανάγνωση του σήματος των μικροσφαιριδίων γίνεται σε ξεχωριστό μηχάνημα της εταιρίας Luminox, συμβατό με την τεχνολογία μικροσφαιριδίων.

3.3 ΑΠΟΤΕΛΕΣΜΑΤΑ ΚΑΙ ΣΥΜΠΕΡΑΣΜΑΤΑ

Η συσκευή αρχικά αξιολογήθηκε με τη χρήση οπτικής μικροσκοπίας για την απεικόνιση παγιδευμένων μικροσφαιριδίων εντός του πλαστικού ρύγχους. Η απεικόνιση δείχνει την επιτυχή παγίδευση των μικροσφαιριδίων με τη χρήση μόνιμων μαγνητών. Τα μικροσφαιρίδια εισήχθησαν στο ρύγχος ως εναιώρημα σε υδατικό διάλυμα. Η παγίδευση παραμένει κατά την εκκένωση του ρύγχους από το διάλυμα. Αφαιρώντας, ωστόσο, το μαγνητικό πεδίο και εισάγοντας ένα νέο διάλυμα, τα μικροσφαιρίδια αιωρούνται εκ νέου. Τα παραπάνω συνηγορούν στο ότι η αρχή λειτουργίας που προτείνεται θα μπορούσε να χρησιμοποιηθεί για τη διεξαγωγή πειραματικών πρωτοκόλλων.

Το σύστημα παγίδευσης αξιολογήθηκε ως προς την αποτελεσματικότητά του στην παγίδευση μικροσφαιριδίων. Χρησιμοποιώντας διαφορετικές αλληλουχίες κινήσεων των εμβόλων της κεφαλής, έγινε παγίδευση μέχρι και 94% των σφαιριδίων για πρωτόκολλο ενός βήματος και μέχρι και 58% για πρωτόκολλα 4 βημάτων.

Η τελική αξιολόγηση του συστήματος έγινε με την εκτέλεση ενός πολυπλεκτικού ανοσολογικού τεστ για αντισώματα έναντι του ιού SARS-CoV-2. Χρησιμοποιώντας δείγματα τριών ασθενών, έγινε έλεγχος των αντισωμάτων έναντι των αντιγόνων N, S1 και RBD και έγινε αντιπαραβολή των αποτελεσμάτων με τα αντίστοιχα εργαστηριακά. Η χρήση της συσκευής έδωσε ίδια αποτελέσματα με τα εργαστηριακά με παρόμοιο συντελεστή μεταβλητότητας.

Τα αποτελέσματα των παραπάνω δοκιμών συνηγορούν στο ότι η συσκευή/μέθοδος που αναπτύχθηκε θα μπορούσε να χρησιμοποιηθεί για κλινική διαγνωστική και για έρευνα, με επόμενα βήματα την περαιτέρω βελτίωση της αποτελεσματικότητας του συστήματος παγίδευσης και δοκιμές μείωσης του χρόνου εκτέλεσης των πρωτοκόλλων.

ΚΕΦΑΛΑΙΟ 4: ΜΙΚΡΟΑΝΤΛΙΕΣ ΕΝΕΡΓΟΠΟΙΟΥΜΕΝΕΣ ΜΕ ΔΕΣΜΗ LASER

Σε αυτό το κεφάλαιο παρουσιάζεται η ανάπτυξη μιας μεθόδου διαχείρισης ρευστών σε μικρορευστονικά κυκλώματα που βασίζεται στη έκθεση θερμοδιαστελλόμενων μικροσφαιριδίων σε ακτινοβολία πηγής laser. Η μέθοδος επιτρέπει τη δημιουργία μικροαντλιών μιας χρήσης που μπορούν να ενσωματωθούν σε μικρορευστονικά κυκλώματα

4.1 ΤΕΧΝΟΛΟΓΙΑ ΜΙΚΡΟΑΝΤΛΙΩΝ

Η υλοποίηση μικρορευστονικών κυκλωμάτων απαιτεί τη χρήση μεθόδων διαχείρισης ρευστών εντός του κυκλώματος για την πραγματοποίηση αλληλουχιών που απαιτούν μεταφορά, ανάμιξη και έκπλυση. Στο κεφάλαιο 2 συζητήθηκαν οι μέθοδοι που χρησιμοποιούνται για την εκτέλεση αυτών των λειτουργιών σε κλινικά συστήματα PoC. Υπάρχουν ωστόσο και άλλες μέθοδοι που έχουν προταθεί στη βιβλιογραφία, όπως οι πνευματικές αντλίες²⁵², η χρήση πιεζοηλεκτρικών στοιχείων²⁴⁷ ή οι επιφάνειες ελεγχόμενης ηλεκτροδιαβροχής²⁶⁴. Τόσο η χρήση εξωτερικών επενεργητών όσο και η ενσωμάτωση περίπλοκων δομών ή άλλων στοιχείων μέσα σε μικρορευστονικά κυκλώματα αποτελούν εμπόδια για την χρήση τους λόγω της δυσκολίας υλοποίησης αυτών των συστημάτων σε αναλώσιμα προϊόντα. Στα πλαίσια αυτής της εργασίας έγινε προσπάθεια ανάπτυξης μιας μεθόδου που δεν απαιτεί σύνδεση με εξωτερικούς επενεργητές ή στεγάνωση με εξωτερικές συνδέσεις και μπορεί να χρησιμοποιηθεί σαν στοιχείο ευέλικτου σχεδιασμού ενός PoC συστήματος.

4.2 ΜΕΘΟΔΟΙ

Για την ανάπτυξη των μικροαντλιών, χρησιμοποιήθηκαν θερμοδιαστελλόμενα μικροσφαιρίδια της εταιρίας AkzoNobel / Nouryon. Πρόκειται για σφαιρίδια αρχικής διαμέτρου μερικών μm που εγκιβωτίζουν μια ποσότητα πεπιεσμένου υδρογονάνθρακα σε υγρή φάση μέσα σε ένα θερμοπλαστικό κέλυφος. Όταν τα μικροσφαιρίδια θερμαίνονται, το κέλυφος μαλακώνει και ο υδρογονάνθρακας διαστέλλεται οδηγώντας σε μέχρι και 40 φορές ογκομετρική αύξηση. Αυτά τα μικροσφαιρίδια ενσωματώθηκαν σε μίγματα που περιλαμβάνουν μήτρα από έλαιο σιλικόνης και έναν παράγοντα τροποποίησης της απορρόφησης του μίγματος στην IR ακτινοβολία. Στη συνέχεια, το μίγμα τοποθετήθηκε μέσα σε μικρορευστονικά κυκλώματα και χρησιμοποιώντας μια δίοδο laser 980 nm και οπτικά εστίασης, μελετήθηκε η συμπεριφορά του ως μικροαντλία μιας χρήσης για διαφορετικές συνθέσεις, ως προς τον μέγιστο όγκο εμβολισμού, ως προς την μεταφορά θερμότητας προς το υπόλοιπο κύκλωμα, ως προς την μέγιστη πίεση εμβολισμού και ως προς την παροχή ρευστού. Επίσης, αναπτύχθηκε μια παραλλαγή της μικροαντλίας που περιλαμβάνει μέθοδο ελέγχου του ακριβούς όγκου εμβολισμού. Σε αυτή την παραλλαγή, μια ποσότητα φωτοπολυμερούς χρησιμοποιείται για να μπλοκάρει τη ροή όταν εκτεθεί στην ακτινοβολία ενός μπλε laser. Για την ποσοτικοποίηση των αποτελεσμάτων χρησιμοποιήθηκε ανάλυση video της κίνησης του ρευστού μέσα στο κύκλωμα.

4.3 ΑΠΟΤΕΛΕΣΜΑΤΑ ΚΑΙ ΣΥΜΠΕΡΑΣΜΑΤΑ

Οι πρώτες δοκιμές αυτού του κεφαλαίου περιλαμβάνουν την αρχική αξιολόγηση της μεθόδου και την επίδραση που έχουν διαφορετικές συνθέσεις του μίγματος στη συμπεριφορά της μικροαντλίας. Η λειτουργία της μικροαντλίας από την ενεργοποίησή της μέχρι την ολοκλήρωση της χρήσης της εμφανίζει τα ακόλουθα στάδια: Μια γραμμική περιοχή διαστολής όπου η παροχή είναι σταθερή ακολουθούμενη από μια μη γραμμική περιοχή όπου η παροχή συνεχώς μειώνεται μέχρι που μηδενίζεται. Μετά την απενεργοποίηση της διόδου, εμφανίζεται μια περιοχή επαναφοράς όπου μέρος του όγκου εμβολισμού αναρροφάται πίσω. Αυτή η περιοχή δεν εμφανίζεται όταν η αρχική διαστολή δεν ξεπερνά τη γραμμική περιοχή. Ως προς την επίδραση της σύνθεσης του μίγματος, φαίνεται πως η χρήση μιγμάτων με μεγαλύτερη περιεκτικότητα σε διαστελλόμενα σωματίδια και παράγοντα απορρόφησης, οδηγεί σε αύξηση του μέγιστου όγκου εμβολισμού αλλά δεν επηρεάζει σημαντικά την παροχή, η οποία στα πειράματα προσδιορίστηκε στα ~2 μl/sec. Μελετώντας ξεχωριστά την περιεκτικότητα του μίγματος σε παράγοντα απορρόφησης, παρατηρούμε πως για μικρές περιεκτικότητες (1%) η παροχή της μικροαντλίας είναι μειωμένη (<0.7 μl/sec) ενώ για μεγαλύτερες περιεκτικότητες αυξάνεται, ωστόσο μεγιστοποιείται στα ~2.8 μl/sec για την διάταξη που χρησιμοποιήθηκε σε αυτά τα πειράματα. Ανάμεσα στις διαφορετικές δοκιμές υπήρχε τυπική απόκλιση μέχρι και 0.3 μl/sec για την παροχή και ~2 μl για τους όγκους εμβολισμού.

Στην επόμενη σειρά πειραμάτων, χρησιμοποιώντας μια ποσότητα φωτοπολυμερούς και μια μπλε πηγή laser, υλοποιήθηκε ένα σύστημα ελέγχου του τελικού όγκου εμβολισμού της μικροαντλίας. Στα πειράματα αυτά μετρήθηκε τυπική απόκλιση του τελικού όγκου εμβολισμού ± 0.27 μl και ολικό εύρος 0.7 μl ανάμεσα σε όλες τις επαναλήψεις της δοκιμής. Για τις δοκιμές μέτρησης της πίεσης που μπορεί να επιτευχθεί μέσω της μεθόδου, έγιναν δοκιμές με αντλία πίεσης και με ενεργοποίηση της μικροαντλίας έναντι ενός κλειστού κυκλώματος χωρίς εκτόνωση της πίεσης. Υπολογίστηκε πως η βαλβίδα λειτούργησε μέχρι μια μέγιστη πίεση 9.2 bar.

Για την εκτίμηση της μεταφοράς θερμότητας από τη μικροβαλβίδα προς το υπόλοιπο κύκλωμα, έγινε προσομοίωση με τη μέθοδο των πεπερασμένων στοιχείων και μετρήσεις με τη χρήση θερμικής κάμερας. Τα αποτελέσματα έδειξαν πως η αύξηση θερμοκρασίας πέραν των 37° C είναι περιορισμένη σε μια μικρή ζώνη γύρω από τη θέση της αντλίας η οποία μπορεί να μειωθεί περαιτέρω με τη χρήση απαγωγών θερμότητας.

Από τις παραπάνω δοκιμές φαίνεται πως η προτεινόμενη μέθοδος μπορεί να χρησιμοποιηθεί για την κατασκευή ενσωματωμένων μικροαντλιών σε μικρορευστονικά κυκλώματα. Στα πλαίσια της παρούσας ερευνητικής εργασίας, αυτές οι μικροαντλίες είναι στοιχεία ευέλικτου σχεδιασμού για την υλοποίηση PoC συστημάτων που μπορούν να διενεργήσουν ανοσολογικές δοκιμές μέσα σε μικρορευστονικό κύκλωμα χρησιμοποιώντας τεχνολογία μικροσφαιριδίων.

ΚΕΦΑΛΑΙΟ 5: ΠΟΡΩΔΕΙΣ ΥΔΡΟΦΟΒΕΣ ΜΙΚΡΟΒΑΛΒΙΔΕΣ

Σε αυτό το κεφάλαιο παρουσιάζεται η ανάπτυξη μιας μεθόδου διαχείρισης ρευστών σε μικρορευστονικά κυκλώματα μέσω της ενσωμάτωσης στο κύκλωμα υδρόφοβων, πορωδών στοιχείων, που λειτουργούν ως βαλβίδες ελεγχόμενες από την πίεση του κυκλώματος. Αναλύεται ο τρόπος κατασκευής των βαλβίδων και τοποθετούνται μέσα σε φυγοκεντρικό μικρορευστονικό κύκλωμα για να αξιολογηθεί η αποτελεσματικότητά τους.

5.1 ΤΕΧΝΟΛΟΓΙΑ ΜΙΚΡΟΒΑΛΒΙΔΩΝ

Οι μικροβαλβίδες είναι απαραίτητα στοιχεία μικρορευστονικών κυκλωμάτων για την υλοποίηση πρωτοκόλλων πολλαπλών βημάτων. Η τεχνολογία μικροβαλβίδων χωρίζεται σε ενεργά και παθητικά στοιχεία. Οι ενεργές βαλβίδες είναι στοιχεία στα οποία απαιτείται επενέργεια για να επιτελέσουν το σκοπό τους, για παράδειγμα πνευματικά ελεγχόμενες on/off βαλβίδες. Οι παθητικές βαλβίδες ανταποκρίνονται στην αλλαγή της πίεσης του κυκλώματος για να μπλοκάρουν ή να επιτρέψουν τη ροή. Στο κεφάλαιο 2 αυτής της εργασίας παρουσιάστηκαν πραγματικές εφαρμογές παθητικών βαλβίδων σε φυγοκεντρικά συστήματα. Αυτές οι βαλβίδες κατασκευάζονται εισάγοντας μια απότομη αλλαγή στη γεωμετρία του κυκλώματος ή/και τοπική αλλαγή της υδροφοβικότητας της δομής. Τυπικές πιέσεις λειτουργίας αυτών των βαλβίδων αναφέρονται στη βιβλιογραφία από τιμές μικρότερες των 500 Pa²⁹⁵ μέχρι και 10⁴ Pa²⁷⁹ για πιο προηγμένες εφαρμογές. Εάν ένα μέτωπο ρευστού βρεθεί σε επαφή με μια τέτοια βαλβίδα, ανάλογα με την περιστροφική ταχύτητα του φυγοκεντρικού συστήματος, είτε θα παραμείνει μπλοκαρισμένο, είτε θα διαβρέξει την επιφάνεια της βαλβίδας, επιτρέποντας έτσι τη ροή διαμέσου της. Η κατασκευή υδρόφοβων και υπερυδρόφοβων βαλβίδων απαιτεί υψηλή ακρίβεια στη δομή του μικρορευστονικού κυκλώματος και περαιτέρω τοπική επεξεργασία με πλάσμα ή χημικά τροποποίησης της διαβροχής της επιφάνειας. Σε αυτό το κεφάλαιο παρουσιάζεται η ανάπτυξη ενός τύπου παθητικής μικροβαλβίδας που κατασκευάζεται εκτός του μικροκυκλώματος και εισάγεται σε αυτό ως ξεχωριστό στοιχείο. Αυτό επιτρέπει τη χρήση της ως στοιχείο ευέλικτου σχεδιασμού για PoC συστήματα.

5.2 ΜΕΘΟΔΟΙ

Η προτεινόμενη μικροβαλβίδα αποτελείται από ένα λεπτό, υδρόφοβο δίσκο ενός λεπτού και πορώδους υλικού. Ο δίσκος εισάγεται μέσα σε μικρορευστονικό κύκλωμα διακόπτοντας τη ροή μέσα σε ένα κανάλι. Για την κατασκευή του στοιχείου χρησιμοποιήθηκε φίλτρο μικροϊνών γυαλιού με πορώδες 700 nm. Το φίλτρο έγινε υδρόφοβο εμβαπτίζοντάς το σε διάλυμα που περιέχει SiO₂ σωματίδια μεγέθους ~100 nm και αφήνοντας το διάλυμα να εξατμιστεί. Η γωνία επαφής του υδρόφοβου υλικού μετρήθηκε στις 149°. Για την κατασκευή του μικρορευστονικού κυκλώματος χρησιμοποιήθηκαν τεχνικές κοπής με laser και μηχανική κατεργασία σε ακρυλικούς δίσκους. Κατασκευάστηκαν ακτινικά κανάλια για χρήση σε φυγοκεντρικό σύστημα διαχείρισης ρευστών. Το πάχος της μικροβαλβίδας και της θέσης έδρασής της ήταν 300 μm. Ένα δεύτερο μικρορευστονικό κύκλωμα κατασκευάστηκε στο οποίο η μικροβαλβίδα τοποθετείται κάθετα στην ακτινική διεύθυνση του δίσκου.

Για τη διεξαγωγή των πειραμάτων σχεδιάστηκε και κατασκευάστηκε διάταξη που επιτρέπει την περιστροφή του δίσκου μέχρι και με 9000 RPM. Σύστημα στροβοσκοπικής όρασης και καταγραφής κατασκευάστηκε και τοποθετήθηκε πάνω από τη διάταξη. Τα πειράματα περιλάμβαναν την εισαγωγή χρωματισμένου υδατικού διαλύματος μέσα στο κύκλωμα και την σταδιακή επιτάχυνσή του μέχρι το σημείο κατάρρευσης της βαλβίδας. Η εκτίμηση του σημείου κατάρρευσης έγινε χρησιμοποιώντας την καταγραφή των πειραμάτων από το στροβοσκοπικό σύστημα όρασης.

5.3 ΑΠΟΤΕΛΕΣΜΑΤΑ ΚΑΙ ΣΥΜΠΕΡΑΣΜΑΤΑ

Στην πρώτη σειρά δοκιμών, οι μικροβαλβίδες δοκιμάστηκαν σε ακτινική τοποθέτηση με αυξανόμενη γωνιακή ταχύτητα του φυγοκεντρικού συστήματος. Από το σύνολο των πειραμάτων (N=8), παρατηρήθηκε μέση ταχύτητα κατάρρευσης της μικροβαλβίδας στα 1867 RPM με τυπική απόκλιση 204 RPM. Χρησιμοποιώντας τη θέση των μετώπων ρευστού, η παραπάνω τιμή αντιστοιχεί σε πίεση 12.5 ± 2.7 kPa. Η πρώτη παρατήρηση είναι πως οι πιέσεις κατάρρευσης είναι σημαντικά μεγαλύτερες από τις αντίστοιχες των γεωμετρικών βαλβίδων και μεγαλύτερες από τις αναφερθείσες στη βιβλιογραφία για βαλβίδες με τροποποίηση επιφάνειας. Η δεύτερη παρατήρηση είναι πως η τυπική απόκλιση είναι αρκετά αυξημένη. Κάνοντας τομές στις χρησιμοποιημένες βαλβίδες, παρατηρήθηκε πως σε ορισμένες περιπτώσεις το ρευστό παρακάμπτει το εσωτερικό της βαλβίδας και ρέει ανάμεσα στη διεπιφάνεια με το κύκλωμα.

Στη δεύτερη σειρά δοκιμών, οι μικροβαλβίδες τοποθετήθηκαν σε γωνία 90° με την ακτινική κατεύθυνση και έγινε επανάληψη του πειράματος. Αξίζει να σημειωθεί πως σε αυτή τη διάταξη χρησιμοποιείται ένα εξάρτημα έδρασης των μικροβαλβίδων που αποτρέπει τη ροή από τη διεπιφάνεια με το κύκλωμα. Εδώ, οι πιέσεις κατάρρευσης ήταν σημαντικά πιο αυξημένες με μέση τιμή 60.5 kPa και τυπική απόκλιση 4.5 kPa.

Τα συμπεράσματα από τις παραπάνω δοκιμές είναι πως η προτεινόμενη μικροβαλβίδα έχει δυνατότητες εφαρμογής σε φυγοκεντρικά μικρορευστονικά κυκλώματα. Η αυξημένη πίεση κατάρρευσης είναι επιθυμητή καθώς επιτρέπει τη χρήση των χαμηλών γωνιακών ταχυτήτων για την εκτέλεση βημάτων όπως ανάδευση και μέτρηση των αντιδρώντων. Επίσης, η ευκολία κατασκευής και τοποθέτησης του στοιχείου μέσα σε μικρορευστονικά κυκλώματα, το κάνει συμβατό με ευέλικτο σχεδιασμό PoC συστημάτων. Σαν επόμενο βήμα, η βελτίωση της στεγάνωσης της διεπιφάνειας του κυκλώματος με τη μικροβαλβίδα θα βοηθήσει στην αύξηση της επαναληψιμότητας λειτουργίας αυτού του στοιχείου.

ΚΕΦΑΛΑΙΟ 6: ΕΦΑΡΜΟΓΕΣ ΣΕ ΡΟC ΣΥΣΤΗΜΑΤΑ

Σε αυτό το κεφάλαιο παρουσιάζονται concept παρακλίνων συστημάτων ανοσολογικών δοκιμών που βασίζονται σε όσα αναπτύχθηκαν στα προηγούμενα κεφάλαια. Όλα τα concept βασίζονται σε τεχνολογία μικροσφαιριδίων ώστε να μοιράζονται τα πρωτόκολλα ανάμεσα στο σύστημα που παρουσιάστηκε στο κεφάλαιο 3 και στα μικρότερα, φορητά συστήματα.

6.1 LAB-ON-A-DISK ΒΑΣΙΣΜΕΝΟ ΣΕ ΣΤΟΙΧΕΙΑ ΕΥΕΛΙΚΤΟΥ ΣΧΕΔΙΑΣΜΟΥ

Το πρώτο concept βασίζεται στην ενσωμάτωση μικροβαλβίδων και μικροαντλιών σε ένα αναλώσιμο μικρορευστονικό κύκλωμα σχεδιασμένο για να πραγματοποιεί sandwich ELISA πρωτόκολλα με υπερπαραμαγνητικά μικροσφαιρίδια. Το κύκλωμα κατασκευάζεται στις 2 πλευρές ενός πλαστικού δίσκου. Οι υδρόφοβες βαλβίδες χρησιμοποιούνται στο πρώτο βήμα του πρωτοκόλλου που είναι η επανασύσταση των λυοφιλοποιημένων αντιδρώντων. Μια ποσότητα ρευστού εισάγεται στο κεντρικό port του δίσκου. Ο δίσκος περιστρέφεται και το ρευστό διαμοιράζεται σε θαλάμους ογκομέτρησης επιμέρους όγκων. Οι έξοδοι αυτών των θαλάμων μπλοκάρονται από υδρόφοβες βαλβίδες οι οποίες ενεργοποιούνται μόλις ολοκληρωθεί η ογκομέτρηση, αυξάνοντας την ταχύτητα περιστροφής. Από τους όγκους ρευστού που περνάνε τις βαλβίδες γίνεται επανασύσταση των αντιδρώντων. Στη συνέχεια τα αντιδρώντα ωθούνται προς τον θάλαμο αντίδρασης με τη χρήση μικροαντλιών. Στον θάλαμο αντίδρασης βρίσκονται και τα μικροσφαιρίδια.

Για την ολοκλήρωση αυτού του πρωτοκόλλου, απαιτείται διάταξη που περιλαμβάνει ένα σύστημα ελεγχόμενης περιστροφής, πηγή laser για την ενεργοποίηση των βαλβίδων, μόνιμους μαγνήτες για βήματα ανάδευσης και παγίδευσης και σύστημα ποσοτικοποίησης των αποτελεσμάτων της δοκιμής.

6.2 LAB-ON-A-DISK ΒΑΣΙΣΜΕΝΟ ΣΕ ΑΥΤΟΝΟΜΟΥΣ INJECTORS

Το δεύτερο concept βασίζεται σε μια παραλλαγή των μικροαντλιών που παρουσιάστηκαν στο κεφάλαιο 4. Με στόχο την περαιτέρω αύξηση της ευελιξίας στον σχεδιασμό PoC συστημάτων, προτείνεται η ενσωμάτωση των μικροαντλιών μέσα σε γυάλινα τριχοειδή σωληνάκια. Με αυτόν το τρόπο, η ενσωμάτωση των μικροαντλιών μέσα στο μικρορευστονικό κύκλωμα επιτυγχάνεται με συναρμολόγηση των τριχοειδών μέσα στον αναλώσιμο δίσκο/chip. Χρησιμοποιώντας και ένα φωτοπολυμερές εντός του τριχοειδούς, υλοποιείται και η λύση ελεγχόμενου εμβολισμού που παρουσιάστηκε στο κεφάλαιο 4. Επιπλέον, υπάρχει η δυνατότητα ενσωμάτωσης και των αντιδρώντων μέσα στο ίδιο τριχοειδές, μετατρέποντάς το σε αυτόνομο injector. Μια ελαστομερής κασέτα θα μπορούσε να χρησιμοποιηθεί. Αρχικά πρωτότυπα έδειξαν πως η προτεινόμενη λύση είναι εφικτή αλλά απαιτεί επίλυση των ζητημάτων στεγάνωσης των injectors με το μικρορευστονικό κύκλωμα.

ΚΕΦΑΛΑΙΟ 7: ΣΥΜΠΕΡΑΣΜΑΤΑ ΚΑΙ ΕΠΟΜΕΝΑ ΒΗΜΑΤΑ

Στα πλαίσια αυτής της εργασίας παρουσιάστηκαν λύσεις για τη δημιουργία ευέλικτων συστημάτων παρακλίνων ανοσολογικών δοκιμών. Παρουσιάστηκε ένα εργαστηριακό σύστημα διεξαγωγής δοκιμών ELISA με χρήση υπερπαραμαγνητικών μικροσφαιριδίων και δοκιμάστηκε με επιτυχία για την ανίχνευση αντισωμάτων έναντι του ιού SARS-CoV-2. Για την μεταφορά αυτής της τεχνολογίας σε μικρότερης κλίμακας συσκευές, προτάθηκαν μια μικροαντλία και μια μικροβαλβίδα και δοκιμάστηκαν με θετικά αποτελέσματα. Συζητήθηκαν πιθανές υλοποιήσεις με χρήση αυτών των στοιχείων. Το επόμενο βήμα στα πλαίσια αυτής της ερευνητικής εργασίας είναι η ανάπτυξη αναλώσιμων δίσκων και αντίστοιχης συσκευής που θα κάνουν χρήση αυτών των στοιχείων για την ολοκλήρωση ενός πρωτοκόλλου sandwich ELISA με μικροσφαιρίδια.

ΔΗΜΟΣΙΕΥΣΕΙΣ

Αποτελέσματα της έρευνας έχουν δημοσιευτεί στις ακόλουθες δύο κύριες δημοσιεύσεις:

-Kanakaris, G. P., N. Fatsis-Kavalopoulos, and L. G. Alexopoulos. "Laser Activated Single-Use Micropumps." *Sensors and Actuators B: Chemical* 220 (December 1, 2015): 549–56. <https://doi.org/10.1016/j.snb.2015.04.101>.

-Kanakaris, G. P., C. Sotiropoulos, and L. G. Alexopoulos. "Commercialized Point-of-Care Technologies." *Portable Biosensors and Point-of-Care Systems*, January 16, 2017, 255–307. https://doi.org/10.1049/PBHE003E_ch14.

Στα πλαίσια της διατριβής έχουν υποστηριχθεί οι ακόλουθες δημοσιεύσεις:

-Ellinas, K., V. Pliaka, G. Kanakaris, A. Tserepi, L. G. Alexopoulos, and E. Gogolides. "Micro-Bead Immunoassays for the Detection of IL6 and PDGF-2 Proteins on a Microfluidic Platform, Incorporating Superhydrophobic Passive Valves." *Microelectronic Engineering, Micro- and Nanotechnology/engineering for Life Sciences and Biology*, 175 (May 5, 2017): 73–80. <https://doi.org/10.1016/j.mee.2017.02.015>.

-Gkousioudi, A., D. S. Tzeranis, G. P. Kanakaris, M. Saloufas, and L. G. Alexopoulos. "Quantifying Cartilage Biomechanical Properties Using a Linearized Frequency-Domain Method." *Annals of Biomedical Engineering* 45, no. 9 (September 1, 2017): 2061–74. <https://doi.org/10.1007/s10439-017-1861-1>.

-Korompili, Georgia, Georgios Kanakaris, Christos Ampatis, and Nikos Chronis. "A Portable, Optical Scanning Microsystem for Large Field of View, High Resolution Imaging of Biological Specimens." *Sensors and Actuators A: Physical* 279 (August 15, 2018): 367–75. <https://doi.org/10.1016/j.sna.2018.06.034>.

-Tzeranis, D. S., I. Panagiotopoulos, S. Gkouma, G. Kanakaris, N. Georgiou, N. Vaindirlis, G. Vasileiou, et al. "A Device for High-Throughput Monitoring of Degradation in Soft Tissue Samples." *Journal of Biomechanics* 74 (June 6, 2018): 180–86. <https://doi.org/10.1016/j.jbiomech.2018.04.040>.

BIBLIOGRAPHY

1. Kikuyama, M. *et al.* Early Diagnosis to Improve the Poor Prognosis of Pancreatic Cancer. *Cancers* **10**, 48 (2018).
2. Wardle, J., Robb, K., Vernon, S. & Waller, J. Screening for prevention and early diagnosis of cancer. *American Psychologist* **70**, 119–133 (2015).
3. Shimura, T. *et al.* Novel urinary protein biomarker panel for early diagnosis of gastric cancer. *Br J Cancer* **123**, 1656–1664 (2020).
4. Lin, Y. D., Garner, S. E., Lau, J. S. Y., Korman, T. M. & Woolley, I. J. Prevalence of HIV indicator conditions in late presenting patients with HIV: a missed opportunity for diagnosis? *QJM: An International Journal of Medicine* **112**, 17–21 (2019).
5. Kim, S., Nhem, S., Dourng, D. & Ménard, D. Malaria rapid diagnostic test as point-of-care test: study protocol for evaluating the VIKIA® Malaria Ag Pf/Pan. *Malaria Journal* **14**, 114 (2015).
6. World Health Organization. *Global Fund: funding proposal development: WHO policy brief*. <https://apps.who.int/iris/handle/10665/252534> (2016).
7. Rong, X. Effect of delay in diagnosis on transmission of COVID-19. *Mathematical Biosciences and Engineering* **17**, 16.
8. Usherwood, T., Zhang, L. & Tripathi, A. The Path Forward for COVID-19 Diagnostics. *Mol Diagn Ther* **24**, 637–639 (2020).
9. St John, A. & Price, C. P. Existing and Emerging Technologies for Point-of-Care Testing. *Clin Biochem Rev* **35**, 155–167 (2014).
10. Carballo, B. L. F. Low-cost point-of-care diagnostic devices for low resource settings. 198.
11. Simpler and faster Covid-19 testing: Strategies to streamline SARS-CoV-2 molecular assays - EBioMedicine. [https://www.thelancet.com/journals/ebiom/article/PIIS2352-3964\(21\)00029-3/fulltext](https://www.thelancet.com/journals/ebiom/article/PIIS2352-3964(21)00029-3/fulltext).
12. COVID-19 Rapid Testing: Every Minute Counts. *Abbott* <https://www.abbott.com/corpnewsroom/diagnostics-testing/covid-19-rapid-testing-every-minute-counts.html>.

13. Weissleder, R., Lee, H., Ko, J. & Pittet, M. J. COVID-19 diagnostics in context. *Science Translational Medicine* (2020).
14. FDA letter, Coronavirus Disease 2019 Testing Basics. 2.
15. MacBeath, G. & Schreiber, S. L. Printing Proteins as Microarrays for High-Throughput Function Determination. *Science* **289**, 1760–1763 (2000).
16. MagPlex® Microspheres. *Luminex Corporation* <https://www.luminexcorp.com/magplex-microspheres/>.
17. Parsa, S. F. *et al.* Early diagnosis of disease using microbead array technology: A review. *Analytica Chimica Acta* **1032**, 1–17 (2018).
18. Luminex Corporation | Complexity Simplified. *Luminex Corporation* <https://www.luminexcorp.com/>.
19. Chandler, M. B. & Chandler, D. J. Microparticles with multiple fluorescent signals and methods of using same. (2005).
20. Pittaro, R., Goldman, B., Lefebvre, R. & King, D. A. Differentiation of flow cytometry pulses and applications. (2014).
21. Multiplexed Cytokines (Luminex) – DartLab. <https://geiselmed.dartmouth.edu/dartlab/immunoassays/multiplexed-cytokines/>.
22. Land, K. J., Boeras, D. I., Chen, X.-S., Ramsay, A. R. & Peeling, R. W. REASSURED diagnostics to inform disease control strategies, strengthen health systems and improve patient outcomes. *Nat Microbiol* **4**, 46–54 (2019).
23. Glucose meter. *Wikipedia* (2021).
24. Pete. *Project 365 #82: 230321 Quite The Year.* (2021).
25. Traugott, M. *et al.* Performance of Severe Acute Respiratory Syndrome Coronavirus 2 Antibody Assays in Different Stages of Infection: Comparison of Commercial Enzyme-Linked Immunosorbent Assays and Rapid Tests. *The Journal of Infectious Diseases* **222**, 362–366 (2020).
26. Dincer, C., Bruch, R., Kling, A., Dittrich, P. S. & Urban, G. A. Multiplexed Point-of-Care Testing – xPOCT. *Trends in Biotechnology* **35**, 728–742 (2017).
27. Murata, K. *et al.* Analytical performance of the Abaxis Piccolo Xpress® point of care analyzer in whole blood, serum, and plasma. *Clinical Biochemistry* **48**, 1344–1346 (2015).
28. Health, C. for D. and R. CLIA Waiver by Application. *FDA* (2020).

29. Stratus CS Acute Care. <https://www.siemens-healthineers.com/cardiac/cardiac-systems/stratus-cs-acute-care>.
30. Abaxis, VCA Team Up On Equipment, Marketing Deal. *Veterinary Practice News* <https://www.veterinarypracticenews.com/abaxis-vca-team-up-on-equipment-marketing-deal/> (2014).
31. Siemens Healthineers – Stratus CS 200 Acute Care Diagnostic System • healthcare-in-europe.com. <https://healthcare-in-europe.com/de/labbook/poct/206-siemens-healthineers-stratus-cs-200-acute-care-diagnostic-system.html>.
32. Holmquist, M. & Jesson, G. Microfluidic assays and microfluidic devices. (2011).
33. Fischer, S. K. *et al.* Evaluation of two point of care technologies for measuring monoclonal antibody therapeutic concentrations in blood. *Bioanalysis* **12**, 1449–1458 (2020).
34. Inganäs, M. *et al.* Integrated Microfluidic Compact Disc Device with Potential Use in Both Centralized and Point-of-Care Laboratory Settings. *Clinical Chemistry* **51**, 1985–1987 (2005).
35. Vashist, S. K. Trends in Multiplex Immunoassays for In Vitro Diagnostics and Point-of-Care Testing. *Diagnostics* **11**, 1630 (2021).
36. AB, G. P. T. Gyrolab xPand | Automated Immunoassays | Gyros Protein Technologies. <https://www.gyrosproteintechnologies.com/gyrolab-xpand-automated-immunoassay-system>.
37. Mora, J. R., Obenauer-Kutner, L. & Vimal Patel, V. Application of the Gyrolab™ platform to ligand-binding assays: a user's perspective. *Bioanalysis* **2**, 1711–1715 (2010).
38. Lequin, R. M. Enzyme Immunoassay (EIA)/Enzyme-Linked Immunosorbent Assay (ELISA). *Clinical Chemistry* **51**, 2415–2418 (2005).
39. AlphaLISA immunoassays: the no-wash alternative to ELISAs for research and drug discovery | Nature Methods. <https://www.nature.com/articles/nmeth.f.230>.
40. Doyle, K. J., Wilkins, P., Withers, M., Cooper, A. & Noell, J. O. Integrated cartridge housings for sample analysis. (2017).
41. Whitesides, G. M. The origins and the future of microfluidics. *Nature* **442**, 368–373 (2006).
42. Xia, Y. & Whitesides, G. M. Soft Lithography. *Angewandte Chemie International Edition* **37**, 550–575 (1998).
43. Balagaddé, F. K., You, L., Hansen, C. L., Arnold, F. H. & Quake, S. R. Long-Term Monitoring of Bacteria Undergoing Programmed Population Control in a Microchemostat. *Science* **309**, 137–140 (2005).

44. Cooksey, G. A., Sip, C. G. & Folch, A. A multi-purpose microfluidic perfusion system with combinatorial choice of inputs, mixtures, gradient patterns, and flow rates. *Lab Chip* **9**, 417–426 (2009).
45. Au, A. K., Lai, H., Utela, B. R. & Folch, A. Microvalves and Micropumps for BioMEMS. *Micromachines* **2**, 179–220 (2011).
46. Gervais, L., de Rooij, N. & Delamarche, E. Microfluidic Chips for Point-of-Care Immunodiagnostics. *Advanced Materials* **23**, H151–H176 (2011).
47. Unger, M. A., Chou, H.-P., Thorsen, T., Scherer, A. & Quake, S. R. Monolithic Microfabricated Valves and Pumps by Multilayer Soft Lithography. *Science* **288**, 113–116 (2000).
48. Sohrabi, S., Kassir, N. & Moraveji, M. K. Droplet microfluidics: fundamentals and its advanced applications. *RSC Adv.* **10**, 27560–27574 (2020).
49. Mugele, F. & Baret, J.-C. Electrowetting: from basics to applications. *J. Phys.: Condens. Matter* **17**, R705–R774 (2005).
50. Li, X., Ballerini, D. R. & Shen, W. A perspective on paper-based microfluidics: Current status and future trends. *Biomicrofluidics* **6**, 011301 (2012).
51. Yamada, K., Shibata, H., Suzuki, K. & Citterio, D. Toward practical application of paper-based microfluidics for medical diagnostics: state-of-the-art and challenges. *Lab Chip* **17**, 1206–1249 (2017).
52. Lymer, P. i-Stat portable clinical analyzer.
53. Kopf-Sill, A. R. & Schembri, C. T. Modified siphons for improving metering precision. (2011).
54. Brenner, T., Müller, C., Reinecke, H., Zengerle, R. & Ducrée, J. Fabrication Chain for Prototyping of Microfluidic Chips in Polymers. 4.
55. Suh, Y. K. & Kang, S. A Review on Mixing in Microfluidics. *Micromachines* **1**, 82–111 (2010).
56. Shi, H. *et al.* Recent progress of microfluidic reactors for biomedical applications. *Chemical Engineering Journal* **361**, 635–650 (2019).
57. Lim, Y. C., Kouzani, A. Z. & Duan, W. Lab-on-a-chip: a component view. *Microsyst Technol* **16**, 1995–2015 (2010).
58. Gubala, V., Harris, L. F., Ricco, A. J., Tan, M. X. & Williams, D. E. Point of Care Diagnostics: Status and Future. *Anal. Chem.* **84**, 487–515 (2012).

59. Kumar, S. *et al.* Aspects of Point-of-Care Diagnostics for Personalized Health Wellness. *Int J Nanomedicine* **16**, 383–402 (2021).
60. Mohammed, M. I., Haswell, S. & Gibson, I. Lab-on-a-chip or Chip-in-a-lab: Challenges of Commercialization Lost in Translation. *Procedia Technology* **20**, 54–59 (2015).
61. McCormick-Baw, C. *et al.* Saliva as an Alternate Specimen Source for Detection of SARS-CoV-2 in Symptomatic Patients Using Cepheid Xpert Xpress SARS-CoV-2. *Journal of Clinical Microbiology* **58**, e01109-20.
62. Stokes, W. *et al.* Acceptable performance of the Abbott ID NOW among symptomatic individuals with confirmed COVID-19. *Journal of Medical Microbiology* **70**, 001372.
63. Campbell, A. R. & Buckland, J. R. Disc pump with advanced actuator. (2018).
64. Andersson, P. *et al.* Structural units that define fluidic functions. (2008).
65. Emeric, P., Davis, G., Ewart, T. & Gershtein, S. Optical assay device with pneumatic sample actuation. (2020).
66. Minicare: Big Mistake Opens Door For Siemens. <https://www.searchinglifescience.com>
<https://www.searchinglifescience.com/media/94/minicare-big-mistake-opens-door-for-siemens>.
67. I. Barbosa, A. & M. Reis, N. A critical insight into the development pipeline of microfluidic immunoassay devices for the sensitive quantitation of protein biomarkers at the point of care. *Analyst* **142**, 858–882 (2017).
68. [biochemistry_panel_plus_package_insert-en.pdf](#).
69. Millet, L. J., Lucheon, J. D., Standaert, R. F., Retterer, S. T. & Doktycz, M. J. Modular microfluidics for point-of-care protein purifications. *Lab Chip* **15**, 1799–1811 (2015).
70. Vasilakis, N., Papadimitriou, K. I., Morgan, H. & Prodromakis, T. Modular Pressure and Flow Rate-Balanced Microfluidic Serial Dilution Networks for Miniaturised Point-of-Care Diagnostic Platforms. *Sensors* **19**, 911 (2019).
71. Zhao, Y. *et al.* Microfluidic Synthesis of Barcode Particles for Multiplex Assays. *Small* **11**, 151–174 (2015).
72. Kanakaris, P., Sotiropoulos, C. & Alexopoulos, L. G. Commercialized point-of-care technologies. *Portable Biosensors and Point-of-Care Systems* 255–307 (2017) doi:10.1049/PBHE003E_ch14.
73. Tang, M., Wang, G., Kong, S.-K. & Ho, H.-P. A Review of Biomedical Centrifugal Microfluidic Platforms. *Micromachines* **7**, 26 (2016).
74. Tokel, O., Inci, F. & Demirci, U. Advances in plasmonic technologies for point of care applications. *Chemical Reviews* **114**, 5728–5752 (2014).

75. Vashist, S. K., Luppia, P. B., Yeo, L. Y., Ozcan, A. & Luong, J. H. T. Emerging Technologies for Next-Generation Point-of-Care Testing. *Trends in Biotechnology* **33**, 692–705 (2015).
76. Warsinke, A. Point-of-care testing of proteins. *Analytical and Bioanalytical Chemistry* **393**, 1393–1405 (2009).
77. Wu, L. & Qu, X. Cancer biomarker detection: recent achievements and challenges. *Chemical Society reviews* 2963–2997 (2015) doi:10.1039/c4cs00370e.
78. Yetisen, A. K., Akram, M. S. & Lowe, C. R. Paper-based microfluidic point-of-care diagnostic devices. *Lab on a Chip* **13**, 2210–2251 (2013).
79. Kim, L. Overview of the microfluidic diagnostics commercial landscape. *Methods in molecular biology (Clifton, N.J.)* **949**, 65–83 (2013).
80. Volpatti, L. R. & Yetisen, A. K. Commercialization of microfluidic devices. *Trends in Biotechnology* **32**, 347–350 (2014).
81. Haber, C. Microfluidics in commercial applications; an industry perspective. *Lab on a chip* **6**, 1118–1121 (2006).
82. Medica tradefair. <http://www.medica-tradefair.com/>.
83. Point-Of-Care Diagnostic Market worth \$27.5 Billion by 2018. <http://www.marketsandmarkets.com/PressReleases/point-of-care-diagnostic.asp>.
84. Michael, I., Kim, T.-H., Sunkara, V. & Cho, Y.-K. Challenges and Opportunities of Centrifugal Microfluidics for Extreme Point-of-Care Testing. *Micromachines* **7**, 32 (2016).
85. covid-19_rat_common-list_en.pdf.
86. Posthuma-Trumpie, G. A., Korf, J. & van Amerongen, A. Lateral flow (immuno) assay: its strengths, weaknesses, opportunities and threats. A literature survey. *Analytical and Bioanalytical Chemistry* **393**, 569–582 (2009).
87. O'Farrell, B. Chapter 2.4 – Lateral Flow Immunoassay Systems: Evolution from the Current State of the Art to the Next Generation of Highly Sensitive, Quantitative Rapid Assays. in *The Immunoassay Handbook* 89–107 (2013). doi:10.1016/B978-0-08-097037-0.00007-5.
88. Wing Cheung Mak Anthony P.F. Turner, V. B. Lateral-flow technology: From visual to instrumental. (2015) doi:10.1016/j.trac.2015.10.017.
89. Sajid, M., Kawde, A. N. & Daud, M. Designs, formats and applications of lateral flow assay: A literature review. *Journal of Saudi Chemical Society* **19**, 689–705 (2015).

90. Chun, P. Colloidal Gold and Other Labels for Lateral Flow Immunoassays. in *Lateral Flow Immunoassay* 1–19 (Humana Press, 2009). doi:10.1007/978-1-59745-240-3_5.
91. Bangs Laboratories. *Lateral Flow Tests*. (2013).
92. Eltzov, E. *et al.* Lateral Flow Immunoassays - from Paper Strip to Smartphone Technology. *Electroanalysis* **27**, 2116–2130 (2015).
93. Pfab, T. *et al.* Rapid immunochromatographic strip test for the detection of albuminuria and brief literature review on albuminuria screening. *European journal of medical research* **11**, 3–6 (2006).
94. Mansfield, M. A. The Use of Nitrocellulose Membranes in Lateral-Flow Assays.
95. Linares, E. M., Kubota, L. T., Michaelis, J. & Thalhammer, S. Enhancement of the detection limit for lateral flow immunoassays: evaluation and comparison of bioconjugates. *Journal of immunological methods* **375**, 264–70 (2012).
96. Brown, M. C. Antibodies: Key to a Robust Lateral Flow Immunoassay. in *Lateral Flow Immunoassay* 1–16 (Humana Press, 2009). doi:10.1007/978-1-59745-240-3_4.
97. Jayasena, S. D. Aptamers: an emerging class of molecules that rival antibodies in diagnostics. *Clinical chemistry* **45**, 1628–50 (1999).
98. Bruno, J. Predicting the Uncertain Future of Aptamer-Based Diagnostics and Therapeutics. *Molecules* **20**, 6866–6887 (2015).
99. Chen, A. & Yang, S. Replacing antibodies with aptamers in lateral flow immunoassay. *Biosensors and Bioelectronics* **71**, 230–242 (2015).
100. Mologic. Aptamer Group and Mologic enter commercial partnership to develop aptamer-based SARS-CoV-2 rapid antigen test. *Mologic* <https://mologic.co.uk/aptamer-group-and-mologic-enter-commercial-partnership-to-develop-aptamer-based-sars-cov-2-rapid-antigen-test/> (2021).
101. Millipore. *Rapid Lateral Flow Test Strips: Considerations for product development*. (2008).
102. Khandker, S. S., Nik Hashim, N. H. H., Deris, Z. Z., Shueb, R. H. & Islam, M. A. Diagnostic Accuracy of Rapid Antigen Test Kits for Detecting SARS-CoV-2: A Systematic Review and Meta-Analysis of 17,171 Suspected COVID-19 Patients. *Journal of Clinical Medicine* **10**, 3493 (2021).

103. Ibrahim, N. *et al.* Screening for SARS-CoV-2 by RT-PCR: Saliva or nasopharyngeal swab? Rapid review and meta-analysis. *PLOS ONE* **16**, e0253007 (2021).
104. Mohit, E., Rostami, Z. & Vahidi, H. A comparative review of immunoassays for COVID-19 detection. *Expert Review of Clinical Immunology* **17**, 573–599 (2021).
105. Juarez, S. I. *et al.* Field evaluation of 4 rapid tests for diagnosis of HIV infection in Panama. *Journal of Clinical Microbiology* JCM.02654-15 (2016) doi:10.1128/JCM.02654-15.
106. Delaney, K. P. *et al.* Evaluation of the performance characteristics of 6 rapid HIV antibody tests. *Clinical infectious diseases : an official publication of the Infectious Diseases Society of America* **52**, 257–63 (2011).
107. Stürenburg, E. & Junker, R. Point-of-care testing in microbiology: the advantages and disadvantages of immunochromatographic test strips. *Deutsches Ärzteblatt international* **106**, 48–54 (2009).
108. Cunningham, J. *et al.* A global comparative evaluation of commercial immunochromatographic rapid diagnostic tests for visceral leishmaniasis. *Clinical infectious diseases : an official publication of the Infectious Diseases Society of America* **55**, 1312–9 (2012).
109. Ramparany, L. *et al.* Evaluation of Four Rapid Immunochromatographic Tests for the Detection of Cardiac Troponin I. *Clinical and Vaccine Immunology* **18**, 414–417 (2011).
110. Monti, A. PRIMA LAB SA www.primahometest.com Easy to use rapid Self-Test for the detection of total cholesterol level in blood INSTRUCTIONS FOR USE.
111. Byrnes, S., Thiessen, G. & Fu, E. Progress in the development of paper-based diagnostics for low-resource point-of-care settings. *Bioanalysis* **5**, 2821–2836 (2013).
112. CHAUMAT, P. METHOD FOR DIAGNOSING AND DIFFERENTIATING HIV-2 INFECTIONS. (2013).
113. ESFANDIARI, J. DUAL PATH IMMUNOASSAY DEVICE. (2006).
114. Anderson, E. V. *et al.* Point of care diagnostic systems. (1998).
115. Eriksson, M. Initial Evaluation of the Meritas Troponin I test for Measurement of Equine Cardiac Troponin I.
116. Mahajan, V. S. & Jarolim, P. How to Interpret Elevated Cardiac Troponin Levels. *Circulation* **124**, 2350–2354 (2011).

117. Yen, C.-W., de Puig, H., Tam, J. O. & Gómez-Márquez, J. Multicolored silver nanoparticles for multiplexed disease diagnostics: distinguishing dengue, yellow fever, and Ebola viruses. *Lab Chip* **15**, 1638–1641 (2015).
118. Strohmeier, O. *et al.* Centrifugal microfluidic platforms: advanced unit operations and applications. *Chemical Society reviews* **44**, 6187–6229 (2015).
119. Ducrée, J. Centrifugal Microfluidics. *Encyclopedia of Microfluidics and Nanofluidics SE - 203* 234–245 (2008) doi:10.1007/978-0-387-48998-8_203.
120. Brenner, T., Glatzel, T., Zengerle, R. & Ducrée, J. A FLOW SWITCH BASED ON CORIOLIS FORCE.
121. Feng, Y., Zhou, Z., Ye, X. & Xiong, J. Passive valves based on hydrophobic microfluidics. *Sensors and Actuators A: Physical* **108**, 138–143 (2003).
122. ANDERSSON, P. & EKSTRAND, G. RETAINING MICROFLUIDIC MICROCAVITY AND OTHER MICROFLUIDIC STRUCTURES. (2003).
123. Burd, T. L. & Schembri, C. T. Reagent container for analytical rotor. (1994).
124. U.S. Pat. Nos. 5,061,381; 5,173,193; 5,186,844; 5,122,284;
125. Schembri, C. T., Burd, T. L., Kopf-Sill, A. R., Shea, L. R. & Braynin, B. Centrifugation and capillarity integrated into a multiple analyte whole blood analyser. *Journal of Automatic Chemistry* **17**, 99–104.
126. Schembri, C. T. Analytical rotor with dye mixing chamber. (1995).
127. Bernstein, I. D. M. *et al.* METHODS FOR PHOTOMETRIC ANALYSIS. (1995).
128. Schembri, C. T., Ostoich, V., Lingane, P. J., Burd, T. L. & Buhl, S. N. Portable simultaneous multiple analyte whole-blood analyzer for point-of-care testing. *Clinical Chemistry* **38**, 1665–1670 (1992).
129. Abaxis - Piccolo Xpress. <http://www.piccoloxpress.com/>.
130. BOEHM, C., LUTZ, S. & SPINKE, J. ROTATABLE CARTRIDGE WITH A METERING CHAMBER FOR ANALYZING A BIOLOGICAL SAMPLE. (2015).
131. BOEHM, C., LUTZ, S. & DOLBINOW, T. ROTATABLE CARTRIDGE FOR MEASURING A PROPERTY OF A BIOLOGICAL SAMPLE. (2015).
132. BOEHM, C. & LUTZ, S. ROTATABLE CARTRIDGE FOR ANALYZING A BIOLOGICAL SAMPLE. (2015).
133. Cobas b 101. <http://www.cobas.com/home/product/point-of-care-testing/cobas-b-101-poc-system.html>.

134. PEDRO SANTOS MANSO CÔRTE-REAL, J. & CORREIA DE MATOS NOLASCO LAMAS, F. FOCUSING METHOD. (2016).
135. CORREIA DE MATOS NOLASCO LAMAS, F., MANUEL DE OLIVEIRA GARCIA DA FONSECA, J., DO ROSÁRIO MAGALHÃES, A. & PEDRO SANTOS MANSO CÔRTE-REAL, J. CELL COUNTING. (2016).
136. Burger, R. *et al.* Plasma extraction by centrifugo-pneumatically induced gating of flow. *Journal of Micromechanics and Microengineering* **23**, 035035 (2013).
137. da Fonseca, J. G. & Reis, N. A. E. Liquid distribution and metering.
138. MANUEL DE OLIVEIRA GARCIA DA FONSECA, J., Reis, N. A. E. & Burger, R. ANALYTICAL ROTORS AND METHODS FOR ANALYSIS OF BIOLOGICAL FLUIDS. (2013) doi:10.1016/j.(73).
139. DE OLIVEIRA GARCIA DA FONSECA, J. M. PHOTOMETRIC DEVICE AND METHOD. (2013).
140. Biosurfit - Spinit. <http://biosurfit.com/solution/>.
141. *Point Grey application example - Biosurfit Spinit.*
142. St John, A. & Price, C. P. Existing and Emerging Technologies for Point-of-Care Testing. *The Clinical biochemist. Reviews / Australian Association of Clinical Biochemists* **35**, 155–67 (2014).
143. Yoo, J. C. Bio-disc reading apparatus and assay method using same. (2010).
144. Samsung LabGeo IB 10. <http://www.samsung.com/global/business/healthcare/healthcare/in-vitro-diagnostics/BCA-IB10/DE>.
145. Egan, R. L. Better and faster: Improving rapid point-of-care testing. (2009).
146. Feng, Y., Zhou, Z., Ye, X. & Xiong, J. Passive valves based on hydrophobic microfluidics. *Sensors and Actuators, A: Physical* **108**, 138–143 (2003).
147. Chew, M. *et al.* Study of a capillary force driven passive valve for a microfluidic package. *Proceedings of the Electronic Packaging Technology Conference, EPTC* 448–453 (2006) doi:10.1109/EPTC.2006.342756.
148. Avram, M., Avram, A. M., Bragaru, A., Ghiu, A. & Iliescu, C. Plasma surface modification for selective hydrophobic control. *Romanian Journal of Information Science and Technology* **11**, 409–422 (2008).
149. Arkles, B. Hydrophobicity, Hydrophilicity and Silanes. *Paint and Coatings industry magazine* **10** (2006).
150. Andersson, H., Van der Wijngaart, W., Griss, P., Niklaus, F. & Stemme, G. Hydrophobic valves of plasma deposited octafluorocyclobutane in DRIE channels. *Sensors and Actuators, B: Chemical* **75**, 136–141 (2001).

151. Ellinas, K. *et al.* CONTROL OF FLOW AND PROTEIN ADSORPTION ON PLASMA NANOTEXTURED POLYMERIC MICROFLUIDICS Fabrication Process of PMMA microchannels. 60228 (2013).
152. Schnabl, K. L., Tarek, M., Cursio, C. & Yip, P. M. Evaluation of the Piccolo Xpress chemistry analyzer for point of care testing of plasma liver function markers, electrolytes and metabolites. *Clinical Biochemistry* **41**, 1284–1285 (2008).
153. Owen, W. E., Caron, J. E. & Genzen, J. R. Liver function testing on the Abaxis Piccolo Xpress: Use in Ebola virus disease protocols. *Clinica Chimica Acta* **446**, 119–127 (2015).
154. Akbas, N., Gonzalez, G., Edwards, R. & Devaraj, S. *Assessment of liver function tests on Piccolo Xpress point of care chemistry analyzer in a pediatric hospital. Practical Laboratory Medicine* vol. 3 (2015).
155. van Gammeren, A. J., van Gool, N., de Groot, M. J. M. & Cobbaert, C. M. Analytical performance evaluation of the Cobas 6000 analyzer – special emphasis on trueness verification. *Clinical Chemistry and Laboratory Medicine* **46**, (2008).
156. Simpson, P., Jolly, L., Tirimacco, R., Gill, J. & Tideman, P. Evaluation of the Lipid Panel on the Abaxis Piccolo Xpress to Determine Its Potential as a Point-of-Care Instrument in a Nonlaboratory Setting. *Point of Care: The Journal of Near-Patient Testing & Technology* **9**, 32–35 (2010).
157. Piccolo Xpress product inserts. <http://www.piccoloxpress.com/products/panels/pls-msds/>.
158. Beckman Coulter- Alanine Aminotransferase Product insert. [https://www.beckmancoulter.com/wsrportal/techdocs?docname=/cis/BAOSR6x07A/%25%25/EN_ALANINE AMINOTRANSFERASE \(ALT\).pdf](https://www.beckmancoulter.com/wsrportal/techdocs?docname=/cis/BAOSR6x07A/%25%25/EN_ALANINE AMINOTRANSFERASE (ALT).pdf).
159. 510(k) SUBSTANTIAL EQUIVALENCE DETERMINATION DECISION SUMMARY ASSAY ONLY TEMPLATE. http://www.accessdata.fda.gov/cdrh_docs/reviews/K071211.pdf.
160. Marieke, C., Stijn, J. & Michel, L. Evaluation of three hemoglobin A1c point - of - care instruments.
161. Lenters-Westra, E. & Slingerland, R. J. Three of 7 Hemoglobin A1c Point-of-Care Instruments Do Not Meet Generally Accepted Analytical Performance Criteria. *Clinical Chemistry* **60**, 1062–1072 (2014).
162. Sreenan, S. & Tormey, W. American Diabetes Association recommendations on haemoglobin A1c use in diabetes diagnosis: time to include point-of-care devices? *Annals of Clinical Biochemistry: An international journal of biochemistry and laboratory medicine* 0004563215619440 (2016) doi:10.1177/0004563215619440.

163. Stijn, J. & Michel, L. Evaluation of the Roche cobas b101 point - of - care instrument for glycated hemoglobin testing in an ambulant hospital setting.
164. Biosurfit Spinit-BC , package insert.
165. Biosurfit - CRP product insert.
166. *Samsung LabGeo IB10 brochure*.
167. Ronkainen, N. J., Halsall, H. B. & Heineman, W. R. Electrochemical biosensors. (2010) doi:10.1039/b714449k.
168. Wang, Y., Xu, H., Zhang, J. & Li, G. Electrochemical Sensors for Clinic Analysis. *Sensors* **8**, 2043–2081 (2008).
169. Daniels, J. S. & Pourmand, N. Label-Free Impedance Biosensors: Opportunities and Challenges. *Electroanalysis* **19**, 1239–1257 (2007).
170. Lauks, I. R. Microfabricated Biosensors and Microanalytical Systems for Blood Analysis. *Accounts of Chemical Research* **31**, 317–324 (1998).
171. Martin, C. L. i-STAT - Combining Chemistry and Haematology in PoCT. *The Clinical biochemist. Reviews / Australian Association of Clinical Biochemists* **31**, 81–4 (2010).
172. Lauks, I. & Andrzej, M. DIAGNOSTIC DEVICES INCORPORATING FLUIDICS AND METHODS OF MANUFACTURE. vol. 1 0–4 (2010).
173. Choi, S. Powering point-of-care diagnostic devices. *Biotechnology Advances* **34**, 321–330 (2016).
174. Wang, X. *et al.* Audio jack based miniaturized mobile phone electrochemical sensing platform. *Sensors and Actuators B: Chemical* **209**, 677–685 (2015).
175. Dario Smart Meter. <http://mydario.co.uk/solution/>.
176. Turner, A. P. F. Biosensors: sense and sensibility. *Chemical Society Reviews* **42**, 3184 (2013).
177. Ohara, T. J., Rajagopalan, R. & Heller, A. Glucose electrodes based on cross-linked [Os(bpy)₂Cl]^{+/2+} complexed poly(1-vinylimidazole) films. *Analytical chemistry* **65**, 3512–7 (1993).
178. Gorton, L. *et al.* Direct electron transfer between heme-containing enzymes and electrodes as basis for third generation biosensors. *Analytica Chimica Acta* **400**, 91–108 (1999).
179. Bakker, E. & Qin, Y. Electrochemical sensors. *Analytical chemistry* **78**, 3965–84 (2006).

180. Freckmann, G. *et al.* System Accuracy Evaluation of 27 Blood Glucose. *Diabetes Technology and Therapeutics* **12**, 221–231 (2010).
181. Freckmann, G. *et al.* System accuracy evaluation of 43 blood glucose monitoring systems for self-monitoring of blood glucose according to DIN EN ISO 15197. *Journal of diabetes science and technology* **6**, 1060–75 (2012).
182. ISO 15197:2003. <http://www.diabetes.co.uk/blood-glucose-meters/iso-accuracy-standards.html>.
183. Heinemann, L. Quality of glucose measurement with blood glucose meters at the point-of-care: relevance of interfering factors. *Diabetes technology & therapeutics* **12**, 847–857 (2010).
184. Hellman, R. Glucose meter inaccuracy and the impact on the care of patients. *Diabetes/Metabolism Research and Reviews* **28**, 207–209 (2012).
185. *Alere IN Ratio Report*.
186. Fernando, R. *et al.* PT / INR Test Performance of the Xprecia Stride Coagulation Analyzer on Capillary Blood is Equivalent to a Reference Laboratory Hemostasis System PT / INR Test Performance of the Xprecia Stride Coagulation Analyzer on Capillary Blood is Equivalent to a Re. (2015).
187. *Cobas - Roche : CoaguChek XS Plus & Pro Systems*.
188. *Abbott I-STAT : PROTHROMBIN TIME / (PT / INR)*.
189. *Alere - Clinical Guidelines for PT / INR Comparisons*. (2007).
190. García-Arroyo, L. *et al.* Benefits and drawbacks of molecular techniques for diagnosis of viral respiratory infections. Experience with two multiplex PCR assays. *Journal of Medical Virology* **88**, 45–50 (2016).
191. Zanolì, L. M. & Spoto, G. Isothermal amplification methods for the detection of nucleic acids in microfluidic devices. *Biosensors* **3**, 18–43 (2013).
192. Holland, C. A. & Kiechle, F. L. Point-of-care molecular diagnostic systems — past, present and future. *Current Opinion in Microbiology* **8**, 504–509 (2005).
193. Niemz, A., Ferguson, T. M. & Boyle, D. S. Point-of-care nucleic acid testing for infectious diseases. *Trends in Biotechnology* **29**, 240–250 (2011).
194. Yan, L. *et al.* Isothermal amplified detection of DNA and RNA. *Molecular bioSystems* **10**, 970–1003 (2014).
195. Mori, Y. & Notomi, T. Loop-mediated isothermal amplification (LAMP): a rapid, accurate, and cost-effective diagnostic method for infectious diseases. *Journal of Infection and Chemotherapy* **15**, 62–69 (2009).

196. New England Biolabs - Isothermal amplification. <https://www.neb.com/applications/dna-amplification-and-pcr/isothermal-amplification>.
197. Cepheid - molecular diagnostics. <http://www.cepheid.com/en/>.
198. Dinnes, J. *et al.* Rapid, point-of-care antigen and molecular-based tests for diagnosis of SARS-CoV-2 infection. *Cochrane Database Syst Rev* **2021**, CD013705 (2021).
199. *Alere -Influenza A & B Package Insert*. (2014).
200. *Alere - Strep A Package Insert*.
201. Fairley, D. J. *et al.* Rapid and accurate detection of *Neisseria meningitidis* DNA in clinical specimens using the HiberGene HG Meningococcus LAMP assay. in.
202. Idylla IFV-RSV Panel Clinical Testing (RP1). <https://clinicaltrials.gov/ct2/show/study/NCT02786381>.
203. Gonzalez, A. L. & Waddell, L. S. Blood Gas Analyzers. *Topics in Companion Animal Medicine* (2016) doi:10.1053/j.tcam.2016.05.001.
204. OPTIMedical - OPTI CCA-TS2. <http://www.optimedical.com/products-services/opti-CCA-TS2.html>.
205. Instrumentation Laboratory - GEM premier 4000. <http://www.instrumentationlaboratory.com/products-services/critical-care-diagnostics/instruments/gem-premier-4000-with-iqm.aspx>.
206. Siemens - RAPIDPoint 500 Systems. <http://usa.healthcare.siemens.com/point-of-care/blood-gas/rapidpoint-500-systems>.
207. Roche - Cobas b 123. <http://www.cobas.com/home/product/point-of-care-testing/cobas-b-123-poc-system.html>.
208. Roche - Cobas b 221. <http://www.cobas.com/home/product/point-of-care-testing/cobas-b-221-system.html>.
209. Accriva Diagnostics - Hemochron Signature Elite. <http://www.accumetrics.com/products/hemochron-signature-elite-whole-blood-microcoagulation-system>.
210. Harris, L. F., Castro-López, V. & Killard, A. J. Coagulation monitoring devices: Past, present, and future at the point of care. *TrAC Trends in Analytical Chemistry* **50**, 85–95 (2013).
211. Coagusense - Coag-Sense. <http://www.coagusense.com/>.

212. Burtis, C. A. & Bruns, D. E. *Tietz fundamentals of clinical chemistry and molecular diagnostics*. (Elsevier Health Sciences, 2014).
213. U.S. Department of Health & Human Services, *Save Request, Mitsubishi Chemical Mediance Co.*
214. Stratus CS 200 Acute Cardiac Care Troponin Analyzer. <http://www.healthcare.siemens.com/point-of-care/cardiac/stratus-cs-200-acute-care>.
215. Siemens. Siemens -DCA Vantage System Reagent Kit product insert. 4 (2008).
216. Alere Afinion HbA1c. <http://www.alere.com/en/home/product-details/afinion-hba1c.html>.
217. Diagon - Coag S system. <http://www.diagon.com/en/pocreagent/coag-s-inr-test-kit>.
218. ANTAL, J., NEUBRANDT, J. & PETŐ, M. PROCEDURE AND MEASURING SYSTEM FOR DETERMINING BLOOD COAGULATION CHARACTERISTICS. (2015).
219. *Alere HemoPoint H2 - Product insert.*
220. Alere Hemopoint H2. <http://www.alere.com/en/home/products-services/brands/hemopoint.html>.
221. Assay device for direct measurement of LDL cholesterol.
222. Method for the determination of HDL cholesterol by means of a rapid diagnostic agent with an integrated fractionating step.
223. High-density lipoprotein assay device and method.
224. Alere Cholestech. <http://www.alere.com/en/home/products-services/brands/cholesteck.html>.
225. *Alere Cholestech LDX GLU product insert.*
226. Menarini Diagnostics Pocketchem BA.
http://www.menarinidiagnostics.com/Products/point_of_care_testing/pocketchem_ba.
227. Francesco, C., Berti, B. & Paoli, C. IMMUNOENZYMATIC ANALYSIS DEVICE FOR ONCE-ONLY USE, AND THE RELATIVE ANALYTICAL METHOD FIELD. (2002).
228. Diesse - Chorus. <http://www.diesse.it/en/Instruments/id:39/>.
229. Rifai, N., Gillette, M. A. & Carr, S. A. Protein biomarker discovery and validation: the long and uncertain path to clinical utility. *Nature Biotechnology* **24**, 971–983 (2006).
230. Seger, C. & Salzman, L. After another decade: LC–MS/MS became routine in clinical diagnostics. *Clinical Biochemistry* **82**, 2–11 (2020).

231. Geyer, P. E., Holdt, L. M., Teupser, D. & Mann, M. Revisiting biomarker discovery by plasma proteomics. *Molecular Systems Biology* **13**, 942 (2017).
232. Kong, F., Yuan, L., Zheng, Y. F. & Chen, W. Automatic Liquid Handling for Life Science: A Critical Review of the Current State of the Art. *J Lab Autom.* **17**, 169–185 (2012).
233. Freedom EVO® - Robotic laboratory workstation by Tecan | MedicalExpo.
<https://www.medicalexpo.com/prod/tecan/product-80772-648989.html>.
234. BR_Tecan_Cavro_components_overview_395351.pdf.
235. Magnum FLX® - Alpaqua. <https://www.alpaqua.com/product/magnum-flx/>.
236. Automated liquid handling, compact and flexible liquid handler | Agilent.
<https://www.agilent.com/en/product/automated-liquid-handling/automated-liquid-handling-platforms/bravo-automated-liquid-handling-platform>.
237. Freedom EVO platform. <https://lifesciences.tecan.com/freedom-evo-platform>.
238. Automated Liquid Handlers | Liquid Handling Equipment.
<https://www.hamiltoncompany.com/automated-liquid-handling>.
239. Κανακάρης, Γ. Π. & Kanakaris, G. P. Ανάλυση και κατασκευή πλατφόρμας αυτοματοποιημένης μέτρησης βιολογικών σημάτων με χρήση μικρομαγνητικών σφαιριδίων. *An automated platform for magnetic-based microbeads manipulation* (2011) doi:10.26240/heal.ntua.9907.
240. Zborowski, M., Fuh, C. B., Green, R., Sun, L. & Chalmers, J. J. Analytical Magnetapheresis of Ferritin-Labeled Lymphocytes. <https://pubs.acs.org/doi/pdf/10.1021/ac00116a014> (2002) doi:10.1021/ac00116a014.
241. Smolkin, M. R. & Smolkin, R. D. Calculation and Analysis of the Magnetic Force Acting on a Particle in the Magnetic Field of Separator. Analysis of the Equations Used in the Magnetic Methods of Separation. *IEEE Transactions on Magnetics* **42**, 3682–3693 (2006).
242. Gijs, M. A. M. Magnetic bead handling on-chip: new opportunities for analytical applications. *Microfluid Nanofluid* **1**, 22–40 (2004).
243. Shevkoplyas, S. S., Siegel, A. C., Westervelt, R. M., Prentiss, M. G. & Whitesides, G. M. The force acting on a superparamagnetic bead due to an applied magnetic field. *Lab Chip* **7**, 1294–1302 (2007).

244. Sasso, L. A. *et al.* Automated microfluidic processing platform for multiplexed magnetic bead immunoassays. *Microfluid Nanofluid* **13**, 603–612 (2012).
245. MagPlex® Microspheres | Magnetic Microspheres for Improved Washing. *Luminex Corporation* <https://www.luminexcorp.com/magplex-microspheres/>.
246. Varela, M. L. *et al.* Optimization of a magnetic bead-based assay (MAGPIX®-Luminex) for immune surveillance of exposure to malaria using multiple Plasmodium antigens and sera from different endemic settings. *Malaria Journal* **17**, 324 (2018).
247. ProtAtOnce. SARS-CoV-2 IgG Serological Assay for Luminex® Instruments. (2021).
248. Dutta, N. K., Mazumdar, K. & Gordy, J. T. The Nucleocapsid Protein of SARS–CoV-2: a Target for Vaccine Development. *Journal of Virology* **94**, e00647-20.
249. Tehrani, Z. R. *et al.* Specificity and Performance of Nucleocapsid and Spike-based SARS-CoV-2 Serologic Assays. *medRxiv* 2020.08.05.20168476 (2020) doi:10.1101/2020.08.05.20168476.
250. Kanakaris, G. P., Fatsis-Kavalopoulos, N. & Alexopoulos, L. G. Laser activated single-use micropumps. *Sensors and Actuators B: Chemical* **220**, 549–556 (2015).
251. Au, A. K., Lai, H., Utela, B. R. & Folch, A. Microvalves and Micropumps for BioMEMS. *Micromachines* **2**, 179–220 (2011).
252. Unger, M. A., Chou, H. P., Thorsen, T., Scherer, A. & Quake, S. R. Monolithic microfabricated valves and pumps by multilayer soft lithography. *Science* **288**, 113–116 (2000).
253. Jeong, O. C. & Konishi, S. Fabrication of a peristaltic micro pump with novel cascaded actuators. *Journal of Micromechanics and Microengineering* **18**, 025022 (2008).
254. Monolithic membrane valves and diaphragm pumps for practical large-scale integration into glass microfluidic devices. <https://groverlab.org/research/2003-01-01-monolithic-membrane-valves.html>.
255. Lai, H. & Folch, A. Design and dynamic characterization of “single-stroke” peristaltic PDMS micropumps. *Lab Chip* **11**, 336–342 (2011).
256. Kim, J. *et al.* Photopolymerized check valve and its integration into a pneumatic pumping system for biocompatible sample delivery. *Lab Chip* **6**, 1091–1094 (2006).

257. Tracey, M. C., Johnston, I. D., Davis, J. B. & Tan, C. K. L. Dual independent displacement-amplified micropumps with a single actuator. *J. Micromech. Microeng.* **16**, 1444–1452 (2006).
258. Valveless micropump with acoustically featured pumping chamber | SpringerLink. <https://link.springer.com/article/10.1007/s10404-009-0533-3>.
259. Computerized microfluidic cell culture using elastomeric channels and Braille displays - Google Search. https://www.google.com/search?newwindow=1&sxsrf=ALeKk03Wh-cfZjfbzQ81pR5g_rxTbW1t6Q%3A1611414490109&ei=2jsMYIKVBrCKlwTb9Ki4Cw&q=Computerized+microfluidic+cell+culture+using+elastomeric+channels+and+Braille+displays&oq=Computerized+microfluidic+cell+culture+using+elastomeric+channels+and+Braille+displays&gs_lcp=CgZwc3ktYWIQAzIJCAAQyQMQFhAeULOOpAVizqQFgk a4BaANwAHgAgAF3iAF3kgEDMC4xmAEAoAECOAEBqgEHZ3dzLXdpesABAQ&sclient=psy-ab&ved=0ahUKEwiC6pLiqrLuAhUwxYUKHVs6CrcQ4dUDCA0&uact=5.
260. Böhm, S., Olthuis, W. & Bergveld, P. An integrated micromachined electrochemical pump and dosing system. *Biomed Microdevices* **1**, 121–130 (1999).
261. Chuan-Hua Chen & Santiago, J. G. A planar electroosmotic micropump. *Journal of Microelectromechanical Systems* **11**, 672–683 (2002).
262. Tovar, A. R. & Lee, A. P. Lateral cavity acoustic transducer. *Lab Chip* **9**, 41–43 (2009).
263. Lemoff, A. V. & Lee, A. P. An AC magnetohydrodynamic micropump. *Sensors and Actuators B: Chemical* **63**, 178–185 (2000).
264. Pollack, M. G., Fair, R. B. & Shenderov, A. D. Electrowetting-based actuation of liquid droplets for microfluidic applications. *Appl. Phys. Lett.* **77**, 1725–1726 (2000).
265. Hosokawa, K., Sato, K., Ichikawa, N. & Maeda, M. Power-free poly(dimethylsiloxane) microfluidic devices for gold nanoparticle-based DNA analysis. *Lab Chip* **4**, 181–185 (2004).
266. Weinert, F. & Braun, D. Light driven Microfluidics. in *2009 International Symposium on Optomechatronic Technologies* 383–386 (2009). doi:10.1109/ISOT.2009.5326137.
267. Takeuchi, M., Hagiwara, M., Haulot, G. & Ho, C.-M. Reconfigurable microfluidic pump enabled by opto-electrical-thermal transduction. *Appl. Phys. Lett.* **103**, 174101 (2013).

268. Griss, P., Andersson, H. & Stemme, G. Expandable microspheres for the handling of liquids. *Lab Chip* **2**, 117–120 (2002).
269. Roxhed, N. *et al.* A compact, low-cost microliter-range liquid dispenser based on expandable microspheres. *J. Micromech. Microeng.* **16**, 2740–2746 (2006).
270. Spieth, S., Schumacher, A., Kallenbach, C., Messner, S. & Zengerle, R. The NeuroMedicator—a micropump integrated with silicon microprobes for drug delivery in neural research. *J. Micromech. Microeng.* **22**, 065020 (2012).
271. Jung, J. H., Han, C., Lee, S. A., Kim, J. & Yang, C. Microfluidic-integrated laser-controlled microactuators with on-chip microscopy imaging functionality. *Lab Chip* **14**, 3781–3789 (2014).
272. Ciurans Oset, M., Nordin, J. & Akhtar, F. Processing of Macroporous Alumina Ceramics Using Pre-Expanded Polymer Microspheres as Sacrificial Template. *Ceramics* **1**, 329–342 (2018).
273. Metref, L. [PDF] Fluid Manipulation Using Thermoexpandable Polymer Based on Ploydimethylsiloxane and Expancel | Semantic Scholar.
274. Blowing agents - Expancel Microspheres. *Nouryon* <https://www.nouryon.com/products/expancel-microspheres/blowing-agents/>.
275. Oh, K. W. & Ahn, C. H. A review of microvalves. *J. Micromech. Microeng.* **16**, R13–R39 (2006).
276. Au, A. K., Lai, H., Utela, B. R. & Folch, A. Microvalves and Micropumps for BioMEMS. *Micromachines* **2**, 179–220 (2011).
277. Vashist, S. K., Luppia, P. B., Yeo, L. Y., Ozcan, A. & Luong, J. H. T. Emerging Technologies for Next-Generation Point-of-Care Testing. *Trends in Biotechnology* **33**, 692–705 (2015).
278. Feng, Y., Zhou, Z., Ye, X. & Xiong, J. Passive valves based on hydrophobic microfluidics. *Sensors and Actuators A: Physical* **108**, 138–143 (2003).
279. Ellinas, K., Tserepi, A. & Gogolides, E. Superhydrophobic, passive microvalves with controllable opening threshold: exploiting plasma nanotextured microfluidics for a programmable flow switchboard. *Microfluid Nanofluid* **17**, 489–498 (2014).
280. Unger, M. A., Chou, H.-P., Thorsen, T., Scherer, A. & Quake, S. R. Monolithic Microfabricated Valves and Pumps by Multilayer Soft Lithography. *Science* **288**, 113–116 (2000).

281. Au, A. K., Lai, H., Utela, B. R. & Folch, A. Microvalves and Micropumps for BioMEMS. *Micromachines* **2**, 179–220 (2011).
282. Bauer, M. *et al.* Burst valves for commercial microfluidics: a critical analysis. *Microfluid Nanofluid* **23**, 86 (2019).
283. Cho, H., Kim, H.-Y., Kang, J. Y. & Kim, T. S. How the capillary burst microvalve works. *Journal of Colloid and Interface Science* **306**, 379–385 (2007).
284. Man, P., Mastrangelo, C. H., Burns, M. & Burke, D. T. Microfabricated capillarity-driven stop valve and sample injector. *Proceedings MEMS 98. IEEE. Eleventh Annual International Workshop on Micro Electro Mechanical Systems. An Investigation of Micro Structures, Sensors, Actuators, Machines and Systems (Cat. No.98CH36176* (1998) doi:10.1109/MEMSYS.1998.659727.
285. Zimmermann, M., Hunziker, P. & Delamarche, E. Valves for autonomous capillary systems. *Microfluid Nanofluid* **5**, 395–402 (2008).
286. Glière, A. & Delattre, C. Modeling and fabrication of capillary stop valves for planar microfluidic systems. *Sensors and Actuators A: Physical* **130–131**, 601–608 (2006).
287. Tang, M., Wang, G., Kong, S.-K. & Ho, H.-P. A Review of Biomedical Centrifugal Microfluidic Platforms. *Micromachines (Basel)* **7**, (2016).
288. Fu, G., Tor, S. B., Hardt, D. E. & Loh, N. H. Effects of processing parameters on the micro-channels replication in microfluidic devices fabricated by micro injection molding. *Microsyst Technol* **17**, 1791–1798 (2011).
289. Yu, L., Koh, C. G., Lee, L. J., Koelling, K. W. & Madou, M. J. Experimental investigation and numerical simulation of injection molding with micro-features. *Polymer Engineering & Science* **42**, 871–888 (2002).
290. Attia, U. M., Marson, S. & Alcock, J. R. Micro-injection moulding of polymer microfluidic devices. *Microfluid Nanofluid* **7**, 1 (2009).
291. Schwemmer, F. *et al.* Centrifugo-pneumatic multi-liquid aliquoting – parallel aliquoting and combination of multiple liquids in centrifugal microfluidics. *Lab Chip* **15**, 3250–3258 (2015).
292. Mark, D. *et al.* Aliquoting on the centrifugal microfluidic platform based on centrifugo-pneumatic valves. *Microfluid Nanofluid* **10**, 1279–1288 (2011).

293. Strohmeier, O. *et al.* Centrifugal microfluidic platforms: advanced unit operations and applications. *Chemical Society Reviews* **44**, 6187–6229 (2015).
294. Gorkin, R. *et al.* Centrifugal microfluidics for biomedical applications. *Lab Chip* **10**, 1758–1773 (2010).
295. Feng, Y., Zhou, Z., Ye, X. & Xiong, J. Passive valves based on hydrophobic microfluidics. *Sensors and Actuators A: Physical* **108**, 138–143 (2003).
296. Andersson, P. & Ekstrand, G. Retaining microfluidic microcavity and other microfluidic structures. (2005).
297. Andersson, P. *et al.* Structural Units That Define Fluidic Functions. (2002).
298. Larsson, A., Allmer, K. & Andersson, P. Microfluidic device. (1999).
299. Brenner, T., Müller, C., Reinecke, H., Zengerle, R. & Ducreé, J. Fabrication Chain for Prototyping of Microfluidic Chips in Polymers. 4.
300. Yasuda, T., Ishizuka, K. & Ezo, M. A Superhydrophobic Microvalve for Manipulating Microliquids Containing Biological Molecules. *IEEJ Transactions on Electrical and Electronic Engineering* **3**, 290–296 (2008).
301. Park, S., Kim, J. & Park, C. H. Superhydrophobic Textiles: Review of Theoretical Definitions, Fabrication and Functional Evaluation. *Journal of Engineered Fibers and Fabrics* **10**, 155892501501000420 (2015).
302. Wu, C.-H. & Kuo, H.-C. Parametric study of injection molding and hot embossing in polymer microfabrication. *J Mech Sci Technol* **21**, 1477 (2007).
303. Παππάς, Ι. & Πάππας, Ι. Διατάξεις και βαλβίδες μικροροϊκών συστημάτων. (2017) doi:10.26240/heal.ntua.14259.